Realization of Human Manipulation Based on Haptics

February 2014

A thesis submitted in partial fulfilment of the requirements for the degree of
Doctor of Philosophy in Engineering

Keio University

Graduate School of Science and Technology
School of Integrated Design Engineering

Takahiro Nozaki

Acknowledgements

Contents

List of Figures

List of Tables

Chapter 1

Introduction

Chapter 1 presents the background and the objective of this dissertation. This chapter also presents previous studies related to the subject of this dissertation.

1.1 Background of This Dissertation

In recent years, the use of robots for factory automation has led to improved productivity, which leads to an increased standard of living. Robotics has shown rapid progress around the industrial field until now. In contrast, robots are expected to improve our quality of life by supporting human motions in the future for the urgent problem of aging societies with falling birthrates and labor shortages [3–6] as shown in Fig. 1-1. This urgent problem requires fundamental innovation. If a breakthrough in the solution is not brought immediately, the aging societies with falling birthrates and labor shortages cause the following serious problems:

(1) Reduction in the number of skilled person.

(2) Increase in care burden.

(3) Decline in young labor force.

One of the great possibility is robotic human assistance. To support human motions and to act as physical agent, robots are required to operate in human environments. Here, "environment" refers to the objects with which robots make contact in their range of movement. Specifically, the environment includes
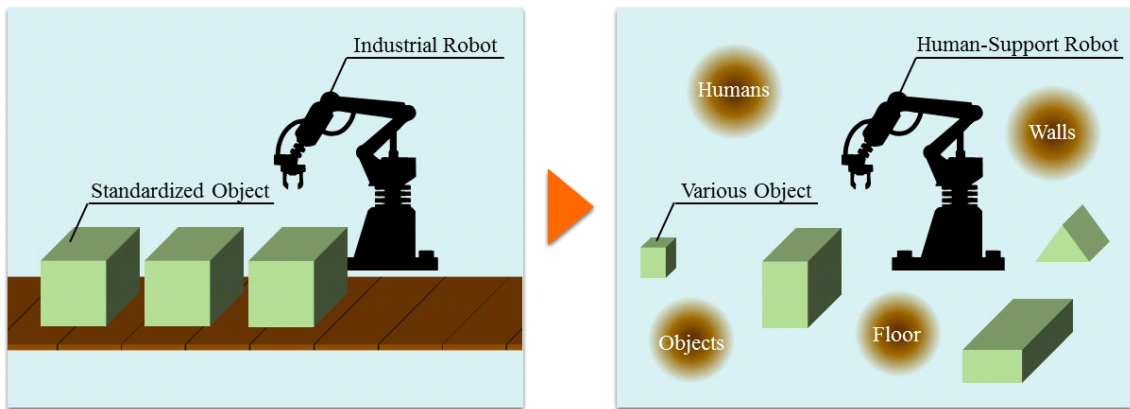
Fig. 1-1: Emerging roles of robots.
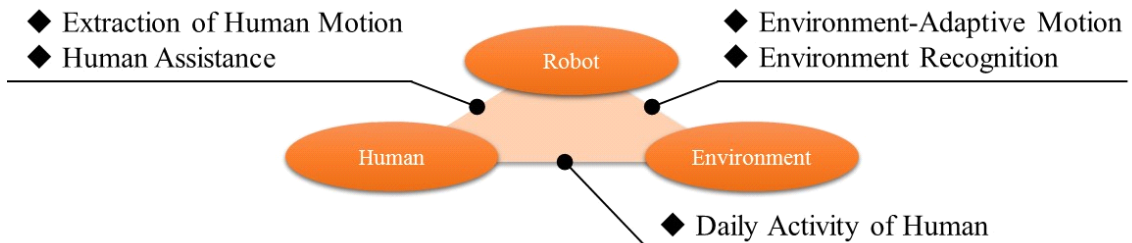
Fig. 1-2: Physical interaction between human, robot, and environment.

target objects, obstacles, floors, and walls. The term "human environment" refers to an environment that includes humans in the robot's range of movement. In many cases, the human environment is the space in which we spend daily lives (e.g., kitchens, living rooms, and bedrooms). The study of robots working in the human environment includes indoor robots [7], physiotherapy robots [8], electric bicycles [9] and electric wheelchairs [10]. Indoor robots have a three-fingered robot hand and open doors like humans do [7]. Physical therapy robots display human joint torque and muscle force during exercise to improve rehabilitation performance [8]. Electric bicycles and electric wheelchairs reduce the force necessary to drive [9, 10]. Thus, a variety of robots has been actively researched for use in daily lives. However, the working area of robots still does not go beyond the bounds of the conventional numerically-controlled machine tools, which can treat only standardized objects. The problem standing in the way of development of robotics is "adaptability."

Recent robots have been developed from numerical control aimed at precise positioning. Control stiffness has been increased as much as possible to be unaffected by external disturbance. However, what

is critically-needed now is adaptive force control. Humans are living in a world of physical interaction. Robots are also held by physical interaction. Humans, robots, and environment have to be in physical contact with each other as shown in Fig. 1-2. In human environment, everything is unstructured object. Even if there is a manufactured object, the size includes product tolerance. Hence knowing the precise position/size of the target object is definitely impossible. Position control and force control have following characteristics:

- Position control

  - This is quite exclusive control and actively makes a plant move to a desired position regardless of the status of the target environment.

- Force control

  - This is highly adaptive control. The position of a plant is not defined and is determined by the character of environment.

If contact motion is performed by using only position control scheme, the target object is going to be broken. Humans achieve their own motions by changing composition of the position control and the force control with every moment. In order to artificially realize adaptive human motion, the composition of the position control and the force control must be designed. One of the effective approach is based on "functionality" [11, 12]. This approach has been used in a field of robotic control. Concept of the functionality in this dissertation is as explained below. To make the concept of functionality clear, Fig. 1-3 and Fig. 1-4 shows the equivalence between electric system and robotic system. For example, in electric systems, personal computer system consists of many units such as print unit and display unit. The units also consists of a lot of circuits. Furthermore, the circuits are composed of a combination of many circuit elements. In this way, electric systems have hierarchy of components. A roles of total system are decomposed into functions, and the functions are assigned to the lower components. Here, "System role" and "Function" are defined as follows:

Definition 1 "System role" is a description of the requirement from a user to a robot control system.

Definition 2 "Function" is a required role of units, circuits, and elements.

Actual circuits are made to satisfy required objective. The circuits are provided to achieve functions by combining physical characteristics of circuit elements. To design a circuit possessing desired function,

designer only have to know what and how circuit element should be connected. In other word, necessary informations are as follows:

- Structure of the connected branches.

- Physical characteristic of branch constructing circuit.

The former is expressed by incidence matrix or topological matrix. The latter is determined by circuit constant and controlled electrical source. As mentioned above, functionality is a way to design total system by decoupling the system into simplified components.

As in the case of electric systems, robotic systems can be decomposed into simple components. For example, hand-over system requires pick and place motion. The pick and place motion consists of precise manipulation and adaptive grasping. Furthermore, the manipulation/grasping are composed of a combination of elements. In this way, robotic systems also have hierarchy of components. as with the electric system, a roles of total system are decomposed into functions, and the functions are assigned to the lower components.

Motions are generated to satisfy required objective. In case requiring stiff motion such as cutting operation, position control is used. In contrast, in case requiring adaptive motion such as grasping, force control is utilized. To achieve desired function, designer only have to know what and how motion element should be connected. In other word, necessary informations are as follows:

- Structure of required motion.

- Desired physical quantity such as movement distance and grasping force.

The former is expressed by modal transformation matrix. The latter is determined by human impedance, environmental impedance, controlled position source, and controlled force source. As mentioned above, the concept of functionality is also useful to design motion control system, as a designer easily get a grip on the system and modify the components. This approach have much better prospects than designing the entire system all together, as a designer have only to design the minimum components separately. The detail is described in Section 3.

1.2   Objective

The objective of this dissertation is clarifying when and how humans integrate position control and force control. Structure and physical quantity such as force of human motion are changing from moment
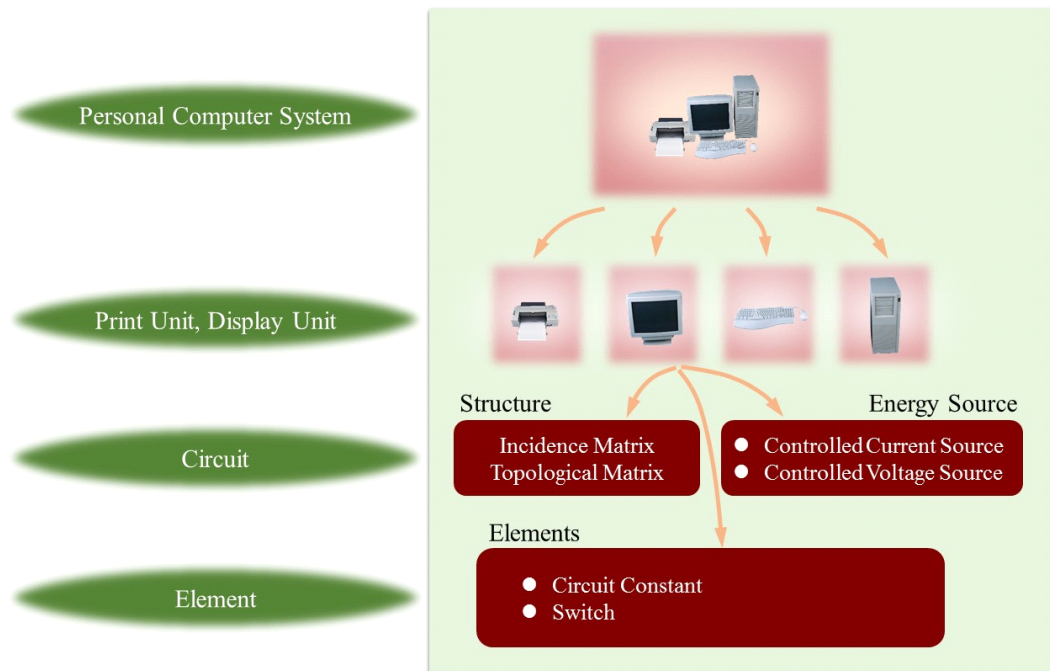
Fig. 1-3: Decomposition of electric system.

to moment. If the structure and physical quantity are clarified, the obtained results make it possible to artificially realize adaptive human motion.

Analyzing and understanding human motions have other two important implications.

- Understanding target
- Improving ability of robots

Since the support target is nothing less than human, understanding human is important. If human motions are precisely measured and extracted, the supported persons can know failure of their body and motion. Furthermore, by using the processing results of the extracted information, robots can understand the state of target person, and can recognize what he/she wants to do. It makes it possible for robots to provide service appropriate for the situation.

In addition, from the analytical results, the implicit knowledge included in the human motions can be clarified. The obtained knowledge can be a key technology to make robots acquire human-like ability. Consequently, human-like dexterous and adaptable motions can be artificially realized by the robots. In other words, understanding of how humans work may enable the development of robots that can work like a human [13–16]
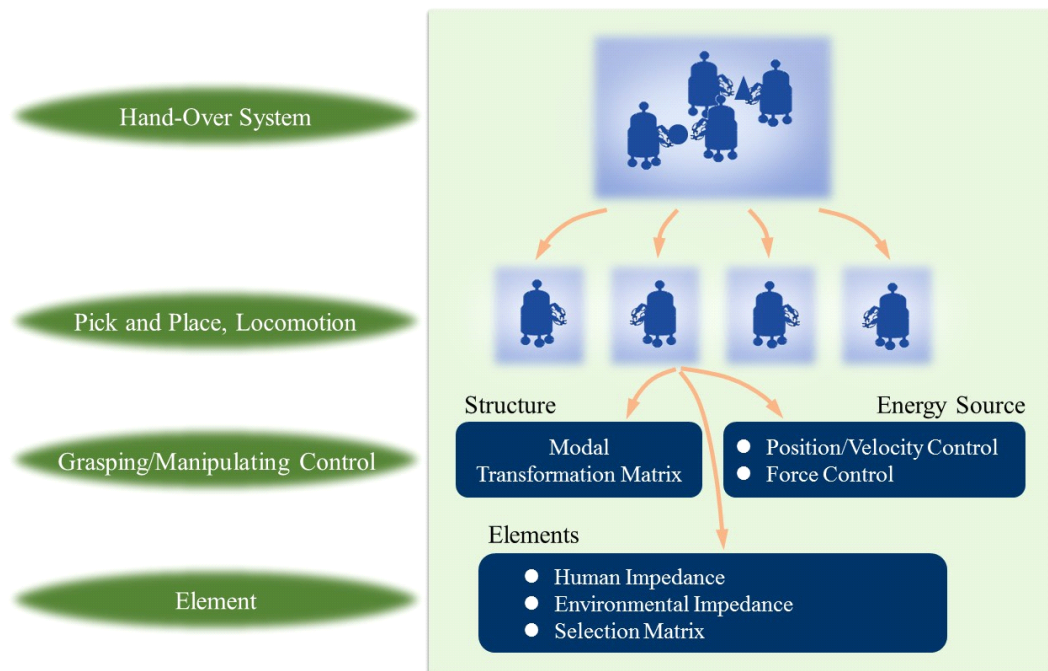
Fig. 1-4: Decomposition of robotic system.

1.3 Approach

This dissertation proposes a quite novel concept and approach for artificial realization of adaptive human manipulation. This dissertation expresses and treats human motions on the basis of functionality. In accordance with the abovementioned strategy, this study accomplishes artificial realization of adaptive human manipulation by dividing into four parts as follows:

- Extraction of Human Motion

- Processing and Recognition

- Analysis and Decomposition

- Artificial Realization of Adaptive Human Manipulation

Through this approach, this dissertation realizes adaptive human motion. The realized motion has high adaptability and performs removal operation of nuts in practice.

Fig. 1-5 shows the expected future that lies ahead of this dissertation. The innovations provided by this technology are as follows:

(1) Robotic systems can extract and preserve skillful human techniques. The recorded motion data is useful for education and training. Therefore, the reduction in skilled person is stopped.
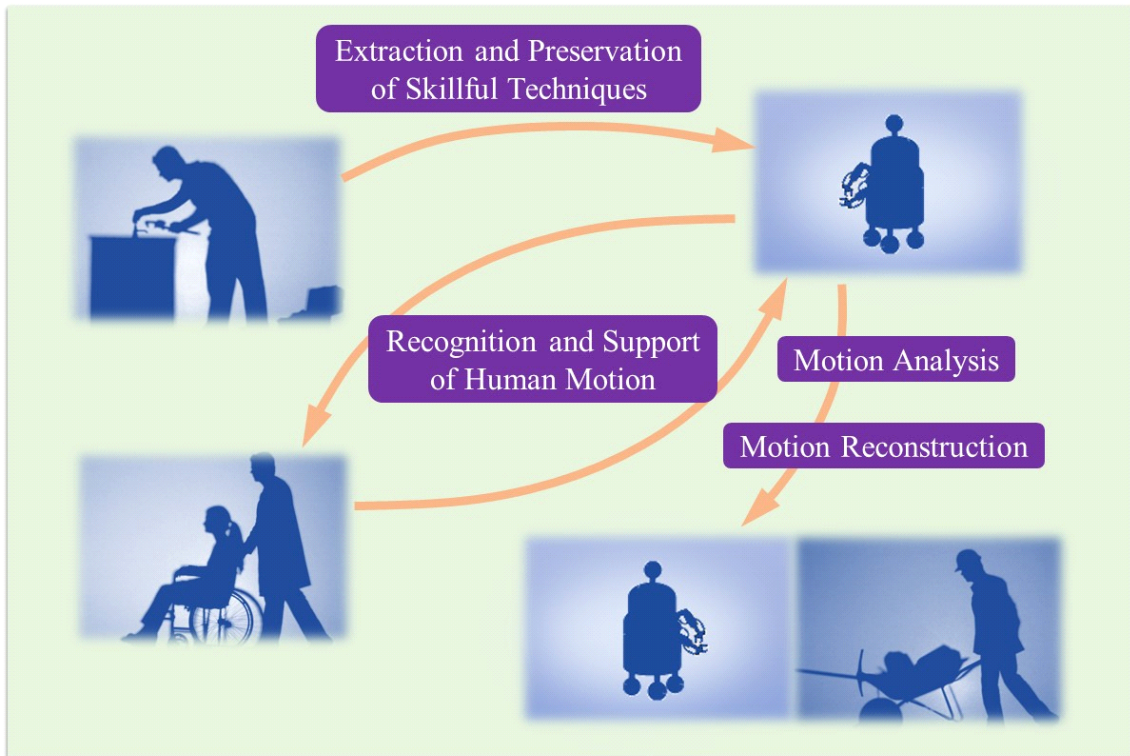
Fig. 1-5: Expected future that lies ahead of this dissertation.

(2) Robotic systems can recognize and understand the situation from motion data. The robotic systems can provide support adequate to what he/she wants to do. Therefore, the caregiver burden is decreased.

(3) Robotic systems can realize human motions. As the reconstructed human motions are both precise and adaptable, robotic systems can perform various tasks. Therefore, they are able to act as an agent of young labors.

1.4   Chapter Organization

Fig. 1-6 shows the chapter organization. Chapter 2 describes fundamental technologies of motion control. Chapter 3 explains the research field of real-world haptics: it reviews the progress of research on real-world haptics. The following chapters are on the basis of the real-world haptics. In addition, chapter 3 shows a decoupling strategy for position and force control on the basis of modal space disturbance observers. This chapter also shows analytical results of the performance and the stability. The utility of
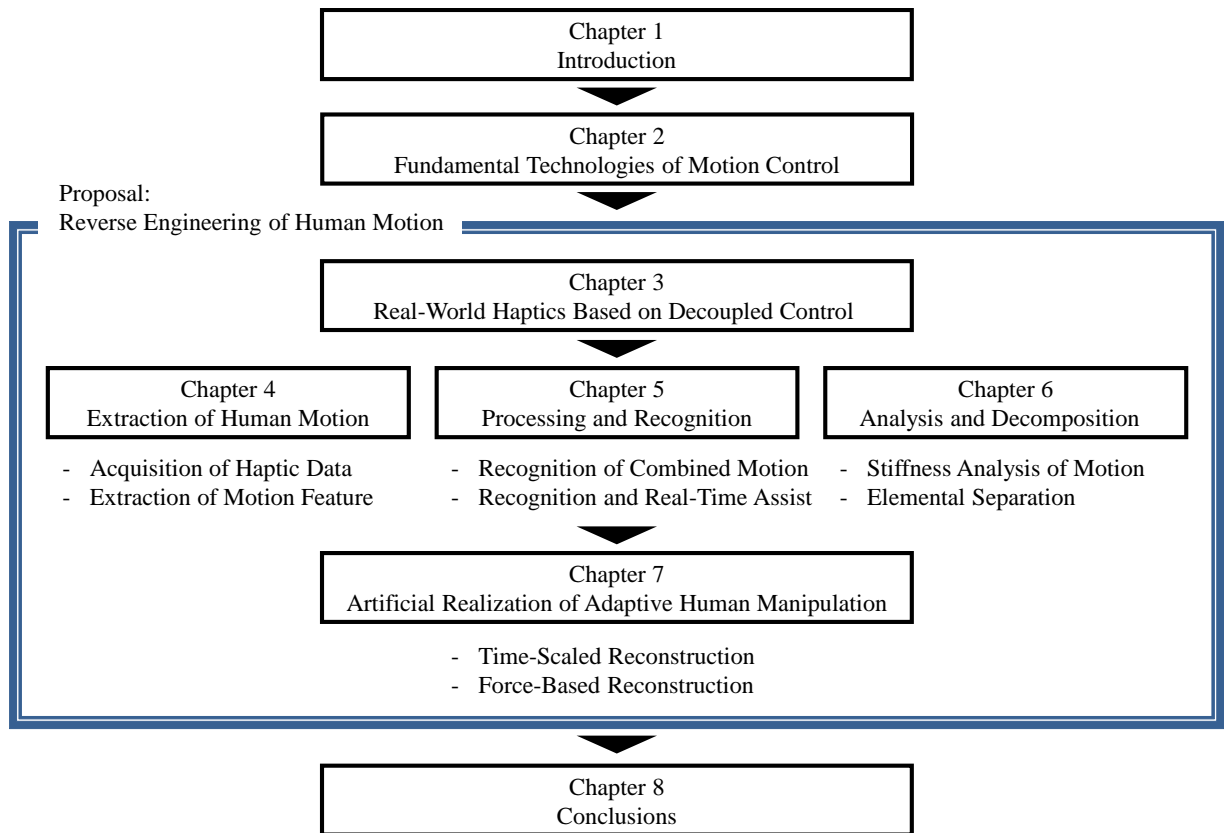
Fig. 1-6: Chapter organization.

the proposed method is experimentally verified by using a multi-degrees-of-freedom (DOF) manipulator. Chapter 4 describes a developed 11-DOF master-slave robot hands using tendon-driven mechanisms. Furthermore, a bilateral control system for tendon-driven robots is proposed. The transmission performance of the proposed system is experimentally verified. Chapter 4 also explains compensation of joint angle error caused by tendon elongation. This proposal is applied to a bilateral control system, and the validity is confirmed by experiments. In addition, Chapter 4 shows a bilateral control technique facilitating intuitive operation. The technique is based on motion features of an operator expressed by principal component analysis. Chapter 5 presents a recognition method of human motions using dynamic programming pattern-matching algorithm. The validity of this recognition method is experimentally verified by using a 5-DOF master-slave robot hands. This chapter also describes an application of above-mentioned recognition method to modal space. In the experiments, the proposed method is applied to grasping motions. Chapter 5 confirms that the proposed method can trigger scaled bilateral control and assists

grasping force of the operator in real-time. Chapter 6 explains a proposed stiffness estimation system using scaled bilateral control. The utility of the proposed method is experimentally verified by using a haptic forceps robot. This chapter also shows a method to clarify the features of human motions by elementally separating haptic information on the basis of the principle of motion control. Chapter 7 presents a time-scaling technology to adapt to different location of target objects. This proposal shows usefulness especially in duration of the contact and amplitude of force. Furthermore, chapter 7 describes reproduction method of human actions. The utility of the proposed method is experimentally verified by applying to a removal operation of a nut. Chapter 7 confirms that the realized motion can remove the nut regardless of the size and shape. Chapter 8 summarizes and concludes this dissertation.

Nomenclature

DOB	Disturbance observer
DOF	Degree-of-freedom
RFOB	Reaction force observer
WOB	Work space disturbance observer
MDOB	Modal space disturbance observer
RMSE	Root mean square error
HDARH	Haptic data acquisition robot hand
TDBC	Tendon-driven bilateral control system
MP	Metacarpophalangeal
PIP	Proximal interphalangeal
DIP	Distal interphalangeal
ABC	Acceleration-based bilateral control
GMC	Grasping and manipulating control
PCA	Principal component analysis
CM	Combination motion
DP	Dynamic programing
PPV	Positive predictive value
NPV	Negative predictive value
x, X	Position
f, F	Force
f^{l}	Load force
f^{motor}	Generative force
$f^{\mathrm{g}}(x)$	Gravity force
$f^{\mathrm{b}}(x, \dot{x})$	Sum of inertial force, Coriolis force, and friction force
m, M	Mass
$\boldsymbol{M_t}$	Equivalent mass
g	Cutoff frequency
p	Equivalent acceleration disturbance
s	Laplace operator
k_{e}	Environmental stiffness
d_{e}	Environmental viscosity
Z_{e}	Environmental impedance
$d(i, j), d(i, j, t)$	Local distance, partial distance
k_{c}	Control impedance
K_{c}	Control stiffness
D_{c}	Control viscosity
κ	Control stiffness

P_{o}	Operationality
P_{r}	Reproducibility
$\boldsymbol{\tau}_{\mathrm{int}}$	Interactive torque vector
$\boldsymbol{\tau}_{\mathrm{ext}}$	Reaction torque vector in force task
$\boldsymbol{D}$	Viscosity coefficient matrix
$\boldsymbol{q}$	Joint angle vector
$\dot{\boldsymbol{q}}$	Angular velocity vector
$\boldsymbol{\tau}_{\mathrm{c}}$	Coulomb friction vector
$\boldsymbol{I}(\boldsymbol{q})$	Joint inertia matrix
$\mathrm{diag}\boldsymbol{I}(\boldsymbol{q})$	Diagonal matrix whose diagonal elements
	have the diagonal elements of $\boldsymbol{I}(\boldsymbol{q})$
$\boldsymbol{I}_{\mathrm{n}}$	Nominal joint inertia matrix
$K_{\mathrm{t}}, \boldsymbol{K}_{\mathrm{t}}$	Torque coefficient, torque coefficient matrix
$K_{\mathrm{tn}}, \boldsymbol{K}_{\mathrm{tn}}$	Nominal torque coefficient, nominal torque coefficient matrix
$\boldsymbol{H}$	Hybrid matrix
$I_{\mathrm{a}}, \boldsymbol{I}_{\mathrm{a}}$	Torque current, torque current vector
$\boldsymbol{I}$	Unit matrix
$\boldsymbol{x}$	Position vector in work space
$\boldsymbol{J}(\boldsymbol{q})$	Jacobian matrix
$\boldsymbol{J}_{\mathrm{t}}$	Modal transformation matrix, task Jacobian
$\boldsymbol{f}$	Force vector in the work space
$\boldsymbol{\tau}$	Torque vector in the joint space
$\boldsymbol{m}_{\mathrm{n}}$	Equivalent mass matrix in the work space
C_{p}	Position controller
C_{f}	Force controller
K_1, K_2	Feedback gain
K_{p}	Position feedback gain
K_{v}	Velocity feedback gain
K_{f}	Force feedback gain
$\boldsymbol{G_t}$	Coordinate transformation matrix
$\boldsymbol{T}$	Transformation matrix
k_1	Start time of motion
k_2	End time of motion
$\mathbf{V}$	Covariance matrix
$\mathbf{M}$	Input combined motion pattern
$\mathbf{R}$	Reference combined motion pattern
$\boldsymbol{G}_{\mathrm{P}}$	Position input pattern
$\boldsymbol{R}_{\mathrm{P}}$	Position reference pattern
$\boldsymbol{G}_{\mathrm{F}}$	Force input pattern

$\boldsymbol{R}_{\mathrm{F}}$	Force reference pattern
$\boldsymbol{D}_{\mathrm{P}}$	Recorded position data
$\boldsymbol{D}_{\mathrm{F}}$	Recorded force data
α, β	Scaling ratio
α (in chapter 5)	Mismatch penalty
$g(i,j), g(i,j,t)$	Cumulative distance
D (in chapter 5)	DP value
I	Lengths of the input combined motion pattern
J	Lengths of the reference combined motion pattern
$p_{[d,k]}$	Position transformed into modal space
$q_{[d,k]}$	Force transformed into modal space
$k_{[d,k]}$	Estimated stiffness
$c_{[d,k]}$	Estimated force offset
$\boldsymbol{R}_{\mathrm{h}}(\theta_{\mathrm{h}})$	Rotation matrix
$\boldsymbol{R}_{\mathrm{h}}(\theta_{\mathrm{h}})$	Rotation matrix
k_{tip}	Unintended stiffness
$\hat{k}_{\mathrm{c}}$	Controlled and conscious stiffness
e	Error signal
V	Loading speed
r	Radius of joint pulleys
N	Matrix for null space calculation
$\boldsymbol{u}_{[k]}$	Eigenvector
$\varepsilon_{[k]}$	Eigenvalue
$\hat{\boldsymbol{\eta}}_{[d,k]}$	Estimated parameter vector
$\boldsymbol{\xi}_{[d,k]}$	Observation vector
$\lambda_{[d,k]}$	Trace gain
$\boldsymbol{\Gamma}, \boldsymbol{\Lambda}$	Selection matrix
λ_1, λ_2	Eigenvalue
Δ	Modeling error
ϕ	Hybrid angle
$^{-}$	Average
$^{\sim}$	Deviation
$^{\wedge}$	Estimation

Superscript

ref	Reference
res	Response
cmd	Command
dis	Disturbance

trans	Translational motion
gras, grasp	Grasping motion
ext	External
th	Thumb finger
in	Index finger
mi	Middle finger
save	Saved motion data

Subscript

record	Recorded motion data
dob	Disturbance observer
rfob, reac	Reaction force observer
ten	Tension control
joi	Joint control
tor	Torque control
ang	Angle control
work	Work space
n	Nominal value
dis	Disturbance
dif, D	Differential mode
com, C	Common mode
int	Interactive
ext	Reaction
c	Coulomb friction
m, M	Master system
s, S	Slave system
r	Right side
l	Left side
b	Bilateral control
h	Human
hpf	High pass filter
int	Internal
cmd	Command
mode	Modal space

This dissertation is written in time domain unless otherwise stated.

"(s)" signs after variables indicate that the variables are in Laplace domain.

Chapter 2

Fundamental Technologies of Motion Control

2.1 Introduction

In this chapter, fundamental technologies for motion control of robotic systems are described. The main objective of the motion control is to control position and force. Acceleration control plays a critical role to deal with position and force. Acceleration derived from force divided by inertia and second order differential of position. Because of this, the acceleration control makes it possible to handle position control and force control in unified framework. The acceleration-based motion control has a significant meaning in this dissertation, as this dissertation employs robotic system with acceleration-based control to extract and reconstruct human motion. Section 2.2 shows a model of actuators and explains a concept of disturbance. Section 2.3 introduces a disturbance observer, which is a helpful technique to achieve acceleration control. Section 2.4 presents a technique to estimate external force on the basis of the disturbance observer. Section 2.5 shows specific configurations of acceleration control. Section 2.5.1 and Section 2.5.2 describe a position control system and a force control system, respectively. This chapter is finally concluded in section 2.6.

2.2 Modeling of Actuator

This chapter shows a modeling of linear actuators. The motion equation is obtained as

$$m\ddot{x} + f^{\mathrm{l}} = f^{\mathrm{motor}}, \tag{2.1}$$
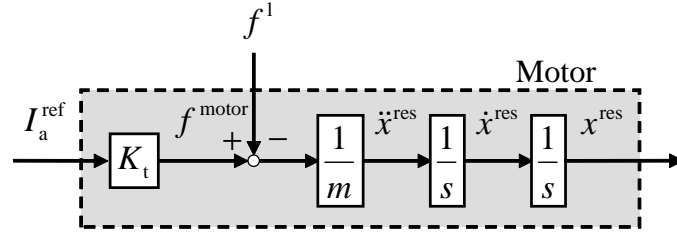
Fig. 2-1: Dynamics of linear motor.

where the m, the x, the f^{l}, and the f^{motor} denote the motor mass, the position, the load force, and the force generated by an actuator, respectively. The load force f^{l} is expressed as

$$f^{\mathrm{l}} = f^{\mathrm{ext}} + f^{\mathrm{g}}(x) + f^{\mathrm{b}}(x, \dot{x}). \tag{2.2}$$

The f^{ext} and the $f^{\mathrm{g}}(x)$ denote the external force and the gravity force, respectively. The $f^{\mathrm{b}}(x, \dot{x})$ is the sum of the inertial force, Coriolis force, and friction force.

The generated force is obtained by multiplication of the armature current and the thrust coefficient. This dissertation assumes that the armature current is exactly the same as the current reference,

$$f^{\mathrm{motor}} = K_{\mathrm{t}} I_{\mathrm{a}} = K_{\mathrm{t}} I_{\mathrm{a}}^{\mathrm{ref}}. \tag{2.3}$$

The motion equation is restated as

$$m\ddot{x} = K_{\mathrm{t}} I_{\mathrm{a}}^{\mathrm{ref}} - \left\{ f^{\mathrm{ext}} + f^{\mathrm{g}}(x) + f^{\mathrm{b}}(x, \dot{x}) \right\}. \tag{2.4}$$

Fig. 2-1 shows the block diagram of the motor dynamics. The parameters of eq. (2.4) (i.e. the mass m and the thrust coefficient K_{t}) vary according to the state of the robot and the distribution of the magnetic flux. When the differences between the nominal values and the real values are expressed by Δm and ΔK_{t}, the following equations are obtained,

$$m = m_{\mathrm{n}} + \Delta m, \tag{2.5}$$

$$K_{\mathrm{t}} = K_{\mathrm{tn}} + \Delta K_{\mathrm{t}}, \tag{2.6}$$

where the subscript n denotes the nominal values. Since the disturbance is the sum of the load force f^{l} and the effect of the parameter variations, the disturbance is presented as

$$
\begin{aligned}
f^{\mathrm{dis}} &= f^{\mathrm{l}} + \Delta m \ddot{x} - \Delta K_{\mathrm{t}} I_{\mathrm{a}}^{\mathrm{ref}} \\
&= f^{\mathrm{ext}} + f^{\mathrm{g}}(x) + f^{\mathrm{b}}(x, \dot{x}) + (m - m_{\mathrm{n}})\ddot{x} + (K_{\mathrm{tn}} - K_{\mathrm{t}}) I_{\mathrm{a}}^{\mathrm{ref}}.
\end{aligned} \tag{2.7}
$$
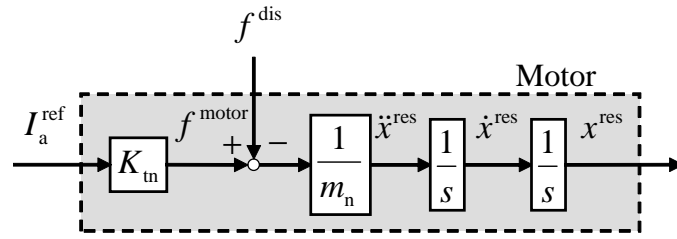
Fig. 2-2: Dynamics of linear motor using nominal mass value.

When the parameter variations are considered, the motion equation of eq. (2.1) is rewritten as

$$(m_{\mathrm{n}} + \Delta \mathrm{m})\ddot{x} = (K_{\mathrm{tn}} + \Delta K_{\mathrm{t}})I_{\mathrm{a}}^{\mathrm{ref}} - f^{\mathrm{l}}. \tag{2.8}$$

By subtracting eq. (2.7) into eq. (2.8),

$$
\begin{aligned}
m_{\mathrm{n}}\ddot{x} &= K_{\mathrm{tn}}I_{\mathrm{a}}^{\mathrm{ref}} - (f^{\mathrm{l}} + \Delta m\ddot{x} - \Delta K_{\mathrm{t}}I_{\mathrm{a}}^{\mathrm{ref}}) \\
&= K_{\mathrm{tn}}I_{\mathrm{a}}^{\mathrm{ref}} - f^{\mathrm{dis}}
\end{aligned}
\tag{2.9}
$$

is obtained. Fig. 2-2 shows the block diagram of eq. (2.9).
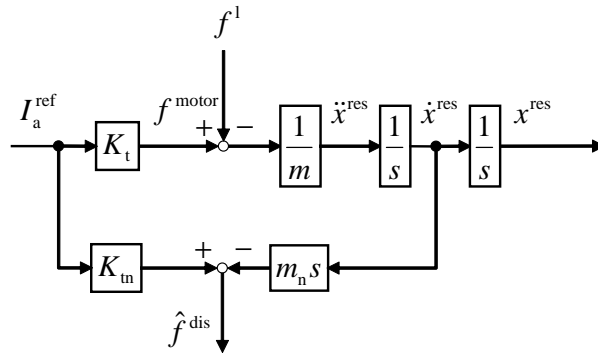
Fig. 2-3: Disturbance calculation based on velocity response.
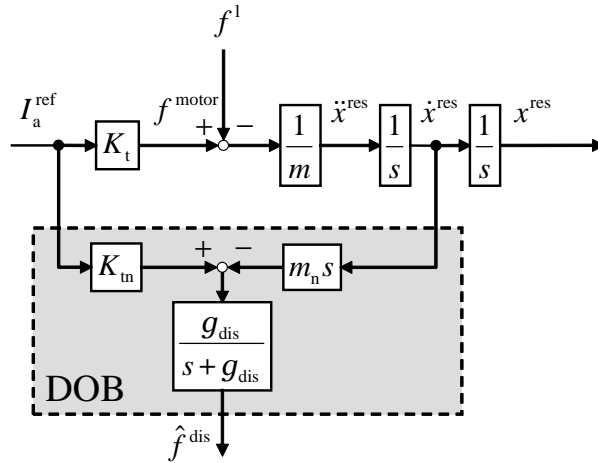
Fig. 2-4: Disturbance estimation in consideration of measurement noise.

2.3 Disturbance Observer

From eq. (2.9),

$$f^{\mathrm{dis}} = K_{\mathrm{tn}}I_{\mathrm{a}}^{\mathrm{ref}} - m_{\mathrm{n}}\ddot{x} \tag{2.10}$$

is obtained. Equation (2.10) shows that the disturbance can be derived by the current reference and the velocity. Fig. 2-3 presents the block diagram of the disturbance calculation. By using the calculated disturbance, suppression of the disturbance becomes possible in feedforward manner.   Since the derivation enhances the noise effect especially in the high frequency domain, a low pass filter (LPF) is employed.
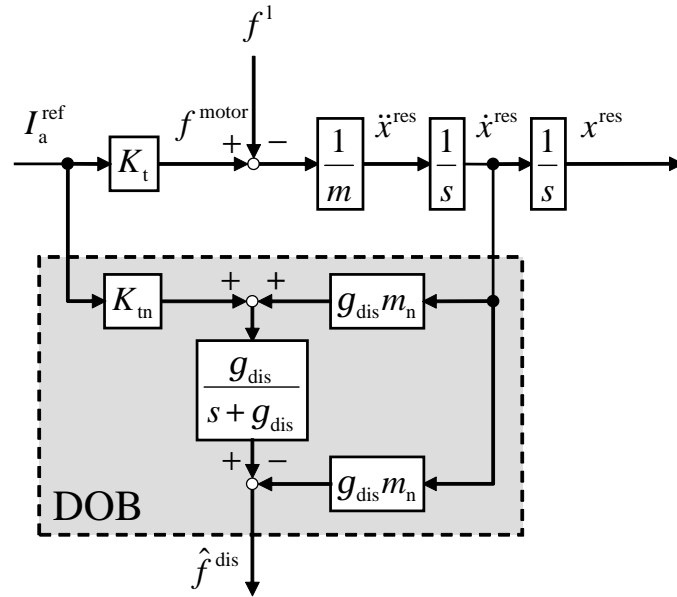
Fig. 2-5: Disturbance calculation using integrator.

Fig. 2-4 shows the disturbance estimation with first-order LPF. The disturbance is estimated as

$$\hat{f}^{\mathrm{dis}}(s) = \frac{g_{\mathrm{dis}}}{s + g_{\mathrm{dis}}} f^{\mathrm{dis}}(s). \tag{2.11}$$

Fig. 2-5 shows a equivalent block diagram of Fig. 2-4. In Fig. 2-5, an integrator is utilized instead of the differentiator. The inside of the dashed line is referred to as disturbance observer (DOB). The compensation current for the disturbance suppression is derived from the disturbance estimated in the structure of Fig. 2-3. When the compensation current is fed back into the system, the disturbance is canceled as shown in Fig. 2-6. If the sampling period is short enough, this structure can be regarded as feedforward equivalently.
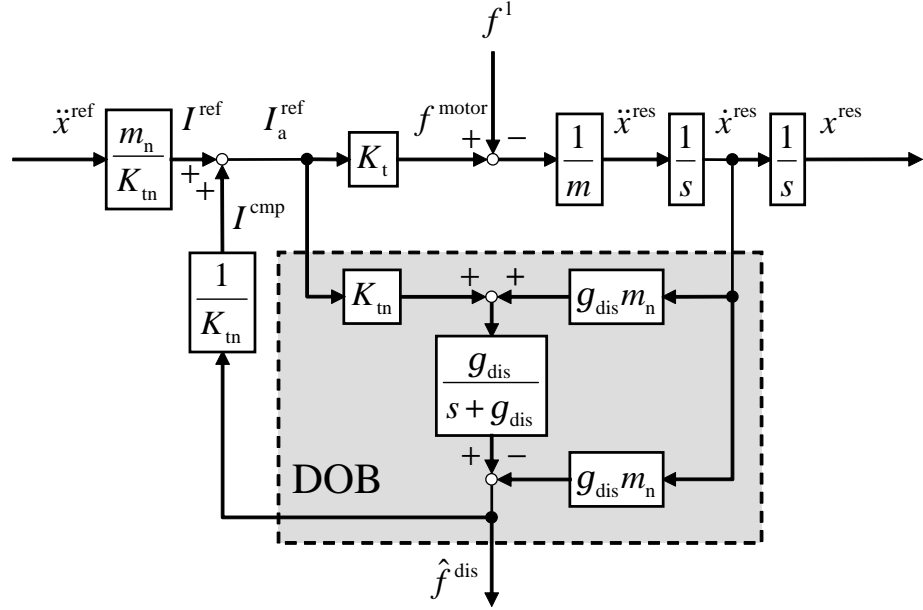
Fig. 2-6: Disturbance feedback.

In the low frequency domain, which is lower than the cutoff frequency g_{dis}, the disturbance is suppressed by DOB. In contrast, in the high frequency domain, the disturbance affects the system. Therefore, Fig. 2-6 is transformed as Fig. 2-7 equivalently. In Fig. 2-7, the disturbance passes through the high pass filter (HPF) and input into the system. The HPF $G_{\text{s}}(s)$ is expressed as

$$G_{\text{s}}(s) = \frac{s}{s + g_{\text{dis}}}. \tag{2.12}$$

Here, p is defined as

$$
\begin{aligned}
p(s) &= s^2 x^{\text{ref}}(s) - s^2 x^{\text{res}}(s) \\
&= m_{\text{n}}^{-1} G_{\text{s}}(s) f^{\text{dis}}(s).
\end{aligned}
\tag{2.13}
$$

p denotes the difference between the acceleration reference and the actual acceleration. By using p, robust control system is shown as Fig. 2-8. p is error of the robust control system. This error is treated in acceleration dimension and is referred to as equivalent acceleration disturbance. The equivalent acceleration disturbance p depends on the abovementioned HPF $G_{\text{s}}(s)$. Although the cutoff frequency g_{dis} should be infinity to suppress all disturbance ideally, the g_{dis} is limited by robust stability.
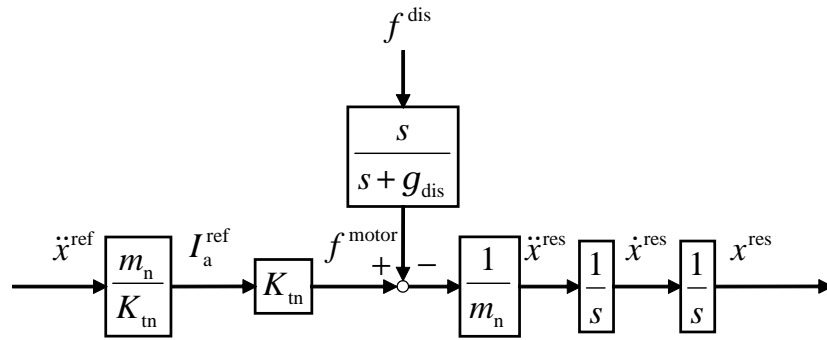
Fig. 2-7: Equivalent block diagram of Fig. 2-5.
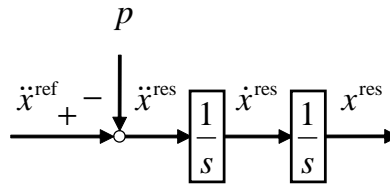
Fig. 2-8: Equivalent acceleration disturbance.

2.4   Reaction Force Observer

Reaction force observer (RFOB) is a structure, which estimates the external force by using DOB. Fig. 2-9 shows the RFOB. RFOB extracts the external force by subtracting the $f^{\mathrm{g}}(x)$, the $f^{\mathrm{b}}(x, \dot{x})$, and the parameter errors from the estimated disturbance, although the subtracted values should be identified in advance.
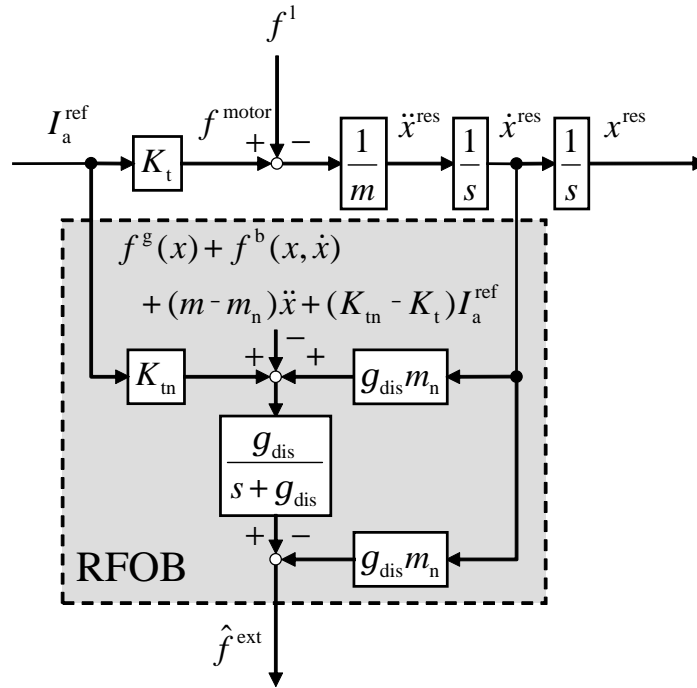
Fig. 2-9: Reaction force observer.

2.5   Motion Control System

To discuss about the references, a second order system with DOB is considered.

2.5.1   Position Control

In the ideal position control, following two characteristics should be achieved:

- Characteristic of command-tracking.
- Characteristic of disturbance rejection.

The first characteristic means: position response should track the desired position, and the second one means: the disturbance should be rejected. In a system shown in Fig. 2-10, the transfer functions are derived as

$$\frac{x^{\mathrm{res}}(s)}{x^{\mathrm{ref}}(s)} = \frac{K_1 K_2}{s^2 + K_1 s + K_1 K_2}, \tag{2.14}$$

$$\frac{x^{\mathrm{res}}(s)}{f^{\mathrm{dis}}(s)} = \frac{p(s)}{s^2 + K_1 s + K_1 K_2}. \tag{2.15}$$

The position feedback and the velocity feedback are employed. To make the transfer function of
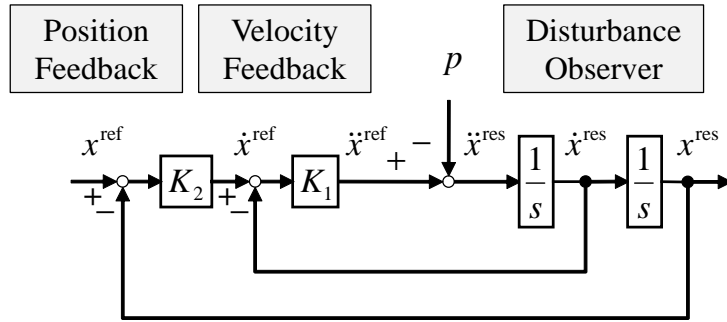
Fig. 2-10: Position control system.
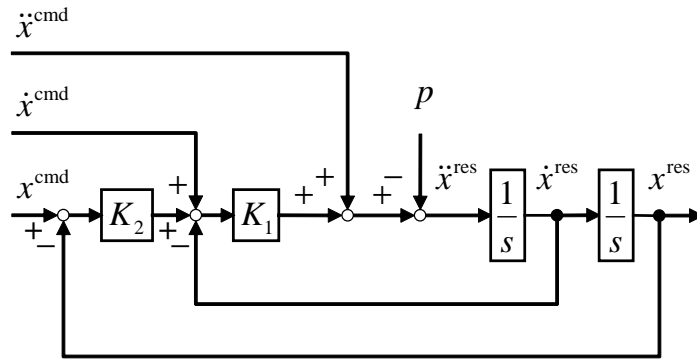
Fig. 2-11: Position control system with feedforward.

eq. (2.14) to 1, the feedforward of the velocity and the acceleration is added as presented in Fig. 2-11. By this feedforward the transfer function becomes

$$x^{\mathrm{res}}(s) = x^{\mathrm{cmd}}(s) - (s^2 + K_1 s + K_1 K_2)^{-1} p(s). \tag{2.16}$$

Since DOB suppresses almost all the disturbance, a little error existing in the high frequency domain is attenuated by the control poles, which are determined by the gains K_1 and K_2.
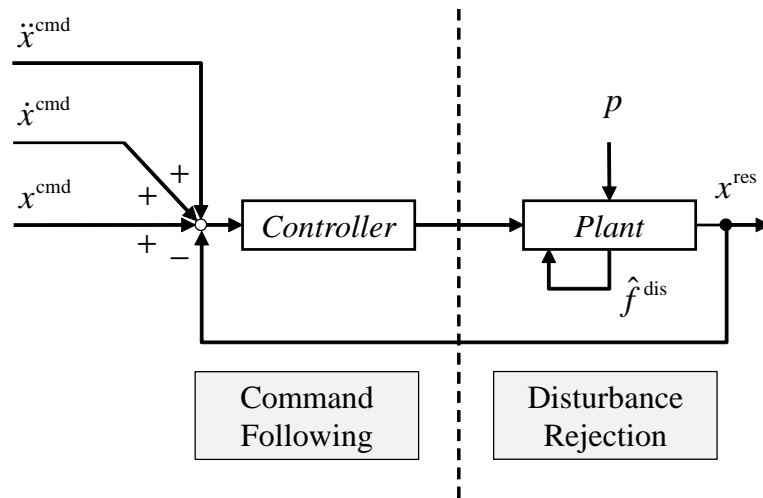
Fig. 2-12: Relationship between feedforward and disturbance observer.

As shown in Fig. 2-12, roughly speaking, DOB takes a role of the disturbance rejection and the feedforward is in charge of the command-following. This structure makes it possible to design these characteristics independently.
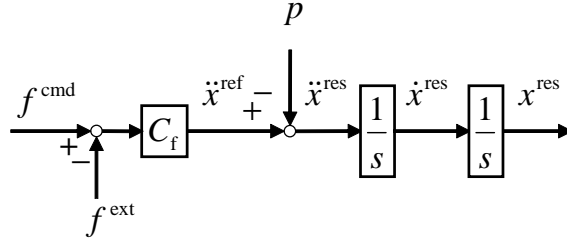
Fig. 2-13: Force controller with DOB.

2.5.2 Force Control

The aim of force control is to control the environmental reaction force to the desired value. From the law of action and reaction, the environmental reaction force is the same as the force, which the end effector applies to the environment. Note that, the applying force is different from the generated force, as the applying force includes not only the applying force but also the gravity force, the friction force, and so on. The acceleration reference of the force control $\ddot{x}^{\text{ref}}$ is calculated as

$$\ddot{x}^{\text{ref}} = C_{\text{f}}(f^{\text{cmd}} - f^{\text{ext}}), \tag{2.17}$$

where the f^{cmd}, the f^{ext}, and the C_{f} denote the force command, the external force, and the force controller. Fig. 2-13 shows the block diagram of the force control system using the disturbance observer. Here, the force controller C_{f} is assumed as a proportional controller

$$C_{\text{f}} = K_{\text{f}}, \tag{2.18}$$

where K_{f} denotes the feedback gain. The relationship between the force command and the external force is described as

$$f^{\text{cmd}} - f^{\text{ext}} = \frac{1}{K_{\text{f}}}\ddot{x}^{\text{res}} - \frac{1}{K_{\text{f}}}p. \tag{2.19}$$

Equation (2.19) shows that if the feedback gain is large the error becomes small. The dimension of K_{f} is $1/\text{kg}$. When the environment is assumed to be parallel connection of the spring element k_{e} and the damping element d_{e}, the environment is expressed as

$$f^{\text{ext}}(s) = (d_{\text{e}}s + k_{\text{e}})x^{\text{res}}(s). \tag{2.20}$$

From eq. (2.19) and eq. (2.20), the transfer function from the force command to the position response is obtained as

$$\frac{x^{\text{res}}(s)}{f^{\text{cmd}}(s)} = \frac{1}{\frac{1}{K_{\text{f}}}s^2 + d_{\text{e}}s + k_{\text{e}}}. \tag{2.21}$$

2.6   Summary

This chapter explained the fundamental technologies of motion control on the basis of acceleration control. Plants are always affected by disturbances such as load force and modeling error. Therefore, handling of the disturbances is a key issue. This chapter introduced the disturbance observer. Since the disturbance observer can derive and compensate the effect of the disturbance in acceleration dimension, this technique is quite helpful and important for motion control. This observer also makes it possible to adjust two characteristics separately. One is the characteristic of command-tracking. The other is the characteristic of disturbance rejection. In addition, this chapter described the structure of the reaction force observer, which can estimate the external force. This chapter also showed the concrete examples of the position control system and the force control system. The above-mentioned technologies make it possible to adjust the effect of the disturbance. While the disturbance observer possess the effect of disturbance suppression, the reaction force observer possess the effect of disturbance acceptance. As these technologies are utilized in the following chapters concerning the extraction, the analysis, and the reconstruction of human motion, the technologies explained in this chapter are quite important in this dissertation.

Chapter 3

Real-World Haptics Based on Decoupled Control

3.1 Introduction

The first half of this chapter introduces the research field of real-world haptics that acts on real-world objects. This part also reviews recent technical advances in real-world haptics, such as functionality and oblique coordinate control. As a catalyst for real-world haptics, a principle of this research area is explained through two simple examples: acceleration-based bilateral control and grasping/manipulating control. These two examples and the cited papers offer the view that a wide variety of system roles can be realized by combining pure position control and pure force control with an appropriate coordinate transformation. Real-world haptics has the capability of contributing toward supporting human activities.

The second half of this chapter extends the diagonalization method on the basis of the modal space disturbance observer (MDOB) for application to a multi-degree of freedom (DOF) system. The aim of this method is to suppress the interference between the position and force control systems, and to realize a bilateral control system. The utility of the proposed method is experimentally verified by using a multi-DOF manipulator. Higher performance of the MDOB-based decoupling method compared with oblique coordinate control is confirmed. Conventional oblique coordinate control causes oscillation in cases where the modeling error is large and the cutoff frequency of an observer is not high enough to change the system dynamics. On the other hand, the MDOB-based decoupling method becomes unstable when the difference in mass is large.

This chapter is organized as follows. Section 3.1.1 describes how real-world haptics evolved. Several

important technologies are introduced. Section 3.1.2 and 3.1.3 show two simple examples to generate concrete descriptions: Section 3.1.2 presents an acceleration-based bilateral control system, and Section 3.1.3 explains a grasping/manipulating control system. In both examples, contact with real-world objects is required. The experimental results are presented in Section 3.1.4. Section 3.2.1 presents an approach to realize a robust controller. Section 3.2.2 describes oblique coordinate control. Section 3.2.3 explains the use of MDOB with multi-DOF systems. Section 3.2.4 shows the analytical results of the performance and the stability. The experimental results are shown in section 3.2.5. This chapter is finally concluded in section 3.3.

3.1.1 Progress of Real-World Haptics

Haptics

Haptics is a research field that deals with information of physical interaction between humans and objects. Haptic information, unlike auditory and visual information, directly presents the size, shape, collision, and location of the objects [17]. For example, a haptic interface has been developed for medical simulations of palpation, which is a physical examination technique devised to check the state of health [18]. However, conventional studies on haptics generally consider only virtual environments [19].

In contrast, real-world haptics is a research field that deals with unstructured objects in the real world [20, 21]. Real-world haptics is expected to make breakthroughs with conventional numerical control, which is not always suitable for adaptation to unknown environments.

Duality

In real-world haptics, controlling the stiffness of a manipulator end effector is important [22]. The control stiffness κ is expressed as

$$\kappa = \frac{\partial f}{\partial x}, \tag{3.1}$$

where x and f denote the position and force, respectively. The control stiffness must be infinity under pure position control and zero under pure force control. Therefore, pure position control and pure force control cannot be achieved in the same direction at the same time.

Compliance Control and Hybrid Control

Two control methods that consider this duality are compliance control and hybrid control. Compliance control achieves intermediate control stiffness between infinity and zero [23, 24]. Hybrid control uses a directionally decoupled motion controller in the operational space [25, 26]. To improve hybrid control, a task description method has been proposed that is based on the construction of generalized task specification matrices to unify references to position control and force control [27].

Motion Control

To improve control systems such as compliance and hybrid control, an acceleration control [28] was developed to realize a robust motion controller. Disturbance observers (DOBs) [29] and sliding mode controls [30, 31] contribute to realizing high robustness.

Disturbance Observer

The DOB, in particular, makes it possible to realize a robust motion controller by estimating and suppressing disturbances that are input into a system: it facilitates decoupling of two kinds of characteristics: disturbance suppression and command following. The structure is a two-degrees-of-freedom (DOF) controller structure [32].

The DOB has another important feature: the estimated disturbance includes a reaction force from the environment. The reaction force observer (RFOB) extracts the reaction force from the disturbance [33]. One study on DOB and RFOB used a decoupling motion control strategy [34]. This strategy decouples motion controllers by determining the equivalent mass matrix in operational space.

Modal Transformation

To break down the overall information–including the position, velocity, and reaction force–into several components, the concept of modes has been introduced to motion control [35]. For example, modes were applied to a biped robot: environmental information measured from the bottom of the foot was decoupled into four modes: heaving, rolling, pitching, and twisting [36]. This decoupling also makes it possible to design controllers for each motion separately. In the study using a biped robot, the Hadamard matrix was utilized for modal transformation. However, the Hadamard matrix can only form modes with 2^n order ($n \in \mathbb{R}$). Therefore, the modal transformation method was extended to deal with odd [37] or arbitrary numbers of modes [38, 39].
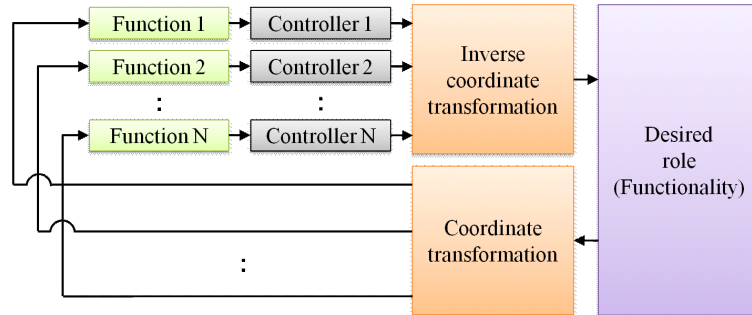
Fig. 3-1: Concept of functionality.

Functionality

Proposed design methods for decentralized control include subsumption architecture [40] and multi-scale robot systems [41]: decentralized control is a promising method to realize complicated and large systems [42]. A decomposition transformation that reduces the total system into a form that can be controlled in blocks has been proposed [43]. The principle of superposition, which implies that a skilled motion can be resolved into elementary motions, was demonstrated [44]. A reduction method that decomposes an entire motion on the basis of a singular value [45] was developed.

Based on the demand for simplification of large-scale system design, the concept of modes was extended, and "functionality" was proposed [46]. In this method, an entire complicated control system for realizing system roles is decoupled into simplified independent components that are defined as functions. In other words, the roles of the entire control system are represented as a superposition of these functions under the assumption that the functions are independent of each other. This property is referred to as functionality [11]. Functions are abstracted and expressed by the function mode. A DOB is applied to cancel the dynamic interference and ensure the independence of each function mode [47]. This design method was applied to a three-dimensional 18-DOF cooperative grasping manipulator, and the detailed design procedure was presented [12]. Fig. 3-1 shows motion realization based on the concept of functionality. Functionality has been used for reconfigurable robots [48], multibody mechanical systems [49], and bilateral control [50].
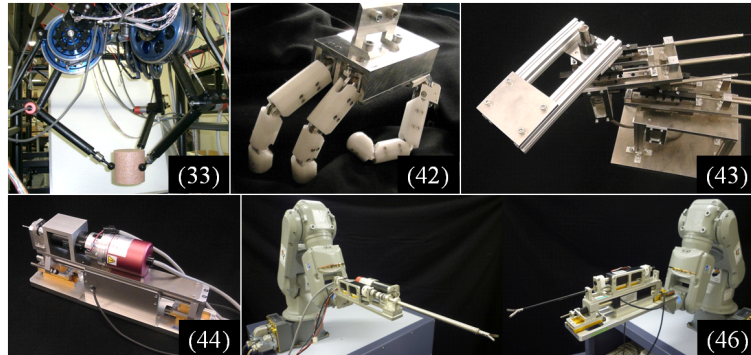
Fig. 3-2: Application examples.

Oblique Coordinate Control

A more general theory was developed, named oblique coordinate control [51, 52]. This theory regards the control of tasks as problems of position/force hybrid control in oblique coordinates and shows that tasks can be realized by appropriate coordinate transformations [53, 54]. This method simply requires the design of a coordinate transformation matrix, which is a task Jacobian.

Application examples

These studies showed that diverse roles and tasks can be completed by combining pure position control and pure force control with appropriate coordinate transformation. Furthermore, artificially designed coordinates make it possible to simultaneously realize both position and force control even if they are on the same axis. Typical applications (Fig. 3-2) include object tracking with different DOF manipulators using visual information [55], an 11-DOF tendon-driven robot hand [56], a two-link manipulator equipped with a biarticular muscle mechanism [57], a telerobotic-assisted bone-drilling system [58], and medical robots [59] such as a 16-DOF telesurgical forceps robot with haptics [60].
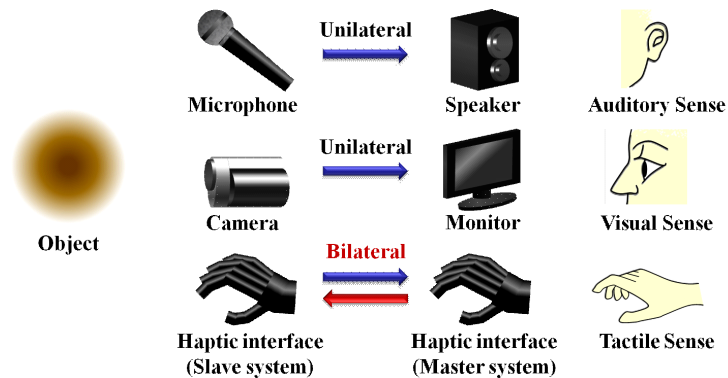
Fig. 3-3: Directional properties of human sensations.

3.1.2 Acceleration-Based Bilateral Control

Fig. 3-3 shows the directional properties of acoustic, visual, and haptic information. Today, methods already exist for acquiring auditory and visual information. Auditory information is extracted by using microphones and reproduced by using speakers. Similarly, visual information is recorded by cameras and then displayed on monitors. On the other hand, haptic sensations have a bilateral property because they are governed by Newton's law of action and reaction in the real world. This bilateral property makes it difficult to realize a system role that involves contact with an unstructured environment.

Bilateral control [61–63] is the most prominent example that requires a system role involving contact motion. In general, a bilateral control system consists of a master system operated by a human and a slave system that makes contact with an object [64], as shown in Fig. 3-4. The aim of the bilateral control system is tactile sense transmission to enable perception of the mechanical impedance of an object existing in a remote place.
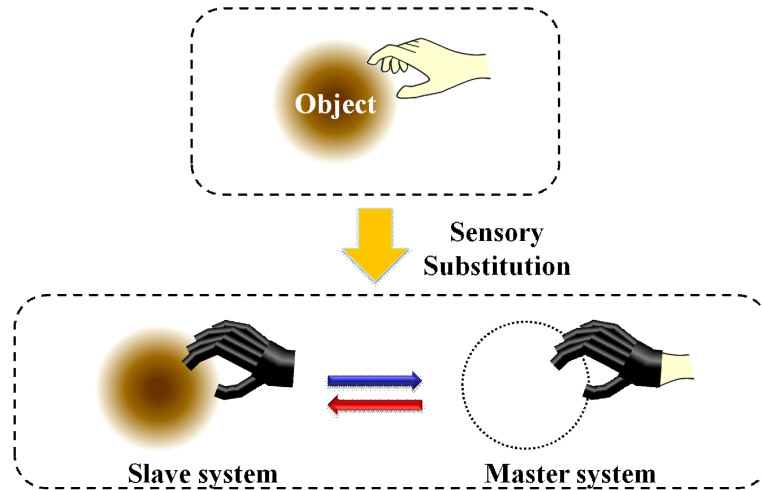
Fig. 3-4: Sensory substitution by ABC.
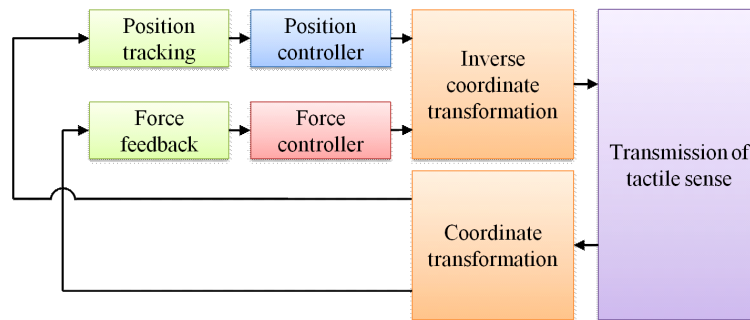
Fig. 3-5: Overall block diagram of ABC system.

Table 3.1: Configuration of ABC.

Function	Modal space	Control system
position tracking	differential mode	position control
force feedback	common mode	force control

Acceleration-based bilateral control (ABC) is based on the concept of modes [65–67]. Fig. 3-5 shows the overall block diagram of ABC. To perform tactile sense transmission, position tracking and force feedback functions are required. In this method, the position tracking function is satisfied in the differential mode, and force feedback function is fulfilled in the common mode. Table 3.1 lists the modal spaces and control systems corresponding to each function. The merit of this approach is not only the explicit controller design but also the high level of performance [68].
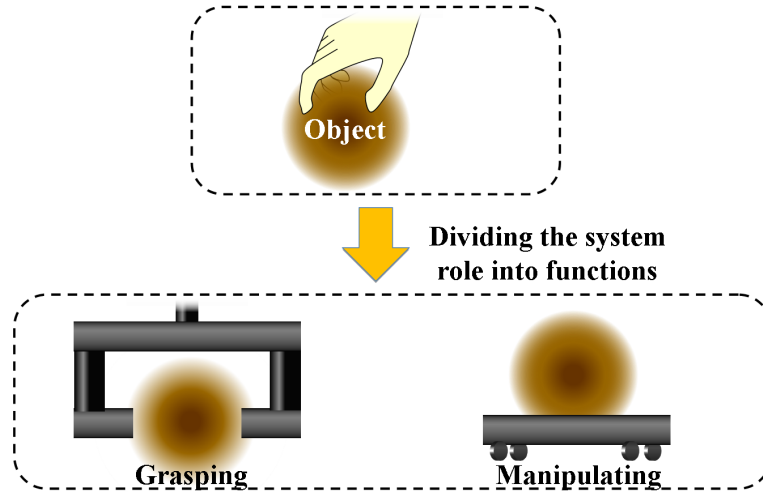
Fig. 3-6: Object transportation by GMC.
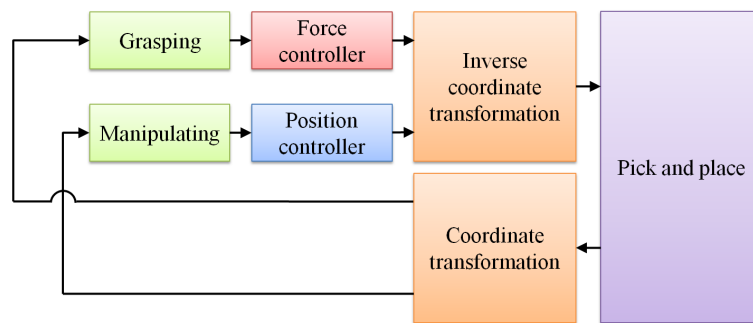
Fig. 3-7: Overall block diagram of GMC system.

Table 3.2: Configuration of GMC.

Function	Modal space	Control system
adaptive grasping	differential mode	force control
precise manipulating	common mode	position control

3.1.3 Grasping and Manipulating Control

Grasping and manipulating control (GMC) [12] is the most prominent example of a system role involving contact motion. The robot has to grip the target object softly enough to not break it. Furthermore, it needs to carry the target object to the desired position. Therefore, the roles of the system can be divided into the functions shown in Fig. 3-6. To perform the role of pick and place, adaptive grasping and precise
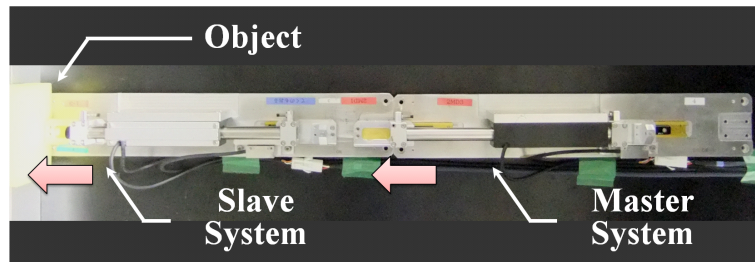
Fig. 3-8: Experimental setup (ABC).

manipulating functions are required [48]. In this method, the adaptive grasping and precise manipulating functions are fulfilled in differential mode and common mode [39], respectively. Fig. 3-7 shows the overall block diagram of the GMC system. Table 3.2 lists the modal spaces and control systems corresponding to each function. While ABC uses a position controller in differential mode and force controller in common mode, GMC needs a force controller in differential mode and position controller in common mode.

3.1.4 Experiments

Experiments were conducted to verify the validity of the functionality-based approach. This section presents two kinds of experiments using the ABC system and using the GMC system. The position was measured by optical encoders, each set on a linear motor. The reaction force from the object was observed using RFOB without force sensors.

Experimental Setups

Fig. 3-8 shows the experimental setup of the ABC system. In this experiment, two linear motors were utilized, as the master system and slave system. An operator moved the master system, which is on the right side. The slave system pushed the object fixed on the left side.
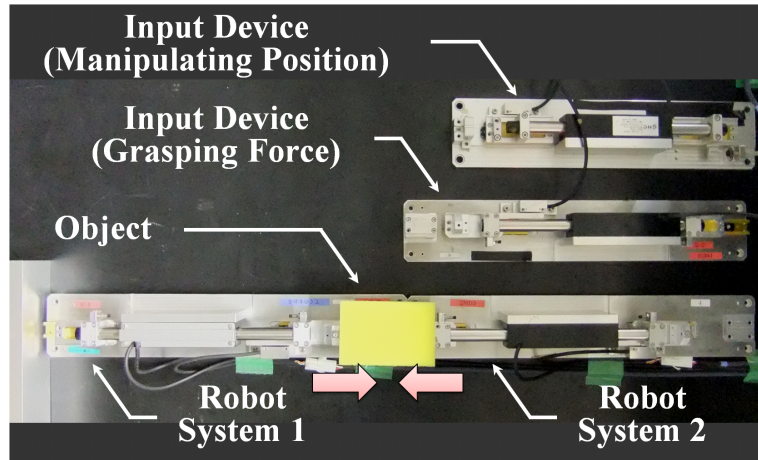
Fig. 3-9: Experimental setup (GMC).

Table 3.3: Experimental parameters.

Position feedback gain	1600 $1/s^2$
Velocity feedback gain	80 $1/s$
Force feedback gain	0.8 $1/kg$
Cutoff frequency of RFOB	500 rad/s
Cutoff frequency of DOB	500 rad/s
Mass	0.5 kg
Sampling time	0.1 ms

Fig. 3-9 shows the experimental setup of the GMC system. Robot system 1 is located on the left side of the object. Robot system 2 is placed on the opposite side. The grasping force and manipulating position were manipulated by input devices, which were the linear motors pictured in Fig. 3-9. An operator pushed the force input device to make robot systems 1 and 2 grasp the object from both sides. The operator also manipulated the position command device.

The experimental parameters used in both experiments are listed in Table 3.3. A sponge was used as a soft object, and an aluminum block was utilized as a hard object. The soft object was slightly smaller than the hard object.
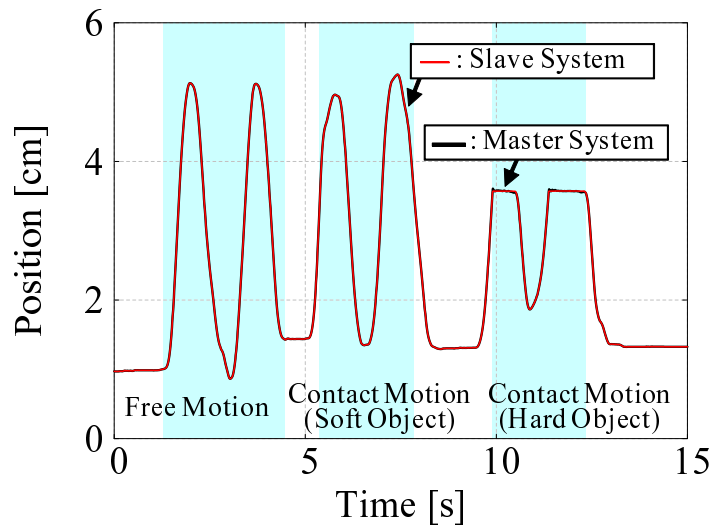
Fig. 3-10: Position response (ABC).
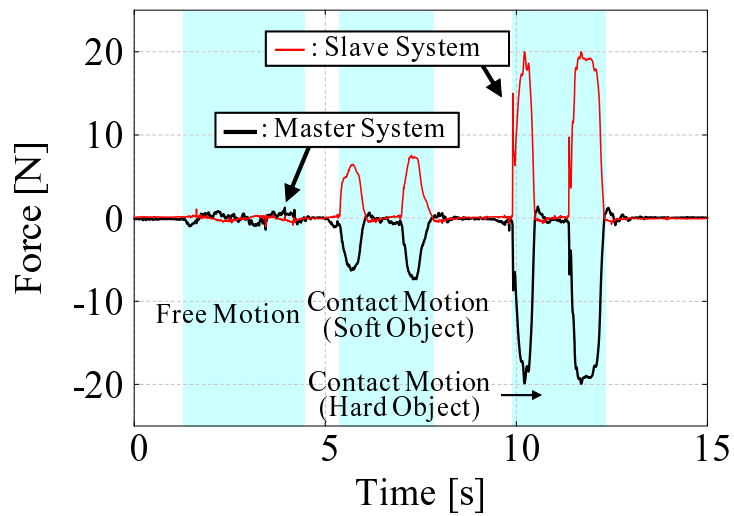
Fig. 3-11: Force response (ABC).

Experimental Results of ABC

Figs. 3-10 and 3-11 show the position and force responses, respectively. From 2.5 s to 4.5 s, the operator moved the robots without contact with any object. The force response in this phase was mainly caused by friction. On the other hand, the slave robot made contact with the soft object from 5.5 s to 8.0 s. The slave robot then made contact with the hard object from 9.8 s to 12.5 s. The thin and heavy
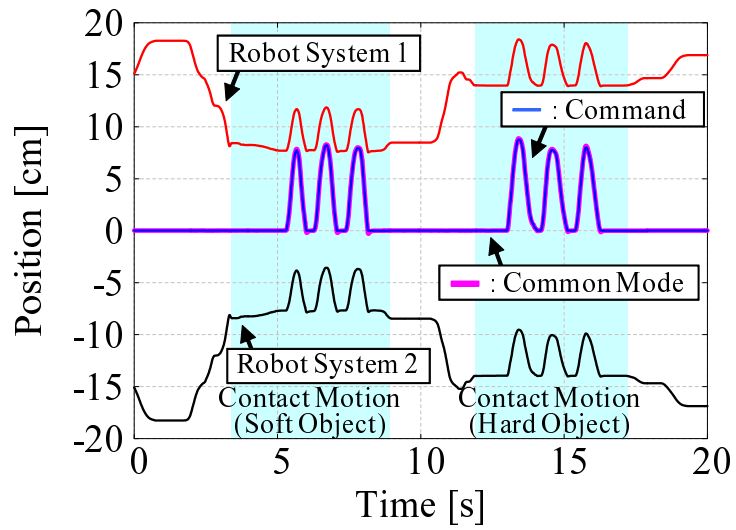
Fig. 3-12: Position response (GMC).
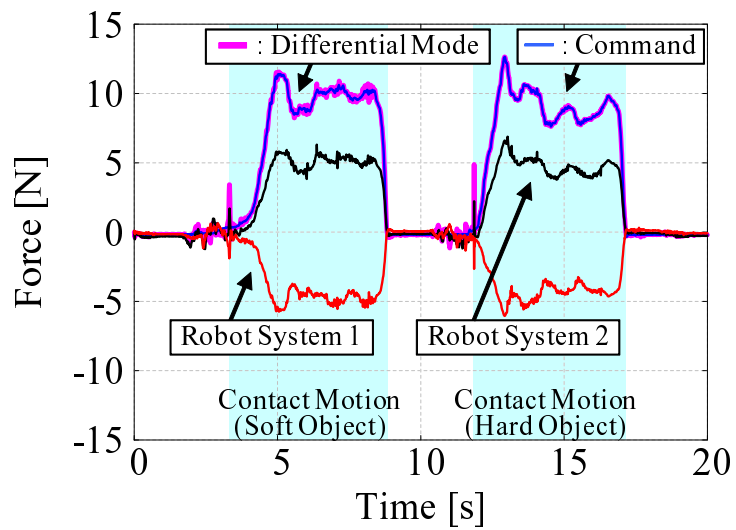
Fig. 3-13: Force response (GMC).

lines indicate the responses of the master and slave systems, respectively. These results confirm that position tracking and force feedback were achieved.

Experimental Results of GMC

Fig. 3-12 shows the position response and position common mode. The GMC system grasped the soft object from 3.0 s to 8.5 s and grasped the hard object from 12.0 s to 17.0 s. The position response did

not change much when the system grasped the hard object. The position common mode, which denotes the midpoint of the two robot systems, tracked the position input. Therefore, this result confirms that the precise manipulating function was achieved.

Fig. 3-13 shows the force response and the differential mode of force. The force differential mode, which was obtained by subtracting the response of robot system 1 from that of robot system 2, tracked the provided force input. The GMC system succeeded in grasping the objects irrespective to the difference in size and stiffness of the objects. In other words, the GMC system adaptively grasped the objects with the manipulated force. Therefore, this result confirms that the adaptive grasping function was achieved.

3.2 Decoupled Control

A technique to simultaneously achieve force control and position control is called hybrid control. Bilateral control can be considered as a kind of hybrid control. Early research on hybrid control was conducted in the early 1980s [25, 26]. Hybrid control uses a directionally decoupled motion controller in the work space. In other words, force control is employed in the normal direction to the contact surface, and position control is employed in the tangential direction. To improve hybrid control, a task description method has been proposed on the basis of the construction of generalized task specification matrices that unify the position control and force control references [27, 69].

In the late 1980s, a hybrid matrix was proposed to indicate the performance of a bilateral control system, and an ideal relationship between the master and the slave systems was constructed on the basis of this hybrid matrix [61]. The ideal relationship was formulated as "transparency" [62]. When the transparency is high, an ideal teleoperation is realized. Since then, numerous bilateral control systems have been proposed to obtain high transparency [63]. One of the most successful systems is an acceleration-based bilateral control system [1, 65].

This system includes three features. Firstly, a disturbance observer (DOB) is employed to suppress the disturbance force and obtain high robustness [29, 70–72]. Secondly, a reaction force observer (RFOB) is employed to estimate the reaction force without using any force sensors [33]. Thirdly, modal decomposition is utilized to decouple the position control and force control [35, 73].

However, when the inertia of the master robot differs from that of the slave robot, interference between position control and force control still occurs. One of the methods used to reduce the interference is oblique coordinate control [52–54, 74]. In this method, a "task mass matrix" is proposed to describe the dynamical relationships between tasks, and the interference is decoupled by using hybrid parameters of the system.

On the other hand, there is another approach to reduce the interference. This approach is a decoupling motion control strategy based on equivalent mass matrices [34]. The equivalent mass matrix is diagonalized to create a decoupling motion controller in the work space. To diagonalize the equivalent mass matrix, the DOB is used in the work space (work space disturbance observer: WOB).

Although the decoupling approach was originally used in the work space, the approach was extended and applied to more general coordinates. In particular, the interference between tasks can be reduced by changing the equivalent mass matrix appropriately [75, 76]. A modal space disturbance observer

(MDOB) was proposed to eliminate this interference [77]. The advantage of implementing disturbance observer in modal space is that it can be possible to design each task independently. However, in these studies, a scaling ratio had an inverse relationship with the inertia ratio. Note that although the idea to implement the disturbance observer in modal space had already proposed before [11], the main aim was canceling the external force, not decoupling, since the applied system has symmetric structure. Furthermore, the performance and stability was not discussed. In another study, MDOB was combined with oblique coordinate control in order to improve the performance [78]. The position and force control systems were decoupled by the diagonalization of the task mass matrix. When a cutoff frequency is high enough, MDOB is able to change the task mass matrix artificially. A previous study described the operationality and reproducibility. In addition, the stability was discussed on the basis of root locus plots. As a result, the utility of MDOB was established, especially in a case where the cutoff frequency of the observers was low. However, the robot that was used in the previous study had only one-degree of freedom (DOF).

Therefore, this section extends the MDOB-based approach to multi-DOF systems. Considering practical use, this section assumes that there is a difference of inertia between the master and the slave systems. The change of the configuration causes the difference of inertia. This section also assumes that cutoff frequency of the disturbance observer cannot be set high. In fact, this kind of situation frequently exists in the industrial fields. The performance and the utility of the proposed method are verified through analyses and experiments. Specifically, achievement of the precise decoupling of the force and position control systems is confirmed even when the inertia of the master robot differs from that of the slave robot. The effect of the position feedback gain, the velocity feedback gain, the force feedback gain, the observer cutoff frequency, and the non diagonal element of the task mass matrix is considered in the analyses. The performance is discussed on the basis of reproducibility and operationality that are indices for the bilateral control system. In addition, the stability of the system is discussed. The performance is experimentally compared with that of oblique coordinate control with a multi-DOF system. Among these processes, this section presents advantages and disadvantages of both the oblique coordinate control and the MDOB-based decoupling method.

3.2.1 Robust Controller Based on Disturbance Observer in Work Space

In this section, the multi-DOF system is modeled in the joint space [33]. The variables in the joint space are transformed into the work space [34, 79, 80]. The framework for the disturbance observer in
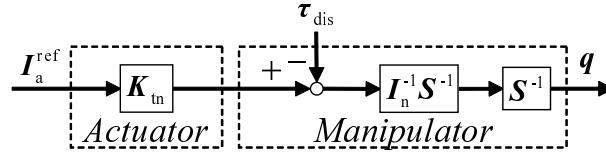
Fig. 3-14: Model of actuator and mechanical manipulator.

the work space is also explained [81, 82].

Modeling

Fig. 3-14 shows a model of the actuator and mechanical manipulator. S is a diagonal matrix whose diagonal elements are Laplace operators. The total effects of the disturbance, τ_{dis}, in the joint space are formulated as

$$\tau_{\mathrm{dis}} = \tau_{\mathrm{int}} + \tau_{\mathrm{ext}} + D\dot{q} + \tau_{\mathrm{c}}$$
$$+ \{\mathrm{diag}I(q) - I_{\mathrm{n}}\}\ddot{q} + (K_{\mathrm{tn}} - K_{\mathrm{t}})I_{\mathrm{a}}^{\mathrm{ref}}, \tag{3.2}$$

where

τ_{int}	interactive torque vector,
τ_{ext}	reaction torque vector in force task,
D	viscosity coefficient matrix,
q	joint angle vector,
$\dot{q}$	angular velocity vector,
$\ddot{q}$	angular acceleration vector,
τ_{c}	Coulomb friction vector,
$I(q)$	joint inertia matrix,
$\mathrm{diag}I(q)$	diagonal matrix whose diagonal elements
	have the diagonal elements of $I(q)$,
K_{t}	torque coefficient matrix,
K_{tn}	nominal torque coefficient matrix,
I_{a}	torque current vector,
superscript ref	reference value, and
subscript n	nominal values.

The motion equation of an m-DOF manipulator in the joint space is expressed as

$$\tau_{\mathrm{dis}} = K_{\mathrm{tn}}I_{\mathrm{a}} - I_{\mathrm{n}}\ddot{q}, \tag{3.3}$$

where

$$\boldsymbol{K}_{\mathrm{tn}} = \mathrm{diag}[\, K_{\mathrm{n}1}, \cdots, K_{\mathrm{n}m}\,], \tag{3.4}$$

$$\boldsymbol{I}_{\mathrm{n}} = \mathrm{diag}[\, I_{\mathrm{n}1}, \cdots, I_{\mathrm{n}m}\,], \tag{3.5}$$

$$\boldsymbol{\tau}_{\mathrm{dis}} = [\, \tau_{\mathrm{dis}1}, \cdots, \tau_{\mathrm{dis}m}\,]^{\mathrm{T}}, \tag{3.6}$$

$$\boldsymbol{I}_{\mathrm{a}} = [\, I_{\mathrm{a}1}, \cdots, I_{\mathrm{a}m}\,]^{\mathrm{T}}, \text{ and} \tag{3.7}$$

$$\boldsymbol{q} = [\, q_1, \cdots, q_m\,]^{\mathrm{T}}. \tag{3.8}$$

Transformation from Joint Space to Work Space

The transformation from the joint space to the work space is represented as

$$\ddot{\boldsymbol{x}} = \boldsymbol{J}(\boldsymbol{q})\ddot{\boldsymbol{q}} + \dot{\boldsymbol{J}}(\boldsymbol{q})\dot{\boldsymbol{q}} \text{ and} \tag{3.9}$$

$$\boldsymbol{f} = \left\{\boldsymbol{J}(\boldsymbol{q})^{\mathrm{T}}\right\}^{-1}\boldsymbol{\tau}, \tag{3.10}$$

where

$\boldsymbol{x}$ position vector in work space,

$\boldsymbol{J}(\boldsymbol{q})$ Jacobian matrix,

$\boldsymbol{f}$ force vector in the work space, and

$\boldsymbol{\tau}$ torque vector in the joint space.

The motion equation in the work space is derived as

$$\boldsymbol{m}_{\mathrm{n}}\ddot{\boldsymbol{x}} = \boldsymbol{f}_{\mathrm{n}} + \boldsymbol{m}_{\mathrm{n}}\dot{\boldsymbol{J}}(\boldsymbol{q})\dot{\boldsymbol{q}} - \boldsymbol{m}_{\mathrm{n}}\boldsymbol{J}(\boldsymbol{q})\boldsymbol{I}_{\mathrm{n}}^{-1}\boldsymbol{\tau}_{\mathrm{dis}} \text{ and} \tag{3.11}$$

$$\boldsymbol{m}_{\mathrm{n}} = \left\{\boldsymbol{J}(\boldsymbol{q})^{\mathrm{T}}\right\}^{-1}\boldsymbol{I}_{\mathrm{n}}\boldsymbol{J}(\boldsymbol{q})^{-1}, \tag{3.12}$$

where $\boldsymbol{m}_{\mathrm{n}}$ denotes the equivalent mass matrix in the work space. The equivalent mass matrix changes according to the configuration of the manipulator.

Disturbance Observer in Work Space

This subsection explains the WOB structure [82, 83]. WOB can change and stabilize the dynamics in the work space by adjusting the nominal value of the equivalent mass matrix. When the nominal equivalent mass matrix is diagonal matrix each axial motion is decoupled. Here, a diagonal mass matrix, $\boldsymbol{m}_{\mathrm{nn}}$, is introduced. The difference, $\Delta\boldsymbol{m}_{\mathrm{n}}$, between the equivalent mass matrix and the diagonal mass matrix

is expressed as

$$
\begin{aligned}
\boldsymbol{m}_{\mathrm{n}} &= \boldsymbol{m}_{\mathrm{nn}} + (\boldsymbol{m}_{\mathrm{n}} - \boldsymbol{m}_{\mathrm{nn}}) \\
&= \boldsymbol{m}_{\mathrm{nn}} + \Delta \boldsymbol{m}_{\mathrm{n}}.
\end{aligned}
\tag{3.13}
$$

The diagonal mass matrix is defined at the initial configuration of the manipulator. The motion equation is restated on the basis of the diagonal mass matrix as

$$
\boldsymbol{m}_{\mathrm{nn}} \ddot{\boldsymbol{x}} = \boldsymbol{f}_{\mathrm{n}} - \boldsymbol{f}_{\mathrm{dis}},
\tag{3.14}
$$

where

$$
\begin{aligned}
\boldsymbol{m}_{\mathrm{nn}} &= \mathrm{diag}[\, m_{\mathrm{nn}1}, \cdots, m_{\mathrm{nn}r} \,], \tag{3.15} \\
\boldsymbol{x} &= [\, x_1, \cdots, x_r \,]^{\mathrm{T}}, \tag{3.16} \\
\boldsymbol{f}_{\mathrm{n}} &= [\, f_{\mathrm{n}1}, \cdots, f_{\mathrm{n}r} \,]^{\mathrm{T}}, \ \ \text{and} \tag{3.17} \\
\boldsymbol{f}_{\mathrm{dis}} &= [\, f_{\mathrm{dis}1}, \cdots, f_{\mathrm{dis}r} \,]^{\mathrm{T}}. \tag{3.18}
\end{aligned}
$$

Here, a work space in an r-dimensional coordinate system is considered. In the work space, the disturbance force vector is restated as

$$
\boldsymbol{f}_{\mathrm{dis}} = \Delta \boldsymbol{m}_{\mathrm{n}} \ddot{\boldsymbol{x}} - \boldsymbol{m}_{\mathrm{n}} \dot{\boldsymbol{J}}(\boldsymbol{q}) \dot{\boldsymbol{q}} + \boldsymbol{m}_{\mathrm{n}} \boldsymbol{J}(\boldsymbol{q}) \boldsymbol{I}_{\mathrm{n}}^{-1} \boldsymbol{\tau}_{\mathrm{dis}}.
\tag{3.19}
$$

The disturbance force $\boldsymbol{f}_{\mathrm{dis}}$ can be derived as

$$
\hat{\boldsymbol{f}}_{\mathrm{dis}} = \boldsymbol{f}_{\mathrm{n}} - \boldsymbol{m}_{\mathrm{nn}} \ddot{\boldsymbol{x}},
\tag{3.20}
$$

where "$\wedge$" denotes the estimated value. However, direct calculation of the disturbance force is difficult, because these signals suffer from noise effects. Therefore, a low-pass filter is inserted to reduce the effects of noises. The disturbance force is estimated as

$$
\hat{\boldsymbol{f}}_{\mathrm{dis}}(s) = \boldsymbol{G}_{\mathrm{H}}^{\mathrm{o}}(s) \{ \boldsymbol{f}_{\mathrm{n}}(s) + \boldsymbol{G}^{\mathrm{o}} \boldsymbol{m}_{\mathrm{nn}} s \boldsymbol{x}(s) \} - \boldsymbol{G}^{\mathrm{o}} \boldsymbol{m}_{\mathrm{nn}} s \boldsymbol{x}(s),
\tag{3.21}
$$

where

$$
\begin{aligned}
\boldsymbol{G}_{\mathrm{H}}^{\mathrm{o}}(s) &= \mathrm{diag}\left[\, \frac{g_1}{s + g_1}, \cdots, \frac{g_r}{s + g_r} \,\right] \ \ \text{and} \tag{3.22} \\
\boldsymbol{G}^{\mathrm{o}} &= \mathrm{diag}[\, g_1, \cdots, g_r \,]. \tag{3.23}
\end{aligned}
$$

Here, g denotes the cutoff frequency of the low-pass filter in each dimension. The estimated disturbance force is fed back to suppress the disturbance force. The motion equation with the feedback is expressed as

$$
\begin{aligned}
\boldsymbol{m}_{\mathrm{nn}} s^2 \boldsymbol{x}(s) &= \boldsymbol{f}_{\mathrm{n}}(s) - \boldsymbol{f}_{\mathrm{dis}}(s) \\
&= \boldsymbol{f}^{\mathrm{ref}}(s) - \boldsymbol{G}_{\mathrm{S}}^{\mathrm{o}}(s) \boldsymbol{f}_{\mathrm{dis}}(s) \approx \boldsymbol{f}^{\mathrm{ref}}(s), \\
&\quad \left(\boldsymbol{f}_{\mathrm{n}}(s) = \boldsymbol{f}^{\mathrm{ref}}(s) + \hat{\boldsymbol{f}}_{\mathrm{dis}}(s) \right)
\end{aligned}
\tag{3.24}
$$

where

$$
\boldsymbol{G}_{\mathrm{S}}^{\mathrm{o}}(s) = \operatorname{diag}\left[\frac{s}{s + g_1}, \cdots, \frac{s}{s + g_r} \right].
\tag{3.25}
$$

If a sufficiently large cutoff frequency, g, is selected to make $\boldsymbol{G}_{\mathrm{S}}^{\mathrm{o}}(s)$ negligibly small, the disturbance force has little effect on the nominal system.
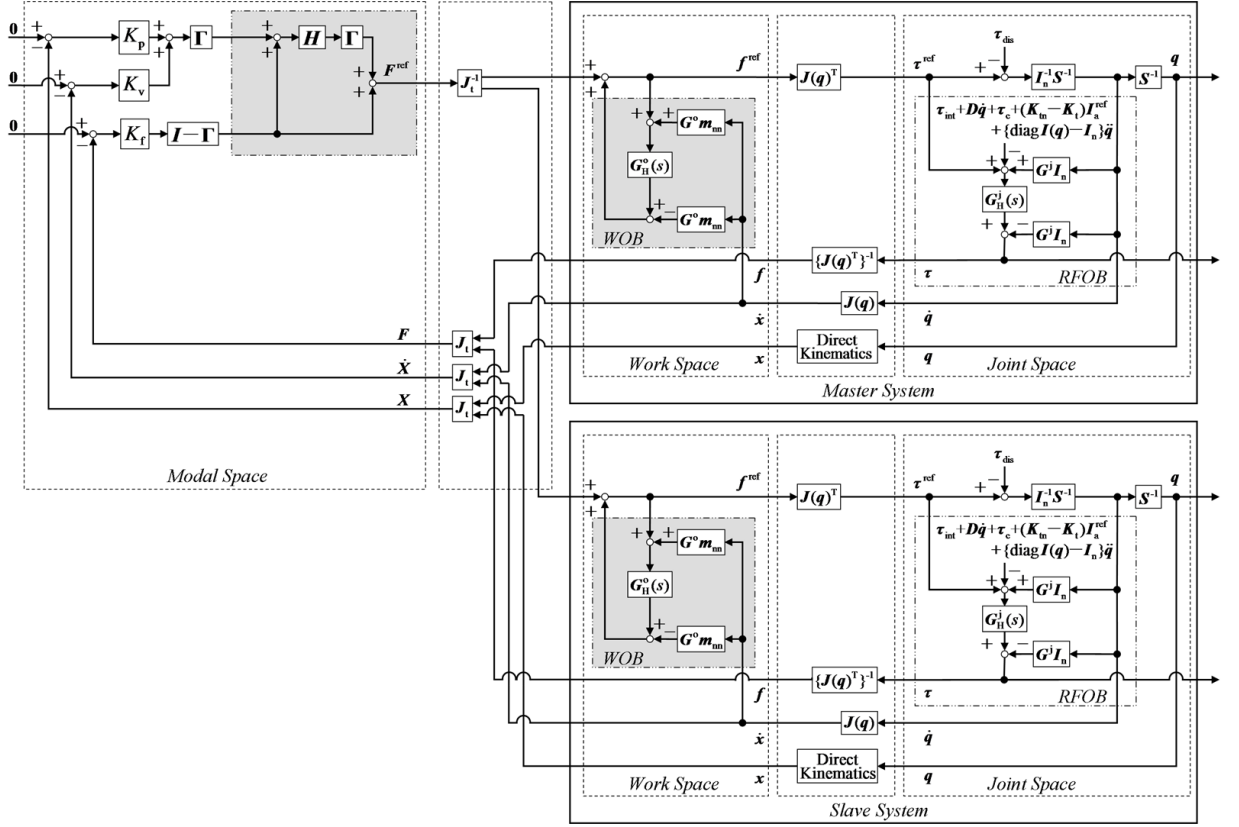
Fig. 3-15: Block diagram of oblique coordinate control. (conventional method)

3.2.2 Oblique Coordinate Control

This section describes a bilateral control on the basis of oblique coordinate control with WOB. Fig. 3-15 shows a block diagram of oblique coordinate control. The equivalent mass and equivalent force of the master and slave systems are used in the following equations. The motion equation is reconstructed as

$$\boldsymbol{m}^* \ddot{\boldsymbol{x}}^* \;=\; \boldsymbol{f}^* - \boldsymbol{f}^*_{\text{dis}}, \tag{3.26}$$

where

$$\boldsymbol{m}^* \;=\; \text{diag}[m_{\text{M}} \, , \, m_{\text{S}}], \tag{3.27}$$

$$\boldsymbol{x}^* \;=\; [x_{\text{M}}, x_{\text{S}}]^{\text{T}}, \tag{3.28}$$

$$\boldsymbol{f}^* \;=\; [f_{\text{M}}, f_{\text{S}}]^{\text{T}}, \; \text{and} \tag{3.29}$$

$$\boldsymbol{f}^*_{\text{dis}} \;=\; [f_{\text{disM}}, f_{\text{disS}}]^{\text{T}}. \tag{3.30}$$

Here, subscripts "M" and "S" denote the master system and slave system, respectively. The goals of the bilateral control are expressed as

- Position tracking

$$J_{11}x_{\mathrm{M}} = J_{12}x_{\mathrm{S}}, \tag{3.31}$$

- Force feedback

$$J_{21}f_{\mathrm{M}} = -J_{22}f_{\mathrm{S}}. \tag{3.32}$$

From these relationships, a modal transformation matrix is obtained as

$$\boldsymbol{J}_{\mathrm{t}} = \left[\begin{array}{cc} J_{11} & -J_{12} \\ J_{21} & J_{22} \end{array} \right], \tag{3.33}$$

where each element denotes a scaling ratio. The transformation from the work space to the modal space is conducted as

$$\boldsymbol{X} = \boldsymbol{J}_{\mathrm{t}}\boldsymbol{x} \text{ and} \tag{3.34}$$

$$\boldsymbol{F} = \boldsymbol{J}_{\mathrm{t}}\boldsymbol{f}, \tag{3.35}$$

where

$$\boldsymbol{X} = [\,X_{\mathrm{M}}, X_{\mathrm{S}}\,]^{\mathrm{T}} \text{ and} \tag{3.36}$$

$$\boldsymbol{F} = [\,F_{\mathrm{M}}, F_{\mathrm{S}}\,]^{\mathrm{T}}. \tag{3.37}$$

Here, X and F denote the position vector and force vector in the modal space, respectively. Usually, the transformation of forces is expressed as

$$\boldsymbol{F} = \left\{\boldsymbol{J}_{\mathrm{t}}^{\mathrm{T}}\right\}^{-1} \boldsymbol{f} \tag{3.38}$$

based on the principle of virtual work. However, the principle of virtual work is not valid for oblique coordinate control. Therefore, to simplify the design, the forces are transformed by $\boldsymbol{J}_{\mathrm{t}}$ which is also utilized for the position transformation. The energy is not conserved before and after the transformation. The modal space dynamics is developed as

$$\boldsymbol{M}_{\mathrm{n}}\ddot{\boldsymbol{X}} = \boldsymbol{F}_{\mathrm{n}} - \boldsymbol{F}_{\mathrm{dis}} \text{ and} \tag{3.39}$$

$$\boldsymbol{M}_{\mathrm{n}} = \boldsymbol{J}_{\mathrm{t}}\boldsymbol{m}^{*}\boldsymbol{J}_{\mathrm{t}}^{-1}, \tag{3.40}$$

where M_{n} denotes the task mass matrix that is an equivalent mass matrix in the modal space. Each element of M_{n}, F_{n}, and F_{dis} is expressed as

$$M_{\mathrm{n}} = \begin{bmatrix} M_{\mathrm{XX}} & M_{\mathrm{XF}} \\ M_{\mathrm{FX}} & M_{\mathrm{FF}} \end{bmatrix}, \tag{3.41}$$

$$F_{\mathrm{n}} = [\, F_{\mathrm{nM}}, F_{\mathrm{nS}} \,]^{\mathrm{T}}, \text{ and} \tag{3.42}$$

$$F_{\mathrm{dis}} = [\, F_{\mathrm{disM}}, F_{\mathrm{disS}} \,]^{\mathrm{T}}. \tag{3.43}$$

An acceleration reference $\ddot{X}_{\mathrm{X}}^{\mathrm{ref}}$ for the position tracking and a force reference $F_{\mathrm{F}}^{\mathrm{ref}}$ to achieve the force feedback are obtained as

$$\begin{bmatrix} \ddot{X}_{\mathrm{X}}^{\mathrm{ref}} \\ F_{\mathrm{F}}^{\mathrm{ref}} \end{bmatrix} = -C_{\mathrm{p}}\boldsymbol{\Gamma}\boldsymbol{X} - C_{\mathrm{f}}(\boldsymbol{I} - \boldsymbol{\Gamma})\boldsymbol{F}, \tag{3.44}$$

where I, C_{p}, and C_{f} denote the 2×2 unit matrix, position controller, and force controller, respectively. The superscript "cmd," subscript "X," and subscript "F" represent the command, the relation with the position control, and the relation with the force control, respectively. Here, $\boldsymbol{\Gamma}$ is the selection matrix, which is defined as

$$\boldsymbol{\Gamma} = \begin{bmatrix} 1 & 0 \\ 0 & 0 \end{bmatrix} \tag{3.45}$$

because one of the two DOFs is utilized for the position control system. The reference values $F_{\mathrm{X}}^{\mathrm{ref}}$ and $\ddot{X}_{\mathrm{F}}^{\mathrm{ref}}$ have to satisfy

$$M_{\mathrm{n}} \begin{bmatrix} \ddot{X}_{\mathrm{X}}^{\mathrm{ref}} \\ \ddot{X}_{\mathrm{F}}^{\mathrm{ref}} \end{bmatrix} = \begin{bmatrix} F_{\mathrm{X}}^{\mathrm{ref}} \\ F_{\mathrm{F}}^{\mathrm{ref}} \end{bmatrix} = \boldsymbol{F}^{\mathrm{ref}}. \tag{3.46}$$

$F_{\mathrm{X}}^{\mathrm{ref}}$ is the force reference for position tracking, and $\ddot{X}_{\mathrm{F}}^{\mathrm{ref}}$ is the acceleration reference for the force feedback. By converting eq. (3.46) into an expression using a hybrid matrix, H,

$$\begin{bmatrix} F_{\mathrm{X}}^{\mathrm{ref}} \\ \ddot{X}_{\mathrm{F}}^{\mathrm{ref}} \end{bmatrix} = H \begin{bmatrix} \ddot{X}_{\mathrm{X}}^{\mathrm{ref}} \\ F_{\mathrm{F}}^{\mathrm{ref}} \end{bmatrix} \tag{3.47}$$

is obtained. The relationship between the hybrid matrix and the task mass matrix is

$$H = \begin{bmatrix} -1 & M_{\mathrm{XF}} \\ 0 & M_{\mathrm{FF}} \end{bmatrix}^{-1} \begin{bmatrix} -M_{\mathrm{XX}} & 0 \\ -M_{\mathrm{FX}} & 1 \end{bmatrix}. \tag{3.48}$$

The force reference vector in the modal space is obtained as

$$\begin{aligned} \boldsymbol{F}^{\mathrm{ref}} &= \begin{bmatrix} F_{\mathrm{X}}^{\mathrm{ref}} \\ 0 \end{bmatrix} + \begin{bmatrix} 0 \\ F_{\mathrm{F}}^{\mathrm{ref}} \end{bmatrix} \\ &= \boldsymbol{\Gamma}H \begin{bmatrix} \ddot{X}_{\mathrm{X}}^{\mathrm{ref}} \\ F_{\mathrm{F}}^{\mathrm{ref}} \end{bmatrix} + (\boldsymbol{I} - \boldsymbol{\Gamma}) \begin{bmatrix} 0 \\ F_{\mathrm{F}}^{\mathrm{ref}} \end{bmatrix}. \end{aligned} \tag{3.49}$$
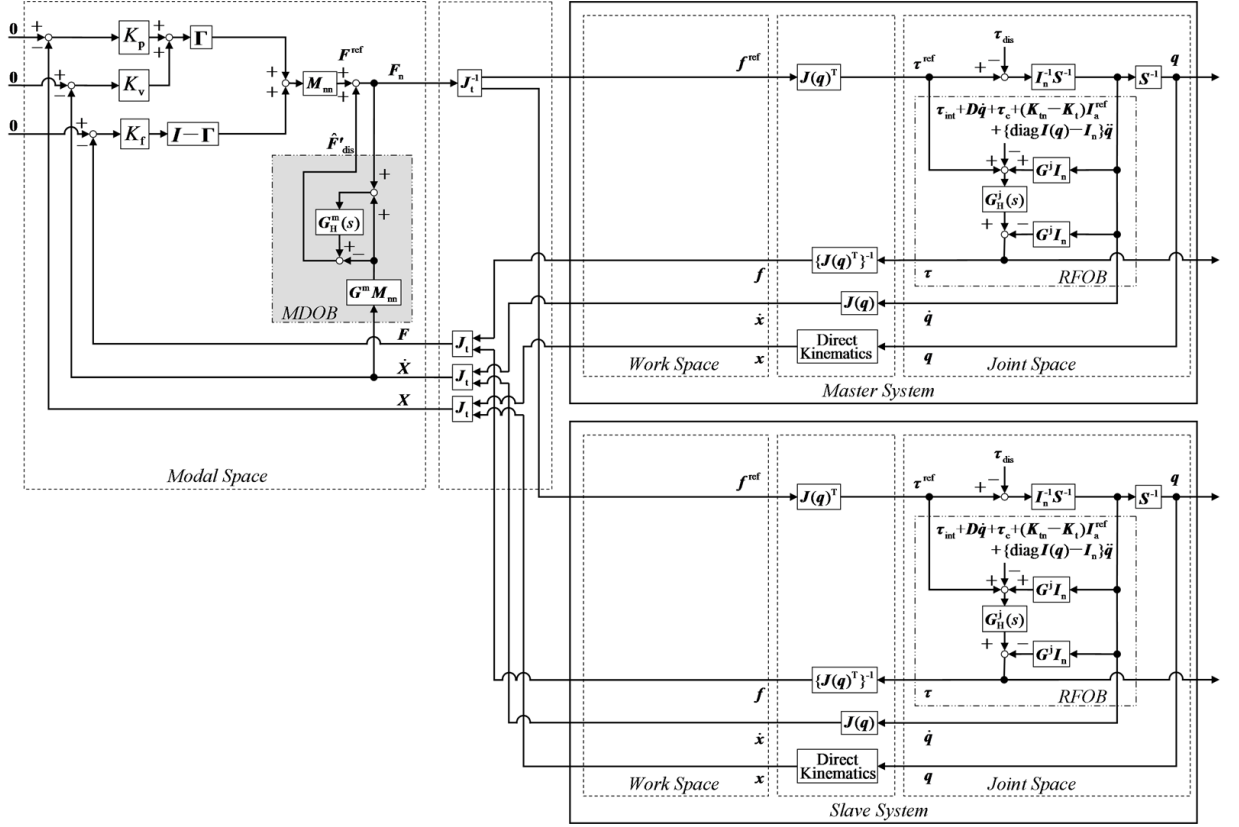
Fig. 3-16: Block diagram of diagonalization method. (proposed method)

The force reference in the joint space is calculated by inversely transforming of $\boldsymbol{F}^{\text{ref}}$ as

$$\boldsymbol{f}^{\text{ref}} \;=\; \boldsymbol{J}_{\text{t}}^{-1}\boldsymbol{F}^{\text{ref}}. \tag{3.50}$$

3.2.3   Modal Space Disturbance Observer

Fig. 3-16 shows a block diagram of the method based on MDOB. MDOB utilizes a nominal value for the task mass matrix. When this nominal value is set to a diagonal matrix, the task mass matrix can be considered as a diagonal matrix artificially. Here, a diagonal mass matrix $\boldsymbol{M}_{\text{nn}}$ is introduced as

$$
\begin{aligned}
\boldsymbol{M}_{\text{n}} &= \boldsymbol{M}_{\text{nn}} + (\boldsymbol{M}_{\text{n}} - \boldsymbol{M}_{\text{nn}}) \\
&= \boldsymbol{M}_{\text{nn}} + \Delta\boldsymbol{M}_{\text{n}}. \tag{3.51}
\end{aligned}
$$

$\boldsymbol{M}_{\text{nn}}$ is composed of diagonal elements of the task mass matrix. $\Delta\boldsymbol{M}_{\text{n}}$ denotes the difference between the two values. A method to suppress the effect of nondiagonal elements is discussed below. A motion

equation in the modal space is expressed as

$$\boldsymbol{M}_{\mathrm{nn}}\ddot{\boldsymbol{X}} \;=\; \boldsymbol{F}_{\mathrm{n}} - \boldsymbol{F'}_{\mathrm{dis}}, \tag{3.52}$$

where

$$\boldsymbol{M}_{\mathrm{nn}} \;=\; \mathrm{diag}[\, M_{\mathrm{XX}}, M_{\mathrm{FF}}\,] \;\; \text{and} \tag{3.53}$$

$$\boldsymbol{F'}_{\mathrm{dis}} \;=\; \boldsymbol{F}_{\mathrm{dis}} + \Delta\boldsymbol{M}_{\mathrm{n}}\ddot{\boldsymbol{X}}. \tag{3.54}$$

The disturbance force $\boldsymbol{F'}_{\mathrm{dis}}$ in the modal space can be calculated as

$$\hat{\boldsymbol{F}}'_{\mathrm{dis}} \;=\; \boldsymbol{F}_{\mathrm{n}} - \boldsymbol{M}_{\mathrm{nn}}\ddot{\boldsymbol{X}}. \tag{3.55}$$

However, direct calculation of the disturbance force is difficult, as these signals suffer from the effects of noises. Therefore, a low-pass filter is inserted to reduce the effects of noises, as is the case in WOB. The disturbance force is estimated as

$$\hat{\boldsymbol{F}}'_{\mathrm{dis}}(s) = \boldsymbol{G}_{\mathrm{H}}^{\mathrm{m}}(s)\left\{\boldsymbol{F}_{\mathrm{n}}(s) + \boldsymbol{G}^{\mathrm{m}}\boldsymbol{M}_{\mathrm{nn}}s\boldsymbol{X}(s)\right\} - \boldsymbol{G}^{\mathrm{m}}\boldsymbol{M}_{\mathrm{nn}}s\boldsymbol{X}(s), \tag{3.56}$$

where

$$\boldsymbol{G}_{\mathrm{H}}^{\mathrm{m}}(s) \;=\; \mathrm{diag}\left[\,\frac{g_{\mathrm{X}}}{s+g_{\mathrm{X}}}, \frac{g_{\mathrm{F}}}{s+g_{\mathrm{F}}}\,\right] \;\; \text{and} \tag{3.57}$$

$$\boldsymbol{G}^{\mathrm{m}} \;=\; \mathrm{diag}[\, g_{\mathrm{X}}, g_{\mathrm{F}}\,]. \tag{3.58}$$

Here, g denotes the cutoff frequency of the low-pass filter in each task. The estimated disturbance force is fed back to cancel out the disturbance force. The motion equation with the feedback is expressed as

$$\begin{aligned}
\boldsymbol{M}_{\mathrm{nn}}s^2\boldsymbol{X}(s) \;&=\; \boldsymbol{F}_{\mathrm{n}}(s) - \boldsymbol{F'}_{\mathrm{dis}}(s) \\
&=\; \boldsymbol{F}^{\mathrm{ref}}(s) - \boldsymbol{G}_{\mathrm{S}}^{\mathrm{m}}(s)\boldsymbol{F'}_{\mathrm{dis}}(s) \approx \boldsymbol{F}^{\mathrm{ref}}(s), \\
&\quad\left(\boldsymbol{F}_{\mathrm{n}}(s) = \boldsymbol{F}^{\mathrm{ref}}(s) + \hat{\boldsymbol{F}}'_{\mathrm{dis}}(s)\right)
\end{aligned} \tag{3.59}$$

where

$$\boldsymbol{G}_{\mathrm{S}}^{\mathrm{m}}(s) \;=\; \mathrm{diag}\left[\,\frac{s}{s+g_{\mathrm{X}}}, \frac{s}{s+g_{\mathrm{F}}}\,\right]. \tag{3.60}$$

Here, sufficiently large cutoff frequencies, g_{X} and g_{F}, are selected so that $\boldsymbol{G}_{\mathrm{S}}^{\mathrm{m}}(s)$ becomes negligibly small. As a result, the disturbance force has little effect on the nominal decoupled system. MDOB

regards the nondiagonal elements of the task mass matrix as the disturbance. The task mass matrix can be expressed in terms of each mass of the master and slave systems as

$$
\boldsymbol{M}_{\mathrm{n}} = \\
\frac{1}{\delta} \begin{bmatrix} J_{11}J_{22}m_{\mathrm{M}} + J_{12}J_{21}m_{\mathrm{S}} & J_{11}J_{12}(m_{\mathrm{M}} - m_{\mathrm{S}}) \\ J_{21}J_{22}(m_{\mathrm{M}} - m_{\mathrm{S}}) & J_{12}J_{21}m_{\mathrm{M}} + J_{11}J_{22}m_{\mathrm{S}} \end{bmatrix}. \tag{3.61}
$$

$$(\delta = J_{12}J_{21} + J_{11}J_{22})$$

Therefore, the nondiagonal elements are zero if the mass of the master system is the same as that of the slave system.

Table 3.4: Parameters.

Common parameters in analyses and experiments	
Slave mass m_S	1.71 kg
Position feedback gain K_p	900 $1/s^2$
Velocity feedback gain K_v	60 1/s
Force feedback gain K_f	0.9
Scaling parameter $J_{11}, J_{12}, J_{21}, J_{22}$	1.0
Cutoff frequency of pseudo derivative (slave side)	100 rad/s
Cutoff frequency of RFOB (slave side)	100 rad/s
Cutoff frequency of WOB (master side)	10 rad/s
Cutoff frequency of MDOB (master side)	10 rad/s
Analyses	
Master mass m_M (Config. A)	1.716650 kg
Master mass m_M (Config. B)	1.226420 kg
Master mass m_M (Config. C)	0.613210 kg
Environmental stiffness	5000 N/m
Environmental viscosity	10 Ns/m
Experiments	
Nominal inertia of 1st link I_{n1}	0.008614 Nm
Nominal inertia of 2nd link I_{n2}	0.000330 Nm
Length of 1st and 2nd link	90 mm
Sampling period	0.1 ms

3.2.4 Analyses

In this section, the operationality and the reproducibility is calculated to evaluate the bilateral control system. Furthermore, the stability is analyzed on the basis of root locus method. The variation of the feedback gain and mass are taken into account. For simplicity, one-DOF manipulator in the joint space is assumed. Table 3.4 lists the parameters used in the analyses and the experiments. In this section, these parameters are set as standard parameters. In order to ensure consistency with the experiments conducted in section 3.2.5, three kinds of mass are considered. The mass of the configuration A is set as a standard parameter.

Performance Analyses

This subsection introduces a concept of the operationality and the reproducibility. These are performance indices of bilateral control systems. The relationship between the position and the force of the bilateral control system can be expressed by a two-port expression as

$$
\begin{bmatrix} f_{\mathrm{M}} \\ x_{\mathrm{S}} \end{bmatrix} = \boldsymbol{T} \begin{bmatrix} x_{\mathrm{M}} \\ f_{\mathrm{S}} \end{bmatrix}.
\tag{3.62}
$$

Here, each element of the matrix $\boldsymbol{T}$ is defined as

$$
\boldsymbol{T} = \begin{bmatrix} T_{11} & T_{12} \\ T_{21} & T_{22} \end{bmatrix}.
\tag{3.63}
$$

From these equations, the relationship between the master position and the master force is derived as

$$
f_{\mathrm{M}} = T_{11} x_{\mathrm{M}} + \frac{T_{12} T_{21}}{1 - T_{22} Z_{\mathrm{e}}} Z_{\mathrm{e}} x_{\mathrm{M}},
\tag{3.64}
$$

where Z_{e} represents environmental impedance that is defined as

$$
f_{\mathrm{S}} = Z_{\mathrm{e}} x_{\mathrm{S}}.
\tag{3.65}
$$

The operationality P_{o} and reproducibility P_{r} are defined as

$$
P_{\mathrm{o}} = T_{11},
\tag{3.66}
$$

$$
P_{\mathrm{r}} = \frac{T_{12} T_{21}}{1 - T_{22} Z_{\mathrm{e}}}.
\tag{3.67}
$$

The operationality shows how much the operator feels operational force in addition to the real environmental force. To achieve comfortable operation, the operationality should be 0. On the other hand, the reproducibility shows how much the environmental impedance is reproduced in the master side. To transmit environmental impedance, the reproducibility should be -1. In order to investigate the effect of the control parameters, Bode diagrams of the operationality and the reproducibility are described. Fig. 3-17 and Fig. 3-18 show the impact of the position feedback gain. The performance of the reproducibility increases with the increasing position feedback gain. Fig. 3-19 and Fig. 3-20 show that the velocity feedback gain has little influence on both the reproducibility and the operationality. Fig. 3-21 and Fig. 3-22 show that the operationality can be progressed by increasing the force feedback gain. Fig. 3-23 and Fig. 3-24 illustrate the effect of cutoff frequency in WOB and MDOB. The performance

of the reproducibility is enhanced by setting the cutoff frequency high. Fig. 3-25 and Fig. 3-26 show the change caused by the difference in mass. To model the equivalent mass of the tip, which depends on the configurations, three kinds of value listed in Table 3.4 were set as the master mass. The reproducibility decreases with the increasing difference of mass. Fig. 3-27 and Fig. 3-28 are the results of performance comparison. The master mass of the configuration A is the most similar to the slave mass. The difference in mass increases in the following order: configuration A, configuration B, configuration C. The higher performance of the MDOB-based decoupling compared with the oblique coordinate control is confirmed, especially in the configuration C.
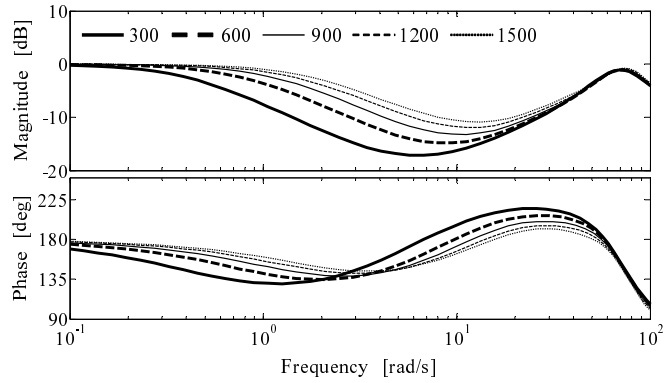
Fig. 3-17: Bode diagram of P_r. ($K_p = 300 \rightarrow 1500$)
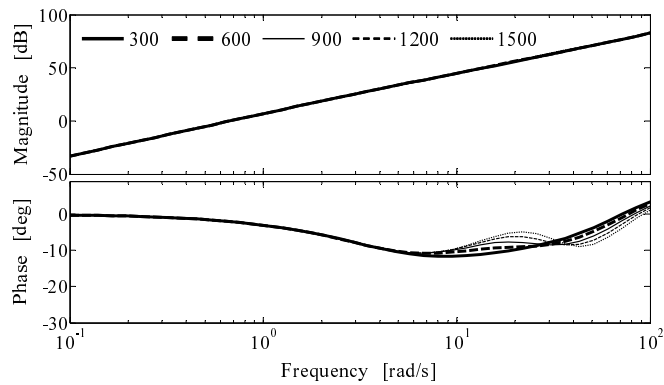
Fig. 3-18: Bode diagram of P_o. ($K_p = 300 \rightarrow 1500$)
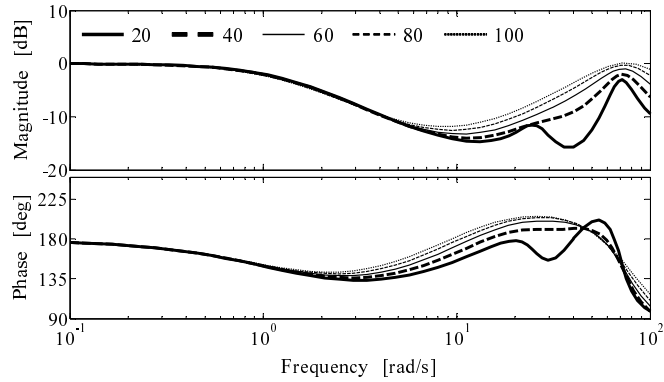
Fig. 3-19: Bode diagram of P_r. ($K_v = 20 \rightarrow 100$)
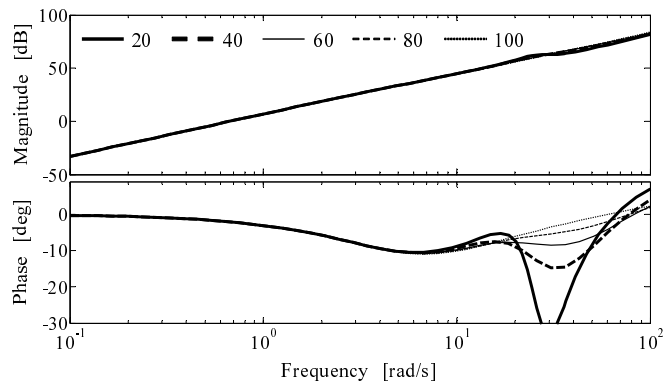
Fig. 3-20: Bode diagram of P_o. ($K_v = 20 \rightarrow 100$)
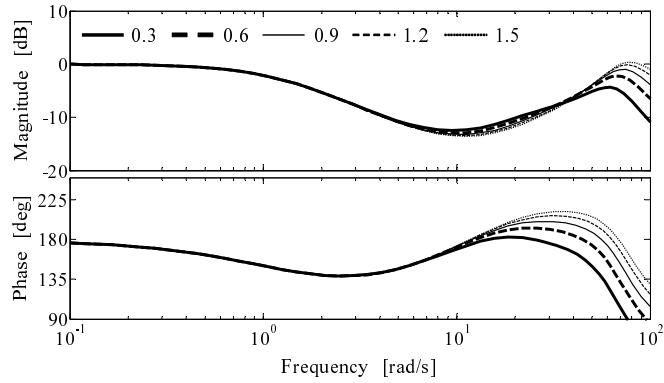
Fig. 3-21: Bode diagram of P_r. ($K_\mathrm{f} = 0.3 \rightarrow 1.5$)
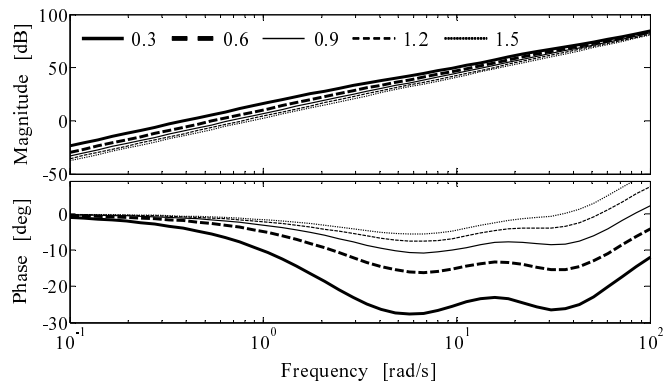
Fig. 3-22: Bode diagram of P_o. ($K_\mathrm{f} = 0.3 \rightarrow 1.5$)
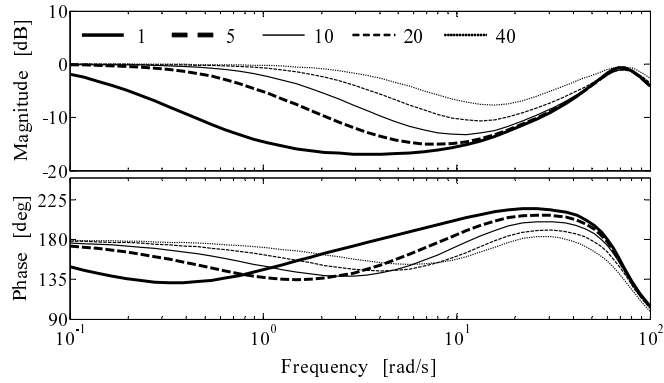
Fig. 3-23: Bode diagram of P_r. ($g_\mathrm{X} = 1 \rightarrow 40$)
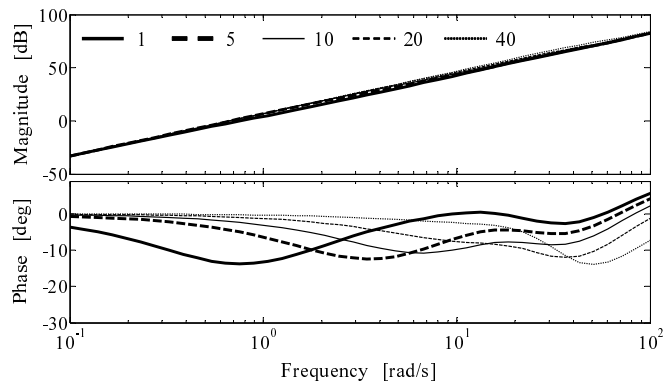
Fig. 3-24: Bode diagram of P_o. ($g_\mathrm{X} = 1 \rightarrow 40$)
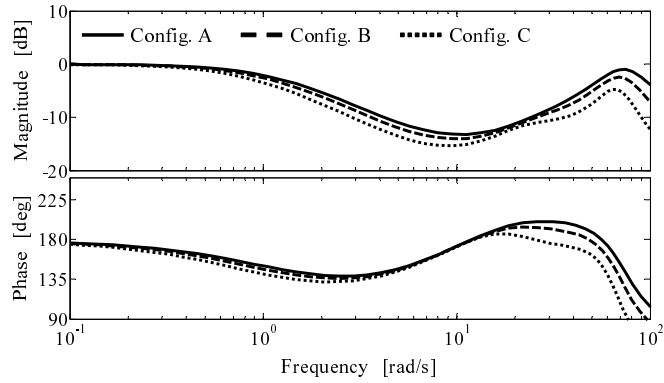
Fig. 3-25: Bode diagram of P_{r}. (Config. A $\rightarrow$ Config. C)
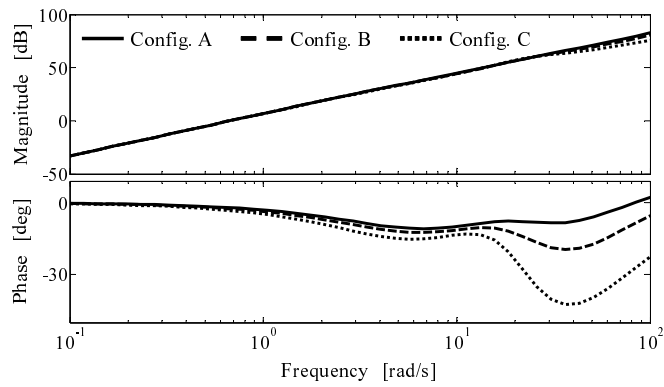
Fig. 3-26: Bode diagram of P_{o}. (Config. A $\rightarrow$ Config. C)
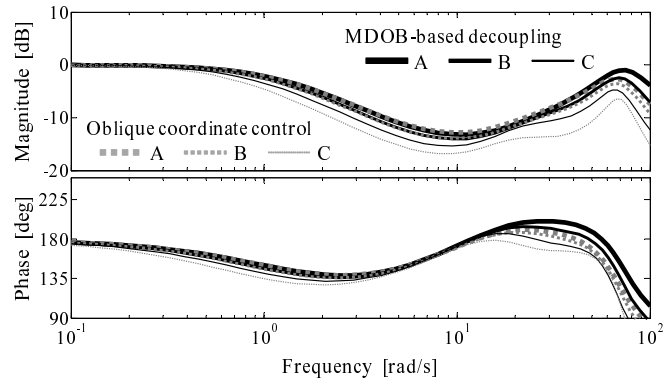
Fig. 3-27: Bode diagram of P_{r}. (performance comparison)
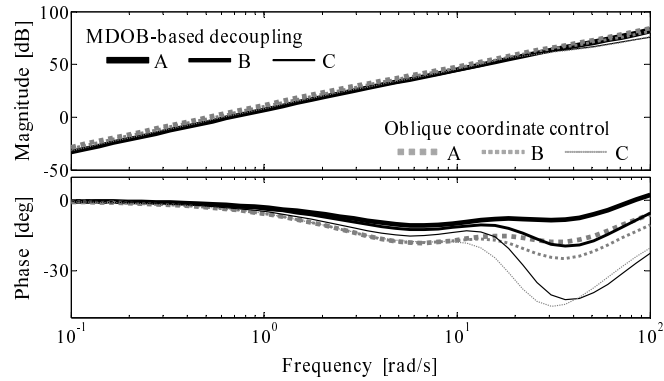
Fig. 3-28: Bode diagram of P_{o}. (performance comparison)
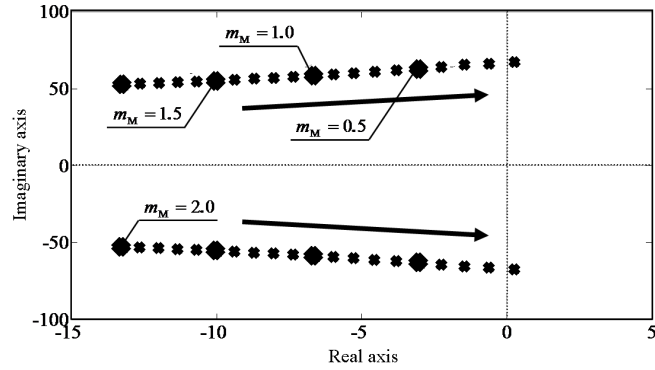
Fig. 3-29: Pole map of oblique coordinate control. ($m_\mathrm{M} = 2.0 \to 0.1$)
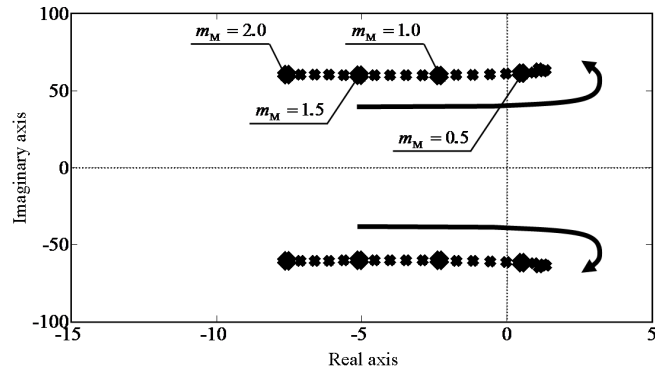
Fig. 3-30: Pole map of MDOB-based decoupling. ($m_\mathrm{M} = 2.0 \to 0.1$)

Stability Analyses

The transfer function from the master force to the master position is obtained as

$$\frac{x_\mathrm{M}}{f_\mathrm{M}} = \frac{1}{P_\mathrm{o} + P_\mathrm{r} Z_\mathrm{e}}. \tag{3.68}$$

The stability of the system can be investigated by checking the poles. Fig. 3-29 and Fig. 3-30 show the pole maps of the oblique coordinate control and the MDOB-based decoupling method, respectively. These figures show the poles when the mass is shifted from 2.0 kg to 0.1 kg, and black dots are plotted every 0.1 kg. MDOB-based decoupling method becomes unstable around 0.6 kg, while the oblique coordinate control is stable.

3.2.5   Experiments on Decoupling

In this section, the validity of the MDOB-based decoupling method is experimentally verified. To confirm the performances, an operator pushed a hard rubber block three times through the bilateral control systems with three different configurations, as presented in Table 3.5. Fig. 3-31 and Fig. 3-32 show the experimental setup. A two-link manipulator and linear forceps robot were used as the master and slave robots, respectively. The external force was observed by RFOB without any force sensors. RFOB has a cost advantage and is widely used in previous research, while it requires precise identification of disturbance other than environmental reaction force such as gravity force and friction force [33, 84]. To avoid the impact of the identification, the above robots were used in this section. The robots used in these experiments were horizontal to the ground and had little friction. Only position encoders were implemented to the motors as sensors. The resolution of the linear encoders and rotary encoders were $0.1\,\mu$m and $81,000$ pulse/rev, respectively. The control software was written in C language under RTAI 3.6.1. The x-axis responses on the master side were transmitted to the slave side. Since the linear forceps robot has one-DOF motion, transformation from the joint space to the work space is not required. The y-axis motion of the master robot was fixed by using position control. Since the two-link manipulator was used on the master side, eq. (3.11) is rewritten as

$$\boldsymbol{m}_{\mathrm{n}} \;\;=\;\; \begin{bmatrix} m_{\mathrm{x}} & m_{\mathrm{xy}} \\ m_{\mathrm{yx}} & m_{\mathrm{y}} \end{bmatrix}. \tag{3.69}$$

The m_{x} denotes the equivalent mass in the direction of the x-axis. The m_{y} denotes similarly the equivalent mass in the direction of the y-axis. The m_{xy} and m_{yx} show the mass of the interference terms.

Table 3.5: Configurations of master manipulator.
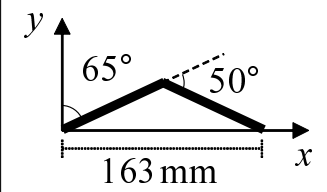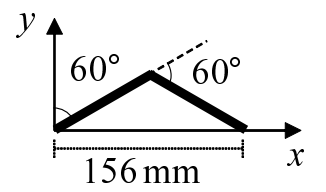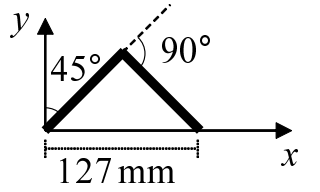
	Configuration A	Configuration B	Configuration C
(q_1, q_2)	(65, 50) [°]	(60, 60) [°]	(45, 90) [°]
$(x,\ y)$	(163, 0) [mm]	(156, 0) [mm]	(127, 0) [mm]
m_{x}	1.716650 kg	1.226420 kg	0.613210 kg
m_{y}	0.323674 kg	0.354486 kg	0.531728 kg

Fig. 3-33 shows the relationship between the configurations of the master manipulator and the elements of the equivalent mass matrices. In configuration A, the element of the equivalent mass matrix $\boldsymbol{m}_{\mathrm{n}}$ for the x-axis in the work space is almost the same as that in the slave system. Therefore, the nondiagonal elements of the task mass matrix $\boldsymbol{M}_{\mathrm{n}}$ are almost zero, as shown in Fig. 3-33(d).

Fig. 3-34, Fig. 3-35, and Fig. 3-36 show the experimental results of oblique coordinate control. On the other hand, Fig. 3-37, Fig. 3-38, and Fig. 3-39 show the experimental results of the decoupling method using MDOB. Fig. 3-40 indicates the root mean square error (RMSE) in each experiment. These figures confirm that the MDOB-based method performs better than oblique coordinate control. In particular, in Fig. 3-34(a) and Fig. 3-34(b), it can be seen that oblique coordinate control caused oscillation. Oblique coordinate control assumes that the system dynamics is nominalized by DOB, but there are some cases where the cutoff frequency is not high enough to change the dynamics in a multi-DOF system. Therefore, these results suggest that the control system was affected by the variation in the equivalent mass matrix, which caused modeling error. In fact, Fig. 3-33(a) indicates a rapid change in the equivalent mass matrix in configuration A. Furthermore, the position error in Fig. 3-35(a) is larger than that in Fig. 3-38(a).

However, Fig. 3-39(a) and Fig. 3-39(b) show that the MDOB-based system tended to be unstable. This result agrees with the analysis of Fig. 3-30. In configuration C, the difference between the equivalent mass of the master system for the x-axis and the slave mass was larger than in the other configurations, as shown in Fig. 3-33(a). This difference formed the nondiagonal elements of the task mass matrix, as shown in Fig. 3-33(d). In the MDOB-based system, the effect of the elements is input into the system as the disturbance force.
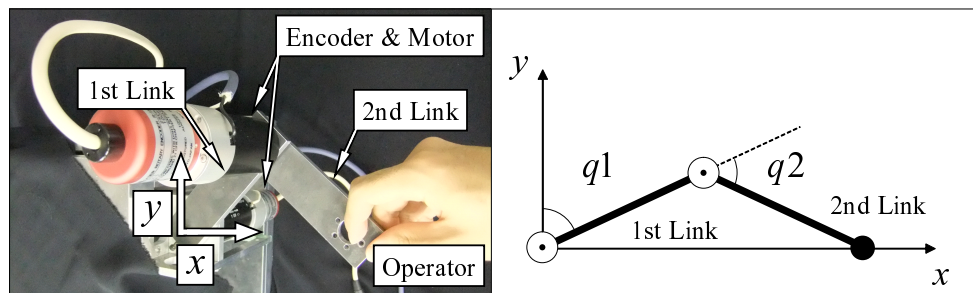
Fig. 3-31: Experimental setup on master side. (two-link manipulator)
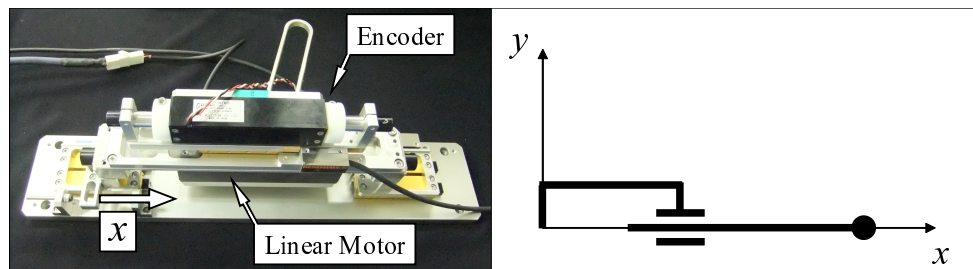
Fig. 3-32: Experimental setup on slave side. (linear forceps robot)
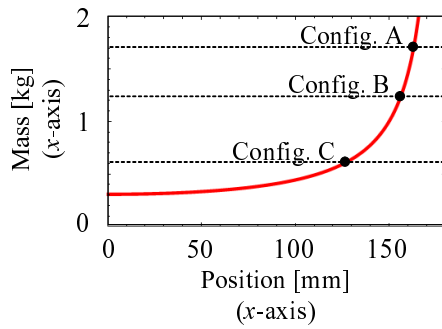
(a) Variation of m_x caused by change of configuration [see eq. (3.69)].
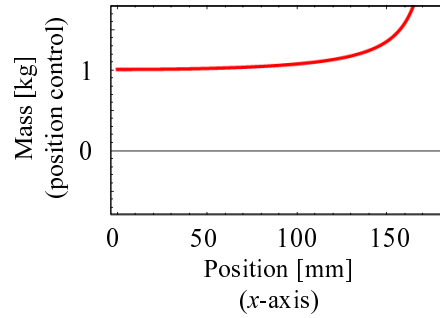
(b) Variation of M_{XX} caused by change of configuration [see eq. (3.41)].
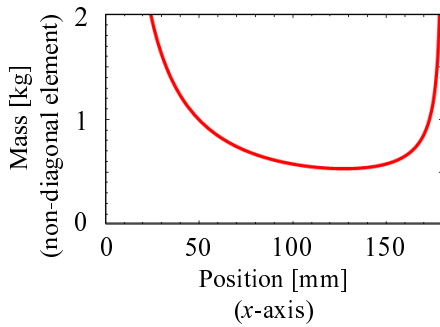
(c) Variation of m_{xy} and m_{yx} caused by change of configuration [see eq. (3.69)].
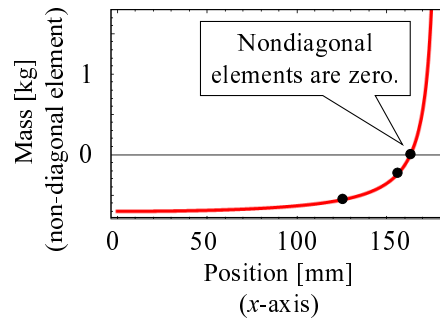
(d) Variation of M_{XF} and M_{FX} caused by change of configuration [see eq. (3.41)].
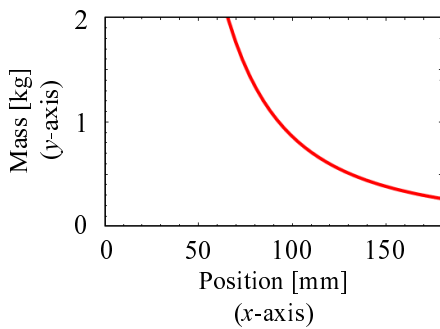
(e) Variation of m_y caused by change of configuration [see eq. (3.69)].
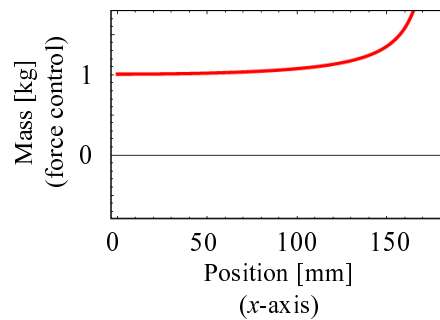
(f) Variation of M_{FF} caused by change of configuration [see eq. (3.41)].

Fig. 3-33: Relationship between configuration of manipulator and elements of equivalent mass matrices.
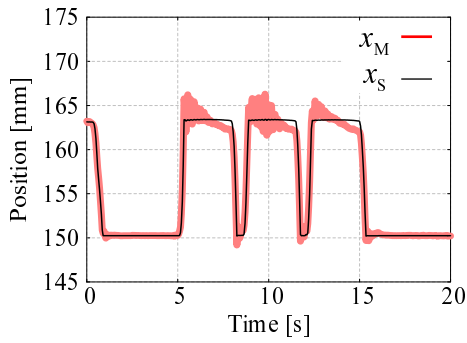
(a) Position response.
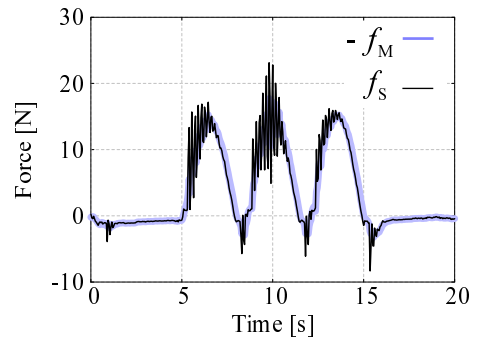
(b) Force response.

Fig. 3-34: Experimental result of oblique coordinate control. (Config. A)
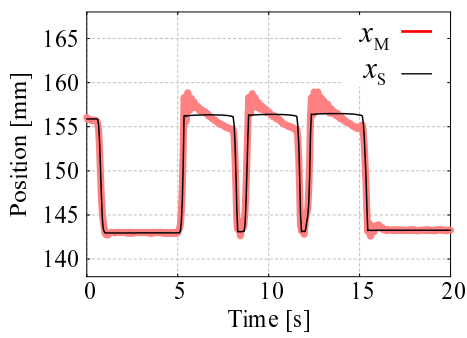
(a) Position response.
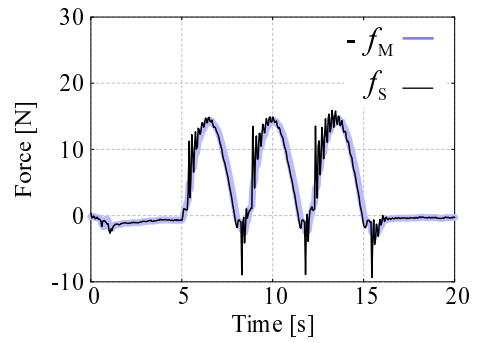
(b) Force response.

Fig. 3-35: Experimental result of oblique coordinate control. (Config. B)
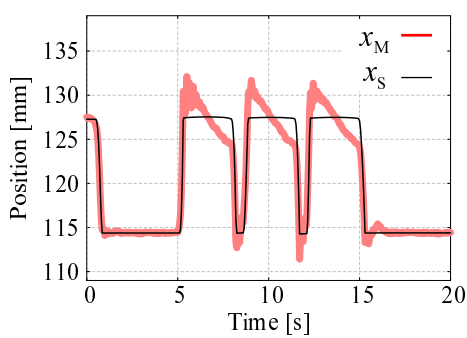
(a) Position response.
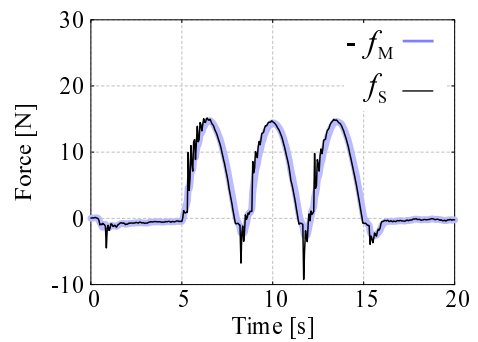
(b) Force response.

Fig. 3-36: Experimental result of oblique coordinate control. (Config. C)
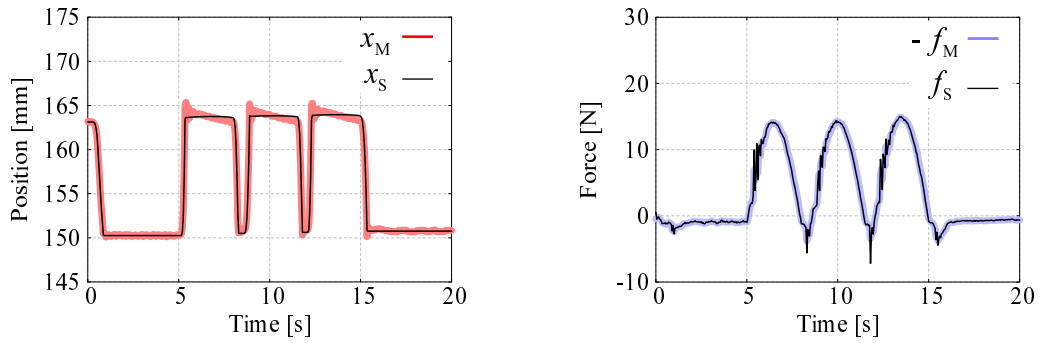
(a) Position response.

(b) Force response.

Fig. 3-37: Experimental result of MDOB-based decoupling. (Config. A)
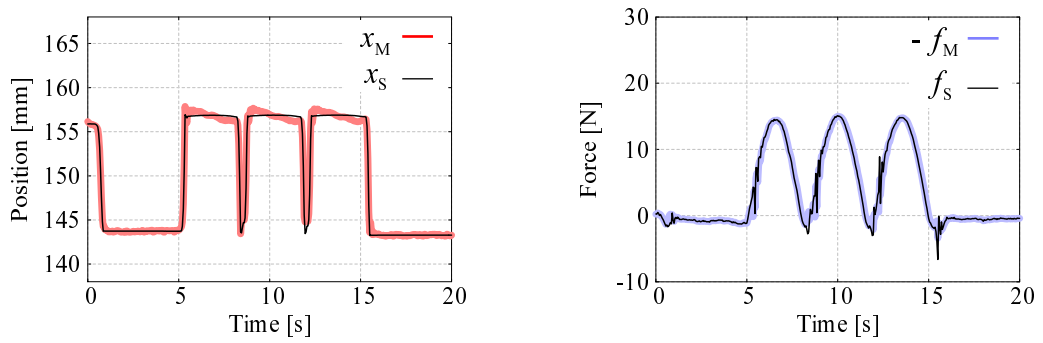
(a) Position response.

(b) Force response.

Fig. 3-38: Experimental result of MDOB-based decoupling. (Config. B)
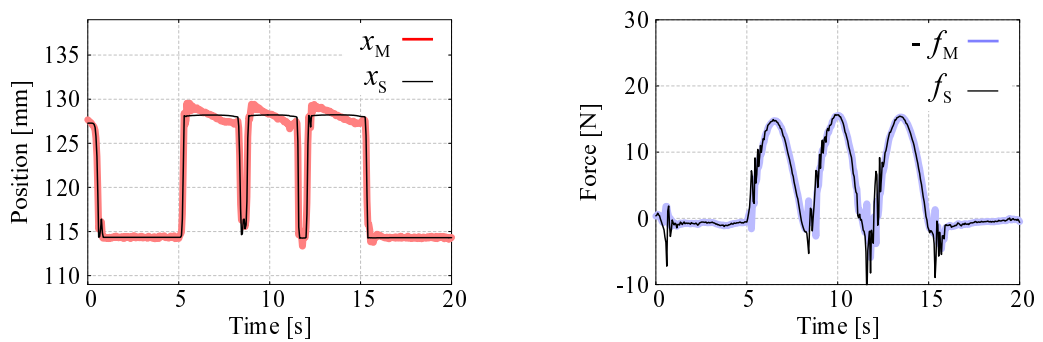
(a) Position response.

(b) Force response.

Fig. 3-39: Experimental result of MDOB-based decoupling. (Config. C)

(a) RMSE of position tracking.

(b) RMSE of force feedback.
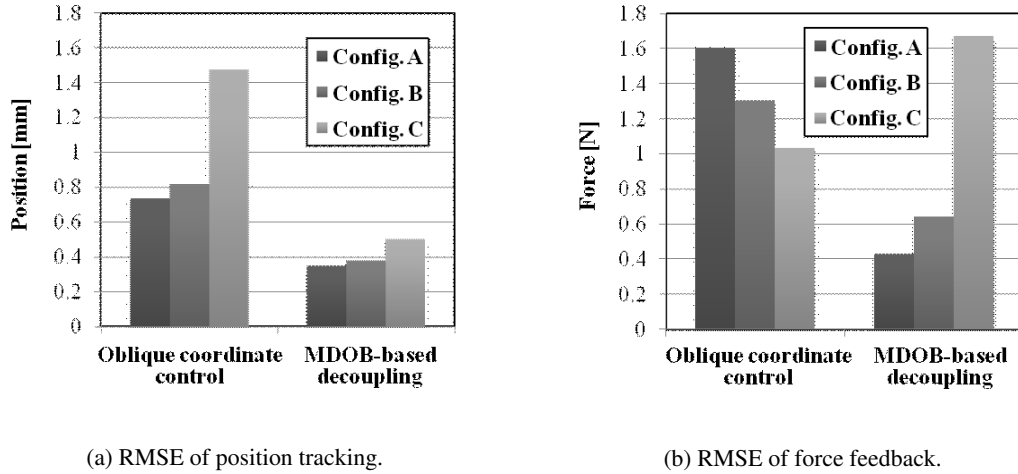
Fig. 3-40: Comparison of control performances.

3.3 Summary

This chapter introduced the research field of real-world haptics. This chapter also reviewed recent technical advances in real-world haptics, such as functionality and oblique coordinate control. The presented studies showed that a wide variety of system roles can be realized by combining pure position control and pure force control with appropriate coordinate transformation. The principle of this view was explained through two simple examples. For more details, please refer to the cited papers.

It has thus far been impossible to support some human activities that require contact with unstructured environments. However, real-world haptics may provide a solution to this problem. This technique has the potential to trigger industrial innovations in various fields, including agriculture, forestry, factories, medical services, and nursing care. This chapter extended the diagonalization method based on the MDOB and applied it to a multi-DOF system. This method succeeded in suppressing the interference between the position and force control systems, and realized a bilateral control system. The utility of the proposed method was experimentally verified by using a multi-DOF manipulator. The MDOB-based decoupling method had better performance comparing with oblique coordinate control. Conventional oblique coordinate control caused oscillation in cases where the modeling error was large and the observer cutoff frequency was not high enough to change the system dynamics. However, the MDOB-based decoupling method became unstable when the difference in mass was large.

Chapter 4

Extraction of Human Motion

Tendon-driven rotary actuators are utilized in various robots because they are small and generate high output. However, if the tendon-driven rotary actuators are utilized in bilateral control system, they have two problems. The first problem is interference. Bilateral control systems with tendon-driven mechanisms require decoupling of angle tracking, torque feedback, and tension control both on the master and the slave side. The second problem is elongation. The tendons are extended by applied force. Therefore, precise control of the angle is difficult.

The first half of this chapter introduces a developed tendon-driven robot hand. Since the developed robot hand has almost the same size as human hand, this robot hand enables to extract human motion adequately. In addition, a bilateral control system for tendon-driven robots are also proposed in this chapter. Both position and force information can be acquired through the developed robot hand by employing the bilateral control. To implement the bilateral control, the characteristic of wires should be taken into account. The wires can transmit only pulling force. To overcome the disadvantage, antagonistic structure is adopted in this proposed control system. Furthermore, the concept of the modal transformation is used to control the tension, the rotation angle, and the torque simultaneously.

In this chapter, a method to compensate the error caused by the tendon elongation for tendon-driven mechanisms is also proposed. The validity of the proposed method is verified by experiments. Elongation is reduced by the proposed method. Experiments are conducted to confirm the validity of the proposed method.

The second half of this chapter proposes a bilateral control system for robots with different configurations. Conventional bilateral controllers have been designed on the basis of a tool coordinate system.

However, from the viewpoint of versatility, a transformation technique based on physical features of an operator is advantageous. Therefore, this chapter proposes a bilateral control technique that can be used to operate slave robots: the technique is based on motion features of an operator and facilitates intuitive operation. Here, motion features imply displacement ratios of joints. A coordinate transformation matrix containing the motion features of the operator is obtained by principal component analyses. The transformation matrix can be used to abstract the motion features, while other transformation matrices require symmetric motion or symmetric sensor placement. The validity of the proposed bilateral control method is experimentally verified. In an experiment, the proposed method is applied to a wearable robot hand and a forceps robot. A grasping motion extracted by the wearable robot hand is transmitted to the forceps robot on the basis of the obtained coordinate transformation matrix.

4.1 Introduction

The first half of this chapter describes acquisition of haptic information. Operators who are on a master side can feel reaction force from an environment that is on a slave side through master-slave systems. However, human hands are small and have a number of DOF over the conventional master-slave systems. The number of DOF is not sufficient to support human activities. A lot of studies about robot hands including Utah/MIT Hand [85] by Jacobsen *et al.*, Omni Hand [86] by Rosheim, DLR Hand [87] by Knoch *et al.*, and Gifu Hand [88, 89] by Kawasaki *et al.* have been conducted. However, these conventional robot hands are not suitable as master-slave systems for real-world haptics because of the friction and backlash. Besides, robot hands become large and heavy if an actuator is employed at each joint.

For increasing the number of DOF, saving the weight of the driven system, and reducing the effect of friction, a study has been conducted to rotate joints by using tendon-driven mechanisms . One of the drawbacks is that the tendon-driven mechanisms can transmit only a pulling motion, as the tendons slack in pushing motion. Antagonistic control [90] can compensate for the shortcoming. There are a lot of studies focusing on only the bilateral control systems or only the tendon-driven robots. However, there are few studies that apply the bilateral control systems to the tendon-driven robots. Recently, several surgery robots have been developed that use tendon-driven mechanisms to reduce the weight of the arms. However, these surgery robots can not transmit haptic sensation, since it has high reduction ratio [91, 92]. Though Suzuki *et al.* tried to transmit haptic sensation by using the bilateral control and thrust wires [93],

the force information was degraded because of the friction and buckling of the wires.

The first half of this chapter describes a developed tendon-driven robot hand (Haptic Data Acquisition Robot Hand : HDARH). In addition, this chapter proposes a bilateral control for tendon-driven robots (Tendon-Driven Bilateral Control System : TDBC). This proposed system controls a joint by two motors. Finally, an multi-DOF robot hand for real-world haptics is realized by employing HDARH on TDBC. HDARH is designed so that the frictional force applied on the wires is reduced, as the aims of this robot hand are not only reducsion in size and weight but also transmition of haptic sense. TDBC is a force-sensorless and acceleration-based control system using DOB [29] and RFOB [34]. The control system is robust against the disturbance. The size and the number of DOF of HDARH are almost equal to human hands. Therefore, this robot hand is suitable to extract haptic information of human. This information is useful for working in a dangerous situation, cultivation of crops, technical tradition of skilled workers, surgery, and care.

There is a research, which put the tendon-driven mechanisms into three categories [94]. Those are N type, N+1 type, and 2N type. Especially, 2N type has superior performance, and utilized in various robot hands [85,95]. Design goals for the antagonistic controller have been investigated [94]. Then, in order to satisfy the design goals, some controllers were proposed [96]. However, because of saturation function, these proposed controllers are not appropriate to achieve bilateral teleoperation. There is a study with a bilateral teleoperation using the tendon-driven mechanisms [56]. However, the elongation was not considered. While there is a study concerning a bilateral teleoperation and elongation, identifications are required to construct wire models [57]. Therefore, the first half of this chapter also proposes a method to compensate wire elongation. Since this compensation method is also on the basis of the modal transformation as follows, it can be applied to the above-mentioned bilateral control without deteriorating the performance.

(1) Position response and force response is transformed into common mode and differential mode.

(2) Tension force is controlled in master side and slave side in common mode.

(3) Length of elongation is calculated in common mode.

(4) Precise angle tracking and torque feedback is achieved by using differential mode for position and differential mode force.

The validity of the proposed method is confirmed by an experiment.

The second half of this chapter describes extraction of motion feature and its transmission. Research related to the bilateral control systems is classified broadly into two types: studies of master-slave systems that have the same configurations and studies of master-slave systems that have different configurations. The design of a control system is easy when the configurations of the master and slave systems are the same, because the ranges of movement and inertia are symmetrical. In many cases, however, the required specifications of the master robot and slave robot are different. For example, small slave robots suitable for detail-related work are required for minimally invasive surgeries and the manipulation of cells. Large slave robots suitable for large-scale work are needed for space-based applications and civil engineering. However, master robots with sizes that are suitable for use by humans are required. In light of these requirements, scaling bilateral control systems that transmit amplified position and force information from the slave side to the master side [97] and bilateral control systems with different inertias have been proposed [98]. In contrast, studies of master-slave systems with different configurations have compared control systems based on joint space [33] to control systems based on work space [99][34] by using multi-link manipulators [100]. In addition, methods to preserve and reproduce human motion have been studied using master-slave systems with different configurations [101]. Studies of master-slave systems with different configurations have focused not only on structural differences but also the required roles of the master and slave robots. Specifically, bilateral control systems with dimensional scaling [102] and bilateral control systems with gyrator properties [103] have been proposed. The dimensional scaling method makes it possible to operate mobile robots by using joysticks with tactile sensation. In bilateral control systems with gyrators, transformer- and gyrator-type mechanisms are integrated, and the velocity of the slave robot responds to the force of the master robot. Furthermore, a method for a multiple master-robot system that controls one slave robot has also been proposed to account for differences between the number of master and slave robots [64].

In the above situations, operators treat a master robot as a tool. However, to allow more intuitive operation, the slave robot should represent the characteristic of human motion. Given that the operators are human, wearable robots are suitable master robots.

In general, wearable sensor systems and vision-based capturing systems have been utilized for abstract motion characteristics [104–106]. However, these conventional systems are not suitable to be applied to teleoperation, because the conventional systems are incapable of acquiring force information or generating a force. Moreover, depending on the coordinate settings, dynamical interference occurs in teleoperation systems.

The second half of this chapter proposes a method to operate slave robots based on motion features. Here, motion features represent the displacement ratios of joints. In the proposed method, position information related to a grasping motion is first extracted using a wearable robot hand. Next, a dominant coordinate system for the grasping motion is calculated by principal component analysis (PCA). The dominant coordinate system is suitable for an abstract representation of the motion features, whereas other transformation matrices used in bilateral control systems (i.e., the Hadamard matrix, quarry matrix, and discrete Fourier transform matrix) require symmetric motion or symmetric sensor placement. Finally, the grasping motion is transmitted to the slave robot based on the calculated coordinate system.

This chapter is organized as follows: The first part of this chapter describes the developed robot hand for motion extraction. Section 4.2.1 presents the developed robot hand. Section 4.2.2 describes the proposed bilateral control system for tendon-driven robots. The experimental results of the proposed bilateral control system are shown in section 4.2.3. The middle part of this chapter shows the compensation method for wire expansion. To compensate wire elongation, section 4.3.1 describes the model of the tendon-driven mechanism. In section 4.3.2, proposed compensation method for the wire elongation for tendon-driven mechanisms is explained. The experimental results of the compensation method are shown in section 4.3.3. The last part of this chapter proposes a bilateral control method for intuitive operation in different structured robots. Section 4.4.1 describes the wearable robot hand (master robot) and forceps robot (slave robot) used in this chapter. Section 4.4.2 presents the results of an analysis of the grasping motion based on PCA. The proposed bilateral control system for master-slave systems with different configurations is explained in section 4.4.3. The experimental results are shown in section 4.4.4. This chapter is finally concluded in section 4.5.
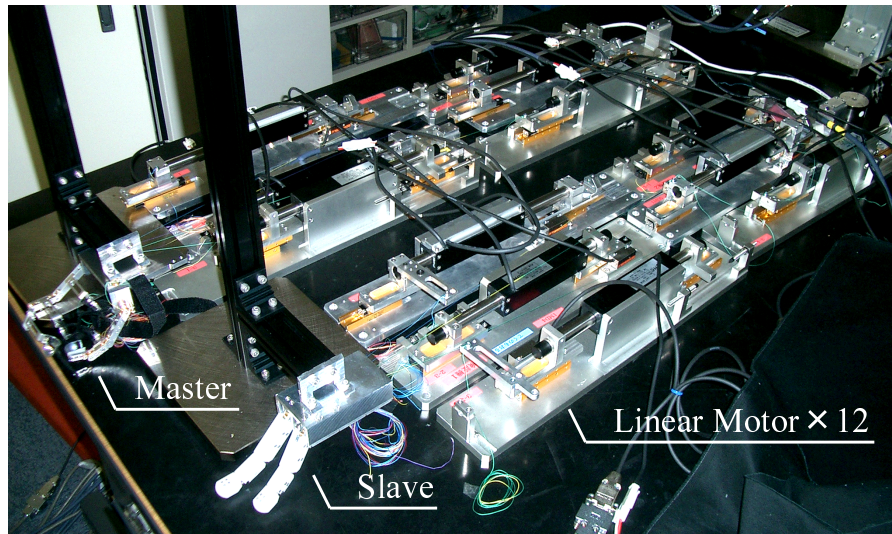
Fig. 4-1: Experimental setup.
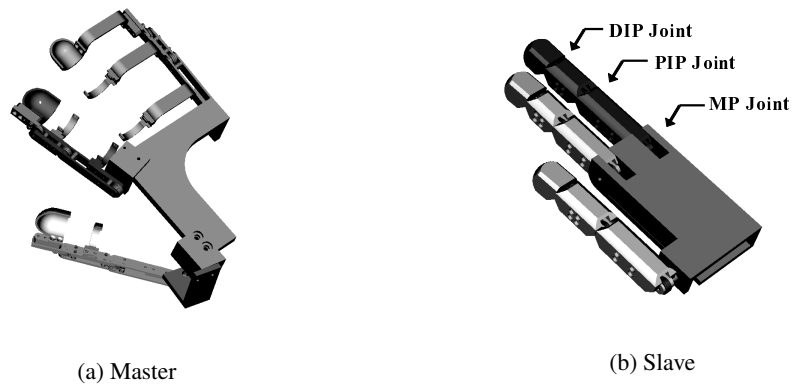
(a) Master

(b) Slave

Fig. 4-2: Overview of haptic data acquisition robot hand.

4.2   Acquisition of Haptic Data

4.2.1   Master-Slave Robot Hands Using Tendon-Driven Mechanisms

An 11-DOF master-slave robot hand has been developed. The name of the robot hand is HDARH. HDARH has a thumb, index, and middle fingers that have 4-DOF, 4-DOF, and 3-DOF, respectively. These composition makes it possible to be the same configulations as human hands. In order to reduce position difference between the operator and environment, master and slave robot have an exoskeleton
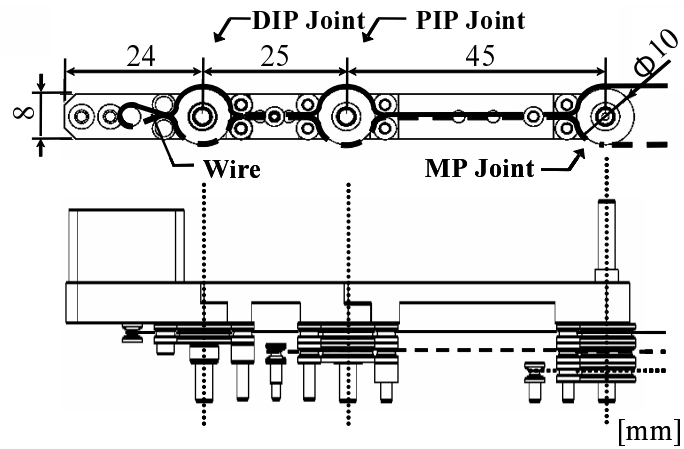
Fig. 4-3: Wire setup.

and an endoskeleton mechanisms, respectively. Fig. 4-1 and Fig. 4-2 show the overview of HDARH. The middle finger has three joints that are referred to as metacarpophalangeal joint (MP joint), proximal interphalangeal joint (PIP joint), and distal interphalangeal joint (DIP joint) in order from the base. Fig. 4-3 shows the setup of the wire. One end of the wire is attached to a linear motor and the other end is attached to a pulley joint. The wires make a contact with the robot hand only at the joint with bearing and guide parts. The little contact surface reduces the effect of friction. Links and wires are arranged in the same manner on the master and slave side. The mechanism makes it possible to avoid interference between the bending of the joints and the length of the wires.

Table 4.1: Four tasks that tendon-driven bilateral control system perform.

Task A	Tension Control in Master Side
Task B	Tension Control in Slave Side
Task C	Position Tracking
Task D	Law of Action and Reaction
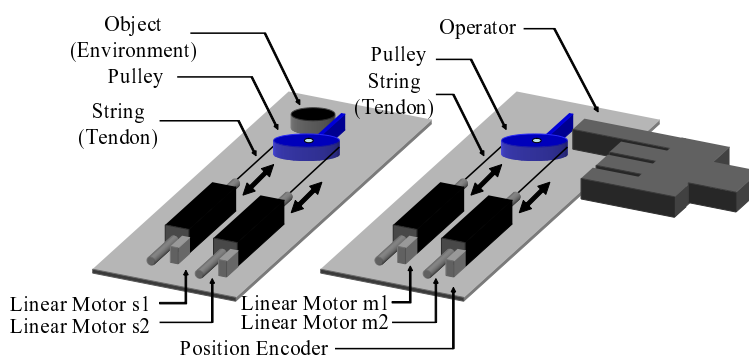
Fig. 4-4: Setup of tendon-driven bilateral control system.

4.2.2 Biletarel Control System for Tendon-Driven Robots

Every joint consists of a joint, wires, and four linear motors, and works as a master-slave system. Fig. 4-4 shows a construction of TDBC that controls one joint. Optical position encoders are employed on the each linear motor to measure the motor position, $x_{\mathrm{m1}}^{\mathrm{res}}$, $x_{\mathrm{m2}}^{\mathrm{res}}$, $x_{\mathrm{s1}}^{\mathrm{res}}$, $x_{\mathrm{s2}}^{\mathrm{res}}$. RFOB is also employed to estimate the reaction force, $\hat{f}_{\mathrm{m1}}^{\mathrm{res}}$, $\hat{f}_{\mathrm{m2}}^{\mathrm{res}}$, $\hat{f}_{\mathrm{s1}}^{\mathrm{res}}$, $\hat{f}_{\mathrm{s2}}^{\mathrm{res}}$. Fig. 4-5 and Fig. 4-6 show the concept of this control system and the block diagram of the proposed TDBC, respectively. TDBC converts 4-DOF of the 4 linear motors into 4 tasks that are shown in Table 4.1.

To control the joints by using wires, the wires must be pulled. Therefore, the wire tensions are controlled to keep at a positive value. This tension control is defined as Task A and Task B on the master side and the slave side, respectively. Position tracking is defined as Task C. Force feedback to achieve law of action and reaction artificially is realized in Task D.

This chapter defines three types of modal space: an actuator space (AS), a muscle modal space (MMS), and a joint modal space (JMS). Actuators are controlled in the actuator space. The tedon driven robots are controlles in the muscle modal space, and reference values for the bilateral control are calculated in the joint modal space. The joint modal space consists of two modes: one is used for position tracking, and the other is employed for force feedback. A transformation matrix from the actuator space to the
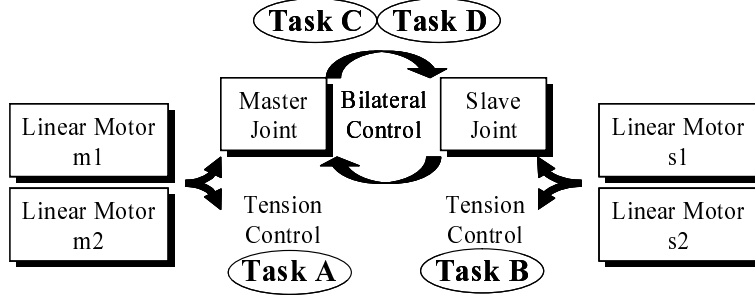
Fig. 4-5: Concept of tendon-driven bilateral control system.
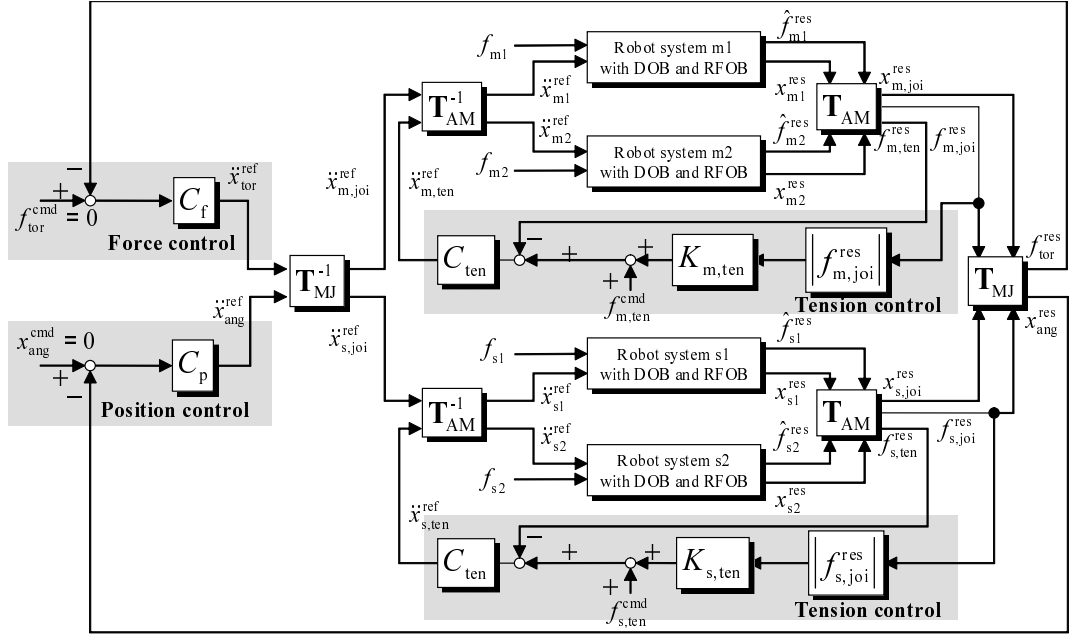
Fig. 4-6: Block diagram of tendon-driven bilateral control system.

muscle modal space is defined as

$$\mathbf{T}_{\mathrm{AM}} \quad := \quad \begin{bmatrix} 1 & 1 \\ 1 & -1 \end{bmatrix}. \tag{4.1}$$

A transformation matrix from the actuator space to the muscle modal space is also defined as

$$\mathbf{T}_{\mathrm{MJ}} \quad := \quad \begin{bmatrix} 1 & 1 \\ 1 & -1 \end{bmatrix}. \tag{4.2}$$

Variables of the muscle modal space, $x_{\mathrm{m,joi}}^{\mathrm{res}}$, $x_{\mathrm{s,joi}}^{\mathrm{res}}$, $f_{\mathrm{m,joi}}^{\mathrm{res}}$, $f_{\mathrm{s,joi}}^{\mathrm{res}}$, $f_{\mathrm{m,ten}}^{\mathrm{res}}$, $f_{\mathrm{s,ten}}^{\mathrm{res}}$ are calculated as

$$
\begin{bmatrix} f^{\mathrm{res}}_{\mathrm{m,ten}} & * \\ f^{\mathrm{res}}_{\mathrm{m,joi}} & x^{\mathrm{res}}_{\mathrm{m,joi}} \end{bmatrix} \quad := \quad \mathbf{T}_{\mathrm{AM}} \begin{bmatrix} \hat{f}^{\mathrm{res}}_{\mathrm{m1}} & x^{\mathrm{res}}_{\mathrm{m1}} \\ \hat{f}^{\mathrm{res}}_{\mathrm{m2}} & x^{\mathrm{res}}_{\mathrm{m2}} \end{bmatrix}, \tag{4.3}
$$

$$
\begin{bmatrix} f^{\mathrm{res}}_{\mathrm{s,ten}} & * \\ f^{\mathrm{res}}_{\mathrm{s,joi}} & x^{\mathrm{res}}_{\mathrm{s,joi}} \end{bmatrix} \quad := \quad \mathbf{T}_{\mathrm{AM}} \begin{bmatrix} \hat{f}^{\mathrm{res}}_{\mathrm{s1}} & x^{\mathrm{res}}_{\mathrm{s1}} \\ \hat{f}^{\mathrm{res}}_{\mathrm{s2}} & x^{\mathrm{res}}_{\mathrm{s2}} \end{bmatrix}. \tag{4.4}
$$

For the sake of ease, the elements that are not used in this chapter are described as "$*$". In the muscle modal space, acceleration references for the achievement of task A and B are calculated as

$$
\ddot{x}^{\mathrm{ref}}_{\mathrm{m,ten}} \quad = \quad C_{\mathrm{ten}}(K_{\mathrm{m,ten}}|f^{\mathrm{res}}_{\mathrm{m,joi}}| + f^{\mathrm{cmd}}_{\mathrm{m,ten}} - f^{\mathrm{res}}_{\mathrm{m,ten}}), \tag{4.5}
$$

$$
\ddot{x}^{\mathrm{ref}}_{\mathrm{s,ten}} \quad = \quad C_{\mathrm{ten}}(K_{\mathrm{s,ten}}|f^{\mathrm{res}}_{\mathrm{s,joi}}| + f^{\mathrm{cmd}}_{\mathrm{s,ten}} - f^{\mathrm{res}}_{\mathrm{s,ten}}). \tag{4.6}
$$

The minimum value of the tension can be set by $f^{\mathrm{cmd}}_{\mathrm{m,ten}}$ and $f^{\mathrm{cmd}}_{\mathrm{s,ten}}$. The effect of generated torque on the tension can be adjust by changing $K_{\mathrm{m,ten}}$ and $K_{\mathrm{s,ten}}$. Propotional controllers are used for tension control as

$$
C_{\mathrm{ten}} = K_{\mathrm{ten}}. \tag{4.7}
$$

Variables of the joint modal space, $x^{\mathrm{res}}_{\mathrm{ang}}$ and $f^{\mathrm{res}}_{\mathrm{tor}}$ are defined as

$$
\begin{bmatrix} f^{\mathrm{res}}_{\mathrm{tor}} & * \\ * & x^{\mathrm{res}}_{\mathrm{ang}} \end{bmatrix} \quad := \quad \mathbf{T}_{\mathrm{MJ}} \begin{bmatrix} f^{\mathrm{res}}_{\mathrm{m,joi}} & x^{\mathrm{res}}_{\mathrm{m,joi}} \\ f^{\mathrm{res}}_{\mathrm{s,joi}} & x^{\mathrm{res}}_{\mathrm{s,joi}} \end{bmatrix}. \tag{4.8}
$$

In the joint modal space, acceleration references for the achievement of task C and D are calculated as

$$
s^2 x^{\mathrm{ref}}_{\mathrm{tor}}(s) \quad = \quad -C_{\mathrm{f}} f^{\mathrm{ref}}_{\mathrm{tor}}(s), \tag{4.9}
$$

$$
s^2 x^{\mathrm{ref}}_{\mathrm{ang}}(s) \quad = \quad -C_{\mathrm{p}}(s) x^{\mathrm{ref}}_{\mathrm{ang}}(s). \tag{4.10}
$$

Proportional controller is used as the force controller, and proportional-derivative controller is utilized as the position controller in this chapter. The force controller and position controller can be expressed as

$$
C_{\mathrm{f}} \quad = \quad K_{\mathrm{f}}, \tag{4.11}
$$

$$
C_{\mathrm{p}}(s) \quad = \quad K_{\mathrm{p}} + K_{\mathrm{v}}s. \tag{4.12}
$$

The acceleration reference of the joint modal space is transformed into the muscle modal space by using the inverse matrix of $\mathbf{T}_{\mathrm{MJ}}$ as

$$
\begin{bmatrix} \ddot{x}^{\mathrm{ref}}_{\mathrm{m,joi}} \\ \ddot{x}^{\mathrm{ref}}_{\mathrm{s,joi}} \end{bmatrix} \quad = \quad \mathbf{T}^{-1}_{\mathrm{MJ}} \begin{bmatrix} \ddot{x}^{\mathrm{ref}}_{\mathrm{tor}} \\ \ddot{x}^{\mathrm{ref}}_{\mathrm{ang}} \end{bmatrix}. \tag{4.13}
$$

Table 4.2: Parameters in experiment.

Parameter	Meaning of The Parameter	Value
K_p	Position feedback gain	1600
K_v	Velocity feedback gain	80
K_f	Force feedback gain	1
K_ten	Force Feedback Gain	1
$K_\mathrm{m,ten}$	Parameter of tension	1
$K_\mathrm{s,ten}$	Parameter of tension	1
g_dis	Cutoff frequency of DOB	700 rad/s
g_reac	Cutoff frequency of RFOB	700 rad/s
M_n	Nominal mass	0.5 kg

Similarly, the acceleration reference of the muscle modal space is transformed into the actuator modal space by using the inverse matrix of $\mathbf{T}_\mathrm{AM}$ as

$$
\begin{bmatrix} \ddot{x}_\mathrm{m1}^\mathrm{ref} & \ddot{x}_\mathrm{s1}^\mathrm{ref} \\ \ddot{x}_\mathrm{m2}^\mathrm{ref} & \ddot{x}_\mathrm{s2}^\mathrm{ref} \end{bmatrix} = \mathbf{T}_\mathrm{AM}^{-1} \begin{bmatrix} \ddot{x}_\mathrm{m,joi}^\mathrm{ref} & \ddot{x}_\mathrm{s,joi}^\mathrm{ref} \\ \ddot{x}_\mathrm{m,ten}^\mathrm{ref} & \ddot{x}_\mathrm{s,ten}^\mathrm{ref} \end{bmatrix}.
\tag{4.14}
$$

As described above, the acceleration references of the linear motors are obtained.
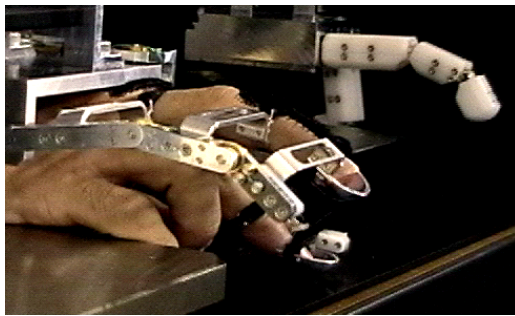
(a) Free motion 1.
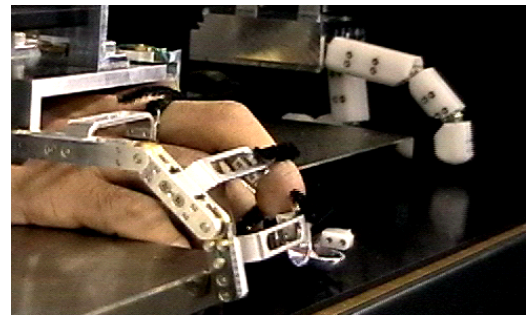
(b) Free motion 2.

Fig. 4-7: Free motion.
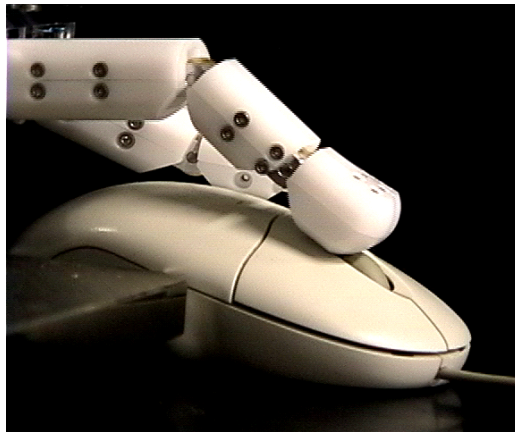
(a) Operating the mouse.
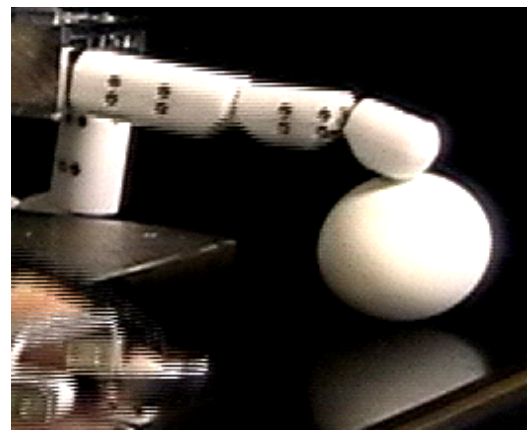
(b) Rolling the egg.

Fig. 4-8: Contact motion.

4.2.3   Experiments

Experiments were conducted by using the middle finger. Totally, 12 linear motors were used to employ TDBC at each joint of HDARH. Table 4.2 lists the experimental parameters. The nominal mass used in DOB was set as equal to the motor shaft, since the mass of the robot fingers were negligibly small in comparison with the motor shafts. Polyethylene lines which were made by YGK Yotuami were used as tendon wires.

HDARH performed poke, roll, stroking, pressing operations. For example, Fig. 4-7, Fig. 4-8(a), Fig. 4-8(b), and Fig. 4-9 show free motion, mouse operation, rolling the egg, and standing the Scotch tape, respectively. These motions require a lot of DOF, precise position control, and fine force control. The conventional robots, which are based on only the position control scheme, are incapable to realize
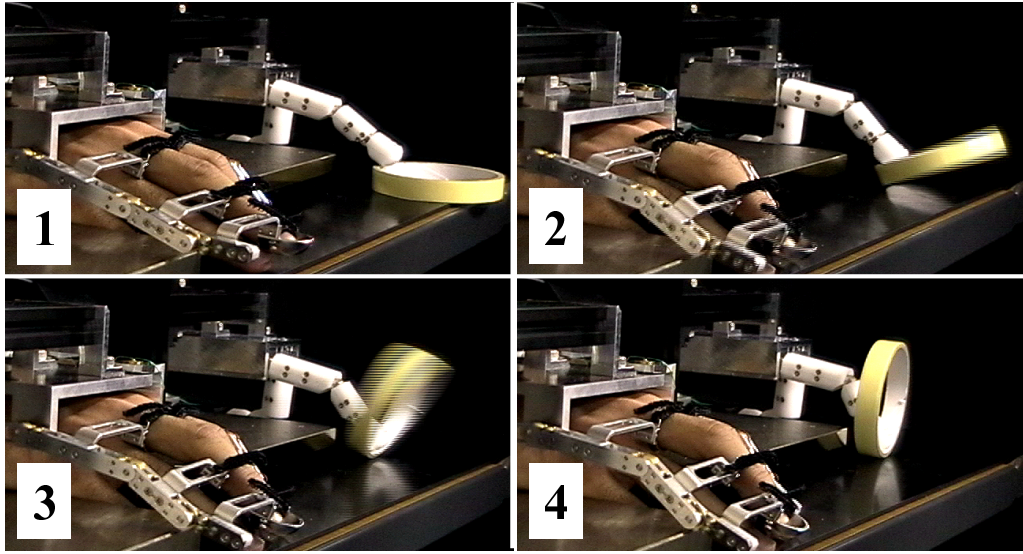
Fig. 4-9: Lifting a roll of Scotch tape such that it becomes vertical.

such kind of motions.

Free Motion and Contact Motion

The operator bended the finger for three times from 20 s to 25 s as a free motion. The slave robot made a contact with soft environment (sponge) for three times from 25 s to 32 s. Similarly, the slave robot made a contact with hard environment (aluminum block) for three times from 32 s to 37 s. Fig. 4-10–Fig. 4-12 show the results. Fig. 4-10, Fig. 4-11, and Fig. 4-12 indicate the results of MP joint, PIP joint, and DIP joint, respectively. Experimental results measured only after 20s are shown, as it took 20 s for the operator to wear the master robot hand. (a) of Fig. 4-10–Fig. 4-12 confirm that task A was achieved at every joint, since $\hat{f}_{\mathrm{m1}}^{\mathrm{res}}$ and $\hat{f}_{\mathrm{m2}}^{\mathrm{res}}$ were always kept as positive value. Similarly, (b) of Fig. 4-10–Fig. 4-12 represent the realization of task B. In (c) of Fig. 4-10–Fig. 4-12, $x_{\mathrm{m,joi}}^{\mathrm{res}}$ is same as the $x_{\mathrm{s,joi}}^{\mathrm{res}}$. Above results confirm that task C was achieved at the every joint. Furthermore, $f_{\mathrm{m,joi}}^{\mathrm{res}}$ is in agreement with $-f_{\mathrm{s,joi}}^{\mathrm{res}}$ in (d) of Fig. 4-10–Fig. 4-12. Therefore, these results show that task D was fulfilled at every joint. As mentioned above, realization of all tasks is confirmed at the all joints.
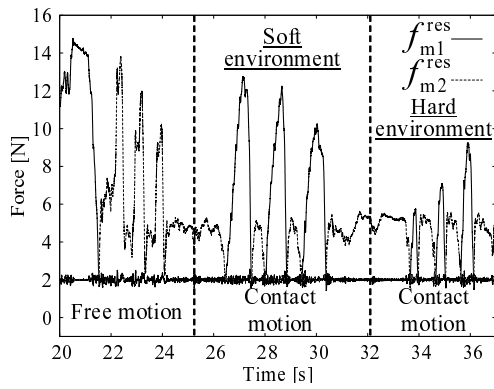
(a) Force response - Task A.
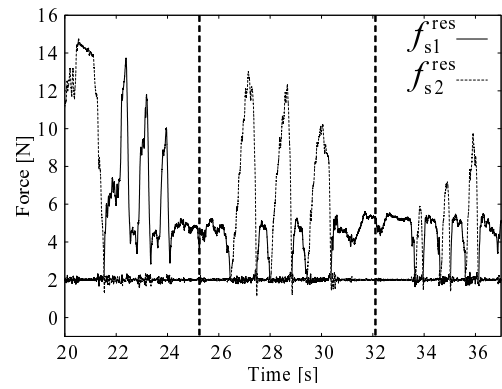
(b) Force response - Task B.
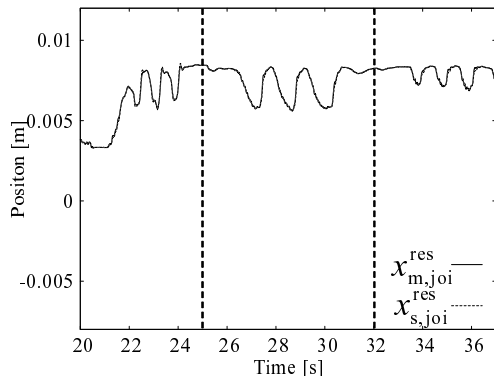
(c) Position response - Task C.
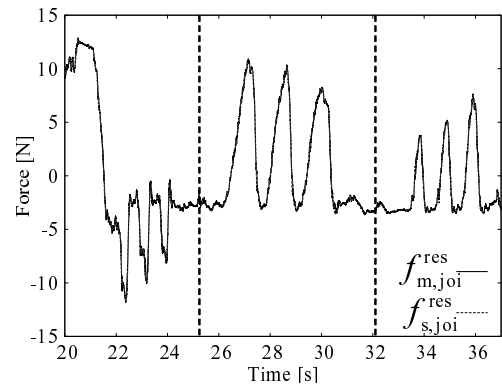
(d) Force response - Task D.

Fig. 4-10: MP joint.
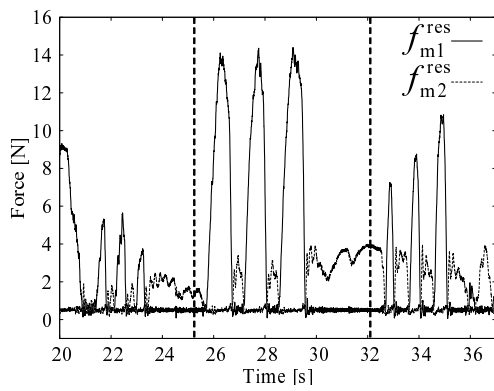
(a) Force response - Task A.
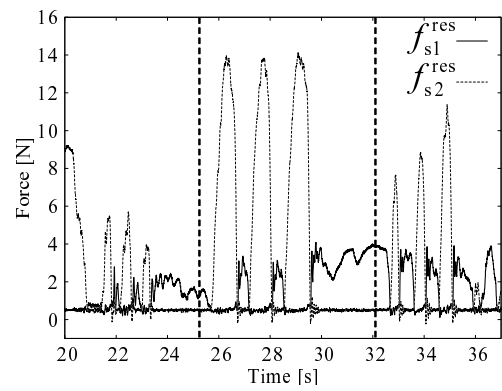
(b) Force response - Task B.
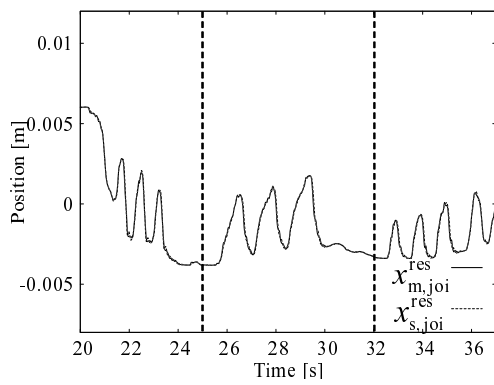
(c) Position response - Task C.
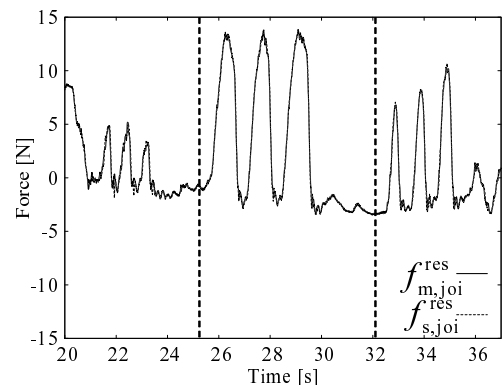
(d) Force response - Task D.

Fig. 4-11: PIP joint.
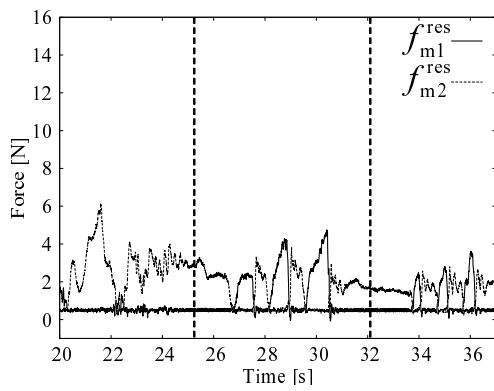
(a) Force response - Task A.
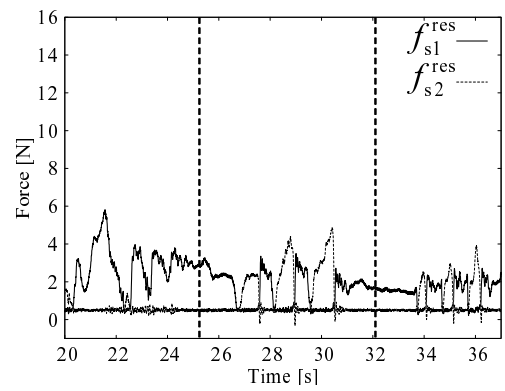
(b) Force response - Task B.
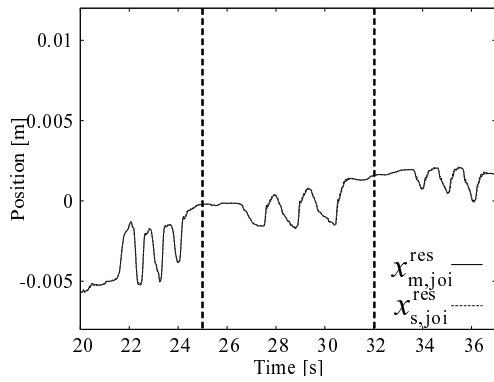
(c) Position response -Task C.
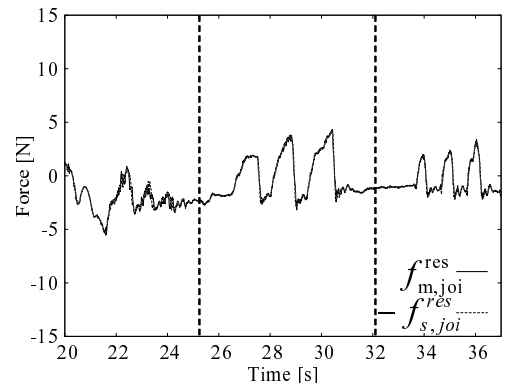
(d) Force response - Task D.

Fig. 4-12: DIP joint.

(a) Force response.

(b) 1st click.

(c) 2nd click.

(d) 3rd click.
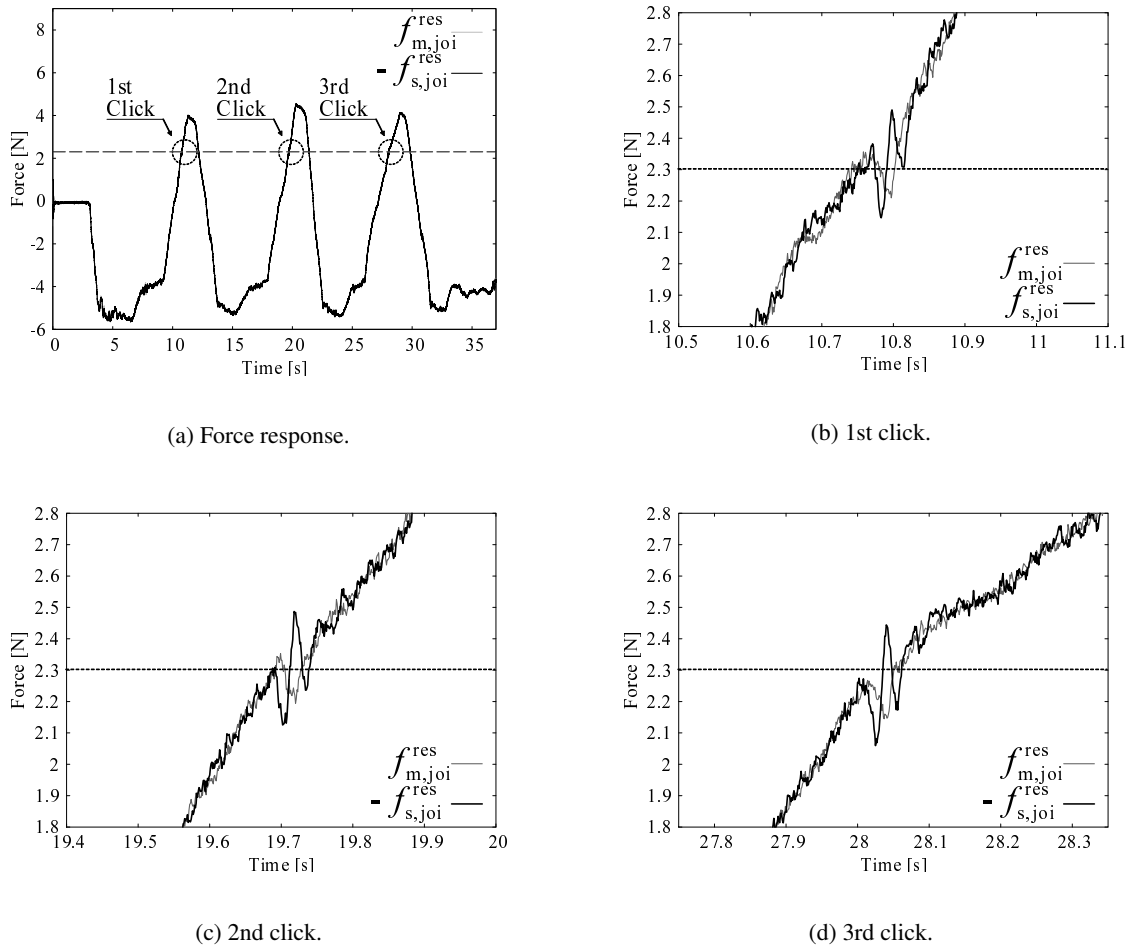
Fig. 4-13: Force response when clicking a motion.

Extraction of Haptic Information

Fig. 4-13 shows the force response of MP joint. The operator clicked the mouse for three times as represented in Fig. 4-13(a). Fig. 4-13(b), Fig. 4-13(c), and Fig. 4-13(d) are magnified figures in the vicinity of 10.80 s, 19.70 s, and 28.05 s, respectively. Haptic information concerning the click operation of the mouse with the force of about 2.3 N was extracted successfully as shown in Fig. 4-13.

(a) Position response.

(b) Force response.
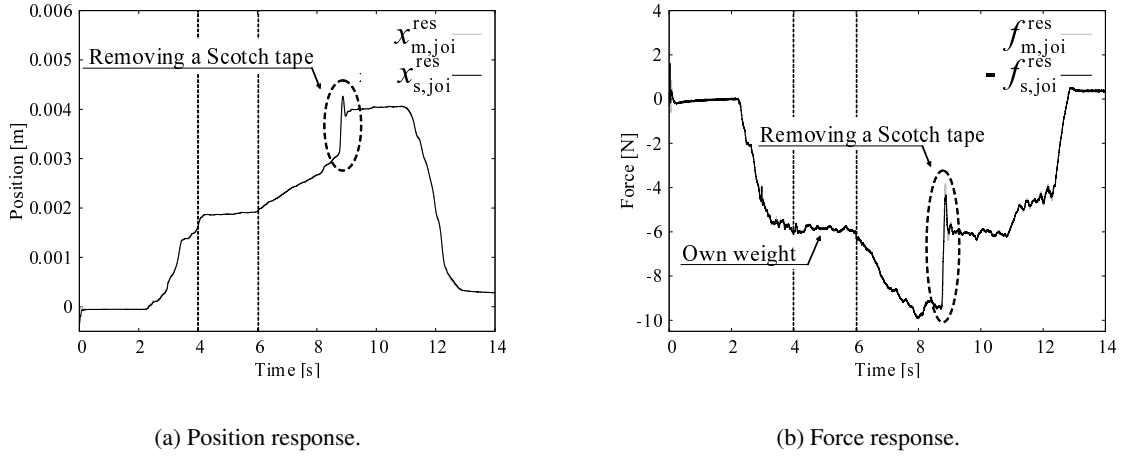
Fig. 4-14: Response when a Scotch tape is removed.

Table 4.3: Remove the Scotch tape.

Time	Motion
0s〜4s	Raise finger
4s〜6s	Keep the position
6s〜8.5s	Pull the Scotch tape
8.5s	Remove the Scotch tape

The operator removed a strip of scotch tape from the floor. One side of the scotch tape was attached to the floor and the other end was attached to HDARH. Fig. 4-14(b) and Fig. 4-14(a) show the force response and position response, respectively. Table 4.3 lists the transitions of the motion. The responses are rapidly changed around 8.5 s. This result shows that haptic information of the removing motion was obtained successfully.
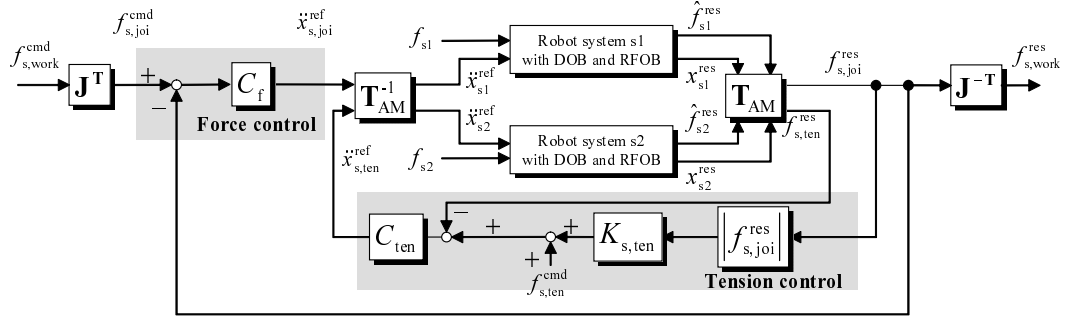
Fig. 4-15: Block diagram of force control.

Frequency Response

The sine wave responses were measured to quantitatively evaluate the performance of this haptic device. Frequency responses between the master and slave robot has been already analyzed by Natori *et al.* [107]. The study showed high transparency up to about 15 Hz. Therefore, force frequency response between the motors and the robot hand was confirmed. A force control system shown in Fig. 4-15 was used, as position and force control can be decoupled in the ideal acceleration-based bilateral control. Command value $f_{\text{s,work}}^{\text{cmd}}$ was given to the motors to drive MP joint. Applied force at the tip of the finger was measured by using a force sensor. The relationships between the joint torque and the tip force was identified in advance, and modeled as

$$f_{\text{s,work}}^{\text{cmd}} \quad = \quad 9.25 \times f_{\text{s,joi}}^{\text{cmd}}. \tag{4.15}$$

Fig. 4-16 shows the experimental results. Resonance, which was caused by the effect of the wire stiffness and the mass of HDARH, was observed in high-frequency domain more than 11.8 Hz, although accurate force control was achieved from 1.0 Hz to 10.0 Hz.
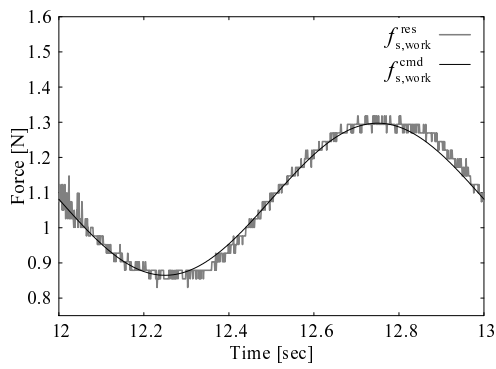
(a) Sine wave response (1.0 Hz).
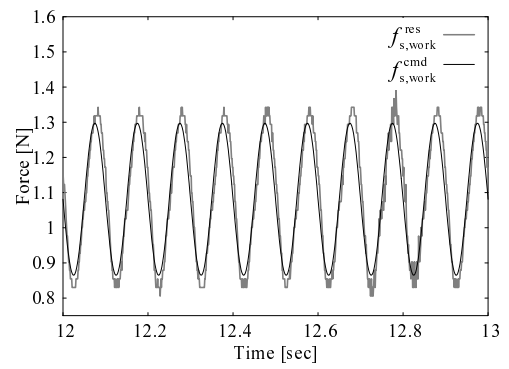
(b) Sine wave response (10.0 Hz).
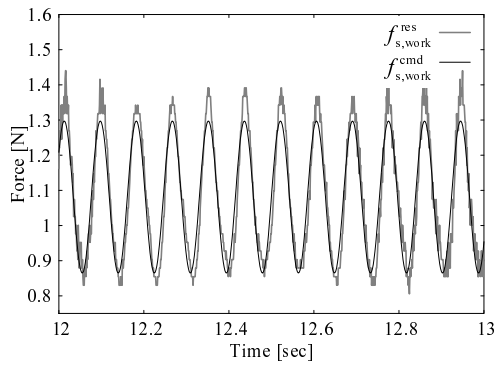
(c) Sine wave response (11.8 Hz).
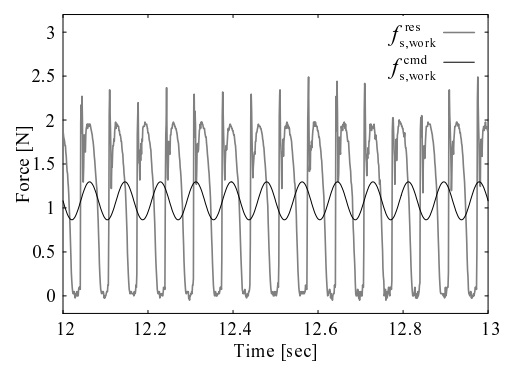
(d) Sine wave response (12.0 Hz).

Fig. 4-16: Force response.
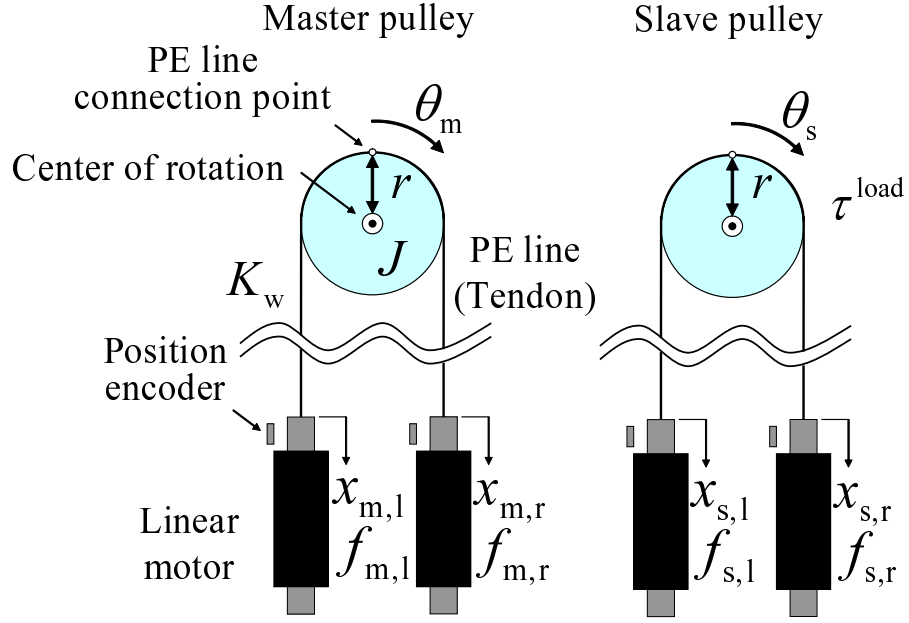
Fig. 4-17: Model of tendon-driven mechanism.

4.3 Compensation of Tendon Expansion

4.3.1 Modeling

The tendon-driven mechanism utilized in this chapter is modeled as Fig. 4-17. Two linear motors are used in master side, and two linear motors are utilized in the slave side as well. An operator moves the master pulley, and the slave pulley makes a contact with environment. The motion equation of the linear motors is

$$\boldsymbol{m}\ddot{\boldsymbol{x}} = \boldsymbol{f}. \tag{4.16}$$

Here,

$$\boldsymbol{m} = \mathrm{diag}\begin{bmatrix} m_{\mathrm{m,r}} & m_{\mathrm{m,l}} & m_{\mathrm{s,r}} & m_{\mathrm{s,l}} \end{bmatrix}, \tag{4.17}$$

$$\boldsymbol{x} = \begin{bmatrix} x_{\mathrm{m,r}} & x_{\mathrm{m,l}} & x_{\mathrm{s,r}} & x_{\mathrm{s,l}} \end{bmatrix}^{\mathrm{T}}, \tag{4.18}$$

$$\boldsymbol{f} = \begin{bmatrix} f_{\mathrm{m,r}} & f_{\mathrm{m,l}} & f_{\mathrm{s,r}} & f_{\mathrm{s,l}} \end{bmatrix}^{\mathrm{T}}, \tag{4.19}$$

and the symbols in the equations represent quantities as follows:

$\boldsymbol{m}$ mass matrix,

$\boldsymbol{x}$ position vector,

$\boldsymbol{f}$ force vector,

m mass,

x position,

f force,

m   (subscript) about master robot,

s   (subscript) about slave robot,

r   (subscript) about right side, and

l   (subscript) about left side.

K_{w}, r, J, and θ denote stiffness of the tendon, radius of the pulley, moment of inertia, and angle of the pulley, respectively.
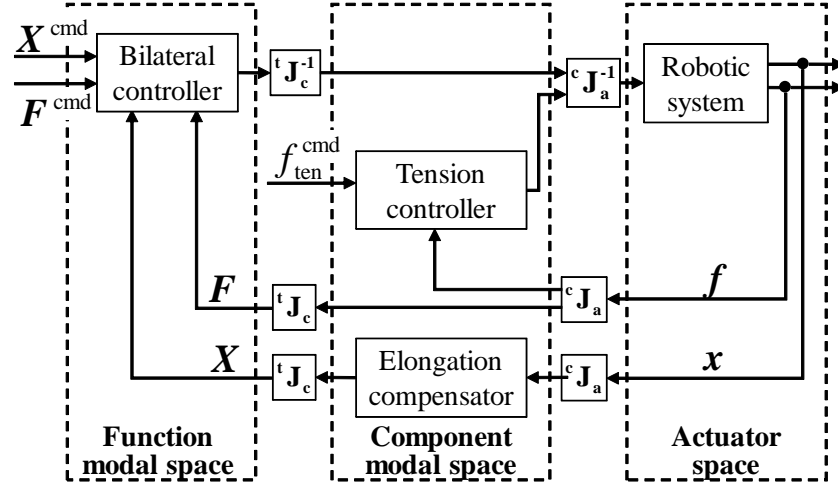
Fig. 4-18: Overview of the proposed method.

4.3.2   Compensation of Wire Elongation Based on Modal Decomposition

Fig. 4-18 shows an overview of the proposed method. This method has four control goals as follows.

- Angle tracking

- Torque feedback

- Tension control in master side

- Tension control in slave side

This chapter defines three kinds of spaces: actuator space, component modal space, and function modal space. The linear motors are controlled in the actuator space. Tension force is generated, and elongation length is calculated in the component modal space. Reference value to achieve angle tracking and torque feedback is obtained in the function modal space. Here,

$$
{}^{\mathbf{c}}\mathbf{J_a} \;=\; \begin{bmatrix} 1 & -1 & 0 & 0 \\ 0 & 0 & 1 & -1 \\ 1 & 1 & 0 & 0 \\ 0 & 0 & 1 & 1 \end{bmatrix} \tag{4.20}
$$

is a transformation matrix from the actuator space to the component modal space, and

$$\mathbf{{}^{f}J_{c}} = \begin{bmatrix} 1 & -1 \\ 1 & 1 \end{bmatrix} \tag{4.21}$$

is a transformation matrix from the component modal space to the function modal space. $\boldsymbol{x}$, $\boldsymbol{f}$ denote position vector and force vector in the actuator space. Position vector and force vector in the component modal space is calculated as

$$\begin{bmatrix} x_{\mathrm{m,dif}} & x_{\mathrm{s,dif}} & x_{\mathrm{m,com}} & x_{\mathrm{s,com}} \end{bmatrix}^{\mathrm{T}} = \mathbf{{}^{c}J_{a}}\boldsymbol{x}, \tag{4.22}$$

$$\begin{bmatrix} f_{\mathrm{m,dif}} & f_{\mathrm{s,dif}} & f_{\mathrm{m,com}} & f_{\mathrm{s,com}} \end{bmatrix}^{\mathrm{T}} = \mathbf{{}^{c}J_{a}}\boldsymbol{f}, \tag{4.23}$$

where subscript "com" and "dif" represent common mode and differential mode. Variables in the common mode are used in component modal space. In addition, variables in the differential mode is transformed into function modal space as

$$\boldsymbol{X} = \begin{bmatrix} X_{\mathrm{dif}} & X_{\mathrm{com}} \end{bmatrix}^{\mathrm{T}} = \mathbf{{}^{f}J_{c}} \begin{bmatrix} x_{\mathrm{m,dif}} & x_{\mathrm{s,dif}} \end{bmatrix}^{\mathrm{T}}, \tag{4.24}$$

$$\boldsymbol{F} = \begin{bmatrix} F_{\mathrm{dif}} & F_{\mathrm{com}} \end{bmatrix}^{\mathrm{T}} = \mathbf{{}^{f}J_{c}} \begin{bmatrix} f_{\mathrm{m,dif}} & f_{\mathrm{s,dif}} \end{bmatrix}^{\mathrm{T}}. \tag{4.25}$$

Fig. 4-19 represents a block diagram of the tendon-driven robot.
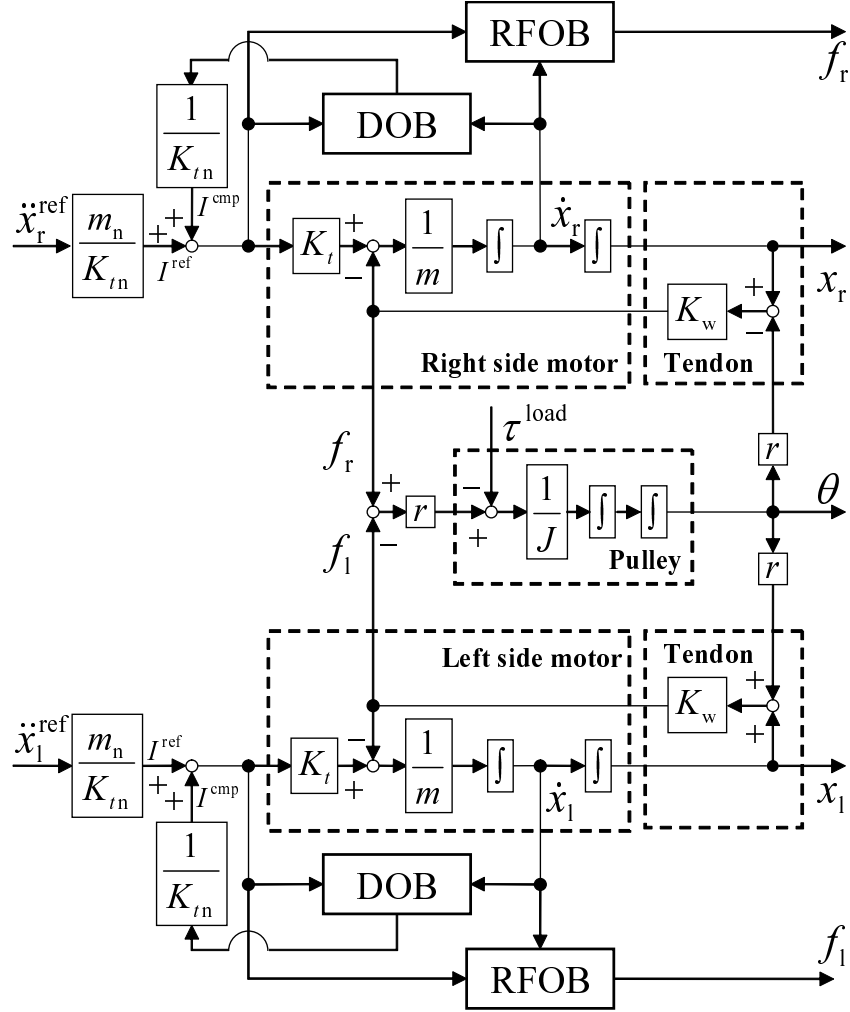
Fig. 4-19: Block diagram of tendon-driven robotic system with DOB and RFOB.

Tension Control

Tension of the tendons (PE line) must be kept to control the pulleys. Therefore, tension of the PE lines is controlled to keep above a constant force. Acceleration references to achieve tension control in component modal space are expressed by

$$\ddot{x}_{\mathrm{m,com}}^{\mathrm{ref}} = C_{\mathrm{ten}}(2f_{\mathrm{ten}}^{\mathrm{cmd}} + |f_{\mathrm{m,dif}}| - f_{\mathrm{m,com}}), \qquad (4.26)$$

$$\ddot{x}_{\mathrm{s,com}}^{\mathrm{ref}} = C_{\mathrm{ten}}(2f_{\mathrm{ten}}^{\mathrm{cmd}} + |f_{\mathrm{s,dif}}| - f_{\mathrm{s,com}}). \qquad (4.27)$$

A lower threshold of the tension is set by $f_{\mathrm{ten}}^{\mathrm{cmd}}$. In this chapter, proportional controller is utilized as the tension controller. Therefore, the gain of the proportional controller K_{ten} is substituted into the tension

controller C_ten as follows:

$$C_\text{ten} = K_\text{ten}. \tag{4.28}$$

Elongation Compensator

The tendons are modeled as springs. The stiffness is denoted by K_f. In this subsection, the pulley in the slave side is focused on for ease of explanation. Additionally, a case where environmental reaction torque is applied into clockwise direction is assumed. Note that following discussion can be applied into master side and counterclockwise direction torque as well.

The tension controller in the subsection 4.3.2 keeps the right side force as

$$f_\text{s,r} = f_\text{ten}^\text{cmd}. \tag{4.29}$$

If there is no environmental reaction force, the left side force is also equal to f_ten^cmd as follows:

$$f_\text{s,l} = f_\text{ten}^\text{cmd}. \tag{4.30}$$

In this case, the whole elongation x_rec is expressed as

$$x_\text{rec} = \frac{2 f_\text{ten}^\text{cmd}}{K_\text{w}}, \tag{4.31}$$

and the elongation value is recorded. Left side force $f_\text{s,l}$ is larger than tension command f_ten^cmd when some environmental reaction force is applied into clockwise direction. Then, whole elongation $x_\text{s,com}$ is expressed as

$$x_\text{s,com} = \frac{f_\text{s,l}}{K_\text{w}} + \frac{f_\text{ten}^\text{cmd}}{K_\text{w}}. \tag{4.32}$$

The difference between the recorded elongation x_rec and the current elongation $x_\text{s,com}$ represents the effect of the environmental reaction force on the elongation, and the difference is expressed as

$$x_\text{s,elo} = x_\text{s,com} - x_\text{rec}. \tag{4.33}$$

The position values in the component modal space are redefined to compensate the error caused by the tendon elongation as

$$x^*{}_\text{m,com} = x_\text{m,com} - \text{sgn}(f_\text{m,dif}) x_\text{m,elo}, \tag{4.34}$$

$$x^*{}_\text{s,com} = x_\text{s,com} + \text{sgn}(f_\text{s,dif}) x_\text{s,elo}. \tag{4.35}$$

The directions of the generated force are different between master side and slave side. Therefore, the directions of the compensation are also different.
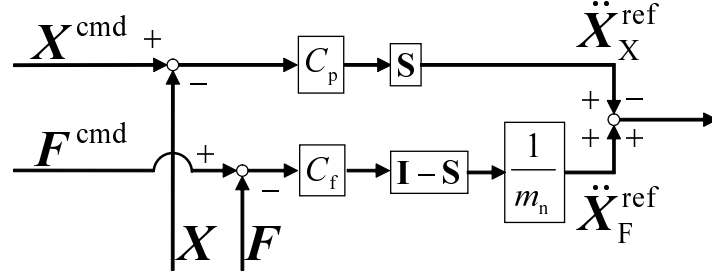
Fig. 4-20: Block diagram of bilateral controller.

Torque Feedback

Fig. 4-20 shows the block diagram of bilateral control. That part is used for torque feedback and angle tracking. An acceleration reference in function modal space to achieve torque feedback is expressed as

$$\ddot{\boldsymbol{X}}_{\mathrm{F}}^{\mathrm{ref}} = -C_{\mathrm{f}}(\mathbf{I} - \mathbf{S})\boldsymbol{F}, \tag{4.36}$$

where C_{f} and $\mathbf{I}$ denote force controller and 2×2 unit matrix. Here,

$$\mathbf{S} = \begin{bmatrix} 1 & 0 \\ 0 & 0 \end{bmatrix} \tag{4.37}$$

is a 2×2 selection matrix. The number of rows is corresponding to the degree of freedom for control. The number of lines is corresponding to the number of control goals. Non-diagonal elements are zero. The number of 1 in the diagonal elements is corresponding to the number of control goals achieved by position control system. In this chapter, proportional controller is utilized for force control. Therefore, the gain of the proportional controller K_{f} is substituted into the controller C_{f} as

$$C_{\mathrm{f}} = K_{\mathrm{f}}. \tag{4.38}$$

Angle Tracking

An acceleration reference value in function modal space to achieve angle tracking is obtained as

$$s^2 \boldsymbol{X}_{\mathrm{X}}^{\mathrm{ref}}(s) = -C_{\mathrm{p}}(s)\mathbf{S}\boldsymbol{X}^{*}(s), \tag{4.39}$$

where "$*$" indicates the compensated position values, which are calculated in the subsection 4.3.2 are used. In this chapter, proportional-derivative controller is utilized for angle control. Therefore, the gain

of the proportional-derivative controller $K_\mathrm{p} + K_\mathrm{v}s$ is substituted into the controller $C_\mathrm{p}(s)$ as

$$C_\mathrm{p}(s) \;=\; K_\mathrm{p} + K_\mathrm{v}s. \tag{4.40}$$

The acceleration references in the function modal space are transformed into the component modal space by

$$\ddot{\boldsymbol{x}}_\mathrm{dif}^{\mathrm{ref}} \;=\; {}^{\mathbf{f}}\mathbf{J}_\mathbf{c}^{-1}(\ddot{\boldsymbol{X}}_\mathrm{F}^{\mathrm{ref}} + \ddot{\boldsymbol{X}}_\mathrm{X}^{\mathrm{ref}}). \tag{4.41}$$

The acceleration references in the actuator modal space are calculated by

$$\ddot{\boldsymbol{x}}^{\mathrm{ref}} \;=\; {}^{\mathbf{c}}\mathbf{J}_\mathbf{a}^{-1} \begin{bmatrix} \ddot{\boldsymbol{x}}_\mathrm{dif}^{\mathrm{ref}} \\ \hline \ddot{x}_\mathrm{m,com}^{\mathrm{ref}} \\ \ddot{x}_\mathrm{s,com}^{\mathrm{ref}} \end{bmatrix}, \tag{4.42}$$

and as represented above, the acceleration reference of each linear motor is calculated.
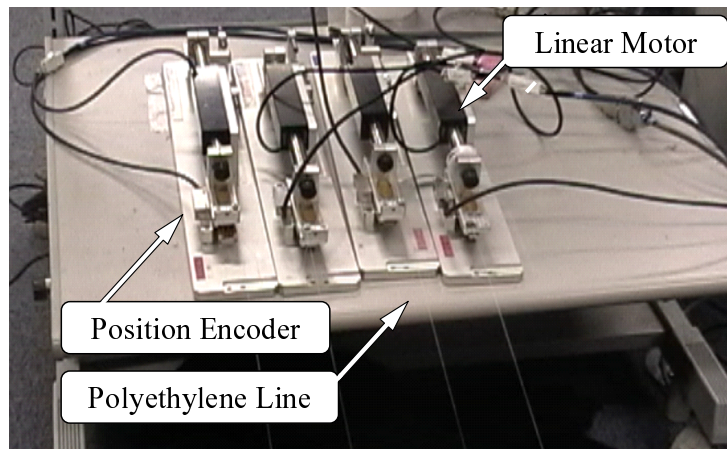
Fig. 4-21: Experimental setup (linear motor side).
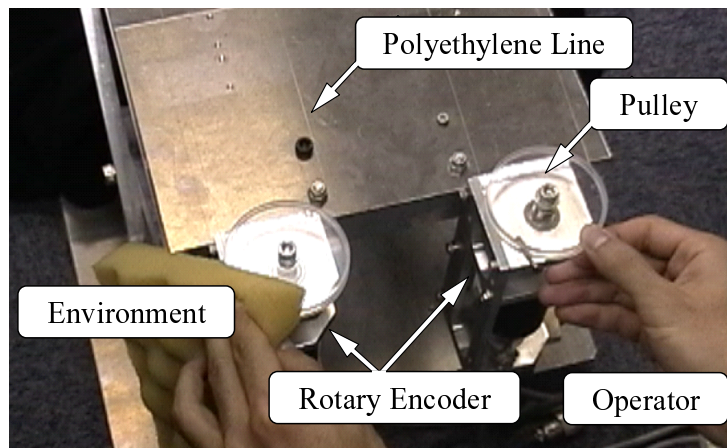
Fig. 4-22: Experimental setup (pulley side).

4.3.3   Experiments

Fig. 4-21 and Fig. 4-22 show the experimental setup. Parameters utilized in the experiment are shown in Table 4.4. The pulley in the master side and slave side were driven by two linear motors respectively. The distance between the pulley and the linear motor was 0.8m. The diameter of the PE line was 0.165mm, and the radius of the pulley was 0.03m.

Fig. 4-23 shows experimental results without elongation compensation. The shaded area from about 0.5s to 5.0s indicates free motion. At this time, slave pulley did not make a contact with environment. On the other hand, the shaded area from 7.5s to 12.0s indicates contact motion, and slave pulley made a contact with environment. Fig. 4-23(a) represents force response in the component modal space. Law of

Table 4.4: Experimental parameters.

Parameter	Meaning of the parameter	Value
K_{p}	Position feedback gain	1600
K_{v}	Velocity feedback gain	80
K_{f}	Force feedback gain	0.8
K_{ten}	Force feedback gain	1.0
g_{dob}	Cut-off frequency of DOB	500 rad/s
g_{rfob}	Cut-off frequency of RFOB	500 rad/s
m_{n}	Nominal mass	0.5 kg

action and reaction was realized. Therefore, torque feedback was achieved, and the operator could feel the actual reaction force applied to the slave pulley. Fig. 4-23(b) and Fig. 4-23(c) show force response in the actuator space of the master side and slave side, respectively. The tensional force was kept larger than $f_{\mathrm{ten}}^{\mathrm{cmd}}$ (=2N) in both side. Therefore, tension controls were achieved. Fig. 4-23(d) is a position response measured by rotary encoder. The rotary encoder was set on the pulleys only for validation, and the measured value was not used in the any controller. In the free motion, the slave pulley tracked the master pulley. Angle tracking was achieved. However, when environmental reaction force was applied to the slave pulley, large margin of tracking error was observed. The tracking error was caused by elongation of the tendons.

Fig. 4-24 shows experimental results with elongation compensation. The shaded area from 0.5s to 4.5s indicates free motion, and the shaded area from 7.0s to 10.5s indicates contact motion. Fig. 4-24(a), Fig. 4-24(b), and Fig. 4-24(c) represent force response in the component modal space, actuator space of the master side and slave side, respectively. From these results, it can be confirmed that torque feedback, tension control in the master side and the slave side are achieved. From these results, achievement of torque feedback, tension control in the master side and the slave side is confirmed. Fig. 4-24(d) is the position response measured by the rotary encoder. Fig. 4-24(d) shows different result from Fig. 4-23(d). In this case, the error in the contact motion was reduced by the effect of the proposed elongation compensator. Therefore, the results verify the validity of the elongation compensator.
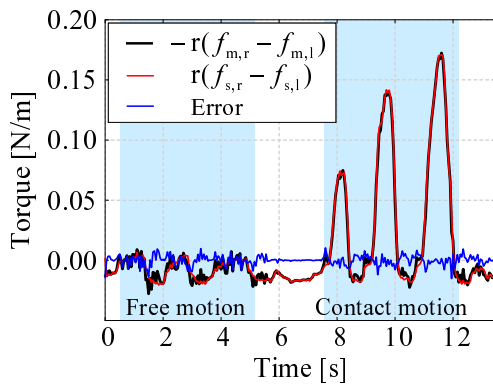
(a) Force response in the component modal space.
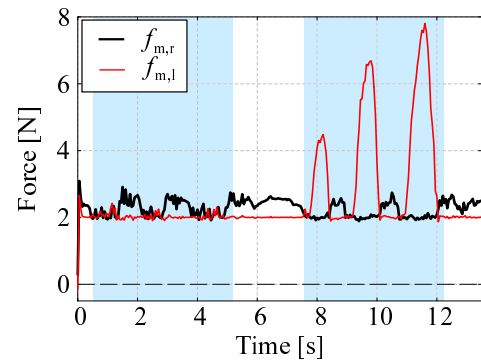
(b) Force response of the master pulley in the actuator space.
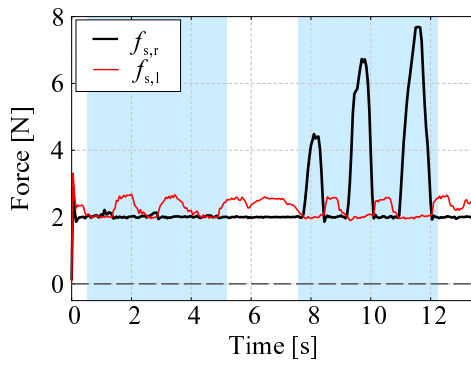
(c) Force response of the slave pulley in the actuator space.
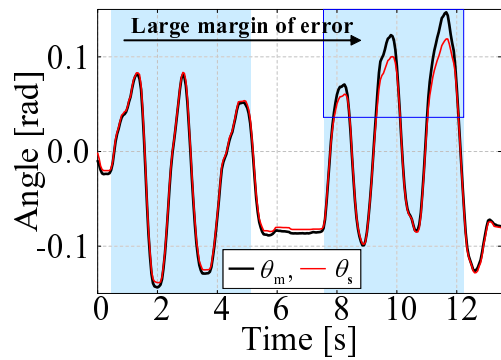
(d) Position response measured by rotary encoder only for validation.

Fig. 4-23: Experimental result (without elongation compensation).
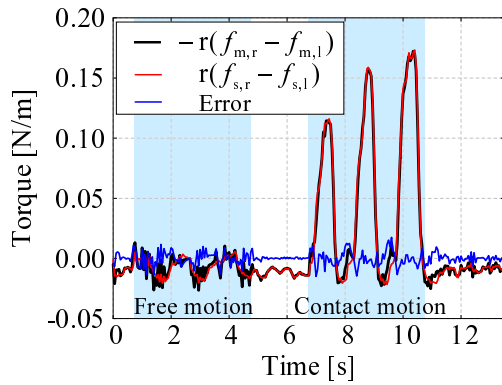
(a) Force response in the component modal space.
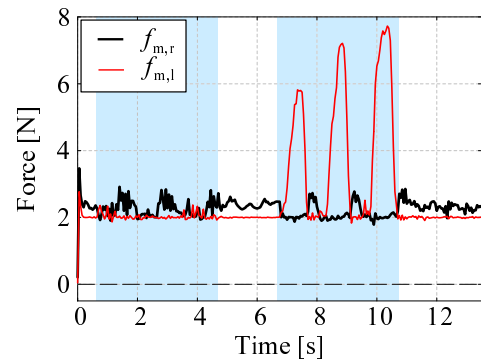
(b) Force response of the master pulley in the actuator space.
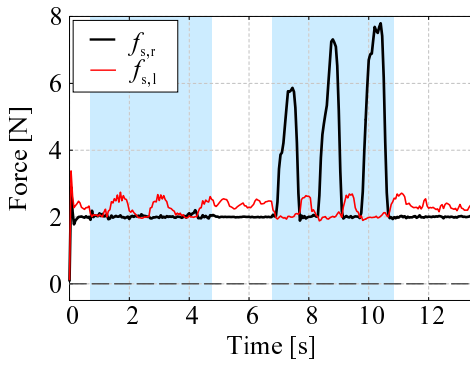
(c) Force response of the slave pulley in the actuator space.
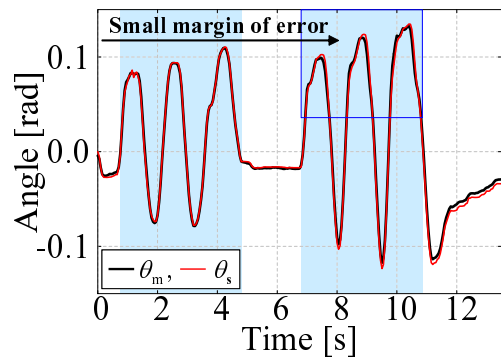
(d) Position response measured by rotary encoder only for validation.

Fig. 4-24: Experimental result (with elongation compensation).
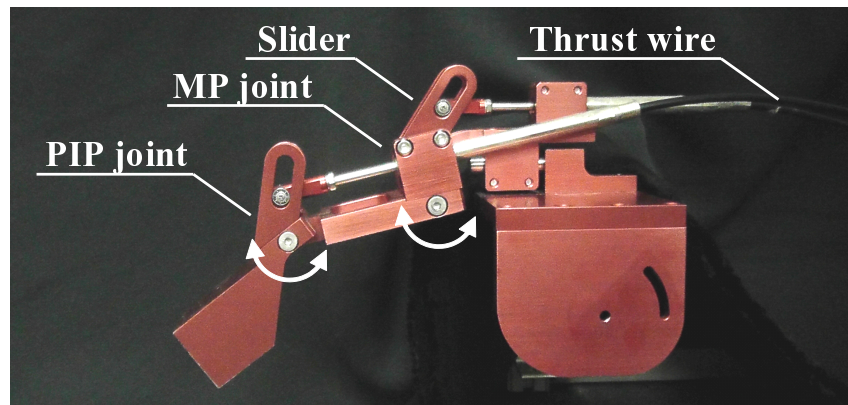
Fig. 4-25: Wearable master robot hand.
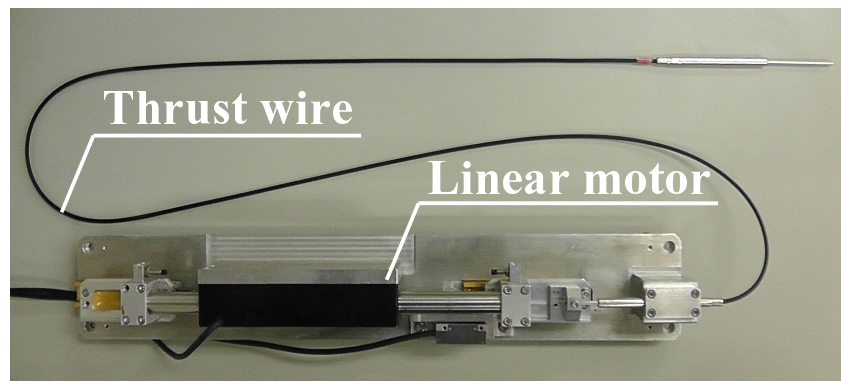
Fig. 4-26: Setup of the thrust wire.

4.4   Extraction of Motion Feature

4.4.1   Master-Slave Systems

Fig. 4-25 shows an overview of the wearable robot hand that is used as a master robot. This robot hand has an exoskeletal structure and two-DOF. The joint located on the base side of the finger is called the MP joint and the joint located on the tip side is called the PIP joint. Fig. 4-26 shows the setup of a thrust wire [108]. The thrust wire connected to each joint is a mechanism for transmitting the driving force from isolated actuators to the driven system. This mechanism makes the driven system lighter. In this chapter, linear motors are used as actuators. Translational motion of the thrust wire is translated into rotational motion by slider-linkage mechanisms in each joint.

Fig. 4-27 shows an overview of the forceps robot that is used as a slave robot. This forceps robot performs grasping and translational motions. The driving force for the grasping motion is generated by
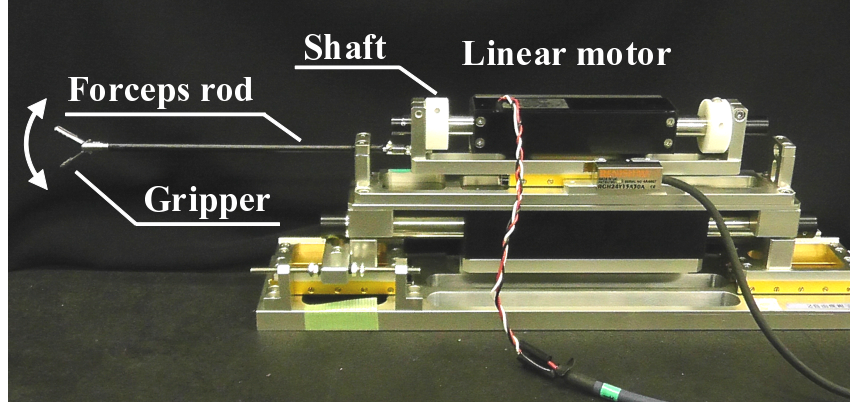
Fig. 4-27: Slave forceps robot.

the linear motor of the upper side. The driving force is transmitted to the gripper through the shaft and the forceps rod, as shown in Fig. 4-27. The driving force for the translational motion is generated by the linear motor, located on the lower side.

4.4.2 Principal Component Analysis

Section 4.4.2 describes the PCA procedure [109] and the required tasks of this study. The projection axis calculated in this section represents the best straight-line approximation of the grasping motion. The coordinate system of the projection axis is suitable for abstracting the motion features.

Abstraction of Principal Components

A matrix $\boldsymbol{x}_{\mathrm{m}}$ is defined as

$$\boldsymbol{x}_{\mathrm{m}} = \left[\begin{array}{c} x^{\mathrm{MP}}[1] \cdots x^{\mathrm{MP}}[d] \cdots x^{\mathrm{MP}}[\mathrm{N}] \\ x^{\mathrm{PIP}}[1] \cdots x^{\mathrm{PIP}}[d] \cdots x^{\mathrm{PIP}}[\mathrm{N}] \end{array} \right]^{\mathrm{T}}, \tag{4.43}$$

where $\boldsymbol{x}_{\mathrm{m}}$ is the position response of the grasping motion. Here, the superscripts "MP" and "PIP" represent the responses of the MP joint and PIP joint, respectively. "N" and "$[d]$" denote the recorded and d-th data of the time-series data, respectively. Deviation from the average is calculated as

$$\tilde{x}^{\mathrm{MP}}[d] = x^{\mathrm{MP}}[d] - \bar{x}^{\mathrm{MP}}, \tag{4.44}$$

$$\tilde{x}^{\mathrm{PIP}}[d] = x^{\mathrm{PIP}}[d] - \bar{x}^{\mathrm{PIP}}, \tag{4.45}$$

where $\bar{x}$ and $\tilde{x}$ denote the average and deviation, respectively. The calculated $\tilde{\boldsymbol{x}}_{\mathrm{m}}$ is defined as

$$\tilde{\boldsymbol{x}}_{\mathrm{m}} = \left[\begin{array}{l} \tilde{x}^{\mathrm{MP}}[1] \cdots \tilde{x}^{\mathrm{MP}}[d] \cdots \tilde{x}^{\mathrm{MP}}[\mathrm{N}] \\ \tilde{x}^{\mathrm{PIP}}[1] \cdots \tilde{x}^{\mathrm{PIP}}[d] \cdots \tilde{x}^{\mathrm{PIP}}[\mathrm{N}] \end{array} \right]^{\mathrm{T}}. \tag{4.46}$$

Covariance matrix $\mathbf{V}$ is calculated by

$$\mathbf{V} = \frac{1}{\mathrm{N}-1} \tilde{\boldsymbol{x}}_{\mathrm{m}}^{\mathrm{T}} \tilde{\boldsymbol{x}}_{\mathrm{m}}. \tag{4.47}$$

Relationships between eigenvalues and eigenvectors are expressed as

$$(\mathbf{V} - \lambda_1 \mathbf{I}) \, \mathbf{t}_1 = 0, \tag{4.48}$$
$$(\mathbf{V} - \lambda_2 \mathbf{I}) \, \mathbf{t}_2 = 0, \tag{4.49}$$

where λ_1 and λ_2 denote the eigenvalues of $\mathbf{V}$, $\mathbf{t}_1$ and $\mathbf{t}_2$ are eigenvectors, and $\mathbf{I}$ is a 2×2 unit matrix. Here, it can be assumed that λ_1 is equal to or larger than λ_2 without loss of generality. $\mathbf{t}_1$ is a projection axis (hereafter referred to as the "feature axis") for the distribution approximation of the original data. Here, "first principal component" and "second principal component" are defined as the physical quantities that are projected to $\mathbf{t}_1$ and $\mathbf{t}_2$, respectively. Thus, the variance of the first principal component is denoted by λ_1 and the variance of the second principal component is denoted by λ_2. Human grasping motion is approximated by the feature axis $\mathbf{t}_1$, because the original data represent the response of the grasping motion extracted by the robot hand. Thus, a transformation matrix is expressed as

$$\mathbf{T}_{\mathrm{C}} = \left[\begin{array}{l} \mathbf{t}_1 \\ \mathbf{t}_2 \end{array} \right]. \tag{4.50}$$

This matrix maps the response of the actuators driving the robot hand on a Cartesian coordinate system with the coordinate axes $\mathbf{t}_1$ and $\mathbf{t}_2$. One feature axis of the first principal component is expressed as

$$\mathbf{t}_1 = [1 \, , \, \omega_1], \tag{4.51}$$

where ω_1 satisfies the following equation:

$$x^{\mathrm{PIP}} = \omega_1 (x^{\mathrm{MP}} - \bar{x}^{\mathrm{MP}}) + \bar{x}^{\mathrm{PIP}}. \tag{4.52}$$

Similarly, a feature axis of the second principal component is expressed as

$$\mathbf{t}_2 = [1 \, , \, \omega_2], \tag{4.53}$$

and

$$x^{\mathrm{PIP}} \quad = \quad \omega_2\big(x^{\mathrm{MP}} - \bar{x}^{\mathrm{MP}}\big) + \bar{x}^{\mathrm{PIP}} \tag{4.54}$$

is satisfied.

Expression of Tasks

The purpose of this study is to demonstrate the operation of a slave robot based on the motion features of an operator, thus providing more intuitive operation. On the master side, the feature axis $\mathbf{t}_1$, which is calculated in subsection 4.4.2, exhibits the features of the grasping motion. However, the slave robot can achieve a grasping motion by moving only one motor. Therefore, the control goals are defined as

$$x^{\mathrm{MP}} + \omega_1\, x^{\mathrm{PIP}} - \alpha^{\mathrm{gras}} x^{\mathrm{gras}} \quad = \quad 0 \ \text{ and} \tag{4.55}$$

$$f^{\mathrm{MP}} + \omega_1\, f^{\mathrm{PIP}} + \beta^{\mathrm{gras}} f^{\mathrm{gras}} \quad = \quad 0, \tag{4.56}$$

where α, β, and the superscripts "trans" and "gras" denote the position scaling ratio, the force scaling ratio, the translational motion of the forceps robot, and the grasping motion of the forceps robot, respectively. The physical quantities projected to the feature axis $\mathbf{t}_2$ have little relation to the grasping motion. Thus, the second principle component is transmitted to the translational motion.
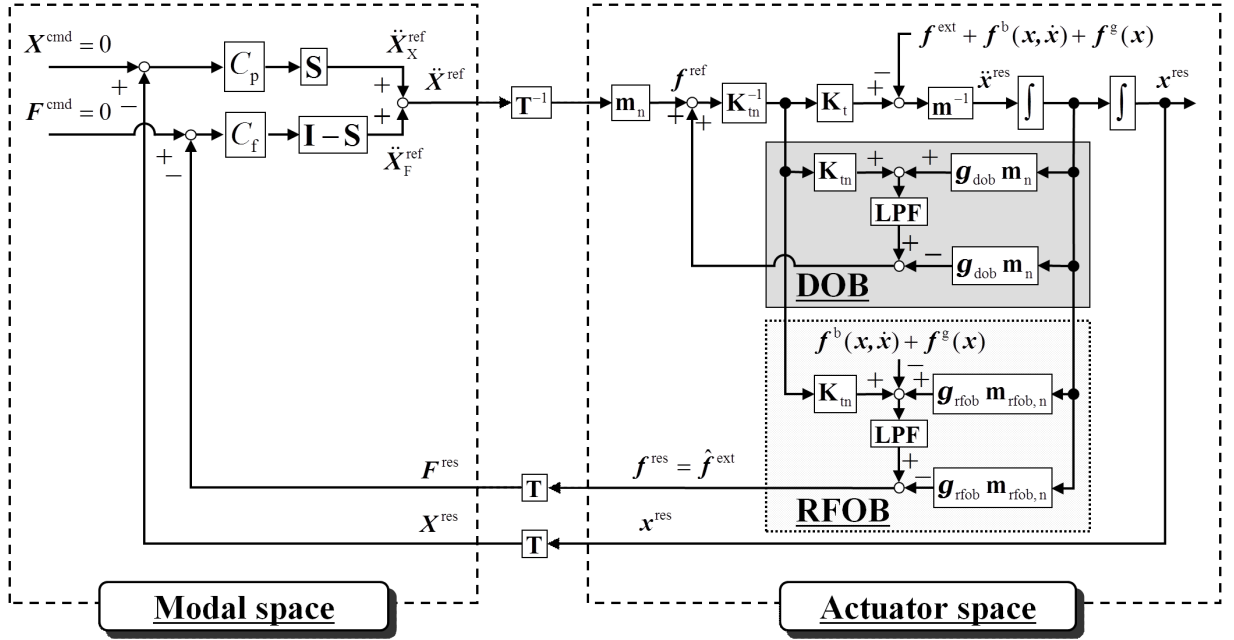
Fig. 4-28: Block diagram.

4.4.3 Bilateral Control System for Different Configurations

Fig. 4-28 shows a block diagram of the bilateral control system used in this study. Disturbances should be suppressed to achieve the desired motion. The disturbance is expressed as

$$\begin{aligned}
\boldsymbol{f}^{\mathrm{dis}} &= \boldsymbol{f}^{\mathrm{ext}} + \boldsymbol{f}^{\mathrm{b}}(\boldsymbol{x}, \dot{\boldsymbol{x}}) + \boldsymbol{f}^{\mathrm{g}}(\boldsymbol{x}) \\
&\quad + (\mathbf{m} - \mathbf{m}_{\mathrm{n}})\ddot{\boldsymbol{x}} + (\mathbf{K}_{\mathrm{tn}} - \mathbf{K}_{\mathrm{t}})\boldsymbol{I}_{\mathrm{a}}^{\mathrm{ref}},
\end{aligned} \tag{4.57}$$

where $\boldsymbol{f}^{\mathrm{ext}}$ and $\boldsymbol{f}^{\mathrm{g}}(\boldsymbol{x})$ denote the external force and gravity force, respectively. $\boldsymbol{f}^{\mathrm{b}}(\boldsymbol{x}, \dot{\boldsymbol{x}})$ is the sum of the inertial force, Coriolis force, and friction force. $\mathbf{K}_{\mathrm{t}}$ and $\boldsymbol{I}_{\boldsymbol{a}}$ denote the thrust coefficient and the armature current, respectively. The superscripts "dis" and "ref" and subscript "n" denote the disturbance, reference, and nominal value, respectively. $\mathbf{m}$ is a mass matrix in the actuator space, and is expressed as

$$\mathbf{m} = \mathrm{diag}\,[\,\mathrm{m}^{\mathrm{MP}}\,,\,\mathrm{m}^{\mathrm{PIP}}\,,\,\mathrm{m}^{\mathrm{trans}}\,,\,\mathrm{m}^{\mathrm{gras}}\,], \tag{4.58}$$

where the superscripts "MP" and "PIP" denote variables related to the MP and PIP joints, respectively. The disturbance can be observed from the force reference and velocity response, and is suppressed by the observed value. The observer is called DOB [29]. In addition, the environmental reaction force is estimated from the observed disturbance and the modeled disturbance. This is a reaction force observer (RFOB) [33]. In this study, the estimated reaction force of the RFOB is used as a force response.

Position is measured by optical encoders set on each linear motor. Response matrices in the actuator space are defined as

$$\boldsymbol{x}^{\mathrm{res}} = [\, x^{\mathrm{MP}} \,,\, x^{\mathrm{PIP}} \,,\, x^{\mathrm{trans}} \,,\, x^{\mathrm{gras}} \,]^{\mathrm{T}}, \tag{4.59}$$

$$\boldsymbol{f}^{\mathrm{res}} = [\, f^{\mathrm{MP}} \,,\, f^{\mathrm{PIP}} \,,\, f^{\mathrm{trans}} \,,\, f^{\mathrm{gras}} \,]^{\mathrm{T}}, \tag{4.60}$$

where the superscript "res" denotes the response. The variables in the actuator space are mapped on a modal space by a transformation matrix that is expressed as

$$\mathbf{T} = \left[
\begin{array}{c|cc}
\mathbf{T}_{\mathrm{C}} & 0 & -\alpha^{\mathrm{gras}} \\
 & -\alpha^{\mathrm{trans}} & 0 \\
\hline
\mathbf{T}_{\mathrm{C}} & 0 & \beta^{\mathrm{gras}} \\
 & \beta^{\mathrm{trans}} & 0
\end{array}
\right]. \tag{4.61}$$

The position response of the slave robot multiplied by α is transmitted to the master side. Similarly, there is a force feedback and the force response of the slave robot multiplied by β is transmitted to the master side. $\mathbf{T}_{\mathrm{C}}$ is the transformation matrix calculated in section 4.4.2.

Dynamics in the modal space is expressed as

$$\mathbf{m}\mathbf{T}^{-1}\ddot{\boldsymbol{X}} = \mathbf{T}^{-1}\boldsymbol{F}, \tag{4.62}$$

where $\boldsymbol{X}$ and $\boldsymbol{F}$ denote position and force, respectively, in the modal space, which are transformed by $\mathbf{T}$.

Usually, the transformation of forces is expressed as

$$\boldsymbol{F} = \mathbf{T}^{-\mathrm{T}}\boldsymbol{f} \tag{4.63}$$

based on the principle of virtual work. However, the principle of virtual work is not valid for scaled bilateral control systems. Therefore, to simplify the design [54], the forces are transformed by $\mathbf{T}$, which is also utilized for the position transformation. The energy is not conserved before and after the transformation.

Mass of the modal space is defined as

$$\mathbf{M} = \mathbf{T}\mathbf{m}\mathbf{T}^{-1}. \tag{4.64}$$

There is no interference the position-control and force-control axes when this mass matrix is a diagonal matrix. Here,

$$(\exists \mathbf{T}^{-1} \in \mathbb{R}^{4\times 4}) \cap (\mathbf{m} = \gamma\mathbf{I}) \Rightarrow \mathbf{M} = \gamma\mathbf{I} \,(\gamma \in \mathbb{R}^{1}). \tag{4.65}$$

The determinant of $\mathbf{T}$, which is represented as

$$
\begin{aligned}
|\mathbf{T}| \;=\;& (\omega_1 - \omega_2)(\alpha^{\mathrm{gras}}\alpha^{\mathrm{trans}} + \alpha^{\mathrm{gras}}\beta^{\mathrm{trans}} \\
& +\alpha^{\mathrm{trans}}\beta^{\mathrm{gras}} + \beta^{\mathrm{gras}}\beta^{\mathrm{trans}}),
\end{aligned}
\tag{4.66}
$$

cannot be zero, because $\mathbf{t}_1$ is orthogonal to $\mathbf{t}_2$

$$
\mathbf{t}_1 \cdot \mathbf{t}_2 = 1 + \omega_1\omega_2 = 0 \quad (\omega_1, \omega_2 \in \mathbb{R}^1),
\tag{4.67}
$$

and every scaling ratio should be positive in a bilateral control system

$$
\alpha^{\mathrm{gras}} \,,\, \alpha^{\mathrm{trans}} \,,\, \beta^{\mathrm{gras}} \,,\, \beta^{\mathrm{trans}} > 0.
\tag{4.68}
$$

Therefore, the existence of $\mathbf{T}^{-1}$ is guaranteed. Furthermore, in this study, every nominal mass is set to the same value in DOB [34].

A proportional-derivative controller is used as a position controller $C_{\mathrm{p}}(s)$, and a proportional controller is used as a force controller C_{f}. These controllers are expressed as

$$
C_{\mathrm{p}}(s) \;=\; K_{\mathrm{p}} + K_{\mathrm{v}}s,
\tag{4.69}
$$

$$
C_{\mathrm{f}} \;=\; K_{\mathrm{f}},
\tag{4.70}
$$

where K_{p}, K_{v}, K_{f} and s denote the position feedback gain, velocity feedback gain, force feedback gain, and Laplace operator, respectively. The master-slave robot has two DOF on the master side and two DOF on the slave side. Therefore, the control system has four DOF in total. The selection matrix $\mathbf{S}$ is expressed as

$$
\begin{bmatrix} \mathbf{I} & \mathbf{0} \\ \mathbf{0} & \mathbf{0} \end{bmatrix}
\tag{4.71}
$$

because two of the four DOF are utilized for position tracking. Here, $\mathbf{I}$ is a 2×2 unit matrix and $\mathbf{0}$ is a 2×2 zero matrix.
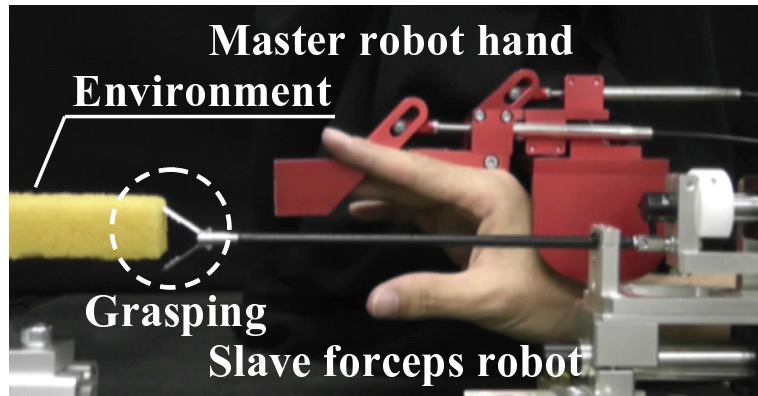
Fig. 4-29: Experimental setup.

4.4.4 Experiments

Position data of the grasping motion were measured and a PCA was conducted to obtain the transformation matrix $\mathbf{T}$. Section 4.4.4 shows the measured data and the PCA result. Section 4.4.4 expresses experimental results for bilateral control based on the feature axis. Fig. 4-29 shows the experimental setup. Four linear motors are utilized in these experiments. Rod-type linear motors are used and there is little friction effect. The external force is observed by the disturbance observer without force sensors. Only a linear encoder is implemented as the sensor of the system. The resolution of the position encoder is $0.1\ \mu$m. The control software is written in C language under RTAI 3.6.1. The sampling time is $100\ \mu$s.
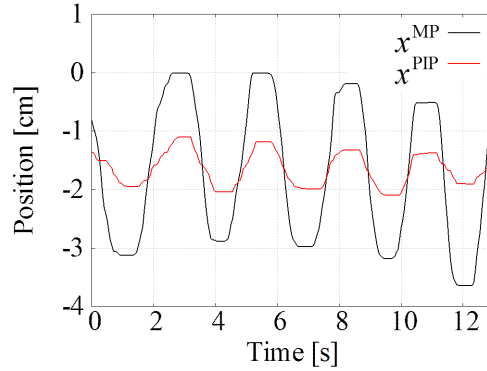
Fig. 4-30: Extraction of grasping motion.
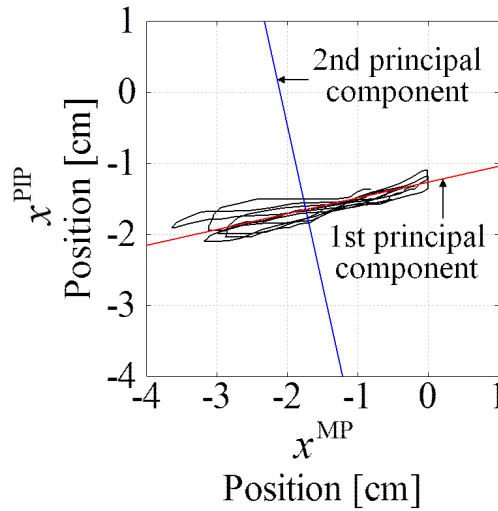
Fig. 4-31: Result of principal component analysis.

Extraction of Feature Axis

Fig. 4-30 shows the position responses of the grasping motion in each linear motor. The operator performed a grasping motion 5 times in 13 s. The feature axis of the grasping motion was calculated from these measured data. Values of ω_1, ω_2, $\bar{x}^{\mathrm{MP}}$ and $\bar{x}^{\mathrm{PIP}}$ are expressed in Table 4.5. Fig. 4-31 shows the result of PCA based on the responses represented in Fig. 4-30.

The results show that the grasping motion of the operator is represented by these displacement variables Δx^{MP} and Δx^{PIP}, with this feature expressed as

$$\Delta x^{\mathrm{MP}} : \Delta x^{\mathrm{PIP}} \;\; = \;\; 1 : \omega_1. \tag{4.72}$$

The feature can be utilized to design the transformation matrix which is explained in eq. (4.61), making

Table 4.5: Results of principal component analysis.

Variable	Value	Variable	Value
ω_1	0.222341139	$\bar{x}^{\mathrm{MP}}$	-0.017379723
ω_2	-4.497593218	$\bar{x}^{\mathrm{PIP}}$	-0.016497062

Table 4.6: Experimental parameters.

Variable	Definition of variable	Value
K_{p}	Position feedback gain	$3600\ 1/\mathrm{s}^2$
K_{v}	Velocity feedback gain	$120\ 1/\mathrm{s}$
K_{f}	Force feedback gain	$0.5\ 1/\mathrm{kg}$
g_{rfob}	Cutoff frequency of RFOB	$300\ \mathrm{rad/s}$
g_{dob}	Cutoff frequency of DOB	$300\ \mathrm{rad/s}$
$\mathrm{m}^{\mathrm{MP}}, \mathrm{m}^{\mathrm{PIP}}$	Measured mass (master side)	$0.5\ \mathrm{kg}$
$\mathrm{m}_{\mathrm{n}}^{\mathrm{MP}}, \mathrm{m}_{\mathrm{n}}^{\mathrm{PIP}}$	Nominal mass (master side)	$0.5\ \mathrm{kg}$
$\mathrm{m}^{\mathrm{trans}}$	Measured mass (slave side)	$1.70\ \mathrm{kg}$
$\mathrm{m}^{\mathrm{gras}}$	Measured mass (slave side)	$0.43\ \mathrm{kg}$
$\mathrm{m}_{\mathrm{n}}^{\mathrm{trans}}, \mathrm{m}_{\mathrm{n}}^{\mathrm{gras}}$	Nominal mass (slave side)	$0.5\ \mathrm{kg}$
	Length of link 1	$5.25\ \mathrm{cm}$
	Length of link 2	$5.72\ \mathrm{cm}$
	Mass of link 1	$0.0560\ \mathrm{kg}$
	Mass of link 2	$0.0610\ \mathrm{kg}$
	Inertia of link 1	$1.33 \times 10^{-5}\ \mathrm{kgm}^2$
	Inertia of link 2	$3.70 \times 10^{-5}\ \mathrm{kgm}^2$
	Sampling time	$0.1\ \mathrm{ms}$

it possible to operate the slave robot.

Experiment of Bilateral Control

Table 4.6 lists the experimental parameters and Table 4.7 presents the transformation matrix. Link 1 and link 2 are ordered from the closest link to the heel of the hand. To decouple the position control and force control systems, the nominal mass value is different from the true value in the DOB. However, the measured mass value is used as the nominal mass value in RFOB. The environment was changed in the

Table 4.7: Parameters for transformation matrix.

Variable	Value	Variable	Value
α^{gras}	5	α^{trans}	20
β^{gras}	1	β^{trans}	1
$\mathbf{t}_1$	$(1, 0.222341139)^{\text{T}}$	$\mathbf{t}_2$	$(1, -4.497593218)^{\text{T}}$

following order:

(1) No environment

(2) Sponge

(3) Balloon

(4) Styrofoam

(5) Aluminum

Fig. 4-32 shows the position response and Fig. 4-33 shows the force response. In Fig. 4-32, realization of the position tracking between the slave robot and the master robot in modal space is confirmed. In Fig. 4-33, attainment of the feedback of the environmental reaction force from the slave side to the master side in modal space is also confirmed. The first principal component of the human grasping motion was transmitted into the tool coordinate on the slave side.

Fig. 4-34 shows an enlarged view of Fig. 4-32 and Fig. 4-33, when the slave forceps robot was making contact with an aluminum block. Although the aluminum block was hard, the slave forceps robot performed a stable contact motion because the force feedback system was designed based on an acceleration control system [110].
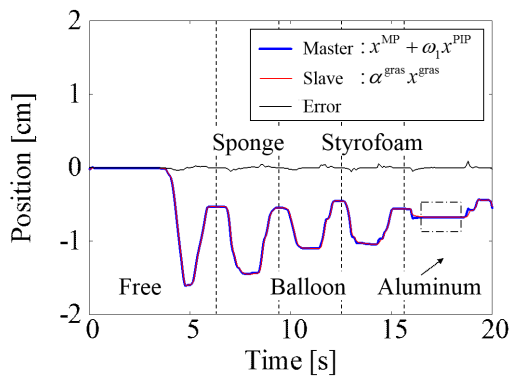
Fig. 4-32: Position response in modal space.
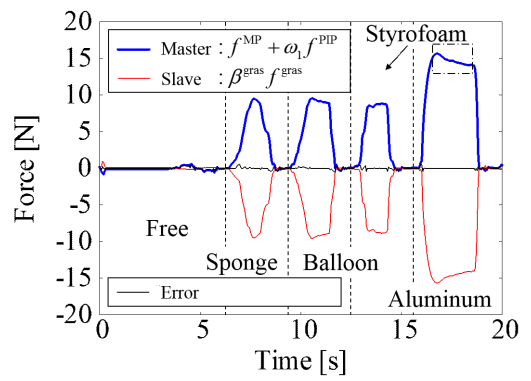
Fig. 4-33: Force response in modal space.
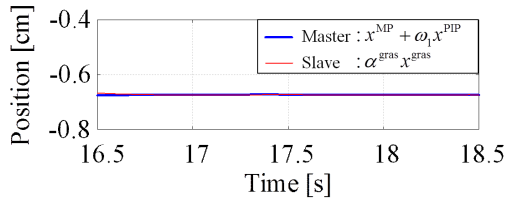
(a) Position response.
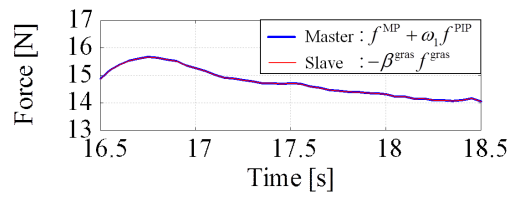
(b) Force response.

Fig. 4-34: Enlarged view of response (aluminum).

4.5   Summary

The first half of this chapter introduced the developed haptic master-slave robot hand named HDARH that has 11-DOF. HDARH consists of the three fingers and the tendon-driven mechanisms. In addition, a novel bilateral control system that is referred to as TDBC was proposed for tendon-driven robots. TDBC can control angles of joints, torque of joints, and tension of wires at the same time. The varidity of HDARH and TDBC was confirmed by the experiments of the middle finger. Fine teleoperation and extraction of haptic information were achieved successfully. The first half of this chapter also proposed the compensator of the tendon elongation. The proposed method was applied to a bilateral control system, and the validity of the proposed method was confirmed by experiments. In the experiment, angle tracking, torque feedback, tension control on master side, and slave side were achieved at the same time. Tendon-driven mechanisms are widely used in many robots because the mechanisms make driven system small and high output. Therefore, the proposed method will make a great contribution to the development of robotics.

The second half of this chapter proposed a method to transform a human grasping motion into the motion of a slave robot to allow intuitive operation. In the proposed method, the physical quantity of the grasping motion first was extracted and mapped onto the physical coordinate using the wearable robot hand. Next, a dominant Cartesian coordinate system, which contains the feature axis of the grasping motion, was calculated based on PCA. Finally, the grasping motion was transmitted to the slave robot using the calculated coordinate system, and intuitive teleoperation system was realized. Decoupling of the position control and force control systems was achieved by setting a nominal mass value of the disturbance observer. The validity of the proposed method was verified using a wearable robot hand and a forceps robot. This proposed bilateral control method has broad utility and facilitates easy teleoperation.

Chapter 5

Processing and Recognition

In this chapter, a motion recognition method that uses haptic information of the human hand is proposed. The haptic information is measured by master and slave robot hands. Human motion recognition systems play an important role in improving the ability of robots to support human life.

The first half of this chapter describes recognition of combinations of successive elementary motions. To handle expansion and contraction of time axes, dynamic programming matching algorithms are introduced. The robot hands have five degrees of freedom, and bilateral control of the robot is implemented. The operator wears the master robot hand and manipulates an object through the slave robot hand. A motion database is prepared, containing haptic information in the form of reference vectors for eight kinds of human motion. The motion database utilizes the cosine similarity to distinguish different human motions on the basis of the haptic information acquired by the master robot. Expansion and contraction of the time axes are corrected by dynamic programming matching, and combination motion is then recognized. The validity of the proposed method is experimentally confirmed.

The second half of this chapter describes the actual application of the above-mentioned recognition method to the real-time power-assist system. Firstly, haptic data are obtained using a bilateral control system. Secondly, the haptic data are divided into action components, using modal transformation. Finally, both the position and the force information in each action component are compared with recorded data. A dynamic programming pattern-matching algorithm is used to recognize the desired motion, and the validity of the proposed method is verified experimentally. In the experiments, the proposed method is applied to a grasping motion. The proposed method can trigger scaled bilateral control and assist the operator in real time.

5.1   Introduction

As mentioned in chapter 1, with the present low birthrate and aging population, there is concern about labor shortages: in workplaces, for housekeeping, and for nursing care. Robots are widely used for industrial applications such as the manufacture of automotive parts or electronic components, and in the future they are expected to spread out into our living environment, thus solving the problems of low birthrate and aging population as well as labor shortages. Specific implementations may include robots that monitor humans' motions and provide support as necessary.

Research on the measurement and extraction of human motions includes motion capture technologies using visual information. There are studies in which hand images are acquired by a camera in plan view and in side view so as to recognize the finger postures [106], and in which human motions are recognized from visual information and are then reproduced by robots [111]. However, as visual information provides only color and position, and recognition of grasping and other motions involving contact is difficult. Therefore, tactile information is needed for the recognition of complex motions. Recently, there has been much research on the transmission, extraction, and storage of tactile information, constituting the field of haptics. In master-slave systems, the transmission of tactile information can be achieved by means of bilateral control [66]. In addition, a motion acquisition system has been proposed to extract and reproduce human operations with objects, such as grasping, translation and rotation, by using coordinate transformations [112]. There has also been research on motion recording systems that simultaneously save the actions of multiple operators [113]. These studies have demonstrated the feasibility of transmission, extraction, and storage of tactile information by robots. Researchers have also investigated such techniques as personal authentication by time-frequency analysis of writing pressure [114], and recognition of road conditions using support vector machines, with feature vectors expressing the friction force between the road surface and the wheels [115]. The modal power has been defined on the basis of function modes [12], and elementary motion recognition has been implemented by linear discrimination algorithms [116]. Function modes are representations of multiple simultaneous motions by their separation in space. These studies show that environmental conditions and human motions can be recognized by using tactile information.

However, the robots dealt with in the above studies have three degrees of freedom at most and are restricted to linear motion. In addition, they do not support the recognition of combinations of successive elementary motions, or expansion and contraction of the time axis. A combination of successive ele-
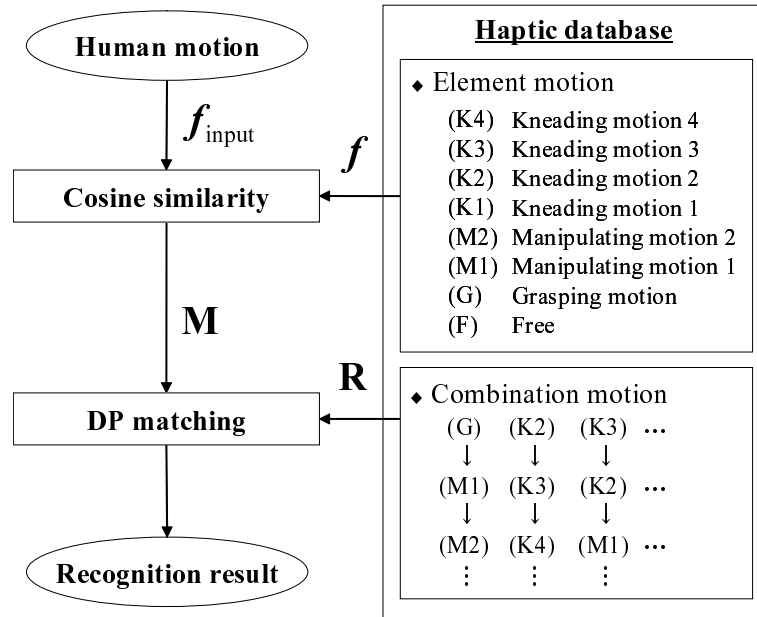
Fig. 5-1: Flow of proposed method.

mentary motions is, for example, "grip, then shake up and shake down". The elementary motions in this combination are "grip", "shake up" and "shake down". Recognition of the combined motion depends strongly on the motion speed.

In the first half of this chapter, firstly, tactile information is acquired by implementing bilateral control of a 5-DOF exoskeleton robot hand. Then the operator's motions are classified into 8 elementary motions by using the cosine similarity. Finally, expansion or contraction time axis is corrected by dynamic programming (DP) matching, and the successive motions in the combination are recognized. The proposed method is verified by experiments. An outline of the proposed method is shown in Fig. 5-1.

In the second half of this chapter, the subject is moved on to the actual application of the above-mentioned recognition method to the real-time power-assist system. In recent years, the number of robots working in the human environment has been increasing. The human environment is the space where we spend our everyday life: it typically includes a living room, kitchen, bedroom, etc. Examples of robots used in the human environment include domestic robots [7], physical therapy robots [8], electric bicycles [9], and electric wheelchairs [10]. Domestic robots have a three-fingered robot hand and open doors like a human does [7]. Physical therapy robots displayed human joint torque and muscle force during exercise to improve rehabilitation performance [8]. Electric bicycles and electric wheelchairs reduce the force necessary to drive [9, 10]. Thus, a variety of robots have been actively researched for

use in our daily lives. In the above cases, human motion recognition systems play a very important role in improving the ability of robots to support human life [13]. If robots understand what we want to do, they can select and provide an appropriate way to support our desires. Wearable sensors were used to recognize human action based on a decision tree structure [117]. Motion-capture technology is a research field wherein human motion is measured and extracted on the basis of visual information [42, 111, 118]. Multiple cameras were used for gesture recognition on the basis of marker-less upper body pose tracking in three dimensions [119]. The importance of recognizing a grasping motion is attracting a lot of attention, because we frequently grasp a wide variety of things in our daily lives [106, 120, 121]. However, it has proven difficult for conventional vision-based hand-capturing systems to recognize the grasping motion. The capturing systems can obtain sufficient information about joint angles and position, but they are incapable of acquiring information on the grasping force [104], [105]. Therefore, a grasping motion recognition method is required that provides both position and force information.

Haptics is a research field on the transmission, extraction, and preservation of position and force information: it has been studied extensively in recent years. Bilateral control [61–63], one of the methods used in teleoperation systems, is often used in haptics. In general, two types of robots are used in bilateral control systems: one is a master robot and the other is a slave robot. The master robot is operated by an operator, and the slave robot makes contact with an environment. The operator can feel the actual environmental reaction force through the master robot. Because of this sensation, robots can be made act as an agent for the operator in hazardous jobs. For this reason, this technique was originally applied to robots working in deep-sea, space, and nuclear containment operations, but the applicable field has been expanding to the human environment.

In the bilateral control system, position and force information can be recorded. This information is called haptic data. Some studies have confirmed that haptic data can be considered as a combination of many action components [12, 112]. Furthermore, an abstraction of the action components has been achieved using modal transformation methods [39, 109]. The modal transformation is one of the coordinate transformations. Fig. 5-2 shows a conventional concept and a proposed concept for the human motion recognition system. In the conventional concept, the haptic data is divided into the action components. Then, the strongest action component is regarded as a dominant motion [122]. However, these conventional decomposition techniques did not take into account two things: one is how to treat the flow of time, and the other is how to integrate the position and force similarities. Specifically, the conventional method can recognize the type of motion the operator performs (e.g., grasping or manipulating),
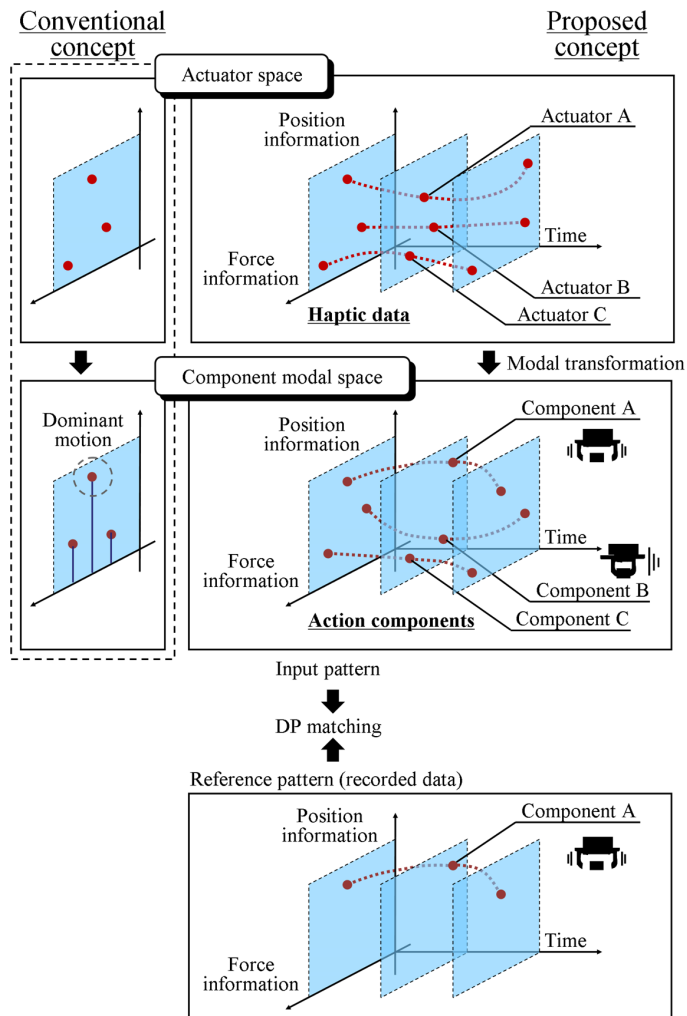
Fig. 5-2: Haptic action component and time variation.

but cannot judge how the performed motion has changed (e.g., transition of grip force). In contrast, in the proposed concept, a time series of the action components is used for motion recognition. The flow of time and the changes in position and force are treated based on a dynamic programming (DP) pattern-matching algorithm. Unintended differences may occur between the speed of the performed motion and the recorded motion. If there is time expansion and contraction between the acquired haptic data (input pattern) and the recorded haptic data (reference pattern), the recognition results are drastically degraded. Pattern-matching using DP [123] is one of the methods to cope with this type of time expansion and contraction: there are some studies that treat the time flow on the basis of this method. One of the studies succeeded in applying DP matching to a pushing motion with a haptic device, although the range of
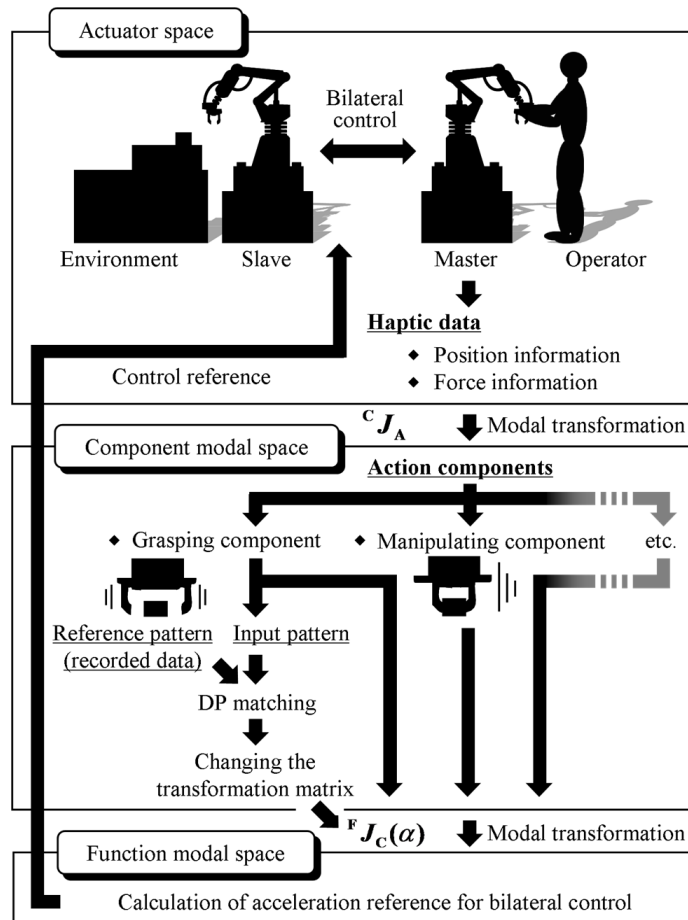
Fig. 5-3: Outline of the proposed method.

motion in the application of this method was limited to one degree of freedom [122]. The difference between our proposal and the previous study [124] is that in our study, the data traveled first to a modal transformation, whereas in the previous research, the data was channeled directly to the DP matching process. Another study [125] extended the previous method to motion with two degrees of freedom. The extended method was also tried to apply the recognition result to a position control system in real time. However, the recognition took a few seconds and the verification was insufficient.

This chapter continues to expand the knowledge in this area by describing a novel motion recognition method based on haptic data. An outline of the proposed method is shown in Fig. 5-3. In this method, the haptic data are first acquired by a bilateral control system. Then, the haptic data are divided into action components such as a grasping component, a manipulating component, and a yawing component by using modal transformation. Both position and force information in the modal space are compared with

a reference pattern using a DP pattern-matching algorithm. Finally, the position and force information are scaled and transmitted to the operator in strict real time. This study also included experiments in which the proposed method was applied to grasping motions.

This chapter is organized as follows: The first half of this chapter proposes a recognition method for combined human motion. In Section 5.2.1, bilateral control systems are explain and in Section 5.2.2 the structure of the robot considered in this chapter is described. The new recognition method is introduced in Sections 5.2.3 and 5.2.4 and experimental results are presented in Section 5.2.5. The second half of this chapter applies the recognition method to modal space, and realizes a power assist system. Section 5.3.1 presents a model of the system used in this chapter. Section 5.3.2 describes the bilateral control for haptic data extraction. Haptic data provide position and force information. Section 5.3.3 explains the proposed method to recognize a grasping motion. The experimental results are shown in section 5.3.4. This chapter is finally concluded in section 5.4.
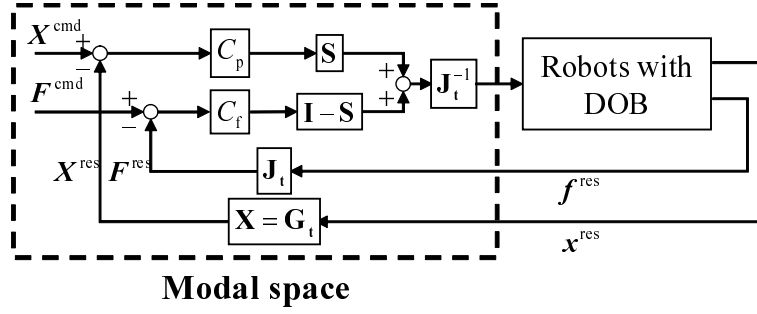
Fig. 5-4: Block diagram of bilateral control.

5.2   Recognition of Combined Motion

5.2.1   Bilateral Control System for Acquisition of Haptic Information

In this study, a robot hand was provided with 4-channel bilateral control to acquire tactile information. The control objectives of the bilateral control system were as follows:

$$x_{\mathrm{m}}^{\mathrm{res}} - x_{\mathrm{s}}^{\mathrm{res}} = 0, \tag{5.1}$$

$$f_{\mathrm{m}}^{\mathrm{res}} + f_{\mathrm{s}}^{\mathrm{res}} = 0. \tag{5.2}$$

eq. (5.1) expresses position tracking between the master and slave, and eq. (5.1) represents the artificial implementation of the action-reaction law. A block diagram of bilateral control using DOB is shown in Fig. 5-4. The generalized position vector x^{res}, generalized force vector f^{res}, task Jacobian J_t, coordinate transformation matrix G_t, mass matrix m, selection matrix S, position command vector X^{cmd}, and

force command vector $\boldsymbol{F}^{\mathrm{cmd}}$ are defined as follows:

$$\boldsymbol{x}^{\mathrm{res}} = [\, x_{\mathrm{m}}^{\mathrm{res}} \,,\, x_{\mathrm{s}}^{\mathrm{res}} \,]^{\mathrm{T}}, \tag{5.3}$$

$$\boldsymbol{f}^{\mathrm{res}} = [\, \hat{f}_{\mathrm{m}}^{\mathrm{res}} \,,\, \hat{f}_{\mathrm{s}}^{\mathrm{res}} \,]^{\mathrm{T}}, \tag{5.4}$$

$$\boldsymbol{J_t} = \begin{bmatrix} 1 & -1 \\ 1 & 1 \end{bmatrix}, \tag{5.5}$$

$$\boldsymbol{G_t} = [\, x_{\mathrm{m}}^{\mathrm{res}} - x_{\mathrm{s}}^{\mathrm{res}} \,,\, 0 \,]^{\mathrm{T}}, \tag{5.6}$$

$$\boldsymbol{m} = \begin{bmatrix} m_{\mathrm{m}} & 0 \\ 0 & m_{\mathrm{s}} \end{bmatrix}, \tag{5.7}$$

$$\boldsymbol{S} = \begin{bmatrix} 1 & 0 \\ 0 & 0 \end{bmatrix}, \tag{5.8}$$

$$\boldsymbol{X}^{\mathrm{cmd}} = 0, \tag{5.9}$$

$$\boldsymbol{F}^{\mathrm{cmd}} = 0. \tag{5.10}$$

The position response $\boldsymbol{X}^{\mathrm{res}}$ and force response $\boldsymbol{F}^{\mathrm{res}}$ in modal space are expressed by means of the coordinate transformation matrix and task Jacobian as follows:

$$\boldsymbol{X}^{\mathrm{res}} = \boldsymbol{G_t} = [\, x_{\mathrm{m}}^{\mathrm{res}} - x_{\mathrm{s}}^{\mathrm{res}} \,,\, 0 \,]^{\mathrm{T}}, \tag{5.11}$$

$$\boldsymbol{F}^{\mathrm{res}} = \boldsymbol{J_t}\boldsymbol{f}^{\mathrm{res}}. \tag{5.12}$$

This study employs a position proportional-derivative controller $C_{\mathrm{p}}(s)$ and force proportional controller C_{f}. The controllers are expressed in terms of feedback gain as follows:

$$C_{\mathrm{p}}(s) = K_{\mathrm{p}} + K_{\mathrm{v}}s, \tag{5.13}$$

$$C_{\mathrm{f}} = K_{\mathrm{f}}. \tag{5.14}$$

The acceleration reference is calculated as follows:

$$\begin{aligned} s^2 \boldsymbol{x}^{\mathrm{ref}}(s) &= \boldsymbol{m}^{-1}\boldsymbol{J_t}^{-1}\left(s^2 \boldsymbol{x}_{\mathrm{dif}}^{\mathrm{ref}}(s) + s^2 \boldsymbol{x}_{\mathrm{com}}^{\mathrm{ref}}(s)\right) \\ &= \boldsymbol{m}^{-1}\boldsymbol{J_t}^{-1}\Big\{ C_{\mathrm{p}}(s)\boldsymbol{S}\left(\boldsymbol{X}^{\mathrm{cmd}}(s) - \boldsymbol{G_t}(s)\right) \\ &\qquad + C_{\mathrm{f}}(\boldsymbol{I} - \boldsymbol{S})\left(\boldsymbol{F}^{\mathrm{cmd}}(s) - \boldsymbol{J_t}\boldsymbol{f}^{\mathrm{res}}(s)\right) \Big\}. \end{aligned} \tag{5.15}$$

Fig. 5-5: Master and slave robots.

(a) Thumb finger.

(b) Index finger and middle finger.
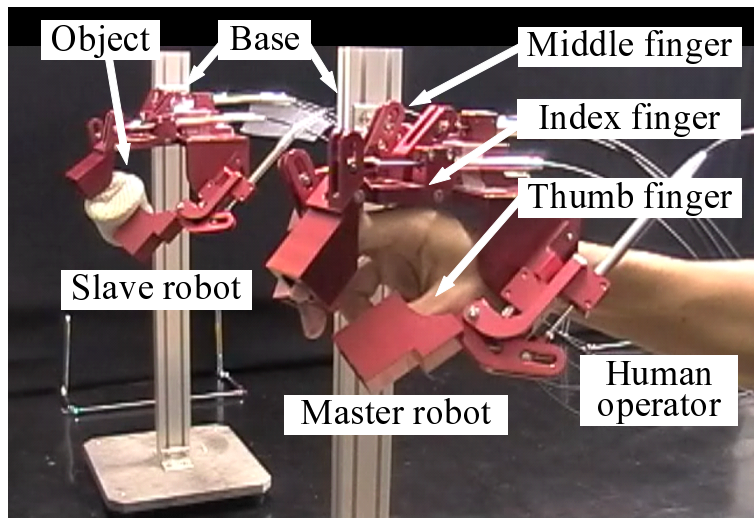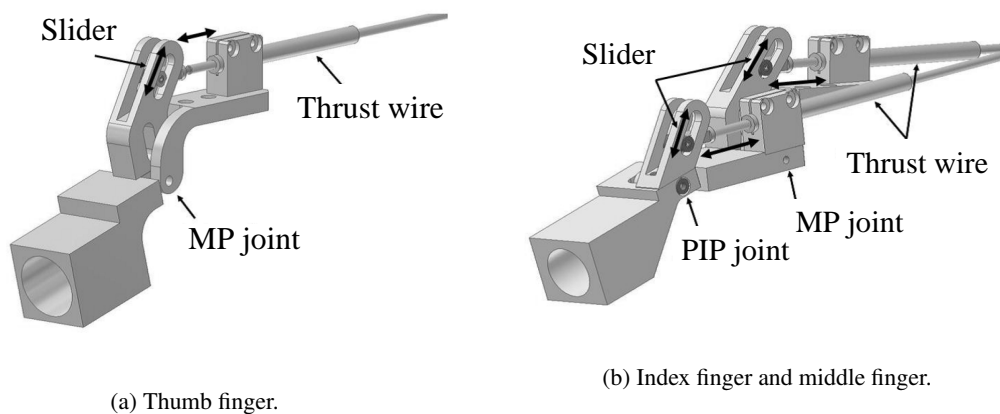
Fig. 5-6: Structure of finger.

5.2.2 Structure of Robot Hand

In this section, the structure of the robot hand used in the experiments is explained. The appearance of the robot hand is shown in Fig. 5-5. An operator wears the master robot hand and manipulates objects via the slave robot hand. Both the master and slave robot hands are exoskeletal structures with three fingers: thumb, index finger, and middle finger. The structure of the thumb is shown in Fig. 5-6(a): the structure of the index and middle fingers is shown in Fig. 5-6(b). The thumb has one joint (MP joint), and the index and middle fingers have two joints (MP joint, PIP joint) each. Thus, both the master and slave robot hands have 5-DOFs each. Only the rotational component of the force applied by the operator
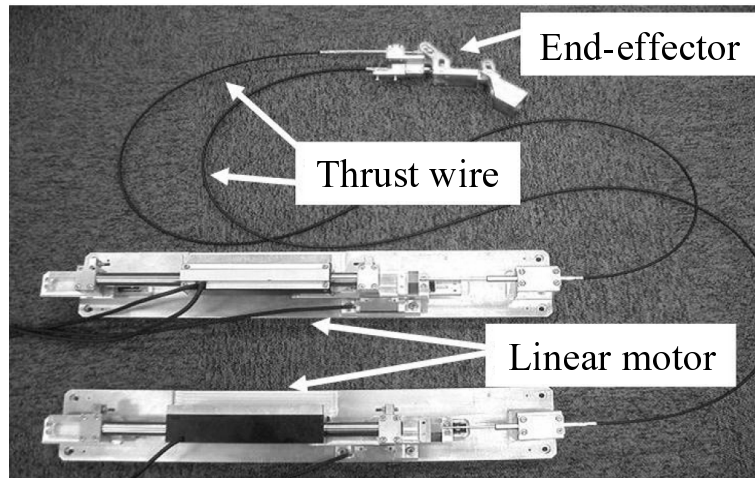
Fig. 5-7: Flexible actuator.

can be observed in each joint, and hence the motion recognition rate diminishes when the orientation of the wrist changes. To avoid such situations, the back of the hand is fixed during manipulations.

The linear motors and actuator unit to drive the joints are connected by thrust wires as shown in Fig. 5-7. The driving force is transmitted from the motors to the end effectors via the thrust wires. The thrust wires have good force transmission characteristics and flexibility, allowing the motors to be arranged arbitrarily. The linear motors, thrust wires, and end effectors are called flexible actuators.

In conventional designs, the master and slave robot hands often have different structures [126] [127], resulting in complicated design. In addition, the actuators are directly embedded in the robot hands, which add to the weight of the hand and the burden on the operator. There is also a design with the same structure of the master and slave robot hands [108], but in that design the motion is restricted to a plane. In contrast, the robot hand used in this study supports three-dimensional grasping and manipulations. The use of the same structure of the master and slave robot hands contributes to simpler design of the bilateral control system. In addition, common components can be used for the master and slave robots, thus reducing the manufacturing cost. Due to the flexible actuators [108], the motor and robot hands can be located on separate locations, thus reducing the burden on the operator caused by the weight of the robot hand.
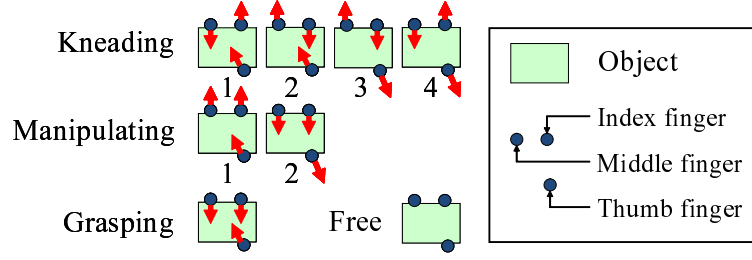
Fig. 5-8: Motion classification.

5.2.3 Classification of Element Motion by Cosine Similarity

In this study, the linear motors attached to each joint are provided with RFOB to classify finger motions. When an object is manipulated on the palm side, 8 major motions are observed depending on the combination of forces applied by the fingers to the object. The motions are shown schematically in Fig. 5-8.

The average values of the reaction force for each operator's elementary motions are stored in a tactile database as five-dimensional vectors (reference vectors). For example, when the operator manipulated an object, the average force in the MP joint of the thumb was calculated as follows:

$$\bar{f}^{\text{th,MP}} \quad = \quad \frac{1}{k_2 - k_1} \sum_{k=k_1}^{k_2} f^{\text{th,MP}}[k], \tag{5.16}$$

Here $f[k]$ denotes the force response at instant k, and k_1 and k_2 respectively denote the start and end points of the elementary motion. The reference vector of an elementary motion is expressed as follows:

$$\boldsymbol{f} = [\bar{f}^{\text{th,MP}} \, , \, \bar{f}^{\text{in,MP}} \, , \, \bar{f}^{\text{in,PIP}} \, , \, \bar{f}^{\text{mi,MP}} \, , \, \bar{f}^{\text{mi,PIP}}]^{\text{T}}. \tag{5.17}$$

Here $\boldsymbol{f}$ is a reference vector composed of the average force values in all joints. In this study, motions were considered only at 3 contact points: since the robot hand was capable of three-dimensional grasping and manipulation, the reference vectors were calculated using the force response at all 5 joints. In addition the same elementary motions can differ depending on the size, weight, and shape of the object, which is reflected in the reference vectors: therefore, reference vectors must be calculated for each object.

The input vectors are defined as five-dimensional vectors whose elements are the force responses at every joint. The input vector at instant k is

$$\boldsymbol{f}_{\text{input}}[k] = [f_{\text{input}}^{\text{th,MP}}[k] \, , \, f_{\text{input}}^{\text{in,MP}}[k] \, , \, f_{\text{input}}^{\text{in,PIP}}[k] \, , \, f_{\text{input}}^{\text{mi,MP}}[k] \, , \, f_{\text{input}}^{\text{mi,PIP}}[k]]^{\text{T}}. \tag{5.18}$$

In this study, difference of the force distributions at the joints for every elemental motion is assumed: thus the input vectors are compared with the reference vectors using the cosine similarity in order to classify elementary motions. The cosine similarity expresses the angular difference between two vectors. Therefore, it can be obtained regardless of the intensity of motion. The cosine similarity is calculated as the inner product of the input and reference vectors divided by their norms. The cosine similarity between the input and reference vectors is found as follows:

$$S = \frac{\boldsymbol{f} \cdot \boldsymbol{f}_{\text{input}}[k]}{\|\boldsymbol{f}\|\|\boldsymbol{f}_{\text{input}}[k]\|}. \tag{5.19}$$

The range of the cosine similarity is

$$-1 \leq S \leq 1. \tag{5.20}$$

When $\|\boldsymbol{f}_{\text{input}}[k]\|$ is small, the cosine similarity becomes unstable. The category of "Free" was applied when $\|\boldsymbol{f}_{\text{input}}[k]\|$ was smaller than 3N. An input motion was assigned to the motion among the 8 elementary motions that had the greatest similarity S. The classification result obtained at instant k is denoted by m_k.

5.2.4   Recognition of Combination Motion by Dynamic Programing Matching

In pattern recognition, the results are significantly degraded in case of expansion or contraction of the time axis. DP matching [128] is a method of aligning the time axes so as to optimize the correspondence relations between time series of feature patterns. The input combined motion pattern $\mathbf{M}$ and the reference combined motion pattern $\mathbf{R}$ are expressed as follows:

$$\mathbf{M} = m_1, m_2, \cdots, m_I, \tag{5.21}$$

$$\mathbf{R} = r_1, r_2, \cdots, r_J. \tag{5.22}$$

In this study, the classification results calculated in Section 5.2.3 were used as time series of feature patterns. I and J denote the lengths (number of data) of the input combined motion pattern and the reference combined motion pattern, respectively. The distance $D(\mathbf{M}, \mathbf{R})$ between patterns is called the DP value and is calculated by the algorithm below. The local distance between the i-th element m_i of the input combined motion pattern and the j-th element r_j of the reference combined motion pattern is found as follows:

$$d(i, j) = \begin{cases} 0 & (m_i = r_j) \\ \alpha & (m_i \neq r_j) \end{cases}, \tag{5.23}$$

Here α is a penalty applied in case of mismatch, and is called the local distance. The initial conditions are set as follows:

$$
\begin{aligned}
g(1,1) &= d(1,1), & (5.24) \\
g(2,2) &= d(1,1) + 2d(2,2), & (5.25) \\
g(2,3) &= d(1,1) + 2d(2,2) + d(2,3), & (5.26) \\
g(3,2) &= d(1,1) + 2d(2,2) + d(3,2), & (5.27)
\end{aligned}
$$

where g is the cumulative distance. The rest of the cumulative distance values $g(i,j)$ are calculated by the following recurrent equations [123]:

$$
g(i,j) = \infty \,, \ \big(i = 1, 2 \cup j = 1, 2\big) \cap \big((i,j) \neq (1,1), (2,2), (2,3), (3,2)\big), \tag{5.28}
$$

$$
g(i,j) = \min
\begin{cases}
g(i-2, j-1) + 2d(i-1, j) + d(i,j) \\
g(i-1, j-1) + d(i,j) \\
g(i-1, j-2) + 2d(i, j-1) + d(i,j)
\end{cases} , \tag{5.29}
$$

In eq. (5.29) the minimum selection area is defined by slope constraints that restrict the expansion or contraction of time axis. The slope of the best path is restricted to values from $1/2$ to 2. DP matching is a method of expanding or contracting the time axis so as to minimize the following DP value under the slope constraints:

$$
D(\mathbf{M}, \mathbf{R}) = g(I, J)/(I + J). \tag{5.30}
$$

From the slope constraints, I is selected within the range of eq. (5.31) to minimize the DP value:

$$
\frac{J}{2} < I < 2J. \tag{5.31}
$$

Here matching is recognized when $D(\mathbf{M}, \mathbf{R})$ is below a threshold τ.

Table 5.1: Parameters in experiments.

Parameter	Meaning of The Parameter	Value
K_p	Position Feedback Gain	900 $1/\mathrm{s}^2$
K_v	Velocity Feedback Gain	60 $1/\mathrm{s}$
K_f	Force Feedback Gain	0.8 $\mathrm{m/Ns}^2$
g_dis	Cut-off Frequency of DOB	200 rad/s
g_reac	Cut-off Frequency of RFOB	500 rad/s
M_n	Nominal Mass	0.5 kg

5.2.5 Experiments

This section describes our experimental verification of the effectiveness of the proposed method. Experimental results are presented on the classification of elementary motions using the cosine similarity in section 5.2.5, and cross-validate the combined motion recognition using the classification results in section 5.2.5. The effect of the classification on the recognition of combined motions is investigated in section 5.2.5. The parameters of bilateral control used for the acquisition of tactile information are given in Table 5.1. In the experiments, the master and slave robot hands were driven by 10 linear motors. The control cycle was 0.1 ms and the data save cycle was 0.1 s. The input vectors were calculated from the force response of the linear motors attached to each joint. Commands were issued to the operator on a PC monitor.
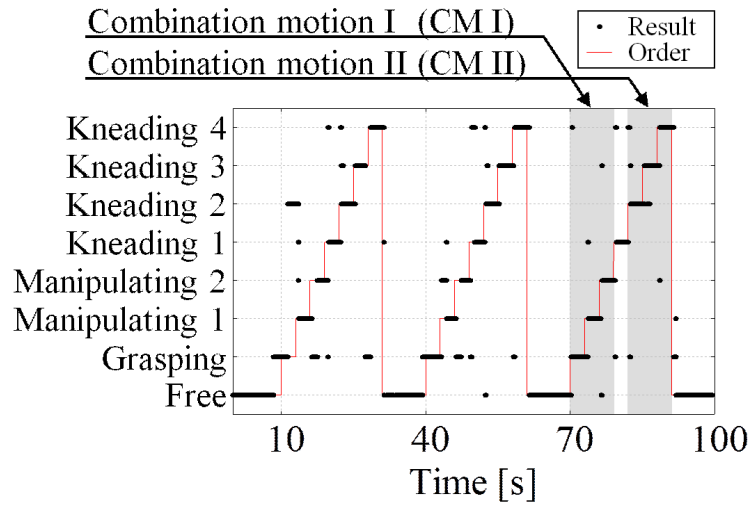
(a) Classification results 1.
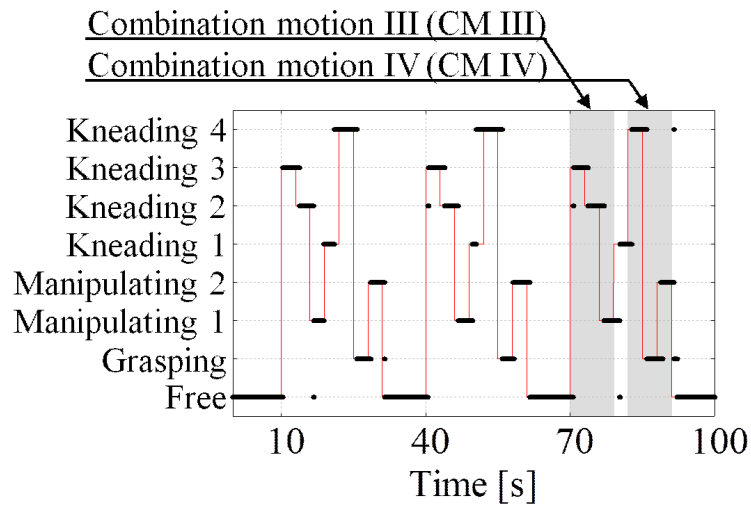
(b) Classification results 2.

Fig. 5-9: Classification results.

Classification of Element Motions

An example of the classification results is shown in Fig. 5-9. In the diagram, the time and elementary motions are represented by the horizontal and vertical axes respectively. The black dots and red lines

Table 5.2: Classification rate.

Order \ Result		K4	K3	K2	K1	M2	M1	G	F
Kneading 4	(K4)	88	4	1	5	1	0	1	0
Kneading 3	(K3)	2	64	23	0	1	0	2	9
Kneading 2	(K2)	2	16	78	3	0	0	2	0
Kneading 1	(K1)	41	0	0	39	6	11	3	0
Manipulating 2	(M2)	6	0	0	3	66	4	21	0
Manipulating 1	(M1)	0	0	18	4	0	75	3	0
Grasping	(G)	19	0	18	0	3	0	58	1
Free	(F)	6	0	0	0	5	1	6	81 [%]

Table 5.3: Cosine similarity between reference vectors.

	K4	K3	K2	K1	M2	M1	G
K4	-	0.14	0.07	0.74	0.73	0.04	0.78
K3	-	-	0.97	0.15	0.76	0.12	0.66
K2	-	-	-	0.21	0.70	0.33	0.64
K1	-	-	-	-	0.55	0.70	0.76
M2	-	-	-	-	-	0.08	0.93
M1	-	-	-	-	-	-	0.35
G	-	-	-	-	-	-	-

represent classification results and commands issued to the operator, respectively. When the black dots lie on the red lines, the classification results are correct. The commands began from "Free", and were changed every 3 s. The classification results for every motion are given in Table 5.2. Cosine similarity between the reference vectors is shown in Table 5.3. In Table 5.2, each row shows the classification results for respective commands. The classification rate shown on the diagonal was 69% on average. Here "Kneading 3" was mistaken for "Kneading 2", "Kneading 1" was mistaken for "Kneading 4", and "Manipulating 2" was mistaken for "Grasping" with probabilities above 20%. These errors can be explained by the high similarity between the reference vectors.

Table 5.4: Combination motions.

-	1st Motion	2nd Motion	3rd Motion
CM I	Grasping	Manipulating 1	Manipulating 2
CM II	Kneading 2	Kneading 3	Kneading 4
CM III	Kneading 3	Kneading 2	Manipulating 1
CM IV	Kneading 4	Grasping	Manipulating 2

Table 5.5: Recognition rate.

Input / Reference	CM I	CM II	CM III	CM IV
CM I	*23/30	0/36	0/36	0/36
CM II	0/36	*28/30	1/36	0/36
CM III	3/36	0/36	*30/30	0/36
CM IV	0/36	0/36	0/36	*26/30
Positive Predictive Value	96.4% (107/111)			
Negative Predictive Value	97.1% (428/441)			

Recognition of Combination Motion

The command series were defined as shown in Table 5.4. The respective responses are called combined motions (CM) I to IV. These four motions were selected at random to show that combined motions can be recognized by the proposed method. Classification of elementary motions was applied 6 times to each combined motion (a total of 24 results). Then one classification result was used as a reference combined motion pattern, and the remaining 23 results were used as input combined motion patterns for cross-validation by DP matching. The mismatch penalty a was set to 10.0, and the threshold τ was set empirically to 3.0. The results of cross-validation are shown in Table 5.5. Here the denominator and numerator represent the number of matching and the number of positive responses, respectively. All non-positive matching results are negative. A matching assumed to be positive is marked by an asterisk *. From the total of 552 matchings, the positive predictive value (PPV) and negative predictive value (NPV) were found to be 96.4% and 97.1%, respectively.

Table 5.6: Recognition rate using ideal reference.

Input / Reference	CM I	CM II	CM III	CM IV
Ideal CM I	∗6/6	0/6	0/6	0/6
Ideal CM II	0/6	∗6/6	0/6	0/6
Ideal CM III	0/6	0/6	∗6/6	0/6
Ideal CM IV	0/6	0/6	0/6	∗5/6
Positive Predictive Value	100.0% (23/23)			
Negative Predictive Value	98.6% (72/73)			

Summary of Experiments

In order to investigate the effect of classification errors, the recognition rate was clarified when the commands issued to the operator were used as reference combined motion patterns, as shown in Table 5.6. Here the PPV was 100.0% and the NPV was 98.6%. These values are higher than the probabilities obtained in section 5.2.5: thus, mistakes in the classification of elementary motions degrade the accuracy of combined motion recognition.

The relationship between the time elapsing after command change and the classification accuracy is illustrated in Fig. 5-10. Here the instant of command change is 0. Fig. 5-10(a) shows the rate of matching between the results of elementary motion classification and the current command. As can be seen from the graph, the match rate is low immediately after motion change. Fig. 5-10(b) shows the rate of matching between the results of elementary motion classification and the current or previous command. As can be concluded from Fig. 5-10(a) and Fig. 5-10(b), motions are often incorrectly classified in accordance with the previous command in transient states. However, this can be corrected by expansion or contraction of the time axis. However, there is no strong correlation between the match rate and time in Fig. 5-10(b), and reduction of such mistakes is an topic for improvement of the proposed method. In this study, DP matching was used for deterministic signal comparison, but one can expect improvements in performance by using stochastic algorithms such as hidden Markov models [129] or dynamic Bayesian networks [130].
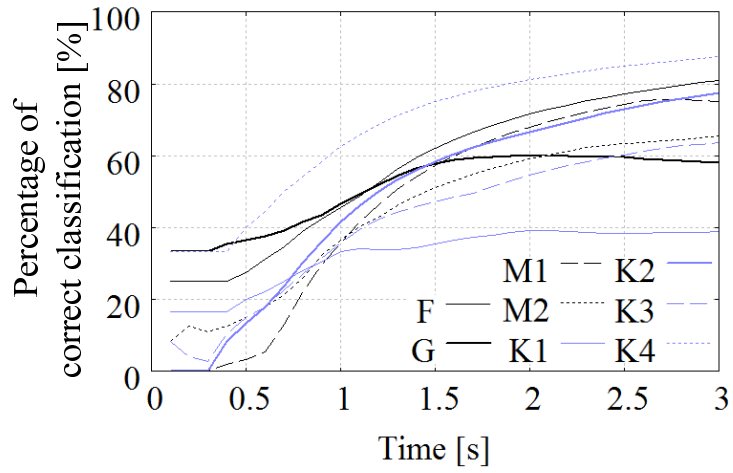
(a) Concordance rate with the current order.
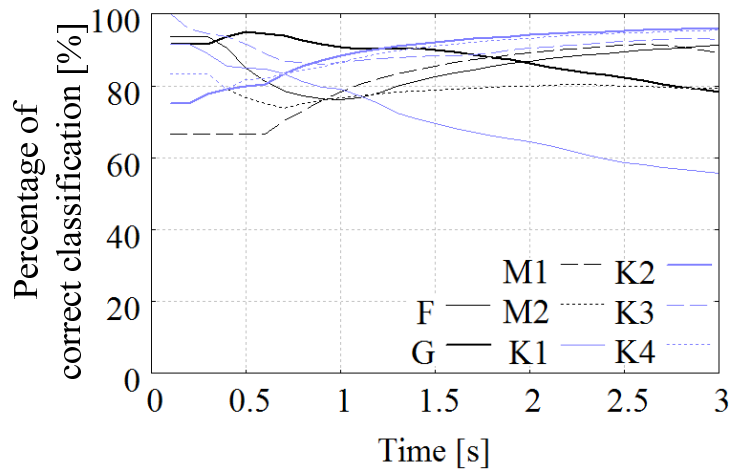
(b) Concordance rate with the previous and current order.

Fig. 5-10: Classification performance.
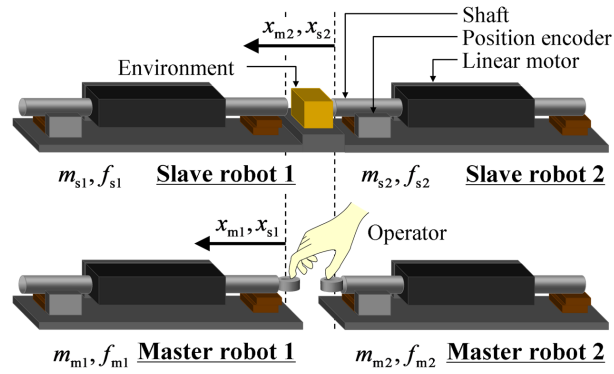
Fig. 5-11: Model of the handling robot.

5.3   Recognition and Real-Time Assist

5.3.1   Modeling

Fig. 5-11 shows a model of the master-slave robot used in this study. Two linear motors are used in each side, as a master robot and a slave robot. The slave robot 1 is located on the left side of the environment. The slave robot 2 is placed on the opposite side. An operator inserts fingers in the rings at the end of each shaft to move the master robot. Then, the slave robot makes contact with the environment. The motion equation is

$$\boldsymbol{m}\ddot{\boldsymbol{x}} \;=\; \boldsymbol{f}. \tag{5.32}$$

Here,

$$\boldsymbol{m} \;=\; \mathrm{diag}\left[\begin{array}{cccc} m_{\mathrm{m1}} & m_{\mathrm{m2}} & m_{\mathrm{s1}} & m_{\mathrm{s2}} \end{array}\right], \tag{5.33}$$

$$\boldsymbol{x} \;=\; \left[\begin{array}{cccc} x_{\mathrm{m1}} & x_{\mathrm{m2}} & x_{\mathrm{s1}} & x_{\mathrm{s2}} \end{array}\right]^{\mathrm{T}}, \tag{5.34}$$

$$\boldsymbol{f} \;=\; \left[\begin{array}{cccc} f_{\mathrm{m1}} & f_{\mathrm{m2}} & f_{\mathrm{s1}} & f_{\mathrm{s2}} \end{array}\right]^{\mathrm{T}}, \tag{5.35}$$

where

m mass matrix,

x position vector,

f force vector,

m mass,

x position,

f force,

m1   (subscript) about master robot 1,

m2   (subscript) about master robot 2,

s1   (subscript) about slave robot 1, and

s2   (subscript) about slave robot 2.

5.3.2 Bilateral Control for Haptic Data Extraction

Our proposal is explained with the practical example of a simple multiple-degree-of-freedom system that can perform grasping and manipulating motions. This method can be applied to a more complex system that has more degrees of freedom if the modal transformation can be conducted. Incidentally, modal transformation techniques for multiple-degree-of-freedom systems have already been proposed [39].

Control Goals and Modal Transformation

In this study, an acceleration-based bilateral control (ABC) system [65] based on oblique coordinate control [53][54] is used to extract haptic data. The most important aim of ABC is the perception of the mechanical impedance of the environment existing in a remote place. This aim can be achieved by two types of elements: one is position tracking between the master and slave robots, and the other is force feedback (realization of the law of action and reaction). Therefore, the control goals are expressed as

$$x_{\mathrm{m1}} = x_{\mathrm{s1}}, \tag{5.36}$$

$$x_{\mathrm{m2}} = x_{\mathrm{s2}}, \tag{5.37}$$

$$f_{\mathrm{m1}} = -f_{\mathrm{s1}}, \tag{5.38}$$

$$f_{\mathrm{m2}} = -f_{\mathrm{s2}}. \tag{5.39}$$

To describe each action component explicitly, these control goals are restated as follows:

- Position tracking of grasping motion

$$x_{\mathrm{m1}} - x_{\mathrm{m2}} \quad = \quad x_{\mathrm{s1}} - x_{\mathrm{s2}}. \tag{5.40}$$

- Position tracking of manipulating motion

$$x_{\mathrm{m1}} + x_{\mathrm{m2}} \quad = \quad x_{\mathrm{s1}} + x_{\mathrm{s2}}. \tag{5.41}$$

- Force feedback of grasping motion

$$f_{\mathrm{m1}} - f_{\mathrm{m2}} \quad = \quad -(f_{\mathrm{s1}} - f_{\mathrm{s2}}). \tag{5.42}$$

- Force feedback of manipulating motion

$$f_{\mathrm{m1}} + f_{\mathrm{m2}} \quad = \quad -(f_{\mathrm{s1}} + f_{\mathrm{s2}}). \tag{5.43}$$

Here, the grasping motion and the manipulating motion are defined as pushing from both sides and as moving in the same direction, respectively.

This chapter defines three types of modal space: an actuator space, a component modal space, and a function modal space. Fig. 5-12 shows the role of each modal space. Actuators are controlled in the actuator space. Action components are expressed in the component modal space, and reference values are calculated in the function modal space. The function modal space consists of two modes: one is used for position tracking, and the other is employed for force feedback. This function modal space makes a valuable contribution to the decomposition of position and force control systems by reducing interferences. A transformation matrix from the actuator space to the component modal space is defined as

$$^{\mathrm{C}}\boldsymbol{J}_{\mathrm{A}} \quad = \quad \begin{bmatrix} 1 & -1 & 0 & 0 \\ 0 & 0 & 1 & -1 \\ 1 & 1 & 0 & 0 \\ 0 & 0 & 1 & 1 \end{bmatrix}. \tag{5.44}$$

This transformation matrix converts the physical quantities of the actuators into the physical quantities of the action components. The variables in the component modal space are described as

$$\begin{bmatrix} x_{\mathrm{m}}^{\mathrm{grasp}} & x_{\mathrm{s}}^{\mathrm{grasp}} & x_{\mathrm{m}}^{\mathrm{mani}} & x_{\mathrm{s}}^{\mathrm{mani}} \end{bmatrix}^{\mathrm{T}} \quad = \quad {}^{\mathrm{C}}\boldsymbol{J}_{\mathrm{A}}\boldsymbol{x}, \tag{5.45}$$

$$\begin{bmatrix} f_{\mathrm{m}}^{\mathrm{grasp}} & f_{\mathrm{s}}^{\mathrm{grasp}} & f_{\mathrm{m}}^{\mathrm{mani}} & f_{\mathrm{s}}^{\mathrm{mani}} \end{bmatrix}^{\mathrm{T}} \quad = \quad {}^{\mathrm{C}}\boldsymbol{J}_{\mathrm{A}}\boldsymbol{f}, \tag{5.46}$$

where the superscripts "grasp" and "mani" represent the grasping and manipulating motions, respectively. The subscript "m" represents the master side, and the subscript "s" represents the slave side. The action component of the grasping motion will be used in section 5.3.3. This study uses the variables of grasping motion to make the explanation of the recognition procedures clear. Note that this method can be applied to any other action component. A transformation matrix from the component modal space to the function modal space is defined as

$$
{}^{\mathrm{F}}\boldsymbol{J}_{\mathrm{C}} \;=\; \begin{bmatrix} 1 & -1 & 0 & 0 \\ 0 & 0 & 1 & -1 \\ 1 & 1 & 0 & 0 \\ 0 & 0 & 1 & 1 \end{bmatrix}. \tag{5.47}
$$

This transformation matrix converts the physical quantities of the action components into the physical quantities of decoupled modes for the bilateral controller. Variables in the function modal space are described as

$$
\boldsymbol{X} \;=\; \left({}^{\mathrm{F}}\boldsymbol{J}_{\mathrm{C}}\,{}^{\mathrm{C}}\boldsymbol{J}_{\mathrm{A}}\right)\boldsymbol{x} = \boldsymbol{J}_t\boldsymbol{x}, \tag{5.48}
$$

$$
\boldsymbol{F} \;=\; \left({}^{\mathrm{F}}\boldsymbol{J}_{\mathrm{C}}\,{}^{\mathrm{C}}\boldsymbol{J}_{\mathrm{A}}\right)\boldsymbol{f} = \boldsymbol{J}_t\boldsymbol{f}, \tag{5.49}
$$

where the product of ${}^{\mathrm{C}}\boldsymbol{J}_{\mathrm{A}}$ and ${}^{\mathrm{F}}\boldsymbol{J}_{\mathrm{C}}$ is called the task Jacobian matrix $\boldsymbol{J}_t$. The variables $\boldsymbol{X}$ and $\boldsymbol{F}$ denote the position and force matrices in the function modal space, respectively. Reference values are calculated from the variables of the function modal space [53, 54].

In contrast, in a scaled bilateral control, control goals are expressed as follows:

$$
\alpha(x_{\mathrm{m1}} - x_{\mathrm{m2}}) \;=\; x_{\mathrm{s1}} - x_{\mathrm{s2}}, \tag{5.50}
$$

$$
\alpha(x_{\mathrm{m1}} + x_{\mathrm{m2}}) \;=\; x_{\mathrm{s1}} + x_{\mathrm{s2}}, \tag{5.51}
$$

$$
\alpha(f_{\mathrm{m1}} - f_{\mathrm{m2}}) \;=\; -(f_{\mathrm{s1}} - f_{\mathrm{s2}}), \tag{5.52}
$$

$$
\alpha(f_{\mathrm{m1}} + f_{\mathrm{m2}}) \;=\; -(f_{\mathrm{s1}} + f_{\mathrm{s2}}). \tag{5.53}
$$

Here, α denotes a scaling ratio. Therefore, the transformation matrix is defined as

$$
{}^{\mathrm{F}}\boldsymbol{J}_{\mathrm{C}}(\alpha) \;=\; \begin{bmatrix} \alpha & -1 & 0 & 0 \\ 0 & 0 & \alpha & -1 \\ \alpha & 1 & 0 & 0 \\ 0 & 0 & \alpha & 1 \end{bmatrix}. \tag{5.54}
$$

This scaled bilateral control can be used for power-assist systems.

Oblique Coordinate Control

An acceleration reference $\ddot{\boldsymbol{X}}_{\mathrm{X}}^{\mathrm{ref}}$ for position tracking and a force reference $\boldsymbol{F}_{\mathrm{X}}^{\mathrm{ref}}$ to achieve the force control are obtained as

$$
\begin{bmatrix} \ddot{\boldsymbol{X}}_{\mathrm{X}}^{\mathrm{ref}} \\ \boldsymbol{F}_{\mathrm{F}}^{\mathrm{ref}} \end{bmatrix} = C_{\mathrm{p}}\mathbf{S}(\boldsymbol{X}^{\mathrm{cmd}} - \boldsymbol{X}^{\mathrm{res}})
$$
$$
+ C_{\mathrm{f}}(\mathbf{I} - \mathbf{S})(\boldsymbol{F}^{\mathrm{cmd}} - \boldsymbol{F}^{\mathrm{res}}), \tag{5.55}
$$

where $\mathbf{I}$, C_{p} and C_{f} denote 2×2 unit matrix, position controller, and force controller, respectively. The superscript "cmd" and the subscripts "X" and "F" represent the command, relation with position control, and relation with force control, respectively. Here, $\mathbf{S}$ is a selection matrix, defined as

$$
\mathbf{S} = \begin{bmatrix} \mathbf{I} & \mathbf{0} \\ \mathbf{0} & \mathbf{0} \end{bmatrix}. \tag{5.56}
$$

Both command values are zero in the case of bilateral control. The reference values in eq. (5.55) have to satisfy

$$
M_t \begin{bmatrix} \ddot{\boldsymbol{X}}_{\mathrm{X}}^{\mathrm{ref}} \\ \ddot{\boldsymbol{X}}_{\mathrm{F}}^{\mathrm{ref}} \end{bmatrix} = \begin{bmatrix} \boldsymbol{F}_{\mathrm{X}}^{\mathrm{ref}} \\ \boldsymbol{F}_{\mathrm{F}}^{\mathrm{ref}} \end{bmatrix} = \boldsymbol{F}^{\mathrm{ref}}, \tag{5.57}
$$

where $\boldsymbol{F}_{\mathrm{X}}^{\mathrm{ref}}$ is a force reference for position tracking and $\ddot{\boldsymbol{X}}_{\mathrm{F}}^{\mathrm{ref}}$ is an acceleration reference for force control. Here, the dynamics in the modal space is developed as

$$
J_t m J_t^{-1} \ddot{\boldsymbol{X}} = \boldsymbol{F}. \tag{5.58}
$$

The equivalent mass is defined as

$$
M_t = J_t m J_t^{-1}, \tag{5.59}
$$

which is called the task mass matrix. Each element of M_t is expressed as

$$
M_t = \begin{bmatrix} M_{\mathrm{XX}} & M_{\mathrm{XF}} \\ M_{\mathrm{FX}} & M_{\mathrm{FF}} \end{bmatrix}. \tag{5.60}
$$

When eq. (5.57) is converted into an expression using a hybrid matrix $\mathbf{H}$, the following equation is obtained,

$$
\begin{bmatrix} \boldsymbol{F}_{\mathrm{X}}^{\mathrm{ref}} \\ \ddot{\boldsymbol{X}}_{\mathrm{F}}^{\mathrm{ref}} \end{bmatrix} = \mathbf{H} \begin{bmatrix} \ddot{\boldsymbol{X}}_{\mathrm{X}}^{\mathrm{ref}} \\ \boldsymbol{F}_{\mathrm{F}}^{\mathrm{ref}} \end{bmatrix}. \tag{5.61}
$$

Fig. 5-12: Entire block diagram.

The relationship between the hybrid matrix and the task mass matrix is

$$
\mathbf{H} = \left[\begin{array}{cc} -\mathbf{I} & M_{\mathrm{XF}} \\ \mathbf{0} & M_{\mathrm{FF}} \end{array} \right]^{-1} \left[\begin{array}{cc} -M_{\mathrm{XX}} & \mathbf{0} \\ -M_{\mathrm{FX}} & \mathbf{I} \end{array} \right].
\tag{5.62}
$$

The force reference in modal space is obtained as

$$
\begin{aligned}
\boldsymbol{F}^{\mathrm{ref}} &= \left[\begin{array}{c} \boldsymbol{F}_{\mathrm{X}}^{\mathrm{ref}} \\ \mathbf{0} \end{array} \right] + \left[\begin{array}{c} \mathbf{0} \\ \boldsymbol{F}_{\mathrm{F}}^{\mathrm{ref}} \end{array} \right] \\
&= \mathbf{SH} \left[\begin{array}{c} \ddot{\boldsymbol{X}}_{\mathrm{X}}^{\mathrm{ref}} \\ \boldsymbol{F}_{\mathrm{F}}^{\mathrm{ref}} \end{array} \right] + (\mathbf{I} - \mathbf{S}) \left[\begin{array}{c} \mathbf{0} \\ \boldsymbol{F}_{\mathrm{F}}^{\mathrm{ref}} \end{array} \right].
\end{aligned}
\tag{5.63}
$$

By inversely transforming $\boldsymbol{F}^{\mathrm{ref}}$, the force reference in actuator space is calculated as

$$
\boldsymbol{f}^{\mathrm{ref}} = \boldsymbol{J}_t^{-1} \boldsymbol{F}^{\mathrm{ref}}.
\tag{5.64}
$$

Fig. 5-12 presents an entire block diagram. $\boldsymbol{f}^{\mathrm{ext}}$ and $\boldsymbol{f}^{\mathrm{g}}(\boldsymbol{x})$ denote the external force and gravity force, respectively. $\boldsymbol{f}^{\mathrm{b}}(\boldsymbol{x}, \dot{\boldsymbol{x}})$ is the sum of the inertial force, Coriolis force, and friction force. The disturbance observer (DOB) [29, 73, 131] is used to obtain high robustness. The reaction force from the environment is observed by using the reaction force observer (RFOB) [33, 70] without force sensors. $\mathbf{K}_t$, $\mathbf{LPF}$, g_{dob}, g_{rfob}, and the subscript "n" denote the thrust coefficient, low pass filter, cutoff frequency of DOB, cutoff frequency of RFOB, and nominal value, respectively.

5.3.3 Dynamic Programming Pattern-Matching

When comparing two patterns, the time-series information should be expanded or contracted to calculate the optimum matching result. DP pattern-matching solves such a problem using a dynamic programming algorithm. A position input pattern $\boldsymbol{G}_\mathrm{P}$ and a position reference pattern $\boldsymbol{R}_\mathrm{P}$ are expressed as

$$\boldsymbol{G}_\mathrm{P} = x_\mathrm{m}^{\mathrm{grasp}}[t - I + 1] \cdots x_\mathrm{m}^{\mathrm{grasp}}[t - I + i] \cdots x_\mathrm{m}^{\mathrm{grasp}}[\mathrm{t}], \tag{5.65}$$

$$\boldsymbol{R}_\mathrm{P} = x_\mathrm{record}^{\mathrm{grasp}}[1] \cdots x_\mathrm{record}^{\mathrm{grasp}}[j] \cdots x_\mathrm{record}^{\mathrm{grasp}}[J], \tag{5.66}$$

where I, J, and t are the number of data recorded as the input pattern, the number of data recorded as the reference pattern, and an index representing the current time, respectively. The subscript "record" represents recorded data. The expressions $i(i = 1, 2, \cdots, I)$ and $j(j = 1, 2, \cdots, J)$ denote the number of data recorded in chronological order. These patterns consisting of data from the action components are acquired in component modal space. The force input pattern and the force reference pattern are expressed as

$$\boldsymbol{G}_\mathrm{F} = f_\mathrm{m}^{\mathrm{grasp}}[t - I + 1] \cdots f_\mathrm{m}^{\mathrm{grasp}}[t - I + i] \cdots f_\mathrm{m}^{\mathrm{grasp}}[t], \tag{5.67}$$

$$\boldsymbol{R}_\mathrm{F} = f_\mathrm{record}^{\mathrm{grasp}}[1] \cdots f_\mathrm{record}^{\mathrm{grasp}}[j] \cdots f_\mathrm{record}^{\mathrm{grasp}}[J] \tag{5.68}$$

where $\boldsymbol{G}_\mathrm{F}$ represents the force input pattern and $\boldsymbol{R}_\mathrm{F}$ represents the force reference pattern. The distance between the two patterns is called the DP value, and the DP value is calculated using the DP pattern-matching algorithm. The DP value represents the similarity between the motion ending at time t and the reference pattern. If the value is small, the similarity is high and vice versa. The partial distance of the i th data of the input pattern and the j th data of the reference pattern is set as

$$d(i, j, t) = \sqrt{(x_\mathrm{record}^{\mathrm{grasp}}[j] - x_\mathrm{m}^{\mathrm{grasp}}[t - I + i])^2 (f_\mathrm{record}^{\mathrm{grasp}}[j] - f_\mathrm{m}^{\mathrm{grasp}}[t - I + i])^2}, \tag{5.69}$$

where, $d(i, j, t)$ denotes partial distance.
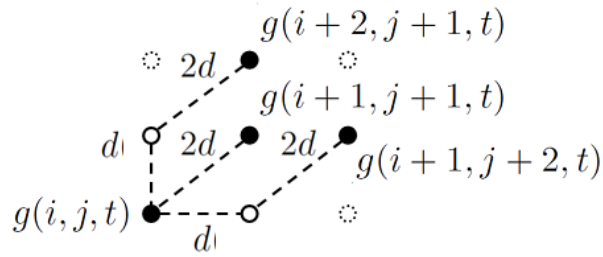
Fig. 5-13: Slope constraint.

Initial conditions are expressed by the following equations:

$$g(I, J, t) = d(I, J, t), \tag{5.70}$$

$$g(I - 1, J - 1, t) = d(I, J, t) + 2d(I - 1, J - 1, t), \tag{5.71}$$

$$g(I - 1, J - 2, t) = d(I, J, t) + 2d(I - 1, J - 1, t) + d(I - 1, J - 2, t), \tag{5.72}$$

$$g(I - 2, J - 1, t) = d(I, J, t) + 2d(I - 1, J - 1, t) + d(I - 2, J - 1, t), \tag{5.73}$$

$$g(i, j, t) = \infty,$$

$$\big(i = I, I - 1 \cup j = J, J - 1\big) \cap$$

$$\big((i, j) \neq (I, J), (I - 1, J - 1), (I - 1, J - 2), (J - 2, I - 1)\big), \tag{5.74}$$

Here, g denotes the cumulative distance. The DP pattern-matching algorithm adjusts the time expansion and contraction, and calculates the optimum path that minimizes the DP value. To avoid extreme time expansion and contraction, a slope constraint is set to between 0.5 and 2 to limit the gradient of the optimum path. This slope constraint is obtained by using a condition in Fig. 5-13 that satisfies the range of the minimum selection, which is expressed as

$$g(i, j, t) = \min \begin{cases} g(i + 2, j + 1, t) + 2d(i + 1, j, t) + d(i, j, t) \\ g(i + 1, j + 1, t) + \ d(i, j, t) \\ g(i + 1, j + 2, t) + 2d(i, j + 1, t) + d(i, j, t) \end{cases}, \tag{5.75}$$
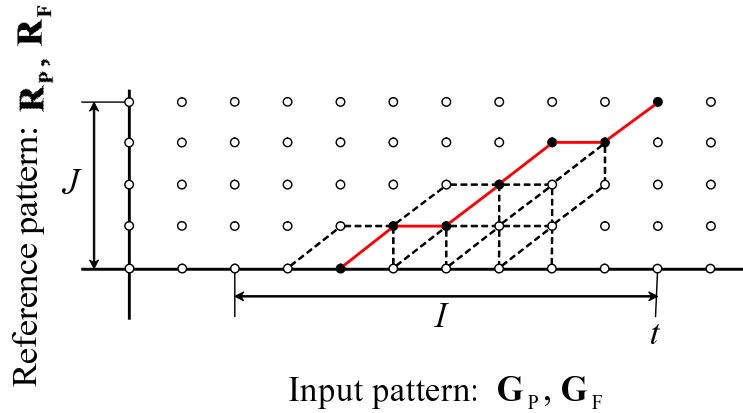
Fig. 5-14: Example of optimum path.

An example of the optimum path is shown in Fig. 5-14. The DP value at t seconds is obtained as

$$D(t) = \min\{g(I - l, 1, t)/(l + J),\ \frac{J}{2} < l < 2J\}. \tag{5.76}$$

5.3.4 Experiments

To verify the validity of the proposal, six types of experiments were conducted as follows:

- Offline recognition

  - Effects of a difference in force

  - Effects of a difference in position

  - Effects of a difference in speed

- Online (real-time) recognition

  - Effects of a difference in the number of motions

  - Effects of modal transformation

  - Application to a power-assist system

In the experiments, both the master robot and the slave robot consisted of two linear motors that performed the grasping motion and the manipulating motion. The linear motors were rod-type motors, and there was little friction effect. The experimental setup is shown in Fig. 5-15. If an operator moved
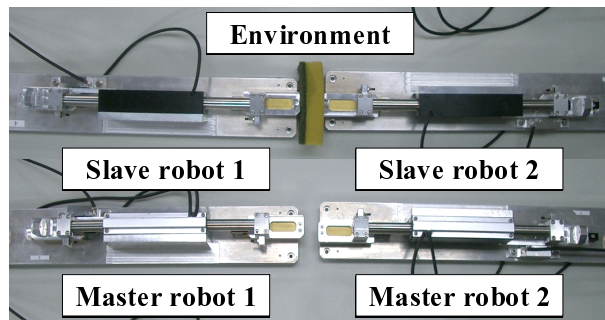
Fig. 5-15: Experimental setup.

| (a) | (b) |
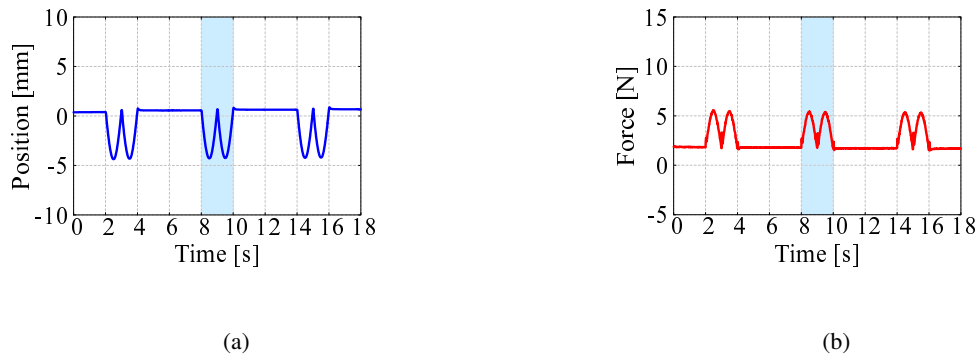
Fig. 5-16: Reference patterns acquired from grasping action component. (a) Position reference pattern. (b) Force reference pattern.

master robots 1 and 2, slave robots 1 and 2 grasped and manipulated objects in the environment. The motion that was searched by the recognition method is shown in Fig. 5-16. The data in the shaded area was set as the reference pattern. The operator grasped the environment twice in two seconds.

In the experiments on offline recognition, three types of objects were used: a melamine sponge, a urethane sponge, and an aluminum block. The hardness of these objects was soft, medium, and hard, respectively. Table 5.7 lists the correspondence between each experiment and object.

Subsections D, E, and F represent real-time recognition cases. In particular, Subsection F describes an example of a practical case, in which the recognition result is used as a trigger for a power-assist system. In the real-time recognition cases, the threshold was set at 0.4 based on a trial-and-error process.

Table 5.7: Difference between each motion and the reference pattern.

◯ : High similarity,   - : Low similarity

Motion	Position	Force	Time	Environment
Results in the difference of force (Fig. 5-17)				
A	◯	-	◯	No environment
B	◯	◯	◯	Urethane sponge(Soft)
C	◯	-	◯	Melamine sponge(Medium)
Results in the difference of position (Fig. 5-18)				
D	-	◯	◯	Melamine sponge(Medium)
E	◯	◯	◯	Urethane sponge(Soft)
F	-	◯	◯	Aluminum block(Hard)
Results in the difference of speed (Fig. 5-19)				
G	◯	◯	-	Urethane sponge(Soft)
H	◯	◯	◯	Urethane sponge(Soft)
I	◯	◯	-	Urethane sponge(Soft)

(a)   (b)   (c)
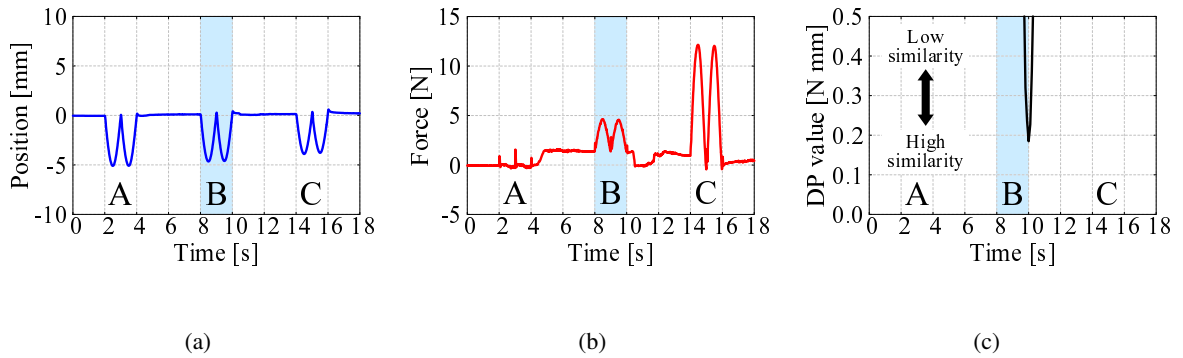
Fig. 5-17: Effects of change in force. (a) Position response. (b) Force response. (c) DP value.

Effects of Difference in Force

Fig. 5-17 shows the effects of a force difference on the motion recognition. The operator performed the desired grasping motion from 8 to 10 s. However, the slave robot did not make contact with the item from 2 s to 4 s, and the force was larger than that of the reference pattern from 14 to 16 s. Fig. 5-17(a) shows the position response and shows that the operator performed three sets of grasping motions. However, the force response clearly expresses the difference between these grasping motions as shown
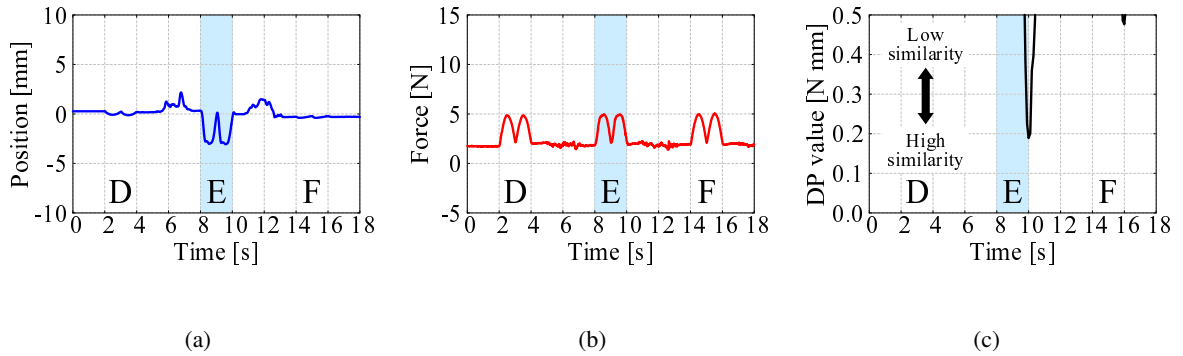
Fig. 5-18: Effects of change in position. (a) Position response. (b) Force response. (c) DP value.
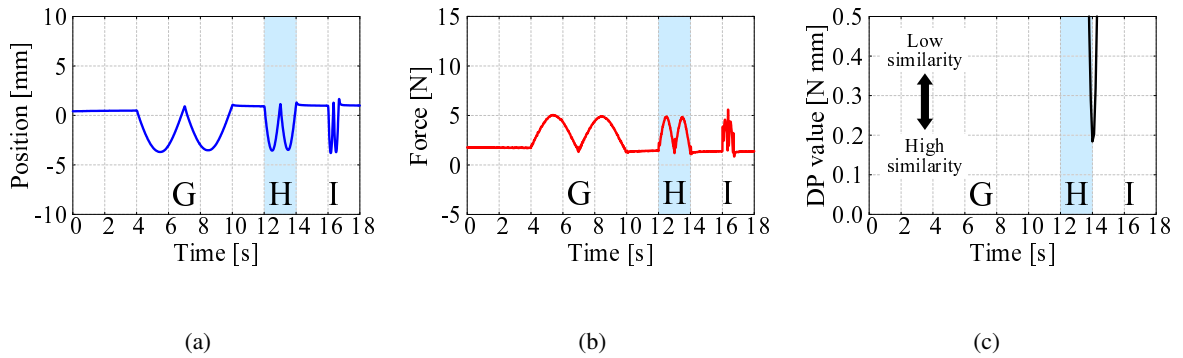
Fig. 5-19: Effects of change in speed. (a) Position response. (b) Force response. (c) DP value.

in Fig. 5-17(b). Fig. 5-17(c) shows that the DP value was small at 10 s. This result shows that the motion ending at 10 s is similar to the reference pattern, and that our method succeeded in expressing the ending time of the desired grasping motion. Incidentally, some force was observed during the unconstrained motion, although the amplitude was small. This force was caused by the effect of inertia and friction.

Effects of Difference in Position

Fig. 5-18 shows the impact of a position difference. The operator performed the desired grasping motion from 8 to 10 s. Meanwhile, the slave robot made contact with two types of objects from 2 to 4 s and from 14 to 16 s. Fig. 5-18(b) shows the force response, which indicates that the operator performed the grasping motion thrice. However, Fig. 5-18(a) clearly shows that the desired grasping motion was performed only from 8 to 10 s. Fig. 5-18(c) tells us that the ending time of the desired grasping motion was 10 s.

(a)　　　　　　　　　　　(b)　　　　　　　　　　　(c)
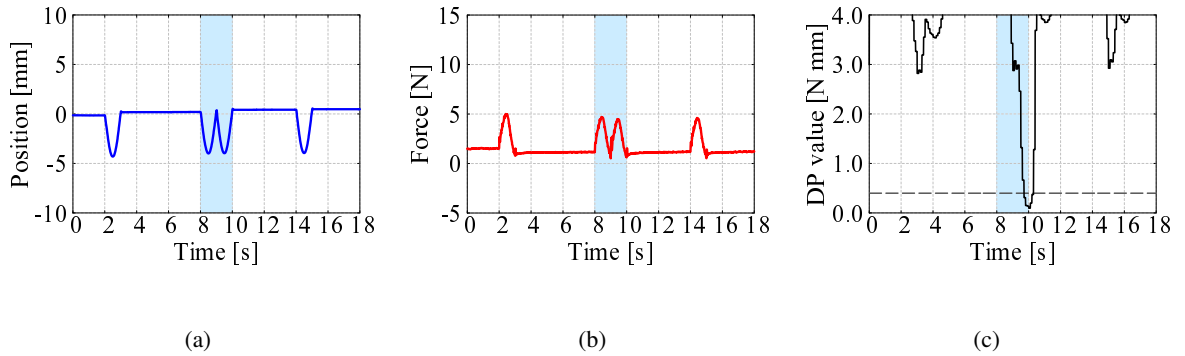
Fig. 5-20: Experimental results of the difference in the number of motion. (a) Position response. (b) Force response. (c) DP value.

Effects of Difference in Speed

The effect of the speed difference is indicated in Fig. 5-19. The operator performed the desired grasping motion from 12 to 14 s. The operator grasped the object slowly from 4 to 10 s and quickly from 16 to 17 s. Fig. 5-19(a) and Fig. 5-19(b) show the position response and force response, respectively. The amplitude was almost the same as the desired grasping motion. However, the moving speed was different from the desired motion. Fig. 5-19(c) shows that the DP value correctly expresses the ending time of the desired grasping motion, and the result suggests that the ending time is around 14 s.

Effects of Difference in Number of Motions

In this experiment, there were periods where the target grasping motion was conducted only once, whereas the grasping motion was conducted twice in the reference pattern. Fig. 5-20 shows the experimental results. The DP values during the periods that included only one grasping motion were lower than that during the other periods, as shown in Fig. 5-20(c). However, the DP values for the single grasping motion were higher than the threshold, whereas the DP values in the presence of the two grasping motions were recognized as being similar to the reference pattern.

Effects of Modal Transformation

This subsection describes the necessity of the modal transformation from the actuator space to the component modal space. The advantage of the modal transformation was confirmed by making a comparison between simple matching in the actuator space and the proposed matching method in the com-
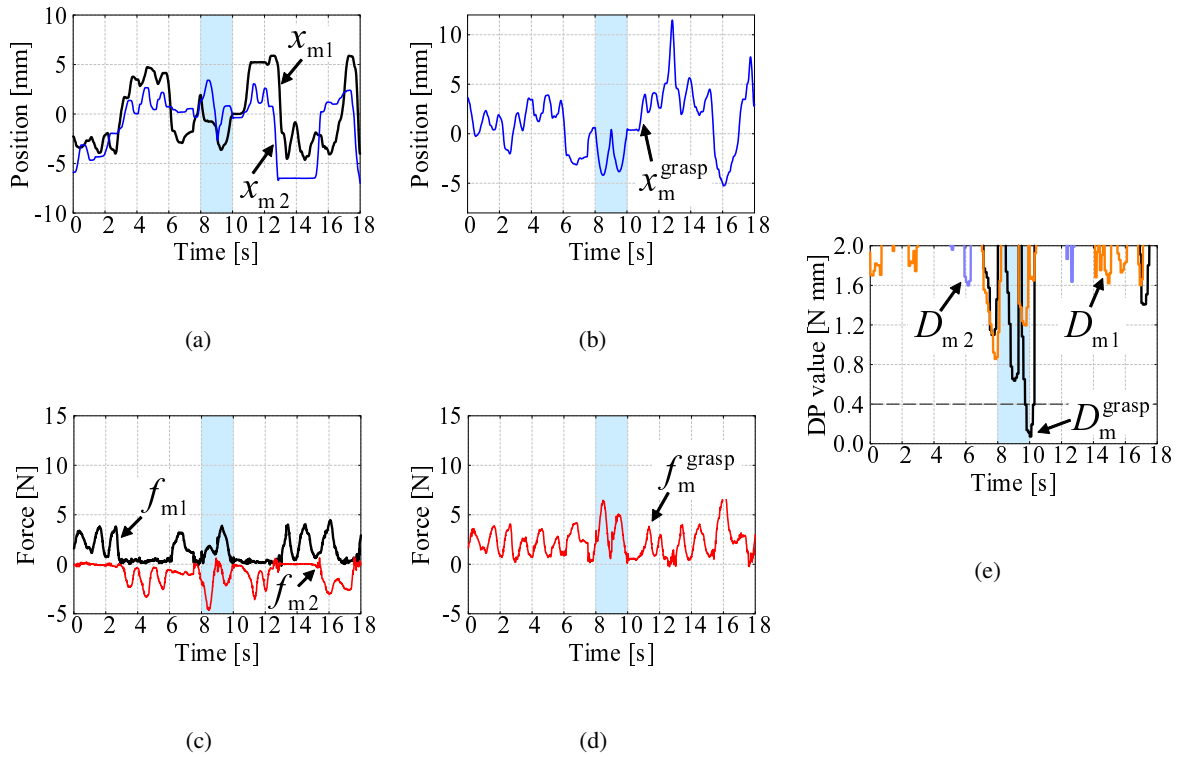
Fig. 5-21: Effects of modal transformation. (a) Position response in the actuator space. (b) Position response in the component modal space. (c) Force response in the actuator space. (d) Force response in the component modal space. (e) DP values.

ponent modal space. Fig. 5-21 shows the experimental results. Fig. 5-21(a) and Fig. 5-21(c) show the responses of the actuator space, where picking out the target motion is difficult due to the mixture of grasping and manipulating motions. In fact, the DP values in Fig. 5-21(e) (D_{m1} and D_{m2}) that were calculated in the actuator space confirm the recognition failure. However, the responses of the component space that are shown in Fig. 5-21(b) and Fig. 5-21(d) explicitly indicate the grasping motion. The DP value (D_m^{grasp}) reached a minimum at the end of the grasping motion.
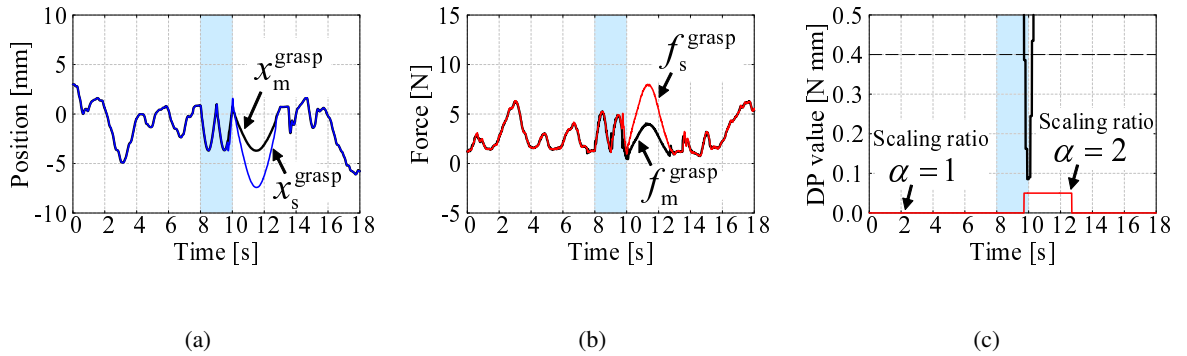
Fig. 5-22: Application to power-assist system. (a) Position response. (b) Force response. (c) DP value.

Application to Power-Assist System

To show the application possibilities, a power-assist system was built based on the proposed recognition method and the scaled bilateral control. Fig. 5-22 shows the experimental results. The operator performed the target grasping motion from 8 to 10 s. Therefore, the DP value was decreased and dropped below the threshold value. In response, the transformation matrix $^\mathrm{F}\boldsymbol{J}_\mathrm{C}(\alpha)$ was shifted from eq. (5.47) to eq. (5.54). In other words, α was shifted from 1 to 2. Fig. 5-22(a) and Fig. 5-22(b) confirm that the position and force was scaled for 3 s after the recognition. The length of the period and the scaling ratio can be set arbitrarily.

5.4   Summary

A method for the recognition of human motions using tactile information have been established in this chapter.

In the first half of this chapter, which describes recognition of combinations of successive elementary motions, firstly, tactile information was acquired by using a 5-DOF exoskeletal robot hand with bilateral control, and stored it in a database for use in classifying the operator's motions into 8 elementary classes. The cosine similarity was employed for comparison between the reference vectors and input vectors. DP matching was used to correct the expansion or contraction of the time axis in the classification results, and performed recognition of combined motions. The proposed method was experimentally verified. In this study the recognition accuracy was verified by using the PPV and NPV for 4 combined actions: in the future, the verification of this recognition method is expected to extend to various transient states.

The second half of this chapter improved the above-mentioned approach to the modal space and to the actual application of the real-time power-assist system. Haptic data was abstracted by a bilateral control system, then divided into action components by a modal transformation. Next, a DP pattern-matching algorithm was used to recognize the desired grasping motion. Finally, experiments were conducted under conditions where there was some difference in position, force, or speed between the input pattern and the reference pattern. In addition, real-time recognition was conducted to examine differences in the number of motions and in modal transformation, and to test the application of the method to a power-assist system. The validity of the proposed method was confirmed by these experiments, and the proposed method was successful in distinguishing the desired motion from other motion.

Chapter 6

Analysis and Decomposition

This chapter analyzes and decomposes the extracted haptic information. From the results, concealed features and implicit knowledge included in the human motion are clarified. These obtained information can be used to improve the ability of the robots.

The objective of the first half of this chapter is to obtain control stiffness of human motion, even if the motion is in contact state. The haptic information is acquired using a scaled bilateral control system. For calculating the control stiffness, dynamic programming matching and the least-squares method are utilized. Dynamic programming matching accommodates the motion speeds the recorded motion data. The derived impedance is fed into a compliance control system, which is used for reproduction. To validate the proposed method the task of removing a sarcoma is performed in experiments, in which three different types of target positions are set. The proposed motion-reproducing system succeeded in removing the sarcoma phantom, whereas the conventional method either failed to grasp it or applied excessive force. The proposed method succeeded in increasing the adaptability of the motion-reproducing system to different environmental locations.

The second half of this chapter describes a method, which decomposes the human motion into fundamental elements of the motion control. Firstly, human motions are extracted as haptic information through a bilateral control system. Then, by using the proposed method, the haptic information is divided into basic elements: transformation matrices, hybrid angles, pure position commands, and pure force commands. The proposed method is validated through simulations as well as experiments with a robotic and a human operator. The obtained results clearly reveal the features of human motions, although recognizing the differences from the original responses is difficult. Nonetheless, this study

provides a motion expression that should contribute toward a greater understanding of human skill.

6.1 Introduction

The first half of this chapter introduces the proposed approach to calculate the control stiffness of human motion, which contributes to understanding and reconstructing human motion. Against a background of a rapidly aging society with a declining birthrate, a growing number of efforts are being made toward the development of automated robotic systems. One of the approaches being used to realize an automated robotic system involves the reproduction of human motion, and many methods have been proposed to achieve such reproduction [111, 132–138].

However, these methods extract human motion based on position information alone. Although these position-based systems are able to obtain sufficient information about joint angles and positions, they are incapable of acquiring force information. Conventional position-based systems are incapable to reproduce a motion that involves direct contact with objects because of the lack of force information. Therefore, there is a definite need for a reproduction method that considers both position and force information.

One of the technologies that consider both position and force information is a bilateral control system [64, 139–141]. This system consists of a master system, which is operated by a human, and a slave system, which makes contact with an object. The most important aim of a bilateral control system is the perception of the mechanical impedance of an object existing in a remote place [61, 62]. Several approaches have been proposed to achieve this aim [63, 142–144].

In contact motions, controlling the stiffness of a manipulator end effector is important [22]. Impedance controls achieve intermediate control stiffness between infinity and zero [23, 24]. There were some studies that combine this impedance control technology with the bilateral control technology. For example, as a means of altering haptic feel, impedance-shaping bilateral control was proposed [145, 146]. A variable damping impedance control of a bilateral teleoperation system was also proposed to obtain better quality teleoperation under a variety of circumstances [147, 148]. Especially, impedance shaping technology is useful for teleoperation between different-scale master-slave systems [149]. These technologies of bilateral control have been improved for practical applicability, such as in microassembly [150]. In particular, methods for operating a small (micro) robot with a large (macro) robot have been referred to as macro-micro bilateral control [151]. In contrast, micro-macro bilateral control uses a smaller robot

on a operator side. Bilateral control utilizing information, which is scaled down or up, is referred to as scaled bilateral control more generally [152, 153]. Cutting-edge research on bilateral control has been directed to the medical field [154].

At the same time, a motion-reproducing system that is a kind of autonomous robotic system has also been proposed [1]. This system reproduces human motion on the basis of data extracted using bilateral control systems. In addition, a method that integrates several sets of haptic data stored in a motion data memory has also been proposed [70]. These conventional motion-reproducing systems contain force controllers that take force information into account. However, the reproduced mechanical impedance, which is called control stiffness, is constant in the reproduction phase. Therefore, conventional motion-reproducing systems are sensitive to changes in the environmental location. For example, end effectors may not make contact with a target object if the object is located far from its position in the phase of human data collection. Another example of this sensitivity is that excessive force may be applied to the target object if the object is nearer than its supposed position. A method that adjusts the position offset depending on the force error of the reproduction phase has been proposed to compensate for changes in the environmental location [155]. Another method that involves the substitution of a velocity controller for a position controller has also been presented [2]. These methods assume that the position relative to the object corresponds to the collected position data, but the aim of the motion is not always intended to correspond to the relative position. For instance, forceps must be pulled out to remove a sarcoma regardless of the position of the organ.

The problem that needs to be solved is that the control stiffness was constant in these conventional motion-reproducing systems. Therefore, this chapter proposes a novel motion-reproducing system that considers the mechanical impedance of human motion. The proposed method includes an approach to determine the control stiffness of the motion-reproducing system on the basis of position, force, and impedance information. The human impedance can be extracted by scaled bilateral control systems even if these are in a contact motion. The haptic data acquired on the slave side are enhanced or weakened prior to transmission in the scaled bilateral control. For calculating human impedance, a dynamic programming matching (DP matching) algorithm [123] is executed to adjust the differences in the speed of each motion. Unexpected differences may occur between the speed of the performed motions. If there is time expansion and contraction between each motion, the calculation results of human impedance are drastically degraded. Pattern matching using DP is one of the well known methods to cope with this type of time expansion and contraction: there are some studies that treat the time flow on the basis of this

method. The main advances proposed in this chapter is adaptability of motion-reproducing system. The reproduction of human impedance enables the realization of automated robotic systems that can adapt to changes in the environmental location.

In the second half of this chapter, the subject is moved on to the method, which separates the human motion into fundamental elements of the motion control. This separation approach can be attained by only one measurement, whereas the method shown in the first half of this chapter require the measurement of human motion more than once.

As mentioned before, it has proven difficult to acquire human motions using conventional vision-based capturing systems. These systems can obtain information about the joint angles, positions, and colors, but not about the contact force [42, 118, 119].

Haptics is a research field that deals with the haptic sense. Initially, research activity in this field was only focused on developing technologies for presenting a virtual environment [18], which was found to be useful for applications such as medical training [156] and computer operations [157]. Research activities then advanced to teleoperation technologies for treating a real environment [73, 158], which came to be known as real-world haptics [70].

Bilateral control [63, 139], a type of teleoperation method, is often used in real-world haptics. Two types of robots are conventionally used in bilateral control systems: a master robot and a slave robot. The master robot is operated by an operator, and the slave robot makes contact with the environment. The operator can feel the actual environmental reaction force through the master robot, thus enabling the robot to easily serve as an agent for the operator when performing dangerous tasks. As such, this technique was initially considered most suitable for deep-sea, space, and nuclear containment operations: having said that, the field of applications has since expanded to our immediate surroundings [64].

In motion control, the importance of realization of desired control stiffness ($\partial f / \partial x$) is well known. The control stiffness must be infinity under pure position control and must be zero under pure force control. Therefore, pure position control and pure force control cannot be achieved in the same direction at the same time. Because of this duality, several control methods were proposed such as impedance control and hybrid control. The impedance control achieves intermediate control stiffness between infinity and zero [23, 24]. The hybrid control uses a directionally decoupled motion controller in the operational space [25–27].

On the other hand, to treat the duality in interactive and complex motions, a concept of mode has been introduced [35]. In mode-based control, robot motion is projected on virtual coordinate system,

which is referred to as modal space. By implementing controllers on each modal space, this approach makes it possible to control each interactive motion, not each end effector. The concept of mode suggested that roles of entire system can be decoupled into simplified components. Now, humans frequently grasp various things in their daily lives, and therefore, studies of hand motions have attracted considerable attention [104, 121, 159–161]. Above-mentioned theory of mode was also applied to handling motion [12, 39]. In [12], cooperative handling motions of multi-degrees-of-freedom (DOF) manipulators were accomplished by assigning various control systems to grasping mode, rolling mode, up-down mode, pitching mode, and yawing mode. In [39], grasping and manipulating motions of a two-finger robot was reconstructed by a three-finger robot. The theory that motions are realized by controlling dual variables (i.e. velocity/position and force) and by transforming appropriate modal space was precisely confirmed in [53, 54, 72]. This theory was applied practically to achieve motions such as obstacle avoidance and limitation control of movable range [162]. To suppress the interference between modal spaces, a modal space disturbance observer was proposed [163].

In an opposite manner, an analytical procedure of hand motion was proposed on the basis of mode [122]. The concept of mode was also applied to a real-time recognition system. This system succeeded to recognize grasping motions and trigger scaled bilateral control to assist the operator [74].

However, there is one problem that the conventional modal transformation should be predetermined. Although a method to derive mode from the haptic information of a human operator was proposed in [109], calculation of the appropriate modal transformation is still difficult when the standard deviation of the haptic information is low. In addition, selecting only one modal transformation out of two, which are obtained from analyses of the position and the force, is also difficult.

There is another serious problem that these mode-based studies have not focused on impedance control [164]. To solve this problem, a concept of hybrid angle has been proposed [165]. This study of the hybrid angle clarified that impedance control can be achieved by combining position and force control in one mode. However, it has not been applied to analysis of human motions. In summary, although the above-mentioned mode-based strategy has greatly expanded the field of application of motion control, the process by which elements are to be determined remains unclear.

This study aims to extract fundamental elements of mode-based control from human motions. Toward this end, it proposes a method for the elemental separation of human motions. The concept of elemental separation, which has commonly been used in the field of motion control, is applied to motion expression. This is the most important and novel feature of our approach. Human motions are extracted through a

bilateral control system and recorded as haptic information. The haptic information of human motion is then broken down into the following basic elements of mode-based control.

- Transformation matrix: the matrix corresponding to functions and determining coordinate referred to as modal space, where controllers are implemented

- Hybrid angle: the ratio between the effect of the position control system and the force control system, which determines control stiffness [165]

- Position command: the value provided to the position controller

- Force command: the value provided to the force controller

The proposed method for understanding human motions is validated through simulations and experiments with a robotic and a human operator.

This chapter is organized as follows. The first half of this chapter proposes a novel method for motion reproduction in consideration of human stiffness. Section 6.2.1 presents the conventional motion-reproducing system. Section 6.2.2 describes the proposed motion-reproducing system. Differences between the conventional method and the proposed method are also explained in Section 6.2.2. The experimental results of the proposed motion-reproducing system are presented in Section 6.2.3. The second half of this chapter proposes an approach of elemental separation in order to reveal human skills. The remainder of this chapter is organized as follows: Section 6.3.1 presents the motion control used for both the human model and the bilateral control. Section 6.3.2 shows an implementation of the bilateral control. Section 6.3.3 explains the proposed expression method for human motion. Sections 6.3.4 and 6.3.5 present the simulation and experimental results, respectively. Finally, Section 6.4 presents the conclusions of this chapter.

6.2 Stiffness Analysis of Motion

6.2.1 Conventional Motion-Reproducing System

This section describes the conventional motion-reproducing systems, which consist of a motion data collection system and a motion data reproduction system. In the motion-reproducing systems, acceleration-based bilateral control systems [53, 54] that employ disturbance observers (DOB) [29] are used, as such systems offer nearly sufficient robustness, transparency, and stability for practical use [166, 167]. Reaction force obserbers (RFOB) [33] are utilized to estimate the force information.
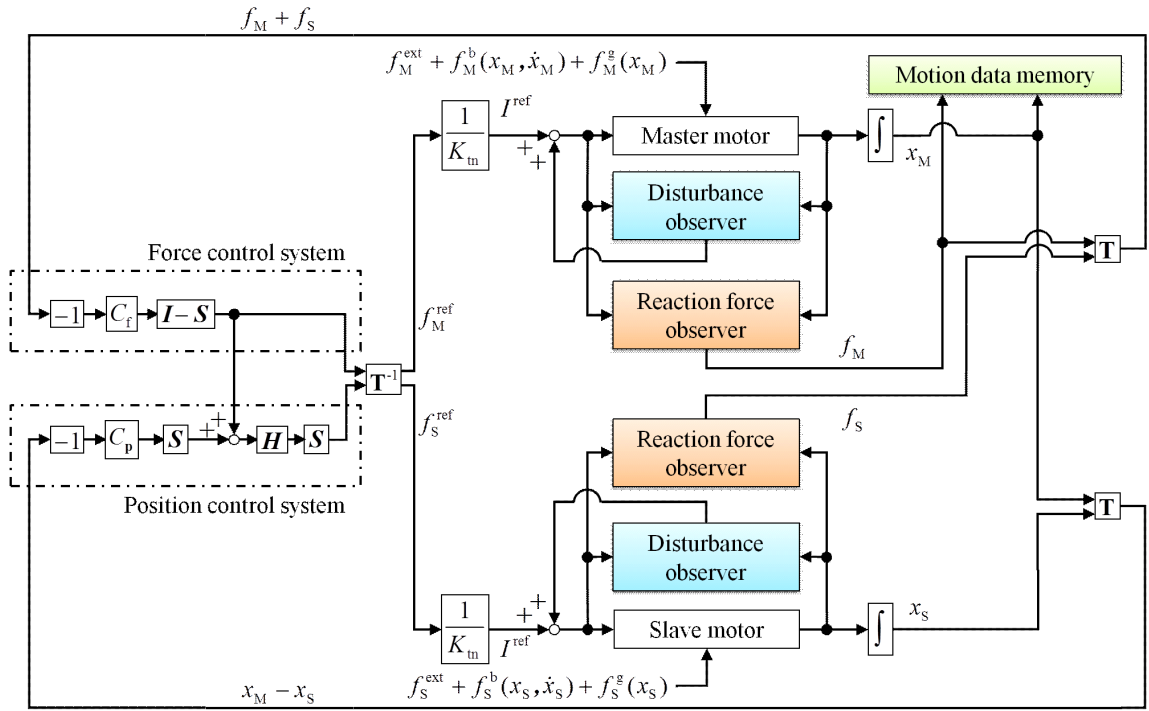
Fig. 6-1: Motion data collection system using bilateral control system.

For ease of explanation, this study takes a forceps robot that can perform translational and grasping motion for practical example. This forceps robot consists of two linear motors and has 2-degree-of-freedom (DOF) although the system is just mechanical combination of 1-DOF motors.

Fig. 6-1 shows a block diagram of a motion data collection system that uses a bilateral control system. Here, $\boldsymbol{f}^{\text{ext}}$ and $\boldsymbol{f}^{\text{g}}(\boldsymbol{x})$ denote the external force and the gravity force, respectively. $\boldsymbol{f}^{\text{b}}(\boldsymbol{x}, \dot{\boldsymbol{x}})$ is the sum of the inertial force, Coriolis force, and friction force. $\boldsymbol{K}_{\text{t}}$ represents the thrust coefficient. The superscripts "ref" and the subscript "n" denote the reference and nominal values, respectively. The disturbance can be observed from the velocity response and the armature current, and it can be suppressed using the observed value. First-order low-pass filters (LPF) are utilized to avoid effects of high-frequency noise.

Position and force information in the actuator space are expressed as

$$\boldsymbol{x}^{\text{trans}} = [\, x_{\text{M}}^{\text{trans}} \,, \, x_{\text{S}}^{\text{trans}} \,]^{\text{T}}, \tag{6.1}$$

$$\boldsymbol{x}^{\text{grasp}} = [\, x_{\text{M}}^{\text{grasp}} \,, \, x_{\text{S}}^{\text{grasp}} \,]^{\text{T}}, \tag{6.2}$$

$$\boldsymbol{f}^{\text{trans}} = [\, f_{\text{M}}^{\text{trans}} \,, \, f_{\text{S}}^{\text{trans}} \,]^{\text{T}}, \tag{6.3}$$

$$\boldsymbol{f}^{\text{grasp}} = [\, f_{\text{M}}^{\text{grasp}} \,, \, f_{\text{S}}^{\text{grasp}} \,]^{\text{T}}, \tag{6.4}$$

where x is the position information and f is the force information. The subscripts "M" and "S" and the superscripts "trans" and "grasp" denote variables concerning the master side, slave side, translational motion, and grasping motion, respectively. The control goals are position tracking and force feedback,

$$x_{\text{M}}^{\text{trans}} = x_{\text{S}}^{\text{trans}}, \tag{6.5}$$

$$x_{\text{M}}^{\text{grasp}} = x_{\text{S}}^{\text{grasp}}, \tag{6.6}$$

$$f_{\text{M}}^{\text{trans}} = -f_{\text{S}}^{\text{trans}}, \tag{6.7}$$

$$f_{\text{M}}^{\text{grasp}} = -f_{\text{S}}^{\text{grasp}}. \tag{6.8}$$

For purposes of brevity, the superscript "trans" and "grasp" is omitted, as following equations are satisfied in both translational motion and grasping motion. These physical quantities in the actuator space are transformed into a modal space as

$$\boldsymbol{X} = \boldsymbol{T}\boldsymbol{x}, \tag{6.9}$$

$$\boldsymbol{F} = \boldsymbol{T}\boldsymbol{f}, \tag{6.10}$$

to simplify the design of the bilateral control system. $\boldsymbol{T}$ is a transformation matrix, which is shown as

$$\boldsymbol{T} = \begin{bmatrix} 1 & -1 \\ 1 & 1 \end{bmatrix}. \tag{6.11}$$

The dynamics in the modal space are given by

$$\boldsymbol{T}\boldsymbol{m}\boldsymbol{T}^{-1}\ddot{\boldsymbol{X}} = \boldsymbol{F}. \tag{6.12}$$

Here, the mass matrices in the actuator space are expressed as

$$\boldsymbol{m} = \text{diag}\,[\, m_{\text{M}}, m_{\text{S}} \,], \tag{6.13}$$

and the mass matrix in the modal space is defined as

$$\boldsymbol{M} \;=\; \boldsymbol{TmT}^{-1} = \begin{bmatrix} M_{11} & M_{12} \\ M_{21} & M_{22} \end{bmatrix}. \tag{6.14}$$

The transformed position and force information are input into a position and a force control system, respectively. Then, the force reference is calculated as

$$\boldsymbol{F}^{\mathrm{ref}} \;=\; -\boldsymbol{SH}\left\{ \boldsymbol{S}C_{\mathrm{p}}\boldsymbol{X} + (\boldsymbol{I} - \boldsymbol{S})C_{\mathrm{f}}\boldsymbol{F} \right\}$$
$$-(\boldsymbol{I} - \boldsymbol{S})C_{\mathrm{f}}\boldsymbol{F}. \tag{6.15}$$

C_{p} and C_{f} are the position controller and force controller, respectively. $\boldsymbol{H}$ is a hybrid matrix that decouples these two control systems [53, 54]:

$$\boldsymbol{H} \;=\; \begin{bmatrix} -1 & M_{12} \\ 0 & M_{22} \end{bmatrix}^{-1} \begin{bmatrix} -M_{11} & 0 \\ -M_{21} & 1 \end{bmatrix}. \tag{6.16}$$

$\boldsymbol{I} \in \mathbb{R}^{2\times 2}$ and $\boldsymbol{S} \in \mathbb{R}^{2\times 2}$ represent the unit matrix and the selection matrix, respectively. The selection matrix is expressed as

$$\boldsymbol{S} \;=\; \operatorname{diag}\left[\,1, 0\,\right], \tag{6.17}$$

as one of the two control goals, which is set for each motion, is related to the position tracking. Then, the force reference in the actuator space is given as

$$\boldsymbol{f}^{\mathrm{ref}} \;=\; \boldsymbol{T}^{-1}\boldsymbol{F}^{\mathrm{ref}}. \tag{6.18}$$

The details of each reference are given as

$$f_{\mathrm{M}}^{\mathrm{ref}} = -C_{\mathrm{p}}(x_{\mathrm{M}} - x_{\mathrm{S}})\left(\frac{m_{\mathrm{M}}m_{\mathrm{S}}}{m_{\mathrm{M}} + m_{\mathrm{S}}} \right)$$
$$-C_{\mathrm{f}}(f_{\mathrm{M}} + f_{\mathrm{S}})\left(\frac{m_{\mathrm{M}}}{m_{\mathrm{M}} + m_{\mathrm{S}}} \right), \tag{6.19}$$
$$f_{\mathrm{S}}^{\mathrm{ref}} = -C_{\mathrm{p}}(x_{\mathrm{S}} - x_{\mathrm{M}})\left(\frac{m_{\mathrm{M}}m_{\mathrm{S}}}{m_{\mathrm{M}} + m_{\mathrm{S}}} \right)$$
$$-C_{\mathrm{f}}(f_{\mathrm{M}} + f_{\mathrm{S}})\left(\frac{m_{\mathrm{S}}}{m_{\mathrm{M}} + m_{\mathrm{S}}} \right). \tag{6.20}$$

Thus, the bilateral control system is configured. The position information (i.e., $x_{\mathrm{M}}^{\mathrm{trans}}$ and $x_{\mathrm{M}}^{\mathrm{grasp}}$) and force information (i.e., $f_{\mathrm{M}}^{\mathrm{trans}}$ and $f_{\mathrm{M}}^{\mathrm{grasp}}$) are recorded to the motion data memory through the bilateral control system.
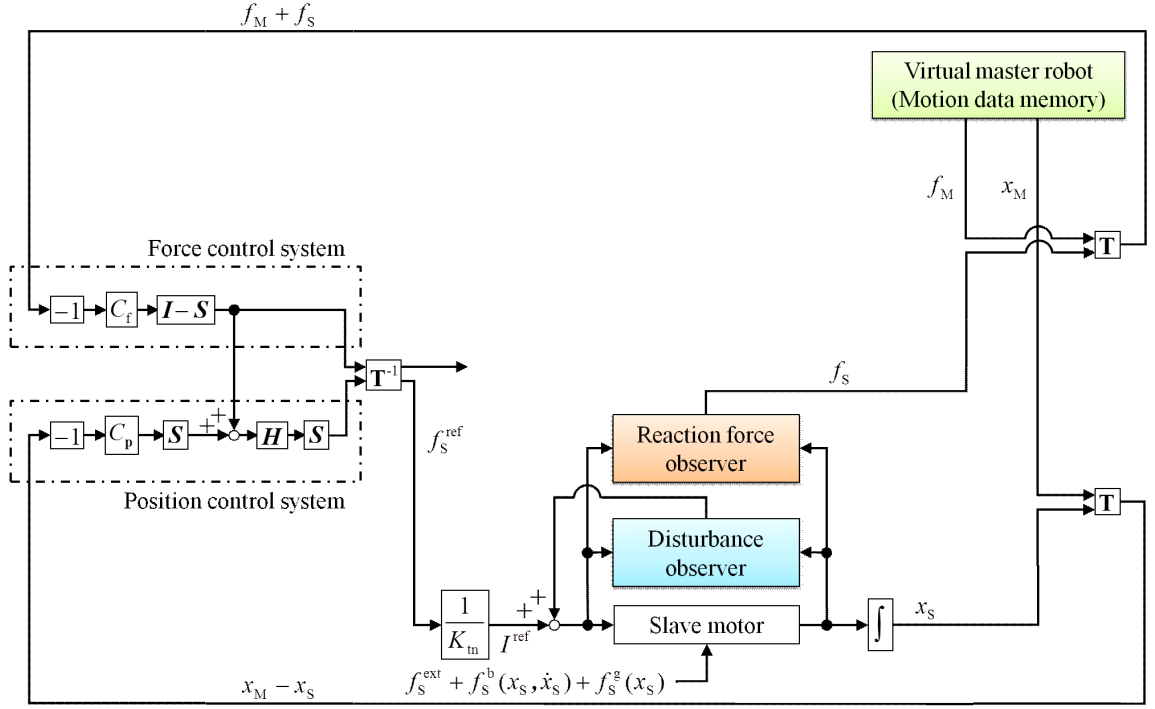
Fig. 6-2: Conventional motion data reproduction system.

Fig. 6-2 shows a block diagram of the conventional motion data reproduction system. Here, in accordance with the conventional method, this chapter assumes that a proportional-derivative controller and a proportional controller are used as the position controller and the force controller, respectively. Hereinafter, K_p, K_v, and K_f stand for the position feedback gain, the velocity feedback gain, and the force feedback gain. In the conventional method, the data collected in the motion data memory are directly used as a virtual master robot. In this case, the force references are derived as

$$f_S^{\text{ref}}(s) = (K_p + K_v s) \left(x^{\text{cmd}}(s) - \frac{f_S(s)}{K_c + sD_c} - x_S(s) \right) \left(\frac{m_M m_S}{m_M + m_S} \right), \qquad (6.21)$$

where

$$x^{\text{cmd}}(s) \;=\; x_M(s) - \frac{K_f}{m_M(K_p + sK_v)} f_M(s), \qquad (6.22)$$

$$K_c \;=\; \frac{m_M K_p}{K_f}, \qquad (6.23)$$

$$D_c \;=\; \frac{m_M K_v}{K_f}. \qquad (6.24)$$
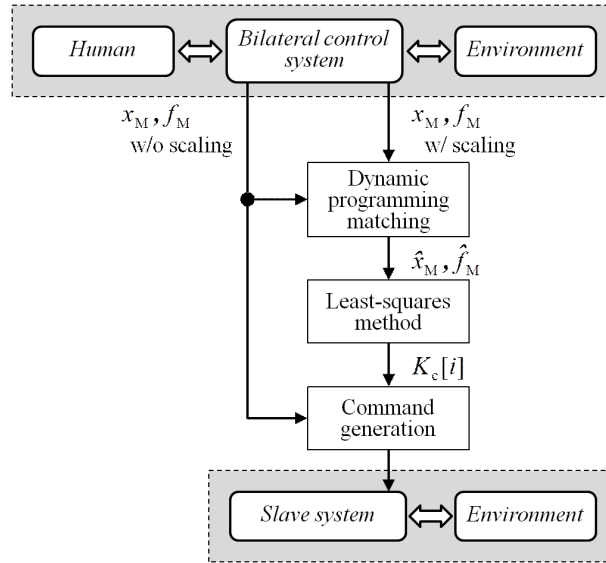
Fig. 6-3: Flowchart.

s, x^{cmd}, K_{c}, and D_{c} denote the Laplace operator, the command of the equilibrium position, the stiffness, and the viscosity, respectively. Eq. (6.23) shows that the stiffness is always constant in a conventional motion-reproducing system. This constant stiffness causes a lack of adaptability to the environmental location.

6.2.2 Proposed Motion-Reproducing System

This chapter shows a novel approach changing the control stiffness, although some viscosity is added to ensure the stability. This study focuses on the stiffness rather than the viscosity, as the aim is improving the above-mentioned adaptability to the environmental location.

Fig. 6-3 shows a flowchart of the proposed motion-reproducing system. The details are described as follows.

If the scaling ratio is represented by α, the transformation matrix can be rewritten as

$$
\boldsymbol{T} \;=\; \begin{bmatrix} 1 & \frac{-1}{\alpha} \\ 1 & \alpha \end{bmatrix} . \tag{6.25}
$$

The force references input into the actuators are derived as

$$f_{\mathrm{M}}^{\mathrm{ref}} = -\frac{C_{\mathrm{p}}}{2}\left(x_{\mathrm{M}} - \frac{x_{\mathrm{S}}}{\alpha}\right)\left(\frac{\alpha^2}{1+\alpha^2}\right)\left(\frac{4m_{\mathrm{M}}m_{\mathrm{S}}}{m_{\mathrm{M}}+m_{\mathrm{S}}}\right)$$
$$-C_{\mathrm{f}}\frac{f_{\mathrm{M}}+\alpha f_{\mathrm{S}}}{1+\alpha^2}\left(1+\alpha^2\frac{m_{\mathrm{M}}-m_{\mathrm{S}}}{m_{\mathrm{M}}+m_{\mathrm{S}}}\right), \tag{6.26}$$

$$f_{\mathrm{S}}^{\mathrm{ref}} = \frac{C_{\mathrm{p}}}{2}\left(x_{\mathrm{M}} - \frac{x_{\mathrm{S}}}{\alpha}\right)\left(\frac{\alpha}{1+\alpha^2}\right)\left(\frac{4m_{\mathrm{M}}m_{\mathrm{S}}}{m_{\mathrm{M}}+m_{\mathrm{S}}}\right)$$
$$-C_{\mathrm{f}}\left(f_{\mathrm{M}}+\alpha f_{\mathrm{S}}\right)\left(\frac{\alpha}{1+\alpha^2}\right)\left(\frac{2m_{\mathrm{S}}}{m_{\mathrm{M}}+m_{\mathrm{S}}}\right). \tag{6.27}$$

The proposed system scales the position and force information. The target motion is performed multiple times with different scaling ratios to calculate the impedance of a human motion.

Here, DP matching is introduced. DP matching is used to accommodate the motion speed of the collected motion data. The recorded position data are represented as

$$\boldsymbol{D}_{\mathrm{P}}[\alpha_1] = \left\{x_{\mathrm{M}}[\alpha_1,1]\cdots x_{\mathrm{M}}[\alpha_1,i]\cdots x_{\mathrm{M}}[\alpha_1,I]\right\}, \tag{6.28}$$

$$\boldsymbol{D}_{\mathrm{P}}[\alpha_2] = \left\{x_{\mathrm{M}}[\alpha_2,1]\cdots x_{\mathrm{M}}[\alpha_2,j]\cdots x_{\mathrm{M}}[\alpha_2,J]\right\}, \tag{6.29}$$

where the first element in the brackets "[ ]" denotes the scaling ratio. The second element in the brackets denotes the number of data recorded in chronological order: i ($i = 1, 2, \ldots, I$) and j ($j = 1, 2, \ldots, J$). "I" and "J" are the number of data recorded as the input pattern and the reference pattern, respectively. Similarly, the recorded force data are represented as

$$\boldsymbol{D}_{\mathrm{F}}[\alpha_1] = \left\{f_{\mathrm{M}}[\alpha_1,1]\cdots f_{\mathrm{M}}[\alpha_1,i]\cdots f_{\mathrm{M}}[\alpha_1,I]\right\}, \tag{6.30}$$

$$\boldsymbol{D}_{\mathrm{F}}[\alpha_2] = \left\{f_{\mathrm{M}}[\alpha_2,1]\cdots f_{\mathrm{M}}[\alpha_2,j]\cdots f_{\mathrm{M}}[\alpha_2,J]\right\}. \tag{6.31}$$

The distance between two patterns is called the DP value, which is calculated using the DP matching algorithm. The partial distance of the i th data of the input pattern and the j th data of the reference pattern are set as

$$d(i,j) = \sqrt{(x_{\mathrm{M}}[\alpha_1,i] - x_{\mathrm{M}}[\alpha_2,j])^2}$$
$$\times \sqrt{(f_{\mathrm{M}}[\alpha_1,i] - f_{\mathrm{M}}[\alpha_2,j])^2}. \tag{6.32}$$

Here, $d(i, j)$ denotes a partial distance. The initial conditions are expressed by the following equations.

$$g(1, 1) = d(1, 1), \tag{6.33}$$

$$g(2, 2) = d(1, 1) + 2d(2, 2), \tag{6.34}$$

$$g(2, 3) = d(1, 1) + 2d(2, 2) + d(2, 3), \tag{6.35}$$

$$g(3, 2) = d(1, 1) + 2d(2, 2) + d(3, 2), \tag{6.36}$$

$$g(i, j) = \infty, \ (i = 1, 2 \cup j = 1, 2) \cap$$
$$\big((i, j) \neq (1, 1), (2, 2), (2, 3), (3, 2)\big), \tag{6.37}$$

$$g(i, j) = \min \begin{cases} g(i - 2, j - 1) + 2d(i - 1, j) + d(i, j) \\ g(i - 1, j - 1) + \ d(i, j) \\ g(i - 1, j - 2) + 2d(i, j - 1) + d(i, j) \end{cases}. \tag{6.38}$$

Here, g denotes a cumulative distance. The range of the minimum selection, which is in the recurrence formula in eq. (6.38), is a slope constraint that is employed to avoid extreme time expansion and contraction. This slope constraint limits the gradient of the optimum path between one-half and two. The DP matching algorithm adjusts the time expansion and contraction and calculates the optimum path. The optimum path is selected to minimize the DP value, which is defined as

$$D = \min \left\{ g(I, J)/(I + J), \ \frac{J}{2} < I < 2J \right\}. \tag{6.39}$$

Here, the optimum path P calculated from $\boldsymbol{D}_\mathrm{P}[\alpha_1]$, $\boldsymbol{D}_\mathrm{P}[\alpha_2]$, $\boldsymbol{D}_\mathrm{F}[\alpha_1]$, and $\boldsymbol{D}_\mathrm{F}[\alpha_2]$ is expressed as

$$P(\boldsymbol{D}_\mathrm{P}[\alpha_1], \boldsymbol{D}_\mathrm{P}[\alpha_2], \boldsymbol{D}_\mathrm{F}[\alpha_1], \boldsymbol{D}_\mathrm{F}[\alpha_2])$$
$$= \{(1, 1), \cdots, (i, j), \cdots, (I, J)\}. \tag{6.40}$$

If the transition of the path fits $(i, j - 1)$ to (i, j) pattern, the reference pattern is accommodated as

$$\hat{x}_\mathrm{M}[\alpha_2, i] = (x_\mathrm{M}[\alpha_2, j - 1] + x_\mathrm{M}[\alpha_2, j])/2, \tag{6.41}$$

$$\hat{f}_\mathrm{M}[\alpha_2, i] = (f_\mathrm{M}[\alpha_2, j - 1] + f_\mathrm{M}[\alpha_2, j])/2. \tag{6.42}$$

Meanwhile, if the transition of the path meets $(i - 1, j - 1)$ to (i, j) pattern, the reference pattern is obtained as

$$\hat{x}_\mathrm{M}[\alpha_2, i] = x_\mathrm{M}[\alpha_2, j], \tag{6.43}$$

$$\hat{f}_\mathrm{M}[\alpha_2, i] = f_\mathrm{M}[\alpha_2, j]. \tag{6.44}$$

In the same way, if the transition of the path fits $(i-1, j)$ to (i, j), the reference pattern is derived as

$$\hat{x}_\mathrm{M}[\alpha_2, i] = x_\mathrm{M}[\alpha_2, j], \tag{6.45}$$

$$\hat{f}_\mathrm{M}[\alpha_2, i] = f_\mathrm{M}[\alpha_2, j]. \tag{6.46}$$

These processes unify the length of each data. Impedance calculation using the accommodated data is carried out by the least-squares method, which is expressed as

$$
K_\mathrm{c}[i] = \frac{N \displaystyle\sum_{k=1}^{N} \left(\hat{x}_\mathrm{M}[\alpha_k, i]\hat{f}_\mathrm{M}[\alpha_k, i] \right)}{N \displaystyle\sum_{k=1}^{N} \hat{x}_\mathrm{M}[\alpha_k, i]^2 - \left(\displaystyle\sum_{k=1}^{N} \hat{x}_\mathrm{M}[\alpha_k, i] \right)^2}
$$
$$
- \frac{\displaystyle\sum_{k=1}^{N} \hat{x}_\mathrm{M}[\alpha_k, i] \displaystyle\sum_{k=1}^{N} \hat{f}_\mathrm{M}[\alpha_k, i]}{N \displaystyle\sum_{k=1}^{N} \hat{x}_\mathrm{M}[\alpha_k, i]^2 - \left(\displaystyle\sum_{k=1}^{N} \hat{x}_\mathrm{M}[\alpha_k, i] \right)^2}, \tag{6.47}
$$

where " $\hat{}$ " denotes the accommodated data. The number of operations is represented by "N." In this least-squares method, first order polynomial is adopted, since this study focuses on the control stiffness. If the calculation result of $K_\mathrm{c}[i]$ is negative, $K_\mathrm{c}[i-1]$ is substituted into $K_\mathrm{c}[i]$, as the stiffness value must be positive.

The obtained stiffness is reproduced by the compliance control system. The force reference for the impedance control is given as

$$f_\mathrm{S}^\mathrm{ref} = m_\mathrm{S} \big\{ K_\mathrm{p} K_\mathrm{c}[i] \left(x_\mathrm{M}[\alpha_1, i] - x_\mathrm{S} \right)$$
$$- K_\mathrm{f} \left(f_\mathrm{M}[\alpha_1, i] + f_\mathrm{S} \right) \big\}. \tag{6.48}$$
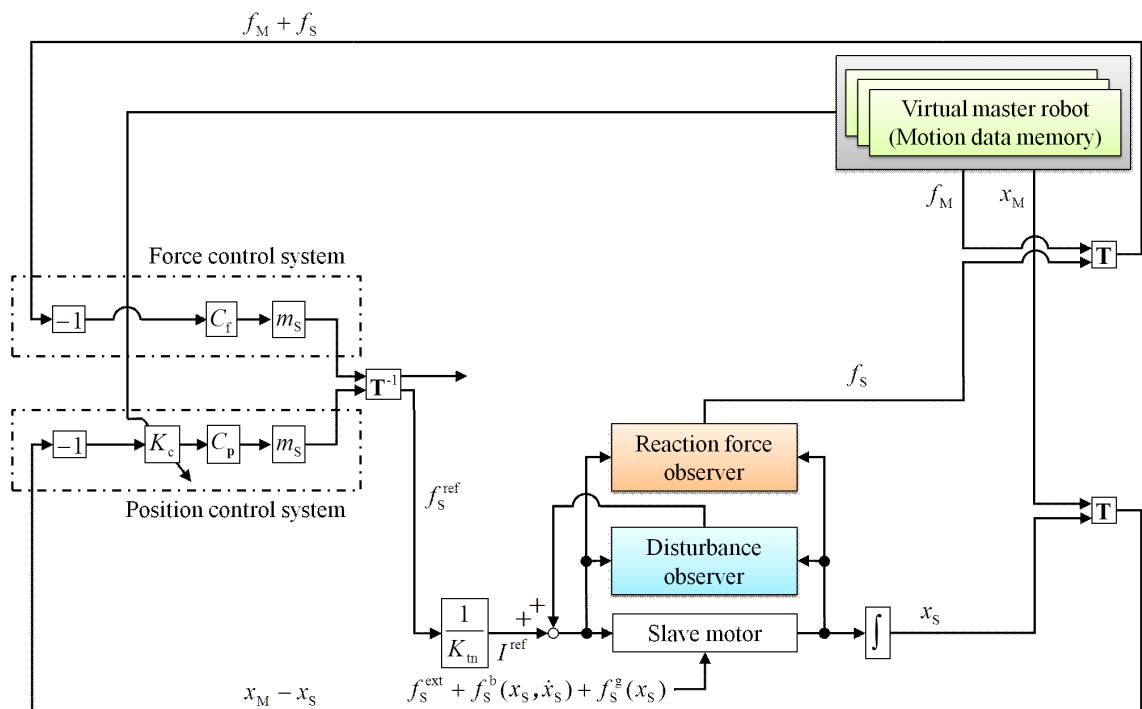
Fig. 6-4: Proposed motion data reproduction system.

Table 6.1: Experimental parameters.

Variables	Definition of variables	Value
$m_{\mathrm{M}}^{\mathrm{trans}}$	Nominal mass	1.70 kg
$m_{\mathrm{S}}^{\mathrm{trans}}$	Nominal mass	1.51 kg
$m_{\mathrm{M}}^{\mathrm{gras}}, m_{\mathrm{S}}^{\mathrm{gras}}$	Nominal mass	0.43 kg
	Position feedback gain	10000 $1/\mathrm{s}^2$
	Velocity feedback gain	200 1/s
	Feedback gain of f^{trans}	0.8 1/kg
	Feedback gain of f^{grasp}	1.6 1/kg
	Cutoff frequency of DOB and RFOB	1000 rad/s
	Sampling time	0.1 ms
Reproduction phase in proposal		
$K_{\mathrm{p}}^{\mathrm{trans}}$	Position feedback gain	0.8 1/kg
$K_{\mathrm{p}}^{\mathrm{gras}}$	Position feedback gain	1.6 1/kg
$K_{\mathrm{f}}^{\mathrm{trans}}$	Force feedback gain	0.8 1/kg
$K_{\mathrm{f}}^{\mathrm{gras}}$	Force feedback gain	1.6 1/kg
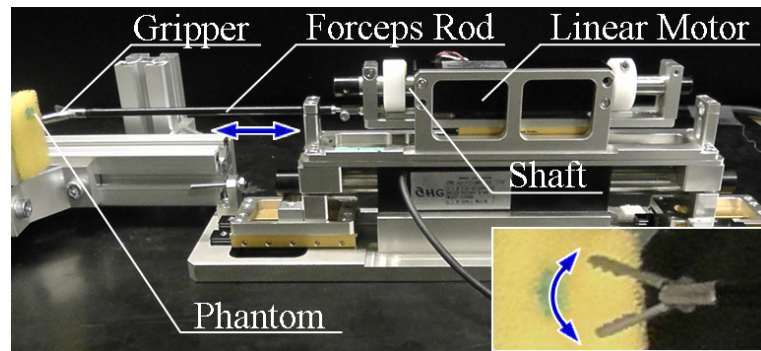
(a) Slave side.
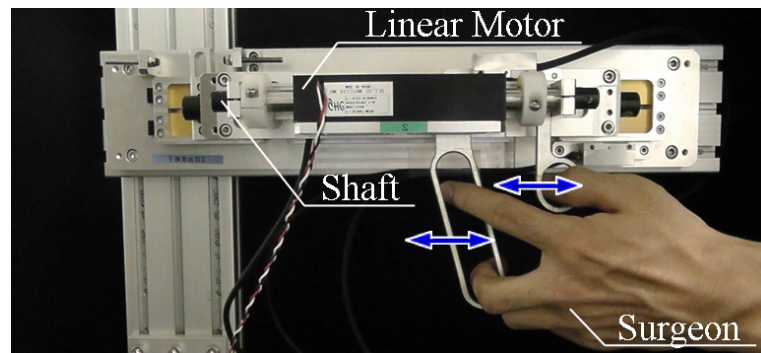
(b) Master side.

Fig. 6-5: Experimental setup of 2-DOF forceps robot which can perform translational motion and grasping motion.

6.2.3 Experiments

Two kinds of experiments were conducted to verify the validity of the proposed motion-reproducing system. One was an experiment for validation of the effectiveness of DP in the stiffness estimation. The other was an experiment of application to the forceps robot. Fig. 6-5 shows the experimental setup. Both the master forceps and the slave forceps consisted of two linear motors that realized the translational motion and the grasping motion. The linear motors were rod-type motors, and there was little friction effect. The external force was observed using the RFOB without force sensors. Only linear encoders were implemented as the sensor of the system. The resolution of the position encoder was 0.1 μm. The object information was an unknown parameter in the control system. The control software was written in C language under RTAI 3.6.1. The sampling time was 100 μs. Table 6.1 lists the experimental

Scaling Ratio α
— 1.0 — 1.5 — 2.0 -- 2.5 -- 3.0

(a) Position response. (without DP)

(b) Force response. (without DP)

(c) Position response. (with DP)

(d) Force response. (with DP)

(e) Estimation result.
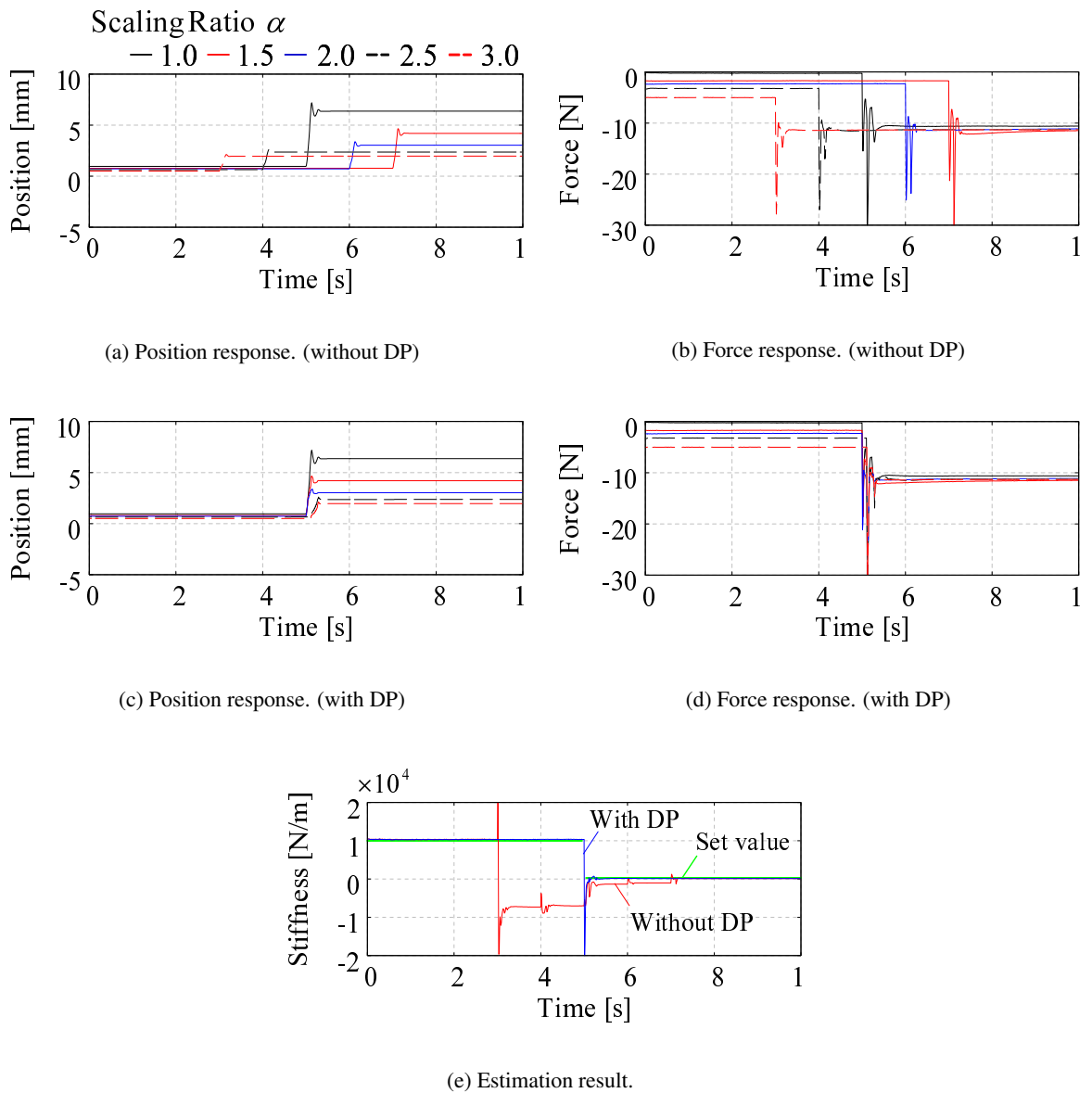
Fig. 6-6: Validation of effectiveness of DP in stiffness estimation.

parameters. In the motion data collection system of this experiment, a proportional-derivative controller was used for position control and a proportional controller was used for force control.

Fig. 6-6 shows the results of the first experiment. A compliance-controlled robot pushed the master forceps. The set stiffness was changed from 10000 N/m to 500 N/m with different switching times. The recorded data were adjusted and the switching times were synchronized by the DP processing as shown

(a) Position response of translational motion.

(b) Position response of grasping motion.

(c) Force response of translational motion.

(d) Force response of grasping motion.
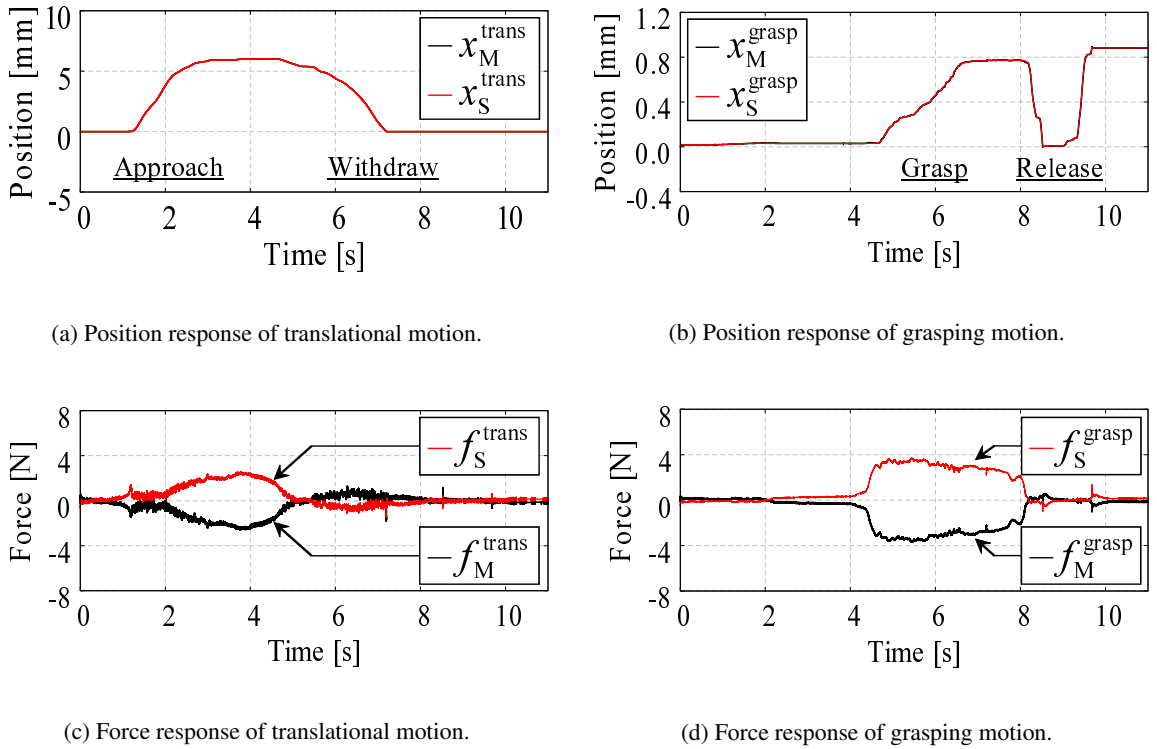
Fig. 6-7: Experimental results of bilateral control.

in Fig. 6-6(c) and Fig. 6-6(d). As the result, the estimation was improved as shown in Fig. 6-6(e).

The second experiment was the application to the forceps robot. A surgeon operated this scaled bilateral control system five times using different scaling ratios. The scaling ratios (α_1, α_2, α_3, α_4, α_5) were 1.0, 1.5, 2.0, 2.5, and 3.0. The purpose of the experiment was the removal of a phantom of sarcoma, which was embedded into a phantom of a healthy tissue. The work procedure and tasks were set as follows: (1) Approach, (2) Grasp, (3) Withdraw, (4) Release. The surgeon was blindfolded while he worked, as the objective of this experiment is to reproduce human motion using haptic information. Fig. 6-7 shows the experimental results of the bilateral control when the scaling ratio was 1.0. These results confirm the achievement of position tracking and force feedback. In other words, the surgeon was able to feel the actual impedance of the target object. Fig. 6-7 (a) presents the position results with regard to translational motion. The results show that the slave system approached the phantom from 1 s to 4 s and withdrew from the surgical field from 6 s to 8 s. Fig. 6-7 (b) presents the position results with regard to grasping motion. The results show that the slave system grasped the phantom from 4 s to 8 s and released it from 8 s to 9 s. Finally, the forceps was closed at 10 s. In the approach phase, force was

Scaling Ratio α

— 1.0 — 1.5 — 2.0 -- 2.5 -- 3.0

(a) Position response of translational motion.

(b) Position response of grasping motion.

(c) Force response of translational motion.

(d) Force response of grasping motion.
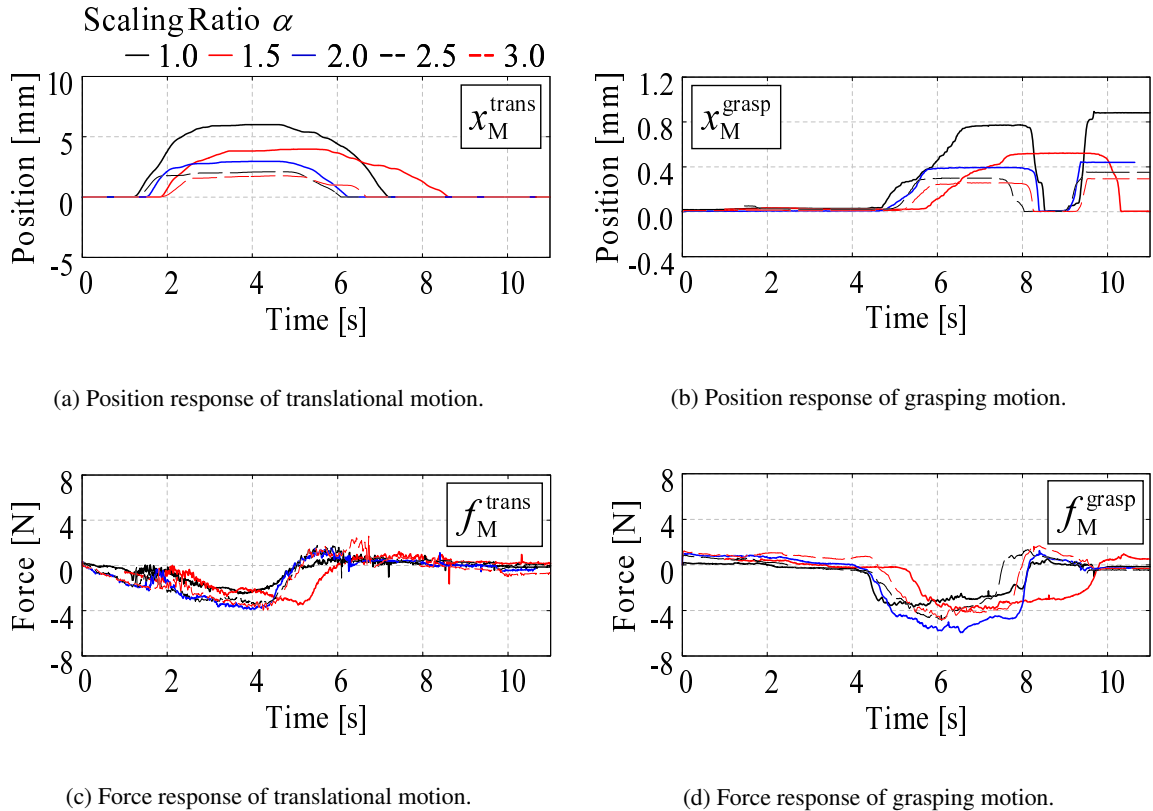
Fig. 6-8: Experimental results of scaled bilateral control.

applied to the forceps robot: the applied force is shown in Fig. 6-7 (c). This force was applied because the surgeon tried to search for the position of the phantom. Fig. 6-7 (d) represents the grasping force. The grasping force, the strength of which was about 3 N, appeared in the grasping phase only.

Fig. 6-8 shows the experimental results for the scaled bilateral control with five different scaling ratios. Only the responses on the master side are represented. There is a variability of motion speed among these five responses. In order to accommodate this variability, DP matching was conducted, and the results are shown in Fig. 6-9. Fig. 6-10 shows the values for the stiffness of the performed motion, which were obtained using the least-squares method with respect to the results shown in Fig. 6-9. In the translational motion, stiffness was high in the first 1 s and the last 2 s. The reason is that when the motion is initiated, the position of the forceps is always the same. In addition, the forceps have to be returned to the starting position in order to be withdrawn from the surgical field. On the other hand, the stiffness of the grasping motion was high at around 5 s, as the forceps was opened to grasp the target phantom.

(a) Position response of translational motion.

(b) Position response of grasping motion.

(c) Force response of translational motion.

(d) Force response of grasping motion.
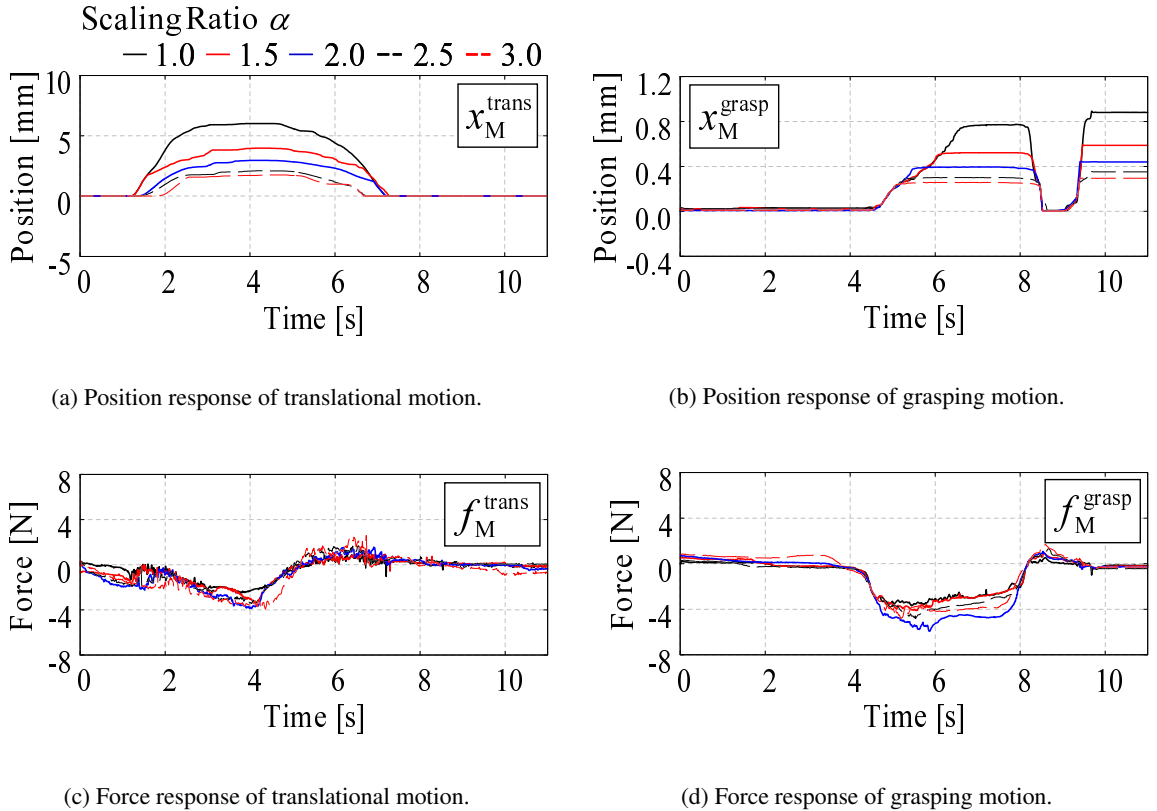
Fig. 6-9: Results of dynamic programming matching.

Fig. 6-11 shows the experimental results of the motion-reproducing system for comparison between the conventional method and the proposed method. In this case, the target phantom was located at the same position as that in the recording phase. Both methods well reproduced the recorded motion, although there was a slight difference with regard to the grasping motion at 1.8 s between the recorded motion and the motion reproduced by the proposed method. In this experimental system, the motor used for the translational motion was located on the base side of the motor generating the grasping motion. Therefore, the rapid acceleration of the translational motion caused the pointed response of the grasping motion.

Fig. 6-12 also shows the experimental results of the motion-reproducing system. In this case, however, the target phantom was located far from its position in the motion data collection phase. In this case, the conventional method could not make contact with the target phantom and failed to execute a grasping motion. Fig. 6-12 (b) shows that the forceps was fully closed without grasping any object.
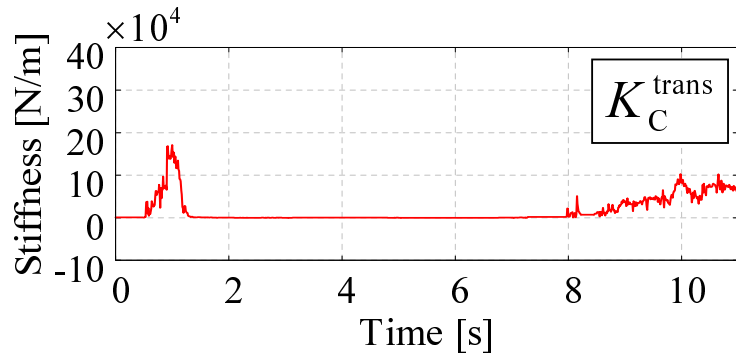
(a) Translational motion.
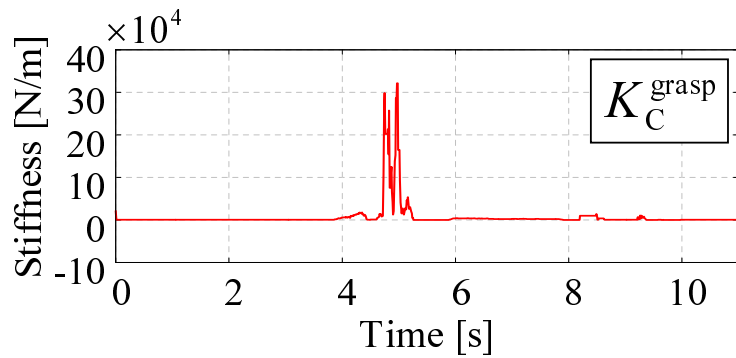
(b) Grasping motion.

Fig. 6-10: Calculated stiffness and force.

In contrast, Fig. 6-13 shows the experimental results of the motion-reproducing system when the target phantom was located near from its position in the collection phase of motion data. In this case, excessive force was applied to the healthy organ, as its surface was nearer than its supposed position. The applied force was four times stronger than that in the recorded motion and that obtained using the proposed method.
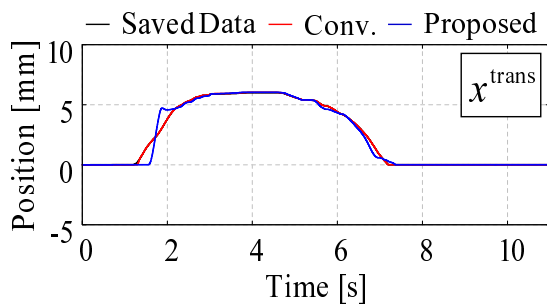
(a) Position response of translational motion.
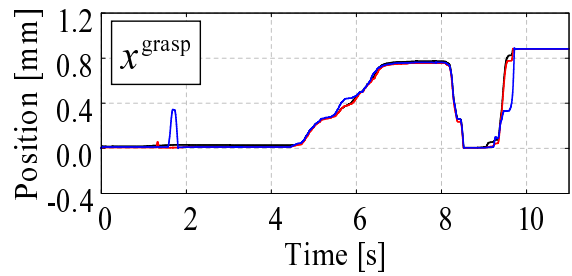
(b) Position response of grasping motion.
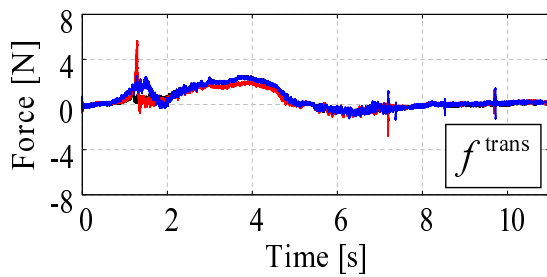
(c) Force response of translational motion.
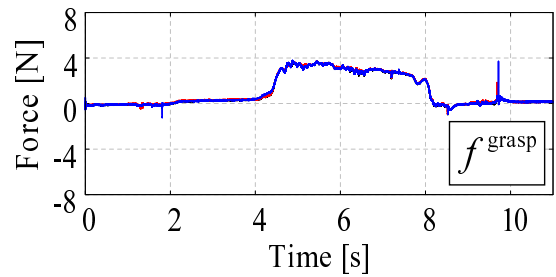
(d) Force response of grasping motion.

Fig. 6-11: Experimental results of motion-reproducing system (phantom was located at the same position as that in the recording phase).
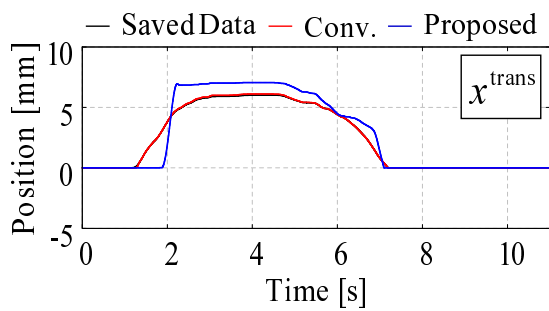
(a) Position response of translational motion.
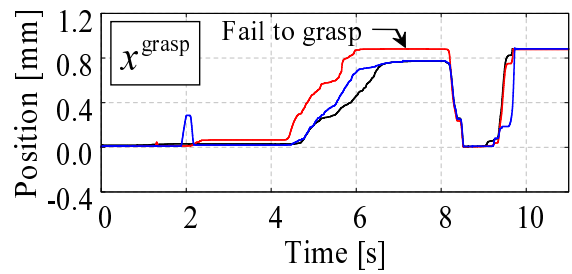
(b) Position response of grasping motion.
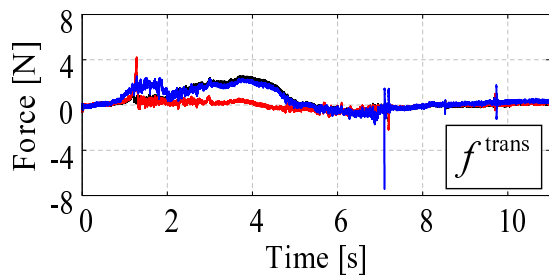
(c) Force response of translational motion.
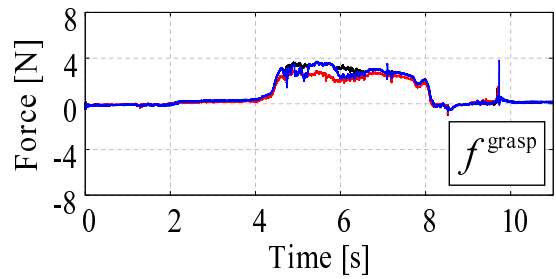
(d) Force response of grasping motion.

Fig. 6-12: Experimental results of motion-reproducing system (phantom was located far from its position in the recording phase).
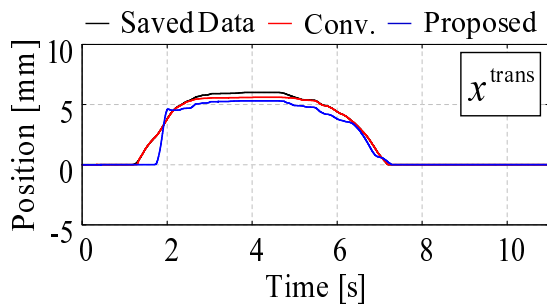
(a) Position response of translational motion.
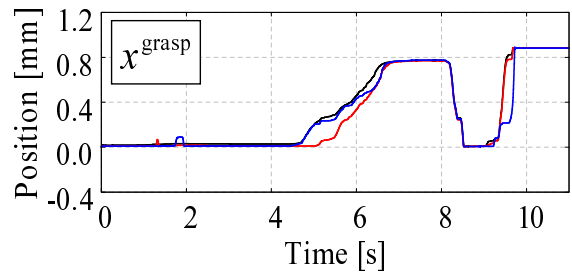
(b) Position response of grasping motion.
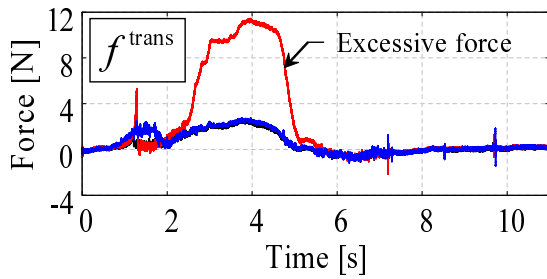
(c) Force response of translational motion.
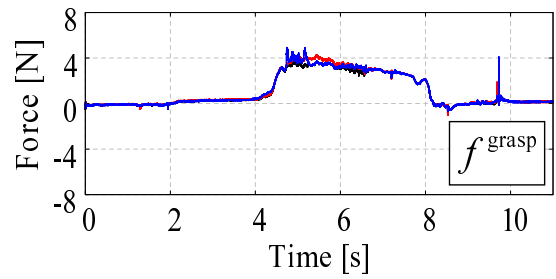
(d) Force response of grasping motion.

Fig. 6-13: Experimental results of motion-reproducing system (phantom was located near from its position in the recording phase).
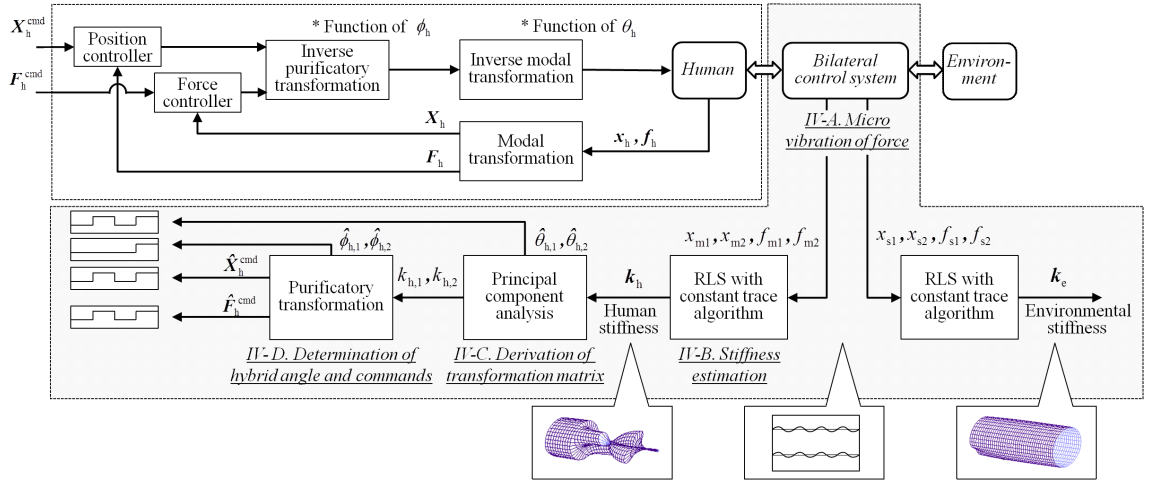
Fig. 6-14: Research outline

6.3   Separation into Elements

6.3.1   Motion Control

Fig. 6-14 shows the research outline. The specific procedures are as follows. Firstly, the haptic information (i.e., position and force information) of human motion is extracted by using a bilateral control system. At this time, a micro force vibration is input into the system to estimate the stiffness of the environment and the human motion independently and simultaneously. Secondly, the haptic information is transformed into various modal spaces. The stiffness of the motion is estimated in each modal space. Finally, the human motion is separated into its basic elements.

Fig. 6-15 shows the block diagram of teleoperation [54] [163]. For simplicity, the mass on the master and the slave sides is assumed to be the same. Disturbance observers (DOBs) [29] are used to realize high robustness. The reaction force from the environment is observed by using the reaction force observers (RFOBs) [33] without force sensors. An acceleration reference is obtained as

$$\ddot{\boldsymbol{X}}^{\mathrm{ref}} = C_{\mathrm{p}}\mathbf{S}_{\mathrm{p}}(\boldsymbol{X}^{\mathrm{cmd}} - \boldsymbol{X}) + C_{\mathrm{f}}\mathbf{S}_{\mathrm{f}}(\boldsymbol{F}^{\mathrm{cmd}} - \boldsymbol{F}). \tag{6.49}$$

Section 6.3.2 explains the determination of the command vectors in detail with a practical example of bilateral control.
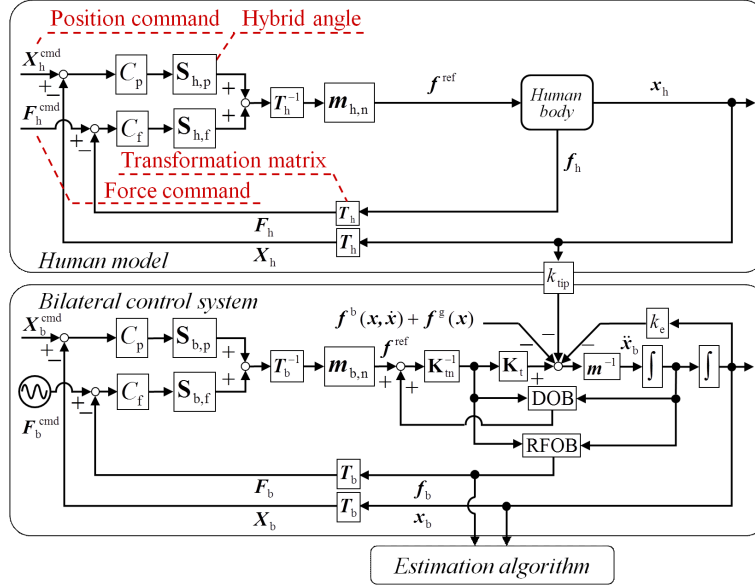
Fig. 6-15: Block diagram of teleoperation.

Here, $\mathbf{S}_p$ and $\mathbf{S}_f$ are respectively defined as

$$\mathbf{S}_p = \operatorname{diag}\left[\cos\phi_1, \cdots, \cos\phi_n\right], \tag{6.50}$$

$$\mathbf{S}_f = \operatorname{diag}\left[\sin\phi_1, \cdots, \sin\phi_n\right]. \tag{6.51}$$

The hybrid angle ϕ is given as the ratio of the effect of a position control system and a force control system [112, 165]. By changing the hybrid angle, pure position control, pure force control, and impedance control can all be expressed. The acceleration reference for each actuator is derived by inverse modal transformation

$$\ddot{\boldsymbol{x}}^{\mathrm{ref}} = \boldsymbol{T}^{-1}\ddot{\boldsymbol{X}}^{\mathrm{ref}}. \tag{6.52}$$

The purpose of the position controller is to suppress the external force and make the control stiffness infinite. On the other hand, the purpose of the compliance or force controller is to control the external force and make the control stiffness zero. An arbitrary control stiffness can be achieved by adjusting the effect of the references obtained from the position and the force controllers. As shown in eq. (6.49), each acceleration reference $\ddot{X}^{\mathrm{ref}}$ is calculated as

$$\ddot{X}^{\mathrm{ref}} = \ddot{X}_{\mathrm{f}}^{\mathrm{ref}}\sin\phi + \ddot{X}_{\mathrm{p}}^{\mathrm{ref}}\cos\phi, \tag{6.53}$$

Table 6.2: Hybrid angle and control impedance.

	Hybrid angle	Control impedance
Force control	$\phi = \frac{\pi}{2}$	0
Impedance control	$0 < \phi < \frac{\pi}{2}$	$\frac{C_\mathrm{p}}{C_\mathrm{f} \tan \phi}$
Position control	$\phi = 0$	∞

where $\ddot{X}_\mathrm{f}^\mathrm{ref}$ and $\ddot{X}_\mathrm{p}^\mathrm{ref}$ are the acceleration references calculated by the position and the force controllers, respectively. These values are expressed as

$$\ddot{X}_\mathrm{f}^\mathrm{ref} = C_\mathrm{f}(F^\mathrm{cmd} - F), \tag{6.54}$$

$$\ddot{X}_\mathrm{p}^\mathrm{ref} = C_\mathrm{p}(X^\mathrm{cmd} - X). \tag{6.55}$$

Table 6.2 lists the relationship between the hybrid angle and the control impedance [23, 24]. When ϕ is 0, the acceleration reference is derived as

$$\ddot{X}^\mathrm{ref} = C_\mathrm{p}(X^\mathrm{cmd} - X). \tag{6.56}$$

In contrast, when ϕ is not 0, the acceleration reference is

$$\ddot{X}^\mathrm{ref} = C_\mathrm{f} \sin \phi \left(f'^\mathrm{cmd} - k_\mathrm{c} x^\mathrm{res} - f^\mathrm{res} \right), \tag{6.57}$$

$$f'^\mathrm{cmd} = f^\mathrm{cmd} + k_\mathrm{c} x^\mathrm{cmd}, \tag{6.58}$$

$$k_\mathrm{c} = \frac{C_\mathrm{p}}{C_\mathrm{f} \tan \phi}, \tag{6.59}$$

where f'^cmd and k_c denote the equivalent force command and impedance, respectively.

6.3.2 Bilateral Control for Extraction of Haptic Information

The implementation of bilateral control is explained through a practical example of a simple multiple-DOF system that can perform grasping and manipulating motions. Two linear motors are assumed to be used in the master and the slave sides, as shown in Fig. 6-16. The operator and the master robots are located on the far side. The environment and the slave robots are located on the near side. The slave robots 1 and 2 are located on opposite sides of the environment. The four shafts can move from side to side. When the operator decreases the distance between the two master robots, the slave robots make contacts with and grasp the environment. When the operator moves the master robots in the same direction, the environment is manipulated and transported horizontally.
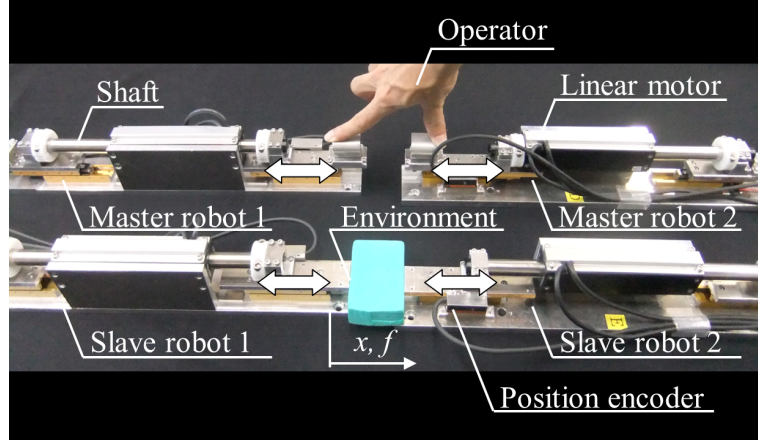
Fig. 6-16: Experimental setup.

The purpose of the bilateral control system is to perceive the mechanical impedance of the remote environment. This can be achieved through two control goals [168]: one is position tracking between the master and slave robots,

$$
\begin{bmatrix}
1 & -1 & 0 & 0 \\
0 & 0 & 1 & -1
\end{bmatrix}
\begin{bmatrix}
x_{m1} & x_{s1} & x_{m2} & x_{s2}
\end{bmatrix}^{T} = \mathbf{0},
\tag{6.60}
$$

and the other is force feedback for realization of the law of action and reaction,

$$
\begin{bmatrix}
1 & 1 & 0 & 0 \\
0 & 0 & 1 & 1
\end{bmatrix}
\begin{bmatrix}
f_{m1} & f_{s1} & f_{m2} & f_{s2}
\end{bmatrix}^{T} = \mathbf{0}.
\tag{6.61}
$$

Therefore, from the left hand sides of eq. (6.60) and eq. (6.61), the transformation matrix is determined as follows [53, 54, 74]:

$$
\boldsymbol{T}_{b} =
\begin{bmatrix}
1 & -1 & 0 & 0 \\
0 & 0 & 1 & -1 \\
1 & 1 & 0 & 0 \\
0 & 0 & 1 & 1
\end{bmatrix}.
\tag{6.62}
$$

Because two out of four control goals are related to the position control system, the selection matrices of the bilateral control are

$$
\mathbf{S}_{p,b} = \mathrm{diag}
\begin{bmatrix}
\cos 0 & \cos 0 & \cos \frac{\pi}{2} & \cos \frac{\pi}{2}
\end{bmatrix},
\tag{6.63}
$$

$$
\mathbf{S}_{f,b} = \mathrm{diag}
\begin{bmatrix}
\sin 0 & \sin 0 & \sin \frac{\pi}{2} & \sin \frac{\pi}{2}
\end{bmatrix}.
\tag{6.64}
$$

The command vectors are determined by the right-hand sides of eq. (6.60) and eq. (6.61) as

$$\boldsymbol{X}_{\mathrm{b}}^{\mathrm{cmd}} = \begin{bmatrix} 0 & 0 & - & - \end{bmatrix}^{\mathrm{T}}, \tag{6.65}$$

$$\boldsymbol{F}_{\mathrm{b}}^{\mathrm{cmd}} = \begin{bmatrix} - & - & 0 & 0 \end{bmatrix}^{\mathrm{T}}. \tag{6.66}$$

Elements that do not affect the control system are expressed as "$-$" for ease of explanation.

6.3.3 Proposed Estimation Algorithm

This section describes the specific procedures of the proposed estimation algorithm. This algorithm estimates the structure and input of human motions. Specifically, this algorithm estimates the following variables: modal transformation matrix $\boldsymbol{T}_{\mathrm{h}}$, hybrid angles ϕ_{h}, position command $\boldsymbol{X}_{\mathrm{h}}^{\mathrm{cmd}}$, and force command $\boldsymbol{F}_{\mathrm{h}}^{\mathrm{cmd}}$.

Micro Vibration of Force

To divide the total haptic information into the environmental information and the human information independently and simultaneously, the micro vibration of the force is input into the system in place of eq. (6.66). The micro vibration is expressed as

$$\boldsymbol{F}_{\mathrm{b}}^{\mathrm{cmd}} = \begin{bmatrix} - & - & A\sin(2\pi ft + \frac{\pi}{2}) & A\sin(2\pi ft) \end{bmatrix}^{\mathrm{T}}, \tag{6.67}$$

where A, f, and t denote the amplitude, frequency, and time, respectively.

Stiffness Estimation

To clarify the control axes, the responses of bilateral control are transformed into several coordinate spaces. When these responses are transformed into N types of modal spaces, the transformation of the k-th time-series data is expressed as

$$\begin{bmatrix} p_{[d,k]} \\ q_{[d,k]} \end{bmatrix}^{\mathrm{T}} = \begin{bmatrix} \cos(\frac{2\pi d}{N}) \\ \sin(\frac{2\pi d}{N}) \end{bmatrix}^{\mathrm{T}} \begin{bmatrix} x_{1[d,k]} & f_{1[d,k]} \\ x_{2[d,k]} & f_{2[d,k]} \end{bmatrix}. \tag{6.68}$$

In this study, the N is selected as 32, although the N can be set higher, as the following procedure is an off-line processing. d denotes the transformation to the d-th space $(1 \leq d \leq N)$. The $p_{[d,k]}$ and the $q_{[d,k]}$ are the position and the force transformed into the modal spaces. The stiffness is calculated
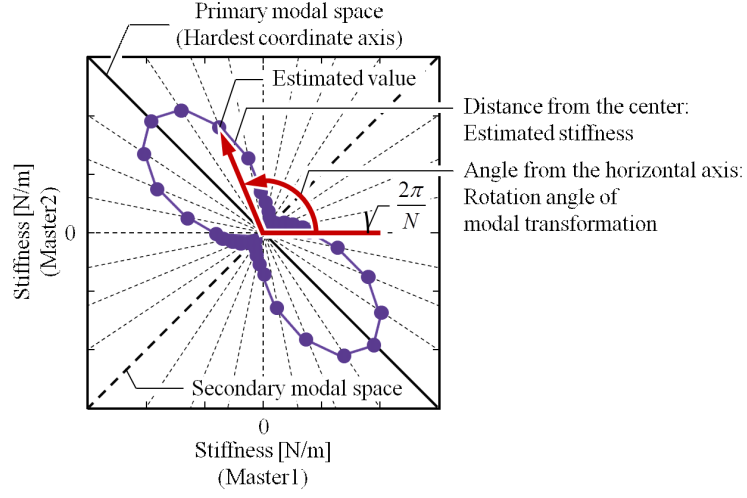
Fig. 6-17: Example of estimation results.

in each modal space. This study employs a recursive least-squares method (RLS) with a constant trace algorithm [169, 170]. An estimated parameter vector $\hat{\boldsymbol{\eta}}_{[d,k]}$ and an observation vector $\boldsymbol{\xi}_{[d,k]}$ are set as

$$\hat{\boldsymbol{\eta}}_{[d,k]} = \left[\begin{array}{cc} k_{[d,k]} & c_{[d,k]} \end{array}\right]^{\mathrm{T}}, \tag{6.69}$$

$$\boldsymbol{\xi}_{[d,k]} = \left[\begin{array}{cc} p_{[d,k]} & -1 \end{array}\right]^{\mathrm{T}}, \tag{6.70}$$

where $k_{[d,k]}$ and $c_{[d,k]}$ denote the stiffness and the force offset, respectively. The algorithms are

$$\hat{\boldsymbol{\eta}}_{[d,k]} = \hat{\boldsymbol{\eta}}_{[d,k-1]} - \frac{\boldsymbol{\Gamma}_{[d,k-1]}\boldsymbol{\xi}_{[d,k]}}{1 + \boldsymbol{\xi}_{[d,k]}^{\mathrm{T}}\boldsymbol{\Gamma}_{[d,k-1]}\boldsymbol{\xi}_{[d,k]}}$$
$$\left(\boldsymbol{\xi}_{[d,k]}^{\mathrm{T}}\hat{\boldsymbol{\eta}}_{[d,k-1]} - q_{[d,k]}\right), \tag{6.71}$$

$$\boldsymbol{\Gamma}_{[d,k]} = $$
$$\frac{1}{\lambda_{[d,k]}}\left(\boldsymbol{\Gamma}_{[d,k-1]} - \frac{\boldsymbol{\Gamma}_{[d,k-1]}\boldsymbol{\xi}_{[d,k]}\boldsymbol{\xi}_{[d,k]}^{\mathrm{T}}\boldsymbol{\Gamma}_{[d,k-1]}}{1 + \boldsymbol{\xi}_{[d,k]}^{\mathrm{T}}\boldsymbol{\Gamma}_{[d,k-1]}\boldsymbol{\xi}_{[d,k]}}\right), \tag{6.72}$$

$$\lambda_{[d,k]} = 1 - \frac{\|\boldsymbol{\Gamma}_{[d,k-1]}\boldsymbol{\xi}_{[d,k]}\|^2}{1 + \boldsymbol{\xi}_{[d,k]}^{\mathrm{T}}\boldsymbol{\Gamma}_{[d,k-1]}\boldsymbol{\xi}_{[d,k]}}\frac{1}{\mathrm{tr}\boldsymbol{\Gamma}_{[d,0]}}, \tag{6.73}$$
$$\left(\boldsymbol{\Gamma}_{[d,0]} = \lambda_{[d,k]}\boldsymbol{I}, \lambda_{[d,k]} > 0\right)$$

where $\lambda_{[d,k]}$ denotes the trace gain, which is determined by initial matrix. We can adjust forgetting rate by changing the trace gain. Through this estimation process, the stiffness of the environment and the human motion can be obtained.

Derivation of Transformation Matrix

Fig. 6-17 shows an example of the estimation results. The distance from the origin presents the estimated stiffness. The angle from the horizontal axis shows the rotation angle used in the modal transformation of eq. (6.68). The bold line shows the hardest coordinate axis where the highest stiffness is estimated. In this study, the space expressed by the hardest coordinate axis is defined as primary modal space. On the other hand, the space expressed by the axis perpendicular to the hardest coordinate axis is defined as secondary modal space. This study employs a principal component analysis to determine the hardest coordinate axis [109]. The sample dataset is set as

$$z_{[k]} = pk_{\mathrm{h}[k]}, \tag{6.74}$$

$$p = \left[\begin{array}{c} \cos(\frac{2\pi}{N}) \cdots \cos(\frac{2\pi d}{N}) \cdots \cos(2\pi) \\ \sin(\frac{2\pi}{N}) \cdots \sin(\frac{2\pi d}{N}) \cdots \sin(2\pi) \end{array} \right], \tag{6.75}$$

$$k_{\mathrm{h}[k]} = \left[\begin{array}{ccc} k_{h[1,k]} \cdots k_{h[d,k]} \cdots k_{h[N,k]} \end{array} \right]^{\mathrm{T}}. \tag{6.76}$$

A covariance matrix v is calculated as

$$v_{[k]} = \frac{1}{N-1} z_{[k]}^{\mathrm{T}} z_{[k]}. \tag{6.77}$$

When the eigenvectors and eigenvalues of the covariance matrix are denoted by $u_{1[k]}$, $u_{2[k]}$, $\varepsilon_{1[k]}$, and $\varepsilon_{2[k]}$,

$$\left(v_{[k]} - \varepsilon_{1[k]} I\right) u_{1[k]} = 0, \tag{6.78}$$

$$\left(v_{[k]} - \varepsilon_{2[k]} I\right) u_{2[k]} = 0, \ (\varepsilon_{2[k]} \le \varepsilon_{1[k]}) \tag{6.79}$$

are satisfied. Here, $u_{1[k]}$ is the hardest coordinate axis. $\varepsilon_{1[k]}$ is the variance of the first principal component. By adjusting the norm, the modal transformation matrix is obtained as

$$\hat{T}_{\mathrm{h}} = \left[\begin{array}{cc} \sqrt{2} \dfrac{u_{1[k]}^{\mathrm{T}}}{\|u_{1[k]}^{\mathrm{T}}\|} & \sqrt{2} \dfrac{u_{2[k]}^{\mathrm{T}}}{\|u_{2[k]}^{\mathrm{T}}\|} \end{array} \right]^{\mathrm{T}}. \tag{6.80}$$

When the rotation matrix is represented as

$$R_{\mathrm{h}}(\theta_{\mathrm{h}}) = \left[\begin{array}{cc} \cos(\theta_{\mathrm{h}}) & -\sin(\theta_{\mathrm{h}}) \\ \sin(\theta_{\mathrm{h}}) & \cos(\theta_{\mathrm{h}}) \end{array} \right], \tag{6.81}$$

the direction of the control axis θ_{h} is defined as

$$\sqrt{2} R_{\mathrm{h}}(\hat{\theta}_{\mathrm{h}}) = \hat{T}_{\mathrm{h}}. \tag{6.82}$$

Table 6.3: Parameter setup of human motion.

	Step 1 (0 s ~ 5 s)	Step 2 (5 s ~ 10 s)	Step 3 (10 s ~ 15 s)	Step 4 (15 s ~ 20 s)
T_h	$\begin{bmatrix} 1 & -1 \\ 1 & 1 \end{bmatrix}$	$\begin{bmatrix} 1 & -1 \\ 1 & 1 \end{bmatrix}$	$\begin{bmatrix} 1 & 1 \\ 1 & -1 \end{bmatrix}$	$\begin{bmatrix} 1 & 1 \\ 1 & -1 \end{bmatrix}$
θ_h	$3\pi/4$	$3\pi/4$	$\pi/4$	$\pi/4$
ϕ_1	0	0	0	$\pi/2$
ϕ_2	0	$\pi/2$	$\pi/2$	$\pi/2$
X_h^{cmd}	$\begin{bmatrix} -0.01 \\ 0.06 \end{bmatrix}$	$\begin{bmatrix} -0.01 \\ - \end{bmatrix}$	$\begin{bmatrix} 0.06 \\ - \end{bmatrix}$	$\begin{bmatrix} - \\ - \end{bmatrix}$
F_h^{cmd}	$\begin{bmatrix} - \\ - \end{bmatrix}$	$\begin{bmatrix} - \\ 0 \end{bmatrix}$	$\begin{bmatrix} - \\ 22 \end{bmatrix}$	$\begin{bmatrix} 0 \\ 22 \end{bmatrix}$

Determination of Hybrid Angles and Commands

Finger tips itself have some stiffness because of the flesh and the skin. By considering this kind of unintended stiffness k_{tip}, the controlled and conscious stiffness $\hat{k}_c$ is calculated as

$$\hat{k}_c = \frac{k_{tip}\hat{k}_h}{k_{tip} - \hat{k}_h}. \tag{6.83}$$

Therefore, the hybrid angle of the human motion can be estimated as

$$\hat{\phi}_h = \tan^{-1}\sqrt{\frac{C_p}{C_f\hat{k}_c}}. \tag{6.84}$$

The commands can be obtained from the calculated transformation matrix and responses as

$$\hat{X}_h^{cmd} = \hat{T}_h x, \tag{6.85}$$

$$\hat{F}_h^{cmd} = \hat{T}_h f. \tag{6.86}$$

6.3.4 Simulation

A simulation was conducted to validate the proposed method. Noticeable basic four examples were set on the simulation, as verification of the validity of the estimation results is difficult by using actual

Table 6.4: Parameters used in this study.

A	Amplitude	2 N
f	Frequency	2 Hz
k_{tip}	Stiffness of the finger tip itself	1800 N/m
k_{e}	Stiffness of environment	12000 N/m
λ	Trace gain	290000
α	Threshold	1000 N/m
	Position feedback gain	900 $1/s^2$
	Velocity feedback gain	60 1/s
	Force feedback gain	1.6 1/kg
	Cutoff frequency of RFOB	500 rad/s
	Cutoff frequency of DOB	500 rad/s
	Mass of motors	0.5 kg
	Mass of fingers	0.3 kg
	Sampling time (control)	0.1 ms
	Sampling time (data)	10.0 ms

human motion The transformation matrix, hybrid angle, position commands, and force commands differ in each step, as listed in Table 6.3. The other simulation parameters are listed in Table 6.4, which were determined by a trial-and-error process while referring to [53]. The micro vibration should be small not to disturb the operation. The environment and the mass were set in accordance with the following experiments. The environment was a spring that simulates a melamine sponge used in the experiments. The required sampling time for data collection is depending on intended tasks in reproduction phase. In this chapter, the sampling time for collection of motion data was determined as 10.0 ms, as it can be thought that it was enough to clarify the correctness of the principle of proposed approach. Note that the data recording rate can be set shorter, as this is off-line processing. Fig. 6-18(a) and Fig. 6-18(b) show the responses obtained from the bilateral control system. The four fundamental parameters of human motion were estimated from these responses despite there being little difference among the steps.

(a) Position response.

(b) Force response.

(c) Stiffness of environment.

(d) Stiffness of human motion.
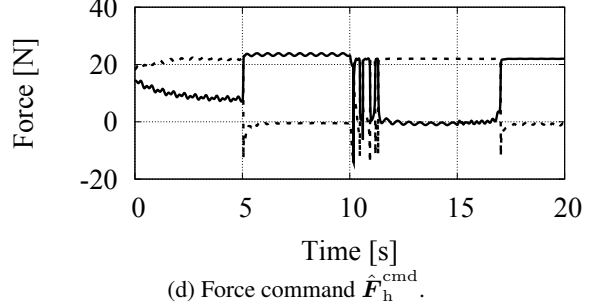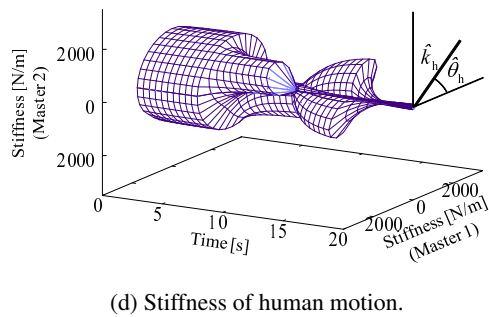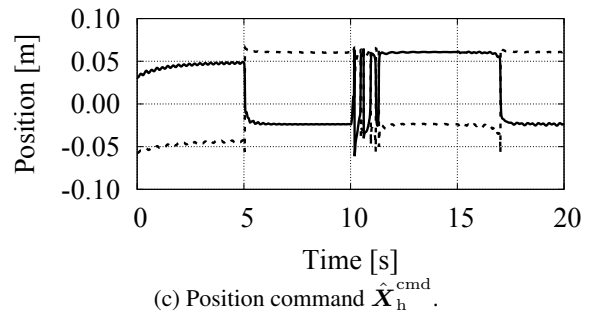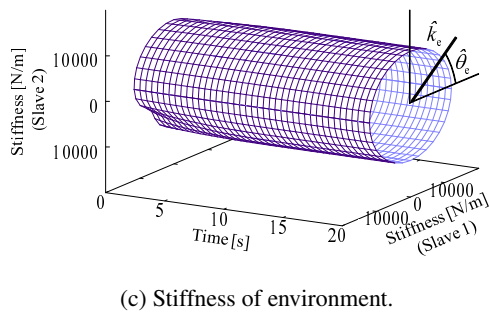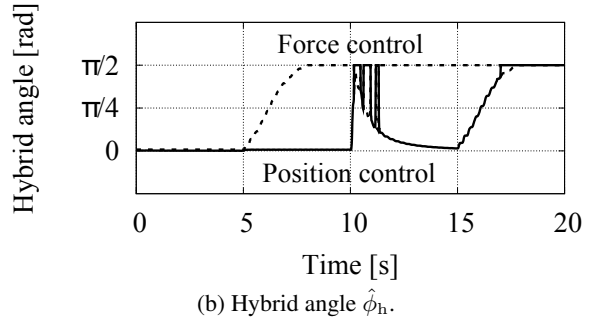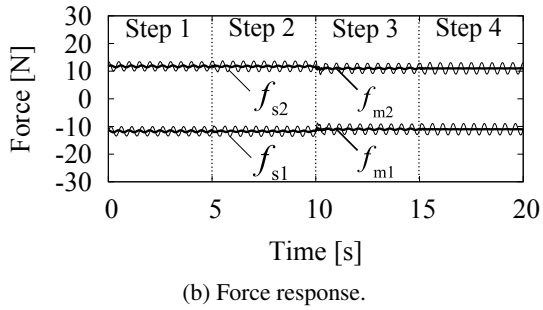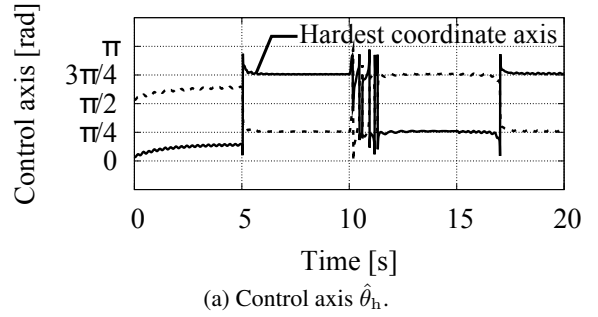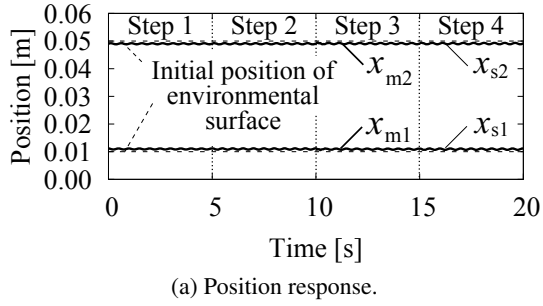
Fig. 6-18: Results of simulation and estimated stiffness.

(a) Control axis $\hat{\theta}_h$.

(b) Hybrid angle $\hat{\phi}_h$.

(c) Position command $\hat{X}_h^{cmd}$.

(d) Force command $\hat{F}_h^{cmd}$.

Fig. 6-19: Basic parameters estimated in simulation.

Fig. 6-18(c) and Fig. 6-18(d) show manifolds that indicate the estimated stiffness of the environment and human motion, respectively. In a plane perpendicular to the time axis, the angle from the horizontal direction indicates $\hat{\theta}_{\mathrm{h}}$, and the distance from the center indicates the stiffness. The environmental result shows a cylinder with radius 12000 N/m. This radius was almost equal to the set stiffness of the environment k_{e}. Separately, the human motion result clearly shows the existence of four types of states. In step 1, the radius of the cylinder was 1800 N/m, which is the same as the value of the unintended stiffness k_{tip}. In ideal position control, the stiffness of the motion is infinite, and only the effect of k_{tip} should appear. Therefore, this result is valid.

In steps 2 and 3, Fig. 6-18(d) shows the directions of the control axes. In the direction of position control, the estimated stiffness was almost 1800 N/m for the same reason as that in step 1. On the other hand, in the direction of force control, the estimated stiffness was almost zero. These results are also valid, because the stiffness must be zero under ideal force control.

The results from 15 to 20 s show the estimated stiffness of force control. As stated above, the stiffness must be zero.

Fig. 6-19 shows the estimated parameters of human motion. The solid lines show the estimated parameters on the primary modal space. The dashed lines show the estimated parameters on the secondary modal space. Fig. 6-19(a) presents the rotation angle of the modal transformation $\hat{\theta}_{\mathrm{h}}$ calculated in eq. (6.82). Fig. 6-19(b) describes the hybrid angle $\hat{\phi}_{\mathrm{h}}$ derived by eq. (6.84). Fig. 6-19(c) and Fig. 6-19(d) show the commands $\hat{\boldsymbol{X}}_{\mathrm{h}}^{\mathrm{cmd}}$, $\hat{\boldsymbol{F}}_{\mathrm{h}}^{\mathrm{cmd}}$ obtained by eq. (6.85) and eq. (6.86). In steps 2 and 3, the parameters were correctly estimated except for immediately after the shift from step 2 to step 3. In steps 1 and 4, both axes were controlled by the same type of control system. Therefore, the orientations of the axes $\hat{\theta}_{\mathrm{h}}$ could not be estimated—they were indefinite and not very important—and the hybrid angle $\hat{\phi}_{\mathrm{h}}$ was correctly estimated.

6.3.5   Experiments

The proposed method was also validated through two experiments: one involving a robotic operator and the other involving human motion. In this experimental setup (Fig. 6-16), the linear motors were 160Q produced by GMC Hillstone Co., Ltd. The linear motors only equipped position encoders as sensors, which were RCH24 produced by Renishaw Inc. The resolution of the position encoders were 0.1 μm. The control software was written in C language under RTAI 3.6.1.

Experiment Using Robotic Operator

The parameters and transitions of the steps were the same as those in the simulation (see Tables 1 and 2). In this experiment, six linear motors were utilized. Of these, two were used to imitate a human operator. The other four were used in the bilateral control system. Fig. 6-20(a) and Fig. 6-20(b) show the responses of the bilateral control system. The parameters of human motion were estimated from these responses, which show little differences among steps. Fig. 6-20(c) and Fig. 6-20(d) show manifolds that indicate the estimated stiffness of the environment and human motion, respectively. The environmental result shows a cylinder with radius 12000 N/m. This was almost equal to the set stiffness of the environment k_e. However, the cross-sectional view of the manifold was elliptical. This is attributed to aftereffects of the stiffness k_{tip} imitating the human finger. In the experiment, the spring has small viscosity. The human motion result clearly shows the existence of four types of states.
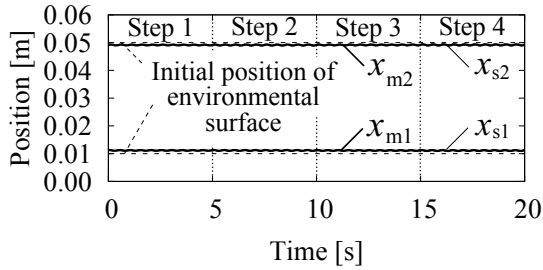
(a) Position response.
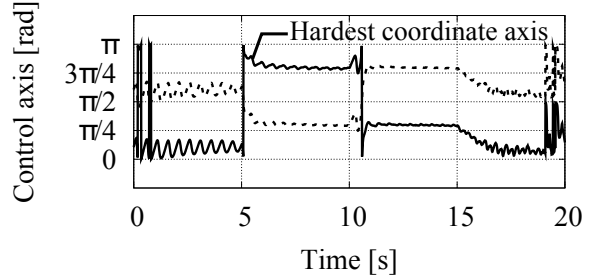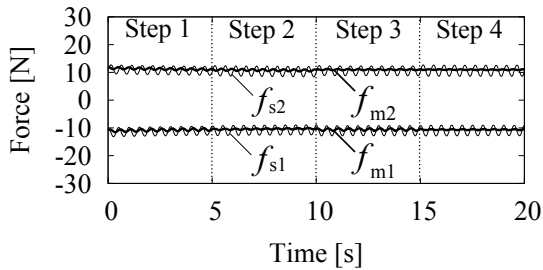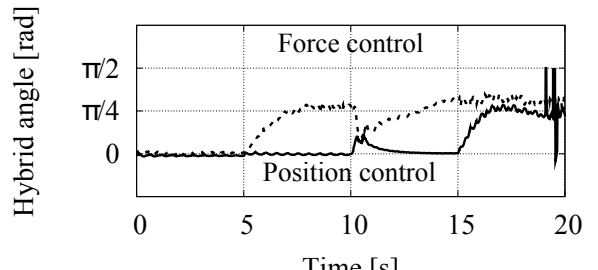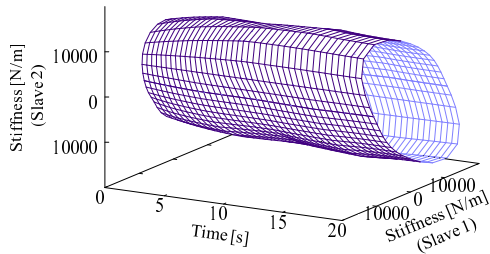
(b) Force response.

(c) Stiffness of environment.
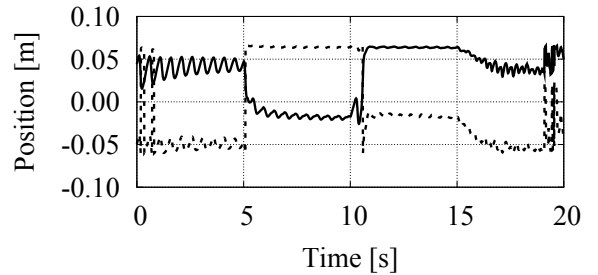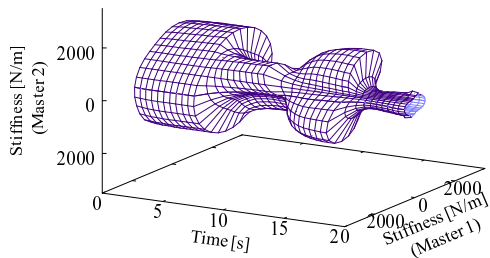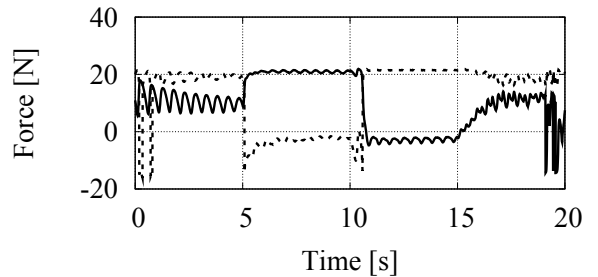
(d) Stiffness of human motion.

Fig. 6-20: Experimental results using robotic operator and estimated stiffness.

(a) Control axis $\hat{\theta}_{h}$.

(b) Hybrid angle $\hat{\phi}_{h}$.

(c) Position command $\hat{X}_{h}^{cmd}$.

(d) Force command $\hat{F}_{h}^{cmd}$.

Fig. 6-21: Basic parameters estimated using robotic operator.

Fig. 6-21 shows the estimation results of the parameters concerning human motion as generated by the robotic operator. The obtained results were quite similar to the simulation results. In steps 2 and 3, the parameters were correctly estimated except for immediately after the shift from step 2 to step 3. In steps 1 and 4, both axes were controlled by the same types of control system. Therefore, the orientations of the axes $\hat{\theta}_h$ could not be estimated—they were indefinite and not very important—and the hybrid angle $\hat{\phi}_h$ was correctly estimated as in the simulation.

Experiment Using Actual Human Motion

In the second experiment, the proposed approach was applied to actual human motion. A human operator added and changed the grasping force from 0 to 10 s and the manipulating force from 10 to 20 s. Fig. 6-22(a) and Fig. 6-22(b) show the human motion extracted by the bilateral control system. From these responses, the environmental stiffness and human stiffness were estimated as shown in Fig. 6-22(c) and Fig. 6-22(d), respectively. These stiffnesses were estimated independently and simultaneously, as in the above-described simulation and experiment.
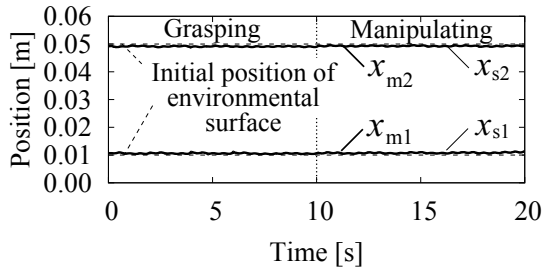
(a) Position response.
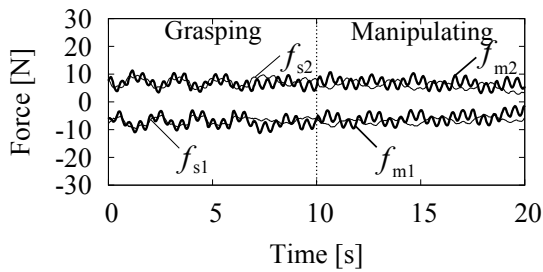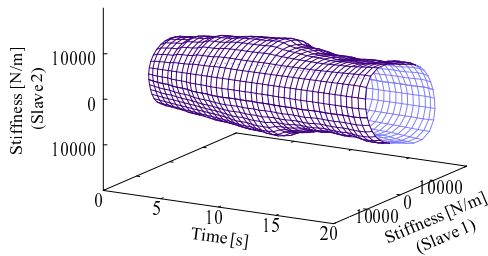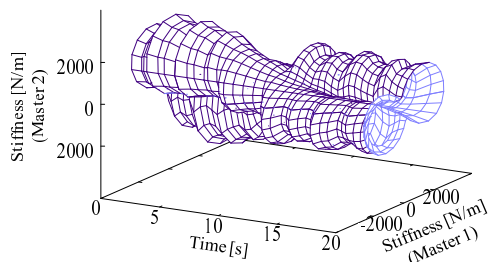
(b) Force response.

(c) Stiffness of environment.

(d) Stiffness of human motion.
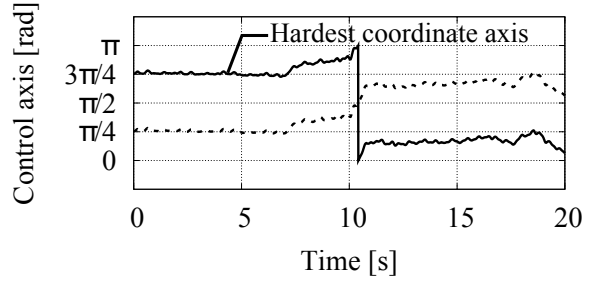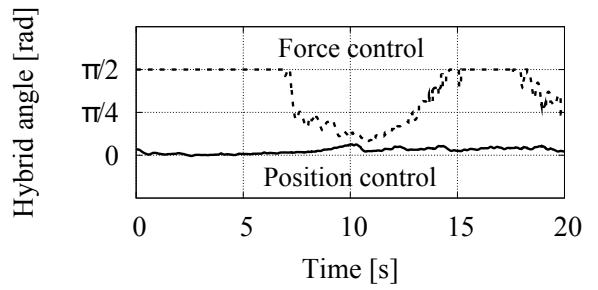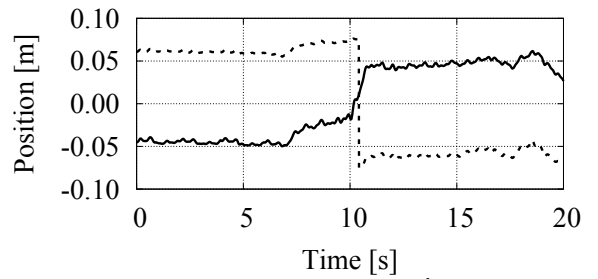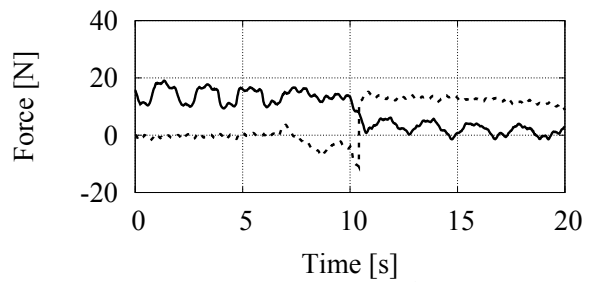
Fig. 6-22: Experimental results for human operator and estimated stiffness.

(a) Control axis $\hat{\theta}_h$.

(b) Hybrid angle $\hat{\phi}_h$.

(c) Position command $\hat{X}_h^{cmd}$.

(d) Force command $\hat{F}_h^{cmd}$.

Fig. 6-23: Estimated basic parameters for experiment by human operator.

Fig. 6-23 shows the estimated parameters. Fig. 6-23(a) shows that the direction of the hardest coordinate axis was shifted from $3\pi/4$ to $\pi/4$ at around 10 s. In the modal space transformed by $\sqrt{2}\boldsymbol{R}_{\mathrm{h}}(3\pi/4)$, the two master robots move in opposite directions. In other words, the axis expressing the grasping motion had the highest stiffness before 10 s had elapsed. Conversely, the transformation by $\sqrt{2}\boldsymbol{R}_{\mathrm{h}}(\pi/4)$ represents the motion in which the two master robots moves in the same direction. The axis expressing the manipulating motion had the highest stiffness after 10 s had elapsed.

Fig. 6-23(d) shows that applied force was changed: in contrast, detection of this change from Fig. 6-22(a) and Fig. 6-22(b) is difficult.

6.4 Summary

The first half of this chapter proposed a novel motion-reproducing system. The system was based on the impedance of a performed motion, which was obtained by using a scaled bilateral control system. For calculating the impedance, DP matching and the least-squares method were utilized. DP matching accommodated the motion speed of the recorded motion data. The derived impedance was input into a compliance control system, where it was reproduced. Three types of experiments that used different target positions were conducted to confirm the validity of the proposed method. In these experiments, the proposed motion-reproducing system succeeded in removing the phantom of a sarcoma, whereas the conventional method either failed to execute a grasping motion or applied excessive force.

In order to extend the proposed method to a multi-DOF system, the followings are required: to process a large amount of data, to select direction to implement the impedance control, and to reduce friction and inertia of the manipulator. Furthermore, if differences of environmental properties between the motion data collection phase and motion data reproduction phase are taken into account, viscosity may have to be changed.

The second half of this chapter aimed to clarify the features of human motions by elementally separating haptic information about human motions. The proposed method used a bilateral control system to extract haptic information and divided the haptic information into basic elements: transformation matrices, hybrid angles, pure position commands, and pure force commands. To validate the proposed method, a simulation and experiment using a robotic and a human operator were conducted. The proposed method successfully clarified the features of human motions despite the fact that recognizing the differences from the original responses extracted through the bilateral control system was difficult.

This study provided mathematical expression of human motion, that contributes toward revealing implicit knowledge. The mathematical expression shows motion features as a combination of the dual variables, control stiffness, and dominant control axes. Furthermore, since these obtained four elements are generally used in the conventional theory of motion control, the human motion can be reproduced from these elements. This approach which is based on the bilateral control has an advantage over the other measurement approaches that use exterior sensors and force sensors, as the slave system itself can be used for the reproduction. The original motion can be certainly reconstructed and improved at the element level before the reproduction. For example, this approach allows us to modify the control stiffness or the grasping force according to the environmental impedance. Therefore, this method is considered

an useful procedure to enhance the dexterity of robots.

In addition, there is another benefit of using the bilateral control system. Since the system can decompose force information into human force and environmental reaction force, independent and simultaneous estimation of the stiffness of the human motion and the environment is possible.

Chapter 7

Artificial Realization of Adaptive Human Manipulation

This chapter proposes a way to artificially realize human motion. As mentioned before, haptic information of human motion can be used for extracting, processing, and analyzing. This chapter reconstructs the human motion by using the haptic information, which is improved by taking the above-mentioned steps.

The first half of this chapter addresses methods to recreate human-like motions involving direct contact with objects in robots. Motion reproduction systems using motion information extracted by bilateral teleoperation have been developed. However, conventional systems lack adaptability to difference in environmental location. The objective of this research is realization of a system, which can accommodate to the difference in environmental location. The proposed method uses position offset and time-scaling techniques. The offset value and the time-scaling ratio vary according to the difference between the extracted and current force information in real-time. The validity of the proposed method is verified by comparative experiments. The proposed method accomplishes to accurate reproduction of the stored motion. This proposed method shows the usefulness especially in duration of the contact state and amplitude of the force.

The objective of the second half of this chapter is reproduction of physical human actions. The information concerning the human actions are extracted by bilateral teleoperation systems using wearable tendon-driven robots. In the bilateral teleoperation systems, modal transformation is applied to achieve three control goals: position tracking, force feedback, and tension control. The extracted information is

provided to the slave robot. To attain the reproduction, a force control scheme is employed. The utility of the proposed method is experimentally verified by applying to a removal operation of a nut.

7.1 Introduction

The first half of this chapter describe a method to reproduce human motion, which has adaptability to difference in environmental location. Industrial robots have been replaced people in menial and repetitive tasks. The industrial robots can execute programmed sequence of motions quickly and tirelessly. This structural change in the labor system has encouraged improvement of productivity. However, the conventional industrial robots are facing two technical challenges. One is facilitation of the instruction procedures conducted by site workers. The other is realization of motions involving direct contact with a target object. Under the expected usage conditions, the site workers do not have sophisticated programming ability, and it takes time to modify the instruction given to the robots. Furthermore, the industrial robots have been mainly used for only welding and painting automation in absence of contact, as position based control has been employed.

One possibility to make the next leap forward is an imitation of human motions. This imitation-based technology is useful for task instruction of robots, since sophisticated programming ability of end-users is not required. The users have only to show target actions or gestures.

This kind of instruction is referred to as "teaching by showing" [132], "assembly plan from observation" [133], "learning from observation" [111], "learning by demonstration" [134], "learning by imitation" [171], and "programming by demonstration" [135–138]. Some of these studies tried to make models of objects and situations, and attempt to find out solutions by integrating components at the symbolic level. In above-mentioned studies, a lot of interesting segmentation strategies and instruction methods have also been proposed. However, it has proven difficult for conventional teaching or observing systems to recognize a motion, which involves direct contact with objects because of the lack of force information. These conventional systems can extract sufficient data concerning angles, positions, and color but they are incapable of acquiring data on the force. Therefore, there is a clear need for a reproduction approach that considers force information.

Although there is a study, which intends to estimate contact force from image data of fingernail coloration [172], its reliability and performance are not enough. While operation system was also introduced to extract grasping skills, the applied field was limited in virtual reality [173]. This operation system al-

lows an operator to control a simulated robotic hand and to grasp only virtual objects. Meanwhile, a motion-reproducing system has also been proposed [1]. This system reproduces human actions on the basis of data extracted through bilateral control systems. In addition, a integration method that couples several sets of haptic data stored in a motion data memory has also been proposed [70, 174]. These aforementioned motion-reproducing systems contain force controllers to take force information into account. However, these are deficient in environmental adaptability, since the mechanical impedance, which is called control stiffness, is positive constant in the reproduction phase. The conventional motion-reproducing systems are sensitive to deference in the environmental location [2]. For example, the end effectors may not make contact with the target objects if the objects are located in the far compared to its position in the saving phase. Another example of this inadaptability is that excessive force may be applied to the target objects if the objects are located in the nearer than its supposed location. To compensate adapt to the difference in environmental location, a method adjusting the position offset depending on the force error of the reproduction phase has been proposed [155]. However, the adjustment of the position offset takes time and results in a reduction in the contact time.

The objective of the first half of this chapter is development of motion reproduction system adapting to the difference in the environmental location. The proposed system introduces a time-scaling technique [175, 176]. The time-scaling ratio is determined by comparing the recorded force information with the current force response, and is always updated. It becomes possible to reproduce the saved motion accurately by reflecting the differences in the force information.

In the second half of this chapter, the subject is moved on to the reproduction of physical human actions. Artificial reproduction of the human action is confirmed with actual removal operation of a nut.

Humans have amazing dexterity to accomplish a wide variety of tasks. In future, robots are expected to have this dexterity to support human life as a physical agent. The main topic of this research is how to reproduce human actions with this dexterity.

To understand human actions, a motion-capture technology has been widely used. Under the expected usage conditions in our daily life, the end-users do not have sophisticated programming ability. Therefore, this technology is useful for task instruction of robots, as sophisticated programming ability of end-users is not required in this method. All end-users need to do is showing target actions or gestures. This kind of instruction is called as "teaching by showing" [132], "assembly-plan-from-observation" [133], "learning from observation" [111], "learning by demonstration" [134], "learning by imitation" [171], or "programming by demonstration" [135–138]. Some of these studies adopted an approach to make

models of objects and situations. In symbolic level, the modeled components of the objects and the situations were treated to find out solutions. In above-mentioned studies, a lot of interesting segmentation strategies and instruction methods have also been proposed. However, the conventional observing-based instruction systems are incapable to recognize a motion that involves direct contact with objects because of the lack of force information. These observing-based systems are incapable of acquiring data on the force, while they can extract sufficient data of angles, positions, and color. Therefore, there is a clear need for a new reproduction approach that considers force information.

Although there was a study to estimate contact force from image data of fingernail coloration, its reliability and performance are not enough [172]. In another study, an operation system of a virtual robot hand was introduced to extract grasping skills. However, the applied field was limited in virtual reality, as this operation system allows an operator to control only a simulated robotic hand and to grasp only virtual objects [173]. Meanwhile, motion-reproducing systems, which realize human actions on the basis of data extracted by bilateral control systems, have also been proposed [1]. In addition, integration methods, that couple several sets of haptic data stored in a motion data memory have also been proposed [70, 174]. These aforementioned motion-reproducing systems employ force controllers, and force information was taken into account. However, these are deficient in environmental adaptability, as the mechanical impedance, which is called control stiffness, is positive constant in the reproduction phase. The conventional motion-reproducing systems are sensitive to deference in the environmental location, size, and shape. For example, end effectors may not make contact with a target object if the object is small compared to its size in the saving phase. Another example of this unadaptability is that excessive force may be applied to the target object if the object is larger than its supposed size.

A method that adjusts the position offset depending on the force error of the reproduction phase has been proposed to compensate for the environmental difference [155]. Another method that involves the substitution of a velocity controller for a position controller has also been presented [2, 177, 178]. Especially, from the view point of adaptability, a force-based reproduction approach demonstrated encouraging results [179]. However, reproduction of human actions could not be achieved, as the robots used in the previous studies had low degree-of-freedom (DOF). Furthermore, verification by specific tasks has not been performed.
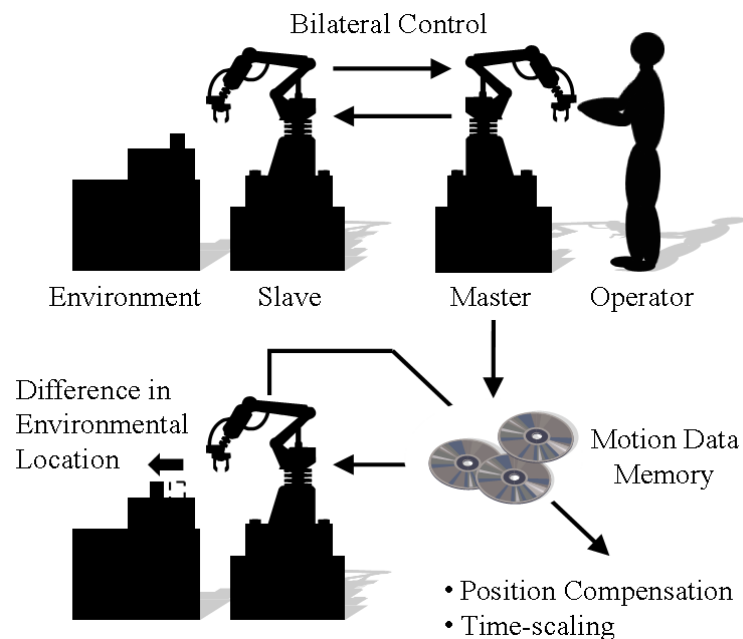
Fig. 7-1: Outline of proposed system.

Fig. 7-1 shows the research overview. Specific procedures are as follows. Firstly, human motions are extracted as position and force information through the bilateral teleoperation system. Secondly, the extracted information is stored in the motion data memory and input into the slave system. Finally, the slave system automatically reproduces the stored motion and adapt to the difference in the environmental location by changing the position offset and the time-scaling ratio in real-time. To verify the validity of the proposed method, following four kinds of method are experimentally compared.

- Motion-reproducing system with virtual master robot: extracted motion information is treated as a virtual master robot [1].

- Motion-reproducing system with velocity regulator: velocity regulator is used instead of position regulator [2].

- Motion-reproducing system with position compensation: compensation value is added to the extracted position information [155].

- Proposed method: this method uses position offset and time-scaling techniques.

The second half of this chapter presents an approach to reproduce human actions using a multi-DOF wearable master-slave robot hand with tendon-driven mechanisms. Fig. 7-2 shows the outline of this
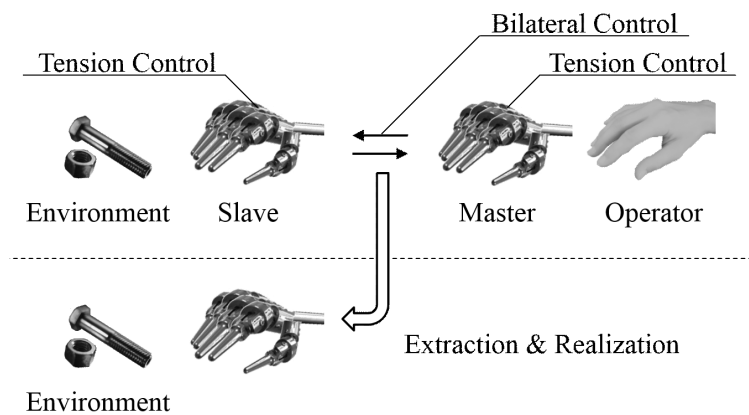
Fig. 7-2: Outline of this approach.

approach. An operator wears the robot hand to manipulate real-world objects through a bilateral control system. An information concerning human actions is extracted through the bilateral teleoperation. In this study, the operator conducts a removal operation of a nut. The extracted information of the physical human actions is used in a reproduction phase, and human actions are realized on the basis of a force control scheme. The utility of the proposed method is experimentally verified.

This chapter is organized as follows. The first half of this chapter proposes a method of reproduction using a time-scaling technique. Section 7.2.1 shows the bilateral teleoperation system for motion extraction. Section 7.2.2 presents the conventional method with position compensation. Section 7.2.3 describes the proposed method with time-scaling. The experimental results are presented in Section 7.2.4. The second half of this chapter proposes a method to artificially realize human motion with high adaptability. Section 7.3.1 presents the wearable master-slave robot hand used for the action extraction. Section 7.3.2 describes the control system. The experimental results are shown in section 7.3.3. This chapter is finally concluded in section 7.4.
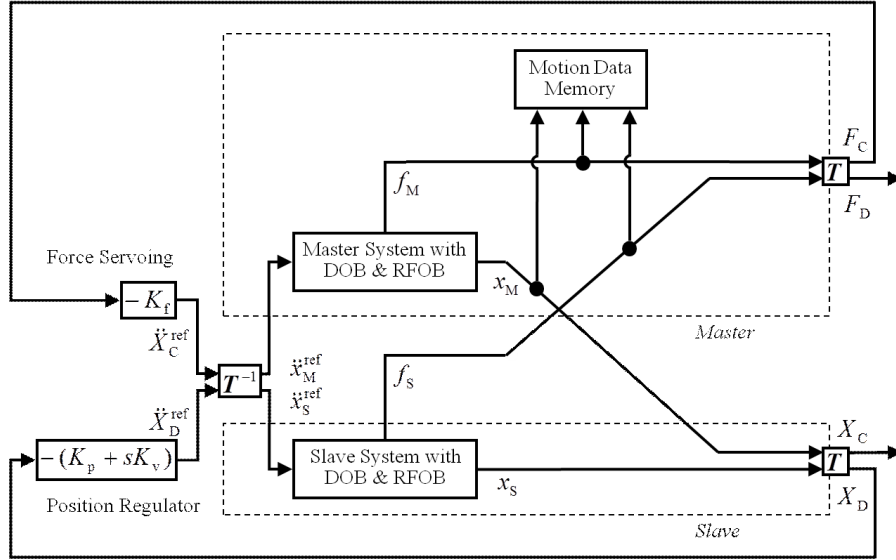
Fig. 7-3: Signal-flow diagram of bilateral control system.

7.2 Time-Scaled Reconstruction

7.2.1 Motion Extraction

This section describes an acceleration-based bilateral control system [53, 54, 74, 163] which is used for motion extraction. The system configuration is determined in accordance with the conventional motion-reproducing method [1, 70]. Control goals are position tracking and force feedback, which are expressed as

$$x_{\mathrm{M}} - x_{\mathrm{S}} \;=\; 0, \tag{7.1}$$

$$f_{\mathrm{M}} + f_{\mathrm{S}} \;=\; 0, \tag{7.2}$$

where the $\boldsymbol{f}$, the $\boldsymbol{x}$, the subscript "M", and the subscript "S" denote the force, the position, the variables of the master system, and the variables of the slave system, respectively. Fig. 7-3 shows a signal-flow diagram of the bilateral control system. $\boldsymbol{T}$ is a matrix, which is described as

$$\boldsymbol{T} = \begin{bmatrix} 1 & -1 \\ 1 & 1 \end{bmatrix}. \tag{7.3}$$

The matrix transforms the responses of the robots into two modes. One is differential mode, which is expressed by the subscript "D", and used for the position tracking. The other is common mode, which is

expressed by the subscript "C", and used for the force feedback. The calculation of the transformation is

$$
\begin{bmatrix} F_{\mathrm{D}} \\ F_{\mathrm{C}} \end{bmatrix} = \boldsymbol{T} \begin{bmatrix} f_{\mathrm{M}} \\ f_{\mathrm{S}} \end{bmatrix},
\tag{7.4}
$$

$$
\begin{bmatrix} X_{\mathrm{D}} \\ X_{\mathrm{C}} \end{bmatrix} = \boldsymbol{T} \begin{bmatrix} x_{\mathrm{M}} \\ x_{\mathrm{S}} \end{bmatrix}.
\tag{7.5}
$$

The capital letters show the transformed variables. Position encoders are implemented on both master and slave systems. Each system employs disturbance observers (DOB) [29], as such systems offer nearly sufficient robustness, transparency, and stability for practical use [167, 180, 181]. Reaction force observers (RFOB) [33] are also utilized to estimate the force applied to the systems. Here, in accordance with the conventional methods, this chapter assumes that a proportional-derivative controller and a proportional controller are used as the position controller and the force controller, respectively. Hereinafter, K_{p}, K_{v}, and K_{f} stand for the position feedback gain, the velocity feedback gain, and the force feedback gain. The control references in the modal space are obtained as

$$
s^2 X_{\mathrm{D}}^{\mathrm{ref}}(s) = -(K_{\mathrm{p}} + sK_{\mathrm{v}})X_{\mathrm{D}}(s),
\tag{7.6}
$$

$$
s^2 X_{\mathrm{C}}^{\mathrm{ref}}(s) = -K_{\mathrm{f}}F_{\mathrm{C}}(s),
\tag{7.7}
$$

where the superscript "ref" denotes the control reference. The force references in the actuator space are given as

$$
\begin{bmatrix} \ddot{x}_{\mathrm{M}}^{\mathrm{ref}} \\ \ddot{x}_{\mathrm{S}}^{\mathrm{ref}} \end{bmatrix} = \boldsymbol{T}^{-1} \begin{bmatrix} \ddot{X}_{\mathrm{D}}^{\mathrm{ref}} \\ \ddot{X}_{\mathrm{C}}^{\mathrm{ref}} \end{bmatrix}.
\tag{7.8}
$$

Through the bilateral teleoperation system, the operators can touch the environment including the target object. During the teleoperation, the motion data memory stores the responses of f_{M}, f_{S}, and x_{M}.
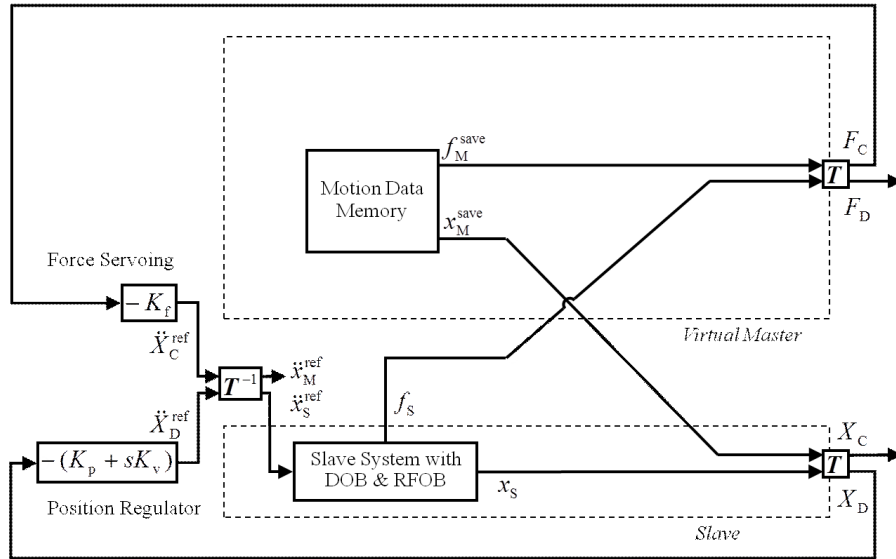
Fig. 7-4: Signal-flow diagram of motion-reproducing system proposed in [1].

7.2.2   Conventional Method to Reproduce Human Motion

Motion Reproduction with Virtual Master Robot

Fig. 7-4 shows a method proposed in [1]. In this method, the extracted motion information is treated as a virtual master system and used as command of the slave system. Hence, the variables in the modal space are calculated as

$$
\begin{bmatrix} F_{\mathrm{D}} \\ F_{\mathrm{C}} \end{bmatrix} = \boldsymbol{T} \begin{bmatrix} f_{\mathrm{M}}^{\mathrm{save}} \\ f_{\mathrm{S}} \end{bmatrix},
\tag{7.9}
$$

$$
\begin{bmatrix} X_{\mathrm{D}} \\ X_{\mathrm{C}} \end{bmatrix} = \boldsymbol{T} \begin{bmatrix} x_{\mathrm{M}}^{\mathrm{save}} \\ x_{\mathrm{S}} \end{bmatrix},
\tag{7.10}
$$

where the superscript "save" denotes the saved information in the bilateral teleoperation in advance.
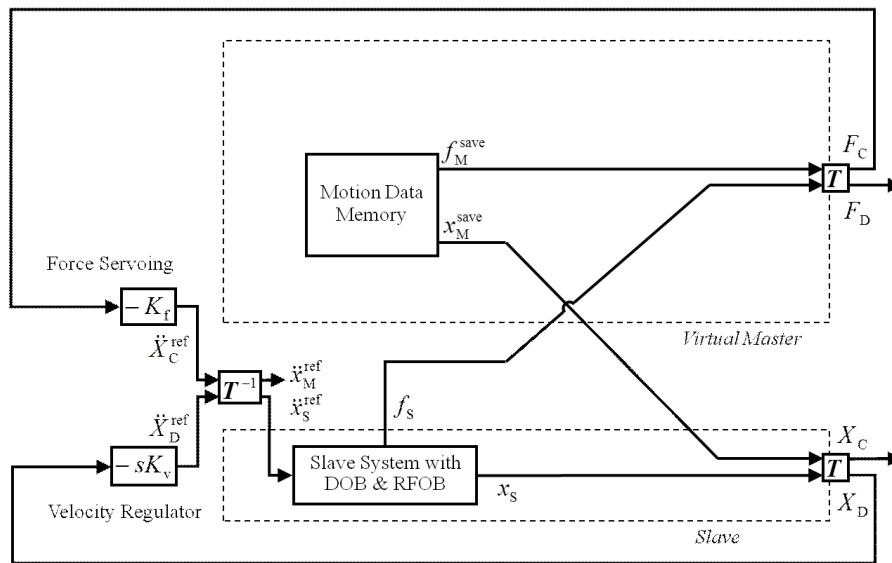
Fig. 7-5: Signal-flow diagram of motion-reproducing system proposed in [2].

Motion Reproduction with Velocity Regulator

Fig. 7-5 shows the signal-flow diagram of a method proposed in [2]. To adapt to the environmental location, the positionfeed back gain is set as zero. Because of this velocity-based structure, the slave system can contact with the environment, even if there is a difference in environmental location.
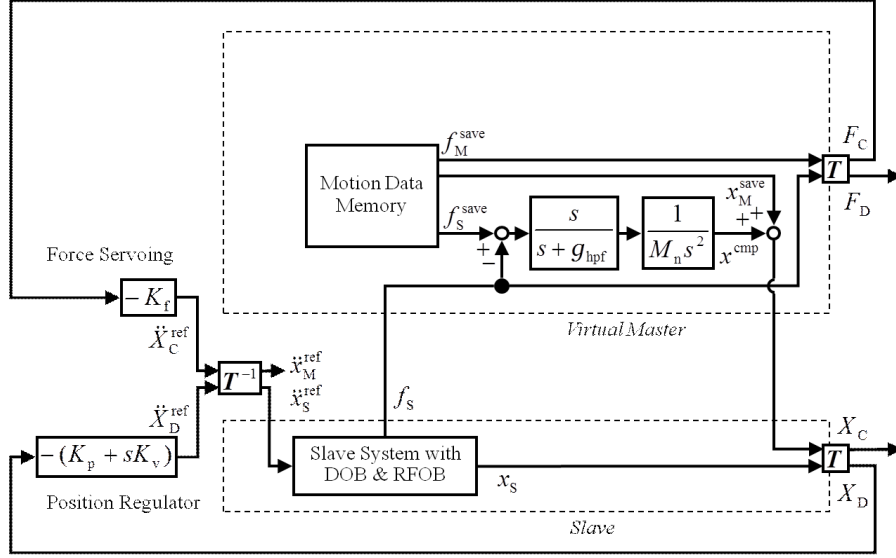
Fig. 7-6: Signal-flow diagram of conventional compensation method.

Motion Reproduction with Position Compensation

Fig. 7-6 shows the signal-flow diagram of the conventional compensation method on the basis of coordinate modification. This approach was proposed in [155]. In the reproduction phase, the saved data of the motions is treated as a virtual master system and used as command of the slave system. In addition, compensation value x^{cmp} is added to the saved position data $x_{\mathrm{M}}^{\mathrm{save}}$ to adapt to the difference in the environmental location. Hence, the variables in the modal space are calculated as

$$
\begin{bmatrix} F_{\mathrm{D}} \\ F_{\mathrm{C}} \end{bmatrix} = \boldsymbol{T} \begin{bmatrix} f_{\mathrm{M}}^{\mathrm{save}} \\ f_{\mathrm{S}} \end{bmatrix}, \tag{7.11}
$$

$$
\begin{bmatrix} X_{\mathrm{D}} \\ X_{\mathrm{C}} \end{bmatrix} = \boldsymbol{T} \begin{bmatrix} x_{\mathrm{M}}^{\mathrm{save}} + x^{\mathrm{cmp}} \\ x_{\mathrm{S}} \end{bmatrix}, \tag{7.12}
$$

The position compensation value is obtained as

$$
x^{\mathrm{cmp}}(s) = \frac{s}{s + g_{\mathrm{hpf}}} \frac{1}{M_{\mathrm{n}}s^2} \big(f_{\mathrm{S}}^{\mathrm{save}}(s) - f_{\mathrm{S}}(s) \big), \tag{7.13}
$$

where the g_{hpf} and the M_{n} denote cutoff frequency of the high pass filter and the nominal inertia [155].
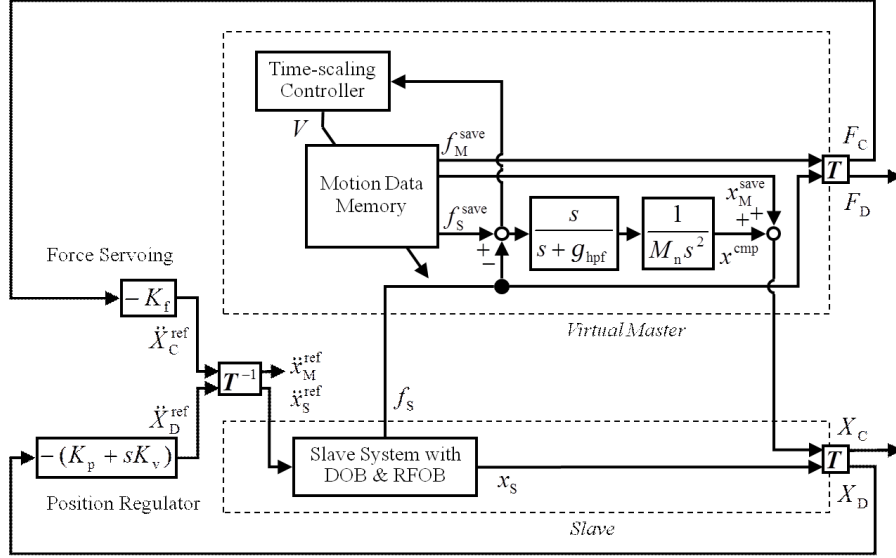
Fig. 7-7: Signal-flow diagram of proposed time-scaling method.

7.2.3 Motion Reproduction with Time-Scaling

In this proposed method, the difference between the saved and current force information is fed back to determine the time-scaling ratio. The time-scaling controller slows down the loading speed of the saved data in the motion data memory when the saved force is weaker than the current response. In contrast, the time-scaling controller makes the loading speed faster when the saved force is stronger than the current response. Fig. 7-7 shows the signal-flow diagram of the proposed time-scaling method. The error signal e, which is input into the time-scaling controller, is calculated as

$$e(s) = \frac{V(s)}{M_\mathrm{n} s} \left(f_\mathrm{S}^\mathrm{save}(s) - f_\mathrm{S}(s) \right). \tag{7.14}$$

When the original sampled data is loaded, the error signal is reflected and reset. The loading speed is set as

$$V = \exp\left(-\frac{e}{k}\right), \tag{7.15}$$

where k is the feedback gain for the time-scaling control.

A linearly-interpolation process and a thinning out process are used in this chapter, although any other signal processes can be applicable. Fig. 7-8 shows the process of the linearly-interpolation. The vertical axis and the horizontal axis are scale of the saved quantity (i.e. force or position) and data number corresponding to the time, respectively. The black dots are saved data, and the white dots are interpolated
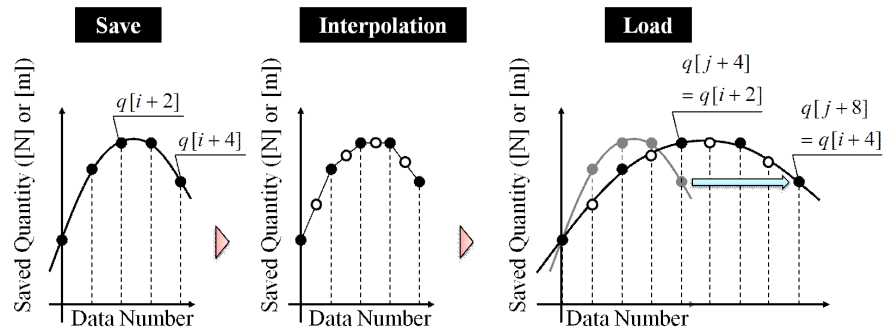
Fig. 7-8: Process of linearly-interpolation for slow loading speed.
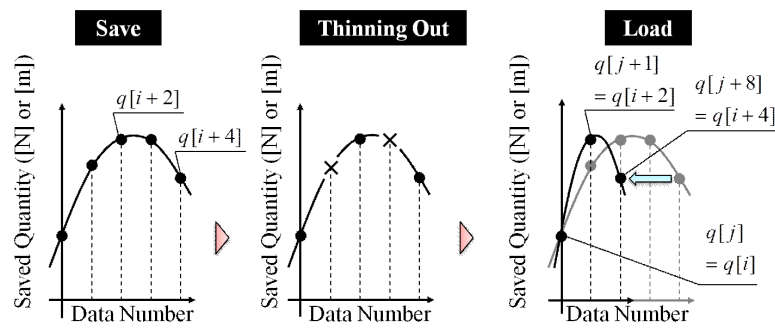
Fig. 7-9: Process of thinning out and skipping for fast loading speed.

data. The i is the data number of the saving phase, and the j is the data number of the loading phase. The linearly-interpolation of the saved data is used to achieve the slow loading speed. For example, if the loading speed is a half after the i th data and the i th data is loaded as j th data, the $i + 2$ th data is loaded as $j + 4$ th data after 4 sampling period. Meanwhile, Fig. 7-9 shows the thinning out and skipping process. The fast loading speed is realized by the thinning out and skipping the saved data. In case of the double speed, the $i + 1$ th data is deleted and the $i + 2$ th data is loaded as $j + 1$ th data after 1 sampling period.

Table 7.1: Parameters used in this chapter.

	Control period	0.1 ms
	Cutoff frequency of DOB	1000 rad/s
	Cutoff frequency of RFOB	1000 rad/s
g_{hpf}	Cutoff frequency of position compensation	1000 rad/s
K_{p}	Position feedback gain	3600 $1/\mathrm{s}^2$
K_{v}	Velocity feedback gain	120 1/s
K_{f}	Force feedback gain	1.6 1/kg
k	Feedback gain for time-scaling	0.0001 $\mathrm{m/s}^2$
M_{n}	Nominal mass of motors	0.5 kg
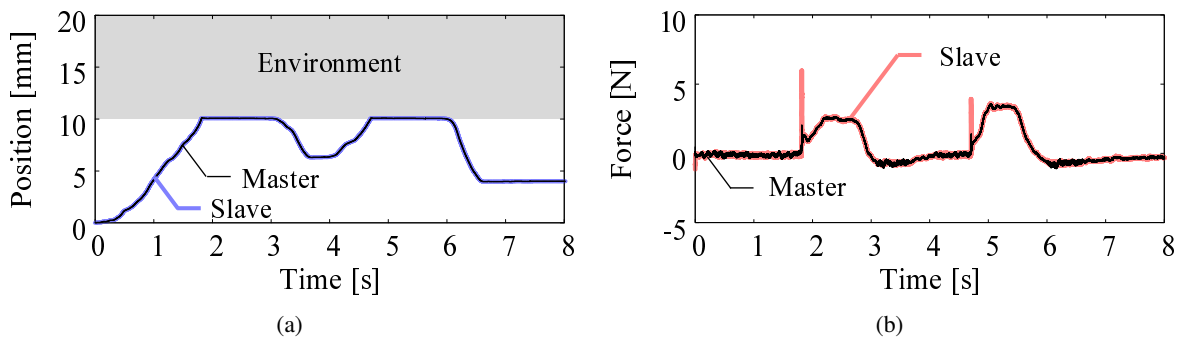
Fig. 7-10: Result of bilateral control. (a) Position response. (b) Force response.

7.2.4 Experiments

To verify the validity of the proposal, three types of experiments were conducted as follows:

- Bilateral control for motion extraction,

- Reproduction without difference in environmental location,

- Reproduction with difference in environmental location.

Table 7.1 lists the parameters used in these experiments.

Bilateral Control for Motion Extraction

Fig. 7-10 shows the experimental results of the bilateral control. The black line and the light-colored line illustrate the reponses of the master system and the slave system, respectively. Fig. 7-10(a) shows the position response. The environment was located at 10 mm. The slave system made 1.5 s of contact with the environment two times. The control goal of position tracking was achieved as can be seen in this position response. Fig. 7-10(b) shows the force response. For comparison, reversal values of positive and negative are plotted as the force response on the master side. About 3 N was applied to the environment during the contact motion. The control goal of force feedback was also realized as is obvious from this figure. Through this bilateral teleoperation, the human motions were extracted and stored as above-mentioned position and force information.

Reproduction without Difference in Environmental Location

Fig. 7-11 shows the experimental results of the motion reproduction with the virtual master system. The black line presents the motion reproduced by the slave system, and the light-colored line illustrates the motion of the master system saved in advance. It can be confirmed that the saved motion was precisely reproduced in the case where there is no difference in the environmental location. Fig. 7-12 shows the experimental results of the motion reproduction with the velocity regulator. In Fig. 7-12(a), the reproduced position is different from the saved motion especially in the free motion, although the force is precisely reproduced in Fig. 7-12(b). This position error was caused by disturbance such as friction. Fig. 7-13 shows the experimental results of the motion reproduction with the conventional compensation method. The light-colored line in Fig. 7-13 is same as the black line in Fig. 7-10. Fig. 7-13(a) and Fig. 7-13(b) are the position response and the force response, respectively. Similarly, Fig. 7-14 shows the experimental results of the motion reproduction with the proposed time-scaling method. Fig. 7-14(a) and Fig. 7-14(b) are the position response and the force response, respectively. In both cases, the environment was located on the same position as the motion extraction phase. As these figures show, both position and force of the saved motion were accurately reproduced.
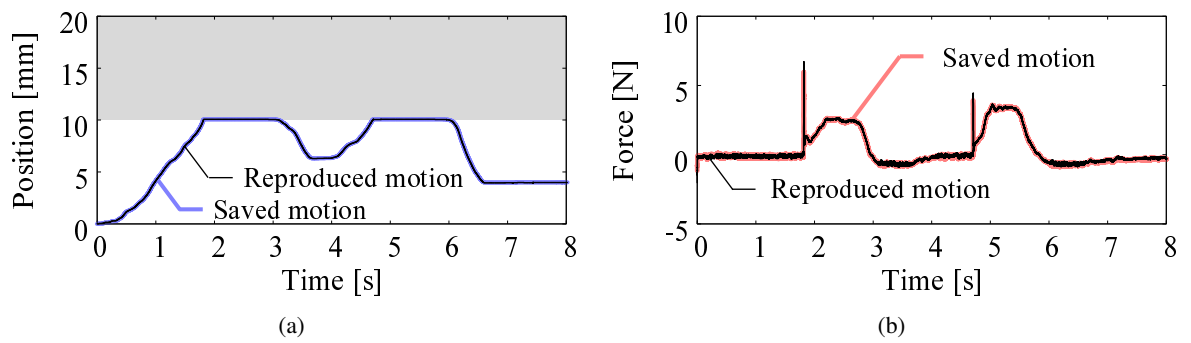
Fig. 7-11: Reproduction using [1] without difference in environmental location. (a) Position response. (b) Force response.
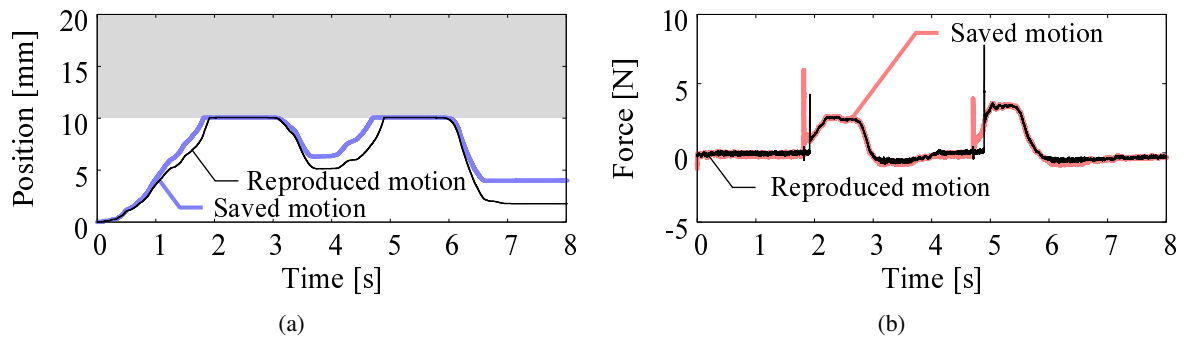
Fig. 7-12: Reproduction using [2] without difference in environmental location. (a) Position response. (b) Force response.
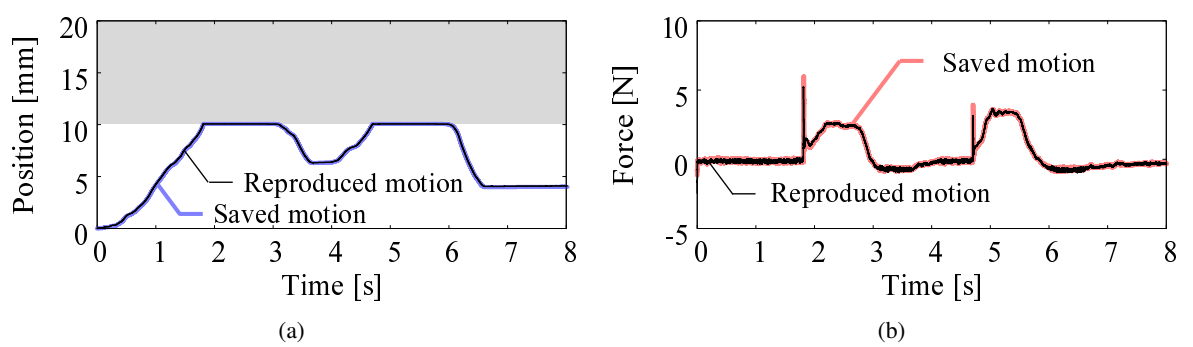
Fig. 7-13: Reproduction by conventional compensation method. (a) Position response. (b) Force response.
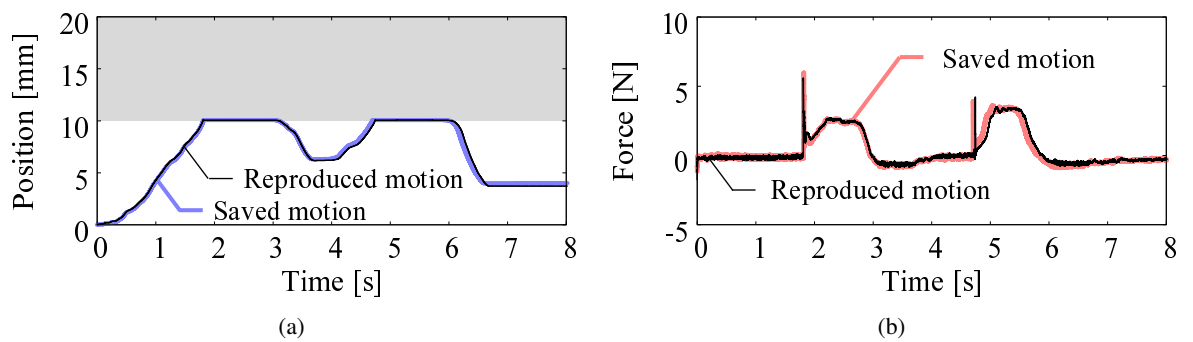
Fig. 7-14: Reproduction by proposed time-scaling method. (a) Position response. (b) Force response.

Reproduction with Difference in Environmental Location

Fig. 7-15, Fig. 7-16, Fig. 7-17, and Fig. 7-18 also show the experimental results of the motion repro-duction. In thess cases, however, the environment was located 5 mm far from its position in the saving phase.

Fig. 7-15 shows the position response of the method of virtual master. The black line and light-colored line present the reproduced motion and the saved motion, respectively. As can be seen in this figure, the reproduced motion could not make a contact with the environment. The reason is that the control stiffness generated by the position controller is positive constant in reproduction phase.

Fig. 7-16 shows the results of the velocity-based approach. In this approach, the control stiffness is almost zero, as the velocity regulator is used instead of the position controller. Because of this structure, the slave system succeeded to contact with the environment. However, as can be seen in Fig. 7-16(a), the position differed from the saved motion even if there is no difference in environmental location.

Fig. 7-17 presents the results of the motion reproduction with position compensation. Fig. 7-17(a) is the position response of the conventional compensation method. The black line presents the motion reproduced by the slave system. The light-colored line starting from 0 mm illustrates the saved motion. The light-colored line starting from 5 mm shows the saved motion 5 mm shifted in a direction toward the environment. As can be seen in this figure, the slave system approached from 2.0 s to 2.6 s and succeeded to contact the environment from 2.6 s to 3.0 s. However, the duration of contact was decreased, as it takes time to reach a contact state. Fig. 7-17(b) suggests that substantial margin of error was caused in the first contact.

Fig. 7-18 shows the results of the proposal. Fig. 7-18(a) shows the position response of the proposed time-scaling method. The black line presents the motion reproduced by the slave system. The light-colored line starting from 0 mm illustrates the original saved motion. The light-colored line starting from 5 mm and 1 s shows the saved motion 5 mm shifted in a direction toward the environment and 1 s shifted in a positive direction of the time axis. Note that, this shifted information is shown only for the comparison and did not used in this experiment. As in the case of the conventional method shown in Fig. 7-17, the slave system adaptively approached to the environment. In contrast, unlike in the case of the conventional method, the proposed time-scaling method provided adequate duration of contact. Fig. 7-18(b) shows the force response of the proposed time-scaling method. the black line presents the motion reproduced by the slave system. The light-colored line starting from 0 s illustrates the original
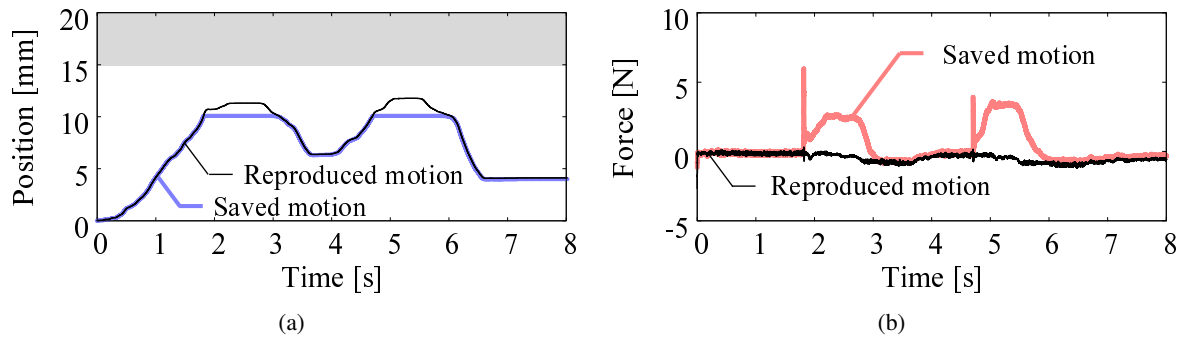
Fig. 7-15: Reproduction using [1] with difference in environmental location. (a) Position response. (b) Force response.
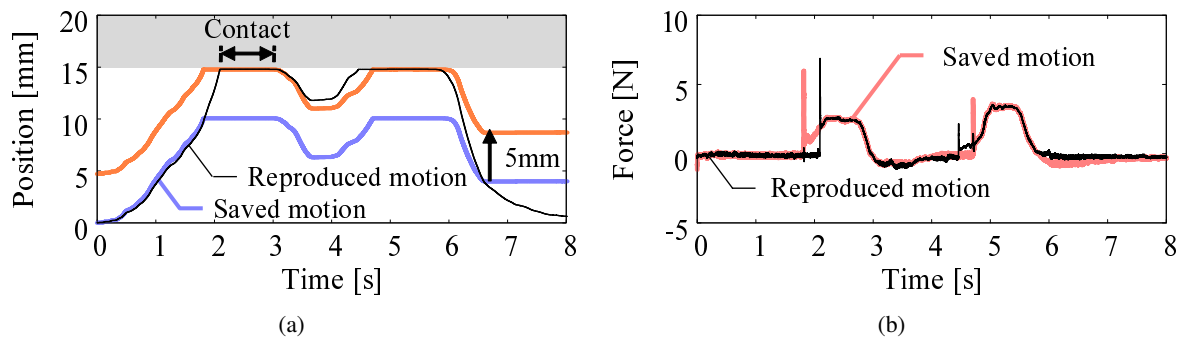
Fig. 7-16: Reproduction using [2] with difference in environmental location. (a) Position response. (b) Force response.

saved motion. The light-colored line starting from 1 s shows the saved motion 1 s shifted in a positive direction of the time axis. Although the starting time of the contact state was different from the stored motion as a matter of course, the duration of contact state and the amplitude of the force were accurately reproduced.

(a)   (b)
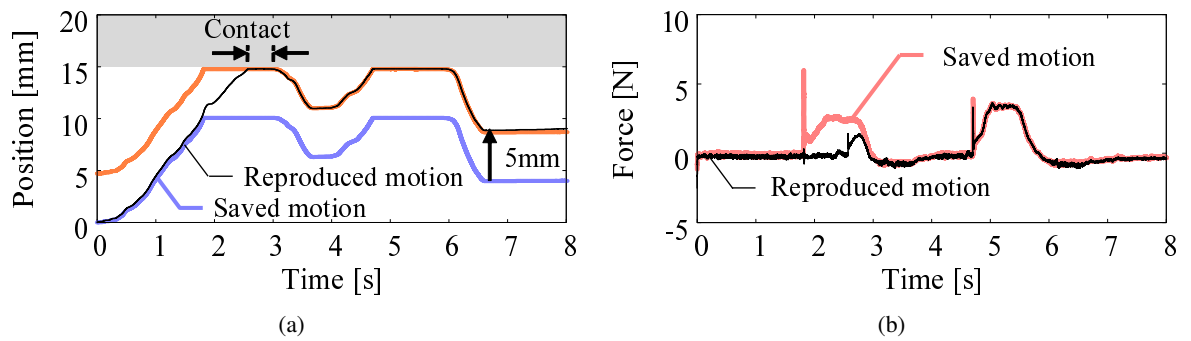
Fig. 7-17: Reproduction by conventional compensation method with difference in environmental loca-
tion. (a) Position response (b) Force response.

(a)   (b)
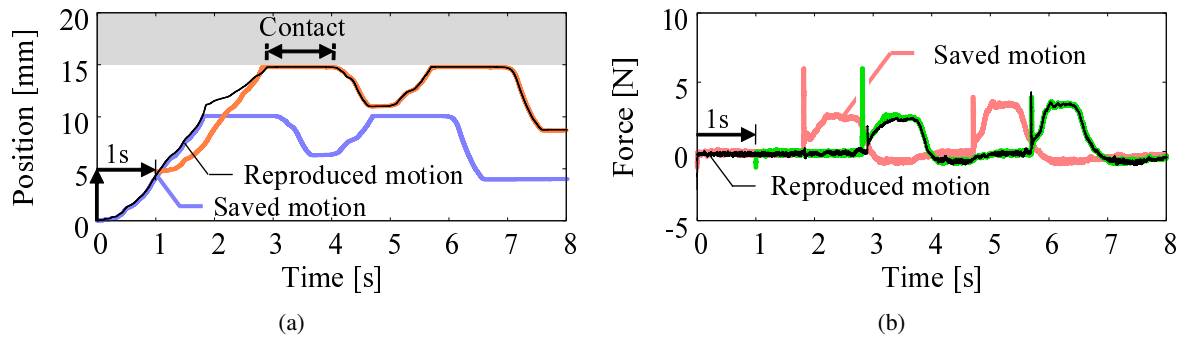
Fig. 7-18: Reproduction by proposed time-scaling method with difference in environmental location. (a)
Position response (b) Force response.
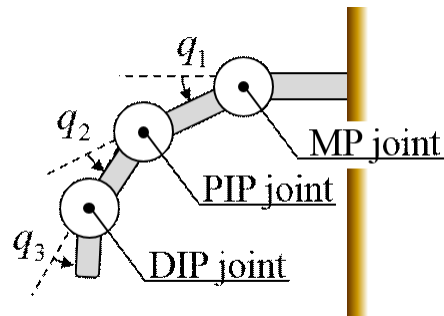
Fig. 7-19: Structure of finger.
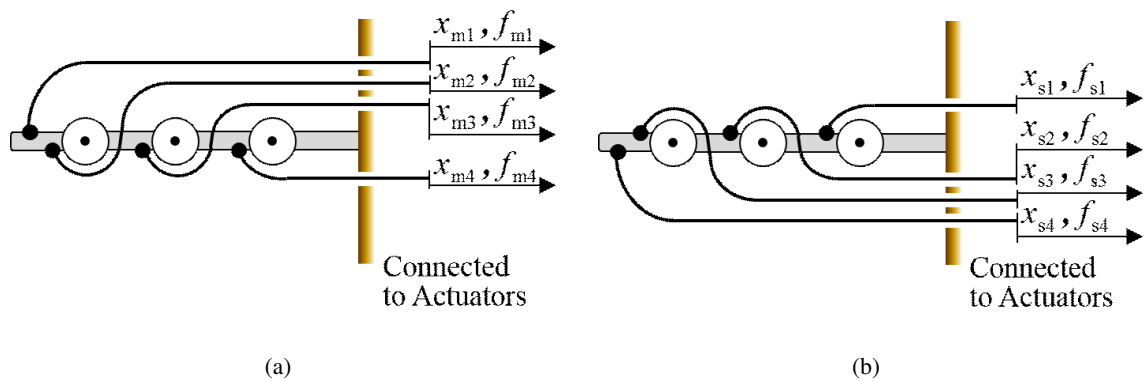
Fig. 7-20: Overview of robot hand. (a) wire arrangement of master hand. (b) wire arrangement of slave hand.

7.3　Force-Based Reconstruction

7.3.1　Robot Hand

To extract information of human action, a wearable master-slave robot hand with tendon-driven mechanisms is used. In general, two types of robots are used in the bilateral control systems: one is a master robot and the other is a slave robot. The master robot is operated by an operator, and the slave robot makes contact with the environment. The operator can feel the actual environmental reaction force through the master robot. Because of this sensation, robots can be made act as a physical agent. Meanwhile, tension control is introduced to keep straining the wire on each side.

Fig. 7-19 shows an overview of the robot hand. The each finger of the master and the slave robot has 3-DOF. The three joints are referred to as "distal interphalangeal: DIP joint", "proximal interphalangeal: PIP joint", and "metacarpophalangeal: MP joint" in the order of location from tip to base. Fig. 7-20

shows the wire arrangement of the index finger, which is used in the experiments. Fig. 7-20(a) and Fig. 7-20(b) show the wire arrangement of the master finger and the slave finger, respectively. In consideration of the direction of the required force, the wires are arranged symmetrically. Four wires are used to rotate the joints, and are connected to actuators. The positive directions of the positions x, the force f, and the angles θ are set as shown in Fig. 7-19 and Fig. 7-20.

7.3.2 Controller Design

In this section, the controller design is described starting from the actuator space. This chapter adopts acceleration-based bilateral controller to achieve haptic transmission [74, 163]. The framework of the disturbance observer (DOB) in the actuator space is also explained [29].

Modeling

Fig. 7-21 shows a block diagram of whole control system. $\boldsymbol{S}$ is a diagonal matrix whose diagonal elements are Laplace operators. The total effects of the disturbance, $\boldsymbol{f}_{\mathrm{dis}}$, in the actuator space are formulated as

$$\boldsymbol{f}_{\mathrm{dis}} = \boldsymbol{f}_{\mathrm{int}} + \boldsymbol{f}_{\mathrm{ext}} + \boldsymbol{D}\dot{\boldsymbol{x}} + \boldsymbol{f}_{\mathrm{c}}$$
$$+ (\boldsymbol{m} - \boldsymbol{m}_{\mathrm{n}})\ddot{\boldsymbol{x}} + (\boldsymbol{K}_{\mathrm{tn}} - \boldsymbol{K}_{\mathrm{t}})\boldsymbol{I}_{\mathrm{a}}^{\mathrm{ref}}, \tag{7.16}$$

where

$\boldsymbol{f}_{\mathrm{int}}$	interactive force vector,
$\boldsymbol{f}_{\mathrm{ext}}$	reaction force vector in force task,
$\boldsymbol{D}$	viscosity coefficient matrix,
$\boldsymbol{x}$	position vector,
$\dot{\boldsymbol{x}}$	velocity vector,
$\ddot{\boldsymbol{x}}$	acceleration vector,
$\boldsymbol{f}_{\mathrm{c}}$	Coulomb friction vector,
$\boldsymbol{m}$	mass matrix,
$\boldsymbol{K}_{\mathrm{t}}$	thrust coefficient matrix,
$\boldsymbol{K}_{\mathrm{tn}}$	nominal torque coefficient matrix,

$$\boldsymbol{I}_{\mathrm{a}} \qquad\qquad \text{torque current vector,}$$

superscript ref   reference value, and

subscript n   nominal values.

The motion equation of the actuators are expressed as

$$\boldsymbol{f}_{\mathrm{dis}} \;=\; \boldsymbol{K}_{\mathrm{tn}}\boldsymbol{I}_{\mathrm{a}} - \boldsymbol{m}_{\mathrm{n}}\ddot{\boldsymbol{x}}, \tag{7.17}$$

where

$$\boldsymbol{K}_{\mathrm{tn}} \;=\; \mathrm{diag}[\, K_{\mathrm{n1}}, K_{\mathrm{n2}}, K_{\mathrm{n3}}, K_{\mathrm{n4}} \,], \tag{7.18}$$

$$\boldsymbol{m}_{\mathrm{n}} \;=\; \mathrm{diag}[\, m_{\mathrm{n1}}, m_{\mathrm{n2}}, m_{\mathrm{n3}}, m_{\mathrm{n4}} \,], \tag{7.19}$$

$$\boldsymbol{f}_{\mathrm{dis}} \;=\; [\, f_{\mathrm{dis1}}, f_{\mathrm{dis2}}, f_{\mathrm{dis3}}, f_{\mathrm{dis4}} \,]^{\mathrm{T}}, \tag{7.20}$$

$$\boldsymbol{I}_{\mathrm{a}} \;=\; [\, I_{\mathrm{a1}}, I_{\mathrm{a2}}, I_{\mathrm{a3}}, I_{\mathrm{a4}} \,]^{\mathrm{T}}, \;\; \text{and} \tag{7.21}$$

$$\boldsymbol{x} \;=\; [\, x_1, x_2, x_3, x_4 \,]^{\mathrm{T}}. \tag{7.22}$$

This equation can stand on both master and slave side.

Observer

This subsection explains the DOB structure. DOB can cancel out the effect of the disturbance and nominalize the system. The motion equation is expressed on the basis of the nominal mass matrix as

$$\boldsymbol{m}_{\mathrm{n}}\ddot{\boldsymbol{x}} \;=\; \boldsymbol{f}_{\mathrm{n}} - \boldsymbol{f}_{\mathrm{dis}}, \tag{7.23}$$

where

$$\boldsymbol{f}_{\mathrm{n}} \;=\; [\, f_{\mathrm{n1}}, f_{\mathrm{n2}}, f_{\mathrm{n3}}, f_{\mathrm{n4}} \,]^{\mathrm{T}}. \tag{7.24}$$

The disturbance force $\boldsymbol{f}_{\mathrm{dis}}$ can be derived as

$$\hat{\boldsymbol{f}}_{\mathrm{dis}} \;=\; \boldsymbol{f}_{\mathrm{n}} - \boldsymbol{m}_{\mathrm{n}}\ddot{\boldsymbol{x}}, \tag{7.25}$$
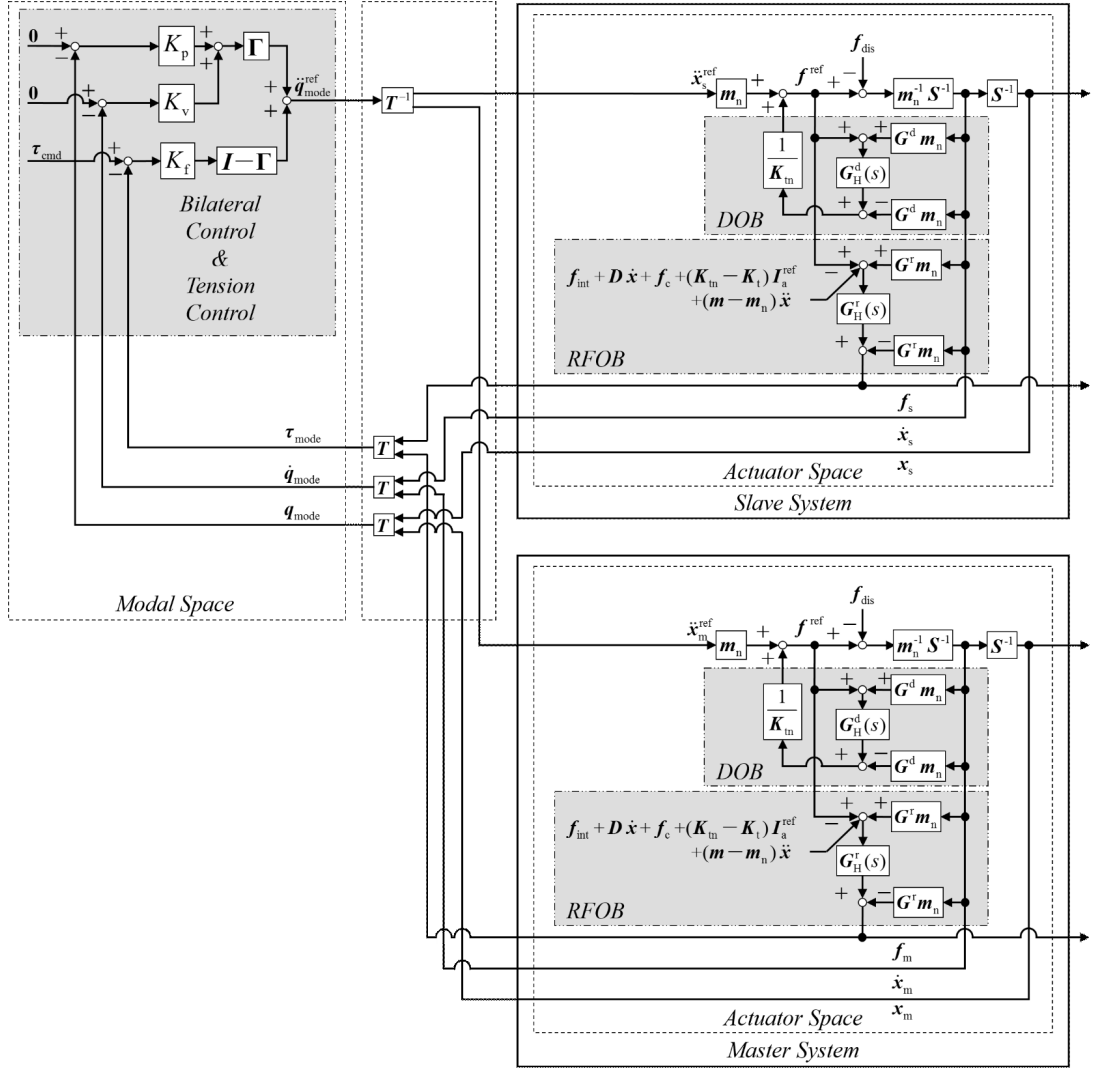
Fig. 7-21: Block diagram of whole control system.

where "$\wedge$" denotes the estimated value. Direct calculation of the disturbance force is impossible, because these signals suffer from noise effects. Therefore, to reduce the effects of noises, a low-pass filter is inserted. The disturbance force is estimated as

$$\hat{\boldsymbol{f}}_{\mathrm{dis}}(s) \;\; = \;\; \boldsymbol{G}_{\mathrm{H}}^{\mathrm{d}}(s)\left\{\boldsymbol{f}_{\mathrm{n}}(s) + \boldsymbol{G}^{\mathrm{d}}\boldsymbol{m}_{\mathrm{n}}s\boldsymbol{x}(s)\right\} - \boldsymbol{G}^{\mathrm{d}}\boldsymbol{m}_{\mathrm{n}}s\boldsymbol{x}(s), \tag{7.26}$$

where

$$\boldsymbol{G}_{\mathrm{H}}^{\mathrm{d}}(s) = \mathrm{diag}\left[\ \frac{g_1}{s+g_1}, \frac{g_2}{s+g_2}, \frac{g_3}{s+g_3}, \frac{g_4}{s+g_4}\ \right] \text{ and} \tag{7.27}$$

$$\boldsymbol{G}^{\mathrm{d}} = \mathrm{diag}\left[\ g_1, g_2, g_3, g_4\ \right]. \tag{7.28}$$

Here, g denotes the cutoff frequency of the low-pass filter in each linear motors pulling the wires. The estimated disturbance force is fed back to suppress the disturbance force. The motion equation with the feedback is expressed as

$$
\begin{aligned}
\boldsymbol{m}_\text{n} s^2 \boldsymbol{x}(s) &= \boldsymbol{f}_\text{n}(s) - \boldsymbol{f}_\text{dis}(s) \\
&= \boldsymbol{f}^\text{ref}(s) - \boldsymbol{G}_\text{S}^\text{d}(s) \boldsymbol{f}_\text{dis}(s) \approx \boldsymbol{f}^\text{ref}(s), \\
&\quad \left(\boldsymbol{f}_\text{n}(s) = \boldsymbol{f}^\text{ref}(s) + \hat{\boldsymbol{f}}_\text{dis}(s) \right)
\end{aligned}
\tag{7.29}
$$

where

$$
\boldsymbol{G}_\text{S}^\text{d}(s) = \text{diag} \left[\frac{s}{s + g_1}, \frac{s}{s + g_2}, \frac{s}{s + g_3}, \frac{s}{s + g_4} \right].
\tag{7.30}
$$

If a sufficiently large cutoff frequency, g, is selected to make $\boldsymbol{G}_\text{S}^\text{d}(s)$ negligibly small, the disturbance force has little effect on the nominal system.

The external force was observed by reaction force observer (RFOB) without using any force sensors [33]. RFOBs are widely used in previous research. While it requires precise identification of disturbance other than environmental reaction force such as gravity force and friction force, RFOB is employed, as it has an advantages of cost, and the cutoff frequency is higher than force sensors.

Modal Transformation

On the master side, the relationship between the actuator space and the joint space is represented as

$$
\begin{aligned}
\boldsymbol{x}_\text{m} &= \boldsymbol{J}_\text{m} \boldsymbol{q}_\text{m}, \\
\boldsymbol{f}_\text{m} &= (\boldsymbol{J}_\text{m}^\text{T})^+ \boldsymbol{\tau}_\text{m},
\end{aligned}
\tag{7.31} \tag{7.32}
$$

where the $\boldsymbol{q}$ denotes the joint angle vector, which is represented as

$$
\boldsymbol{q}_\text{m} = \begin{bmatrix} q_\text{m1} & q_\text{m2} & q_\text{m3} \end{bmatrix}^\text{T},
\tag{7.33}
$$

and, in case of Fig. 7-20,

$$
\boldsymbol{J}_\text{m} = r \begin{bmatrix} 1 & 1 & 1 \\ 1 & 1 & -1 \\ 1 & -1 & 0 \\ -1 & 0 & 0 \end{bmatrix}.
\tag{7.34}
$$

The "+" and the r denote the Moore-Penrose pseudoinverse and the radius of the joint pulleys. The relationship of the velocity and the acceleration are derived as

$$\dot{\boldsymbol{x}}_{\mathrm{m}} \;=\; \frac{\mathrm{d}}{\mathrm{d}t}\left(\boldsymbol{J}_{\mathrm{m}}\boldsymbol{q}_{\mathrm{m}}\right) = \boldsymbol{J}_{\mathrm{m}}\dot{\boldsymbol{q}}, \tag{7.35}$$

$$\ddot{\boldsymbol{x}}_{\mathrm{m}} \;=\; \frac{\mathrm{d}}{\mathrm{d}t}\left(\boldsymbol{J}_{\mathrm{m}}\dot{\boldsymbol{q}}_{\mathrm{m}}\right) = \boldsymbol{J}_{\mathrm{m}}\ddot{\boldsymbol{q}}, \tag{7.36}$$

since $\boldsymbol{J}_{\mathrm{m}}$ is not a function of the position. Similarly, the relationship between the actuator space and the joint space on the slave side is expressed as

$$\boldsymbol{x}_{\mathrm{s}} \;=\; \boldsymbol{J}_{\mathrm{s}}\boldsymbol{q}_{\mathrm{s}}, \tag{7.37}$$

$$\boldsymbol{f}_{\mathrm{s}} \;=\; (\boldsymbol{J}_{\mathrm{s}}^{\mathrm{T}})^{+}\boldsymbol{\tau}_{\mathrm{s}}, \tag{7.38}$$

where

$$\boldsymbol{J}_{\mathrm{s}} \;=\; r\begin{bmatrix} 1 & 0 & 0 \\ -1 & 1 & 0 \\ -1 & -1 & 1 \\ -1 & -1 & -1 \end{bmatrix}. \tag{7.39}$$

To utilize the null space, $\boldsymbol{N}_{\mathrm{m}}$ and $\boldsymbol{N}_{\mathrm{m}}$ are introduced, which satisfies

$$\boldsymbol{N}_{\mathrm{m}}\boldsymbol{J}_{\mathrm{m}} \;=\; 0, \tag{7.40}$$

$$\boldsymbol{N}_{\mathrm{s}}\boldsymbol{J}_{\mathrm{s}} \;=\; 0. \tag{7.41}$$

In this study, the null space is used to achieve tension control. By using the null space, the wire tension is kept without affecting to the joint motion. The $\boldsymbol{N}_{\mathrm{m}}$ and the $\boldsymbol{N}_{\mathrm{m}}$ are obtained by

$$\boldsymbol{N}_{\mathrm{m}} \;=\; \boldsymbol{\Lambda}_{\mathrm{m}}\left(\boldsymbol{I} - \boldsymbol{J}_{\mathrm{m}}\boldsymbol{J}_{\mathrm{m}}^{+}\right), \tag{7.42}$$

$$\boldsymbol{N}_{\mathrm{s}} \;=\; \boldsymbol{\Lambda}_{\mathrm{s}}\left(\boldsymbol{I} - \boldsymbol{J}_{\mathrm{s}}\boldsymbol{J}_{\mathrm{s}}^{+}\right), \tag{7.43}$$

where the $\boldsymbol{I}$ and the $\boldsymbol{\Lambda}$ denote the unit matrix and the selection matrix, respectively.

Bilateral Control in Modal Space

In this study, an acceleration-based bilateral control system [65] is used to extract human actions. The main aim of the bilateral control system is transmission of the mechanical impedance of the environment. This aim can be achieved by two types of elements: one is angle tracking between the master robot and the slave robot, and the other is torque feedback (realization of the law of action and reaction). The control goals are expressed as

- Angle tracking

$$\boldsymbol{q}_{\mathrm{m}} \quad = \quad \boldsymbol{q}_{\mathrm{s}}, \tag{7.44}$$

- Torque feedback

$$\boldsymbol{\tau}_{\mathrm{m}} \quad = \quad -\boldsymbol{\tau}_{\mathrm{s}}. \tag{7.45}$$

Therefore, a modal transformation matrix is determined as

$$\boldsymbol{T} = \begin{bmatrix} \boldsymbol{J}_{\mathrm{m}}^{+} & -\boldsymbol{J}_{\mathrm{s}}^{+} \\ \boldsymbol{J}_{\mathrm{m}}^{\mathrm{T}} & \boldsymbol{J}_{\mathrm{s}}^{\mathrm{T}} \\ \boldsymbol{N}_{\mathrm{m}} & 0 \\ 0 & \boldsymbol{N}_{\mathrm{s}} \end{bmatrix} \tag{7.46}$$

$$= \begin{bmatrix} \frac{2}{11r} & \frac{2}{11r} & \frac{4}{11r} & -\frac{3}{11r} & -\frac{3}{11r} & \frac{4}{11r} & \frac{2}{11r} & \frac{2}{11r} \\ \frac{3}{11r} & \frac{3}{11r} & -\frac{5}{11r} & \frac{1}{11r} & \frac{1}{11r} & -\frac{5}{11r} & \frac{3}{11r} & \frac{3}{11r} \\ \frac{1}{2r} & -\frac{1}{2r} & 0 & 0 & 0 & 0 & -\frac{1}{2r} & \frac{1}{2r} \\ r & r & r & -r & r & -r & -r & -r \\ r & r & -r & 0 & 0 & r & -r & -r \\ r & -r & 0 & 0 & 0 & 0 & r & -r \\ r & r & 2r & 4r & 0 & 0 & 0 & 0 \\ 0 & 0 & 0 & 0 & 4r & 2r & r & r \end{bmatrix}. \tag{7.47}$$

To achieve these control goals, the variables are transformed into the modal space. The transformation is expressed as

$$\boldsymbol{\tau}_{\mathrm{mode}} \quad = \quad \boldsymbol{T} \begin{bmatrix} \boldsymbol{f}_{\mathrm{m}} & \boldsymbol{f}_{\mathrm{s}} \end{bmatrix}^{\mathrm{T}}, \tag{7.48}$$

$$\boldsymbol{q}_{\mathrm{mode}} \quad = \quad \boldsymbol{T} \begin{bmatrix} \boldsymbol{x}_{\mathrm{m}} & \boldsymbol{x}_{\mathrm{s}} \end{bmatrix}^{\mathrm{T}}, \tag{7.49}$$

$$\dot{\boldsymbol{q}}_{\mathrm{mode}} \quad = \quad \boldsymbol{T} \begin{bmatrix} \dot{\boldsymbol{x}}_{\mathrm{m}} & \dot{\boldsymbol{x}}_{\mathrm{s}} \end{bmatrix}^{\mathrm{T}}. \tag{7.50}$$

Here, the subscripts "mode" denotes the variables of the modal space. The angler acceleration reference in the modal space is calculated as

$$\ddot{\boldsymbol{q}}_{\mathrm{mode}}^{\mathrm{ref}} = -C_{\mathrm{p}}\boldsymbol{\Gamma}\boldsymbol{q}_{\mathrm{mode}} + C_{\mathrm{f}}(\boldsymbol{I} - \boldsymbol{\Gamma})\left(\boldsymbol{\tau}_{\mathrm{cmd}} - \boldsymbol{\tau}_{\mathrm{mode}}\right), \tag{7.51}$$
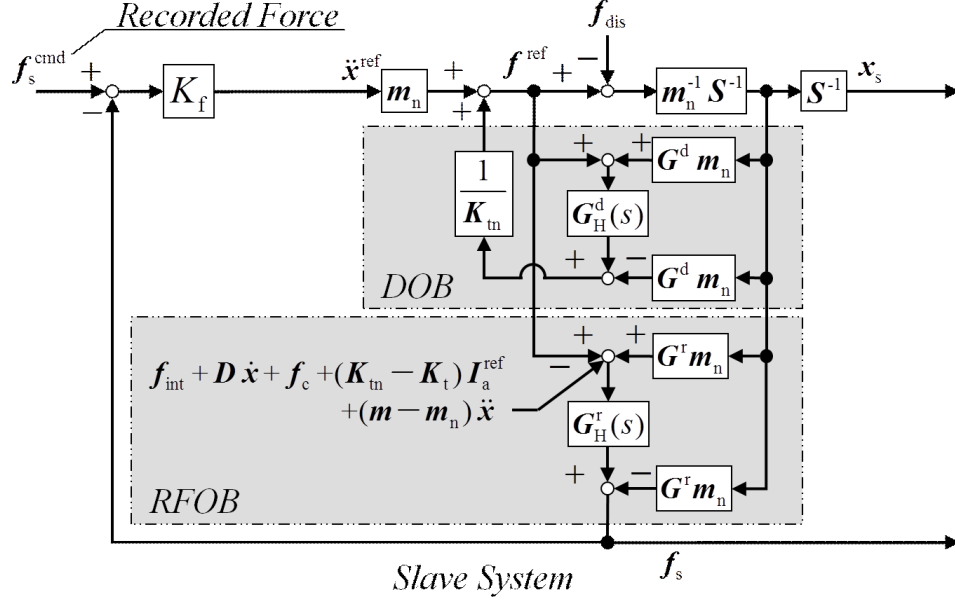
Fig. 7-22: Block diagram of action realization.

where C_p and C_f denote the unit matrix, position controller, and force controller, respectively. The torque command matrix in the modal space τ_{cmd} is expressed as

$$\tau_{cmd} = \begin{bmatrix} 0 & 0 & 0 & 0 & 0 & 0 & \tau_{cmd,m} & \tau_{cmd,s} \end{bmatrix}, \tag{7.52}$$

where $\tau_{cmd,m}$ and $\tau_{cmd,s}$ are the tension commands. Here, Γ is the selection matrix, which is defined as

$$\Gamma = \text{diag} \begin{bmatrix} 1 & 1 & 1 & 0 & 0 & 0 & 0 & 0 \end{bmatrix}. \tag{7.53}$$

By inverse transforming the modal space references

$$\ddot{x}^{ref} = T^{-1}\ddot{q}^{ref}_{mode}, \tag{7.54}$$

the acceleration references in the actuator space are obtained.

Force-based Reproduction of Human Action

Fig. 7-22 shows the block diagram of the force control system used in the realization of the human actions. The acceleration references are calculated as

$$\ddot{x}^{ref} = K_f(f^{cmd}_s - f_s), \tag{7.55}$$

where K_f and f^{cmd}_s denote the force feedback gain and the force command, respectively. The force command is what is extracted from the human actions by using the bilateral control system.

Table 7.3: Parameters used in this chapter.

	Control period	1 ms
	Cutoff frequency of DOB	700 rad/s
	Cutoff frequency of RFOB	700 rad/s
K_{p}	Position feedback gain	3600 $1/\mathrm{s}^2$
K_{v}	Velocity feedback gain	120 1/s
K_{f}	Force feedback gain	0.9
M_{n}	Nominal mass of motors	0.5 kg
$\tau_{\mathrm{cmd,m}}$	Tension command	80 N
$\tau_{\mathrm{cmd,s}}$	Tension command	80 N
$\boldsymbol{\Lambda}_{\mathrm{m}}$	Selection matrix	$\begin{bmatrix} 0\ 0\ 11r\ 0 \end{bmatrix}$
$\boldsymbol{\Lambda}_{\mathrm{s}}$	Selection matrix	$\begin{bmatrix} 0\ 11r\ 0\ 0 \end{bmatrix}$

7.3.3 Experiments

Linear motors were used as the actuators pulling the wires. The resolution of the linear encoders were 0.1 μm. The control software was written in C language under RTAI 3.6.1. Eight stainless steel wires with diameter of 0.27mm were used. Table 7.3 lists the parameters used in the experiments. Fig. 7-23 is a snapshot of the experiments concerning motion extraction. The operator and the master robot are located on the far side. The nut, which is set as environment, and the slave robot are located on the near side. The removal action was extracted and realized in order to show the validity of this approach. The index finger was used, and the removal action to the hexagonal nut (M8) was performed. The hexagonal nut was connected with the rotary encoder. In the removal action, the operator stretched and bended the index finger three times, and the hexagonal nut was rotated to the clockwise direction. The force information was stored during the experiment of the teleoperation. In the realization phase, three kinds of hexagonal nuts were used: M6, M8, and M10. The width across the flats of the nuts the size of M6, M8, and M10 were 10 mm, 13 mm, and 16 mm, respectively. The removal action to the hexagonal nut (M8) was applied to the above-mentioned three kinds of hexagonal nuts to confirm the adaptability and usefulness of this approach.

Fig. 7-24 is a snapshot of the experiments concerning motion reproduction. The slave finger succeeded to make contacts with the nut three times, and the nut was rotated. Fig. 7-25 shows the responses of the encoder connected with the target nuts. The solid line is the angle response of the extraction phase,
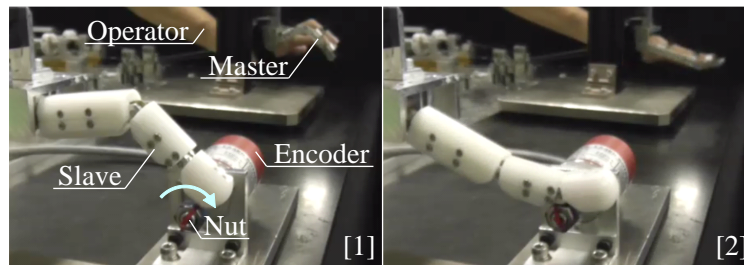
Fig. 7-23: Snapshot of experiments concerning motion extraction.
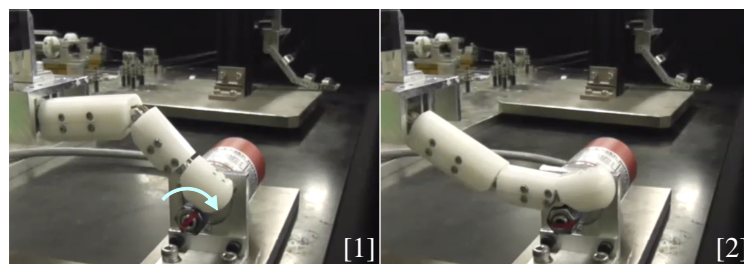
Fig. 7-24: Snapshot of experiments concerning motion reproduction.
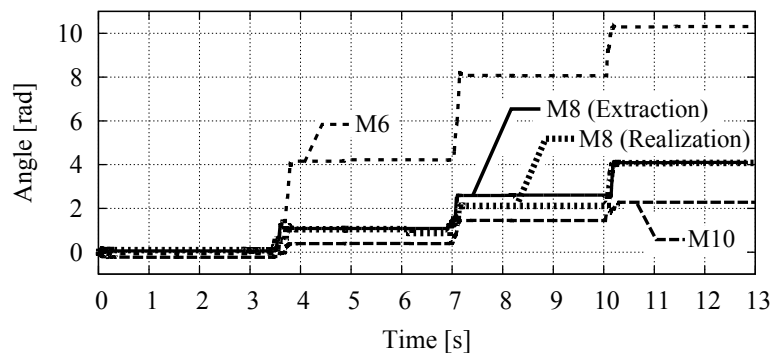
Fig. 7-25: Response of encoder connected with target nut.

and the dashed line illustrates the angle response of the reproduction phase. The dashed line ending at 10 rad, 4 rad, and 2 rad show the reprodused removal action to the M6, M8, and M10 nuts, respectively. As can be seen in Fig. 7-25, the target nut of M8 in the reproduction phase behaved in the same way as that in the extraction phase. In other word, this system succeeded to artificially realize the removal action. Furthermore, the extracted motion could adapt to the other hexagonal nuts and sucsseeded to rotate without any modification.

7.4 Summary

The first half of this chapter proposed a method to facilitate the instruction of motions involving direct contact with objects. The bilateral teleoperation system was introduced to directly extract human motions. The extracted information was used to automatically reproduce the motions. The main focus of this study was adaptation to the difference in location of target objects in the reproduction phase. The proposed method employed the position offset and the time-scaling technique. These were determined by the difference between the extracted and current force information in real-time. The validity of the proposed method was verified by comparative experiments. The proposed method succeeded to accurately reproduce the stored motion. Especially, this proposed method behaved extremely well in the duration of the contact state and the amplitude of the force.

The second half of this chapter presented a method to realize physical human actions. The human actions were extracted by the bilateral control system using wearable tendon-driven robot, which has master-slave structure. The force control scheme and the modal transformation were employed in this study. To experimentally verify the utility, the proposed approach was applied to the removal operation of a nut. The realized action succeeded to rotate the target nuts. This chapter showed a quite practical approach to realize physical human actions. The experimental results suggested extremely high possibility that robots can be physical agent of humans.

Chapter 8

Conclusions

Chapter 2 described fundamental technologies of motion control as the base of this dissertation. The acceleration control is especially explained, which is employed to improve the robustness. Controlled plants are always exposed to the disturbance, and the core essence of the motion control is to handle the disturbance such as the load force and the modeling error. This chapter introduced the disturbance observer, which is one of the most useful techniques to suppress the disturbance. By using this observer, it can be possible to design two characteristics independently: characteristic of command-following and characteristic of disturbance rejection. This concept makes the design guide clear. Furthermore, this chapter introduced the reaction force observer. The reaction force observer makes it possible to estimate and to feedback the external force. In short, by using these two observers the effect of the disturbance is arbitrary adjusted. This chapter also showed the concrete examples of the position control system and the force control system. In position control, the disturbance should be suppressed. In contrast, the disturbance (although it is external force strictly) should be accepted by the controlled plant in force control. As these technologies were employed in the other chapters, which described the extraction, the analysis, and the reconstruction of human motion.

Chapter 3 explained the research field of real-world haptics; it reviewed the progress of research on real-world haptics such as functionality and oblique coordinate control. Furthermore, chapter 3 introduced the important theory that a wide variety of system roles can be realized by combining pure position control and pure force control with appropriate coordinate transformation. This dissertation is on the basis of the real-world haptics. Although it has far been impossible to support some human activities that require contact with unstructured environments, real-world haptics provides a solution to this problem.

This technique has the potential to trigger industrial innovations in various fields, including agriculture, forestry, factories, medical services, and nursing care. The principle of this view was explained through two simple examples: acceleration-based bilateral control and grasping/manipulating control. Since the decoupling of the position control system and the force control system is critical in the above-mentioned theory, chapter 3 also extended the diagonalization method, and proposed a decoupling strategy for position and force control on the basis of modal space disturbance observers. To confirm the advantage of the proposed approach, this chapter showed analytical results of the performance and the stability. The utility of the proposed method was experimentally verified by using a multi-degrees-of-freedom (DOF) manipulator. This method succeeded in suppressing the interference between the position and force control systems, and realized a bilateral control system. This chapter clarified that proposed disturbance observer has high decomposition performance of the position control system and the force control system. It was confirmed that the MDOB-based decoupling method had better performance than oblique coordinate control. Conventional oblique coordinate control caused oscillation in cases where the modeling error was large and the observer cutoff frequency was not high enough to change the system dynamics. However, the MDOB-based decoupling method became unstable when the difference in mass was large.

Chapter 4 described a newly developed 11-DOF master-slave robot hands using tendon-driven mechanisms. These robot hands were developed to acquire haptic data of human motion. These robot hand consist of the three fingers and has the tendon-driven mechanisms. Furthermore, a bilateral control system for tendon-driven robots was proposed. This proposed control system uses the technique of modal decomposition, which makes it possible to control angles of joints, torque of joints, and tension of wires simultaneously. The transmission performance of the proposed system was experimentally verified. It was succeeded to achieve fine teleoperation and extraction of haptic information. Chapter 4 also proposed a compensation method of joint angle error caused by tendon elongation. This proposal was applied to a bilateral control system, and the validity was confirmed by experiments. Tendon-driven mechanisms are used extensively in a lot of robots, as the tendon-driven mechanisms make driven systems small and generate high output. Therefore, the proposed method contributes to the improvement of the field of robotics. In addition, chapter 4 showed a bilateral control technique facilitating intuitive operation. The proposed method transforms a human grasping motion into the motion of a slave robot to allow intuitive operation. In particular, firstly the physical quantity of the grasping motion was extracted and mapped onto the physical coordinate using the wearable robot hand. Next, a dominant Cartesian coordinate system, which contains the feature axis of the grasping motion, was calculated based on PCA.

Finally, the grasping motion was transmitted to the slave robot using the calculated coordinate system, and intuitive teleoperation system was realized. Decoupling of the position control and force control systems was achieved by setting a nominal mass value of the disturbance observer. The validity of the proposed method was verified using a wearable robot hand and a forceps robot. This proposed bilateral control method has broad utility and facilitates easy teleoperation. As above, chapter 4 showed that the developed robot hand offer a new avenue to extract human motion.

Chapter 5 established a recognition method of human motions using the haptic information and dynamic programming pattern-matching algorithm. The first half of chapter 5 described recognition of combinations of successive elementary motions. The haptic information was acquired by using a 5-DOF exoskeletal robot hand with bilateral control, and stored it in a database for use in classifying the operator's motions into 8 elementary classes. To compare the reference vectors with the input vectors, the cosine similarity was employed. DP matching was used to correct the expansion or contraction of the time axis in the classification results, and performed recognition of combined motions. The proposed method was experimentally verified. In this study the recognition accuracy was verified by using the PPV and NPV for 4 combined actions; in the future, the verification of this recognition method is expected to be extended to various transient states. The second half of chapter 5 described an application of above-mentioned recognition method to modal space. In the experiments, the proposed method was applied to grasping motions. Haptic information was abstracted by a bilateral control system, then divided into action components (e.g. grasping component and manipulating component) by a modal transformation. To recognize the target grasping motion, a DP pattern-matching algorithm was used. Finally, experiments were conducted under conditions where there was some difference in position, force, or speed between the input pattern and the reference pattern. In addition, real-time recognition was conducted to examine differences in the number of motions and in modal transformation, and to test the application of the method to a power-assist system. The validity of the proposed method was confirmed by these experiments, and the proposed method was successful in distinguishing the desired motion from the other motion. It was confirmed that the proposed method can trigger scaled bilateral control and assist grasping force of the operator in real-time. As above, chapter 5 showed that the proposed recognition method attains actual human support.

Chapter 6 explained a proposed novel motion-copying system using estimated control stiffness of human motion. The control stiffness of performed human motion is calculated by using a scaled bilateral control system, DP matching algorithm, and the least-squares method. DP matching accommodates the

motion speed of the saved data. The derived impedance was input into a compliance control system, where it was reproduced. The utility of the proposed method was experimentally verified by using a haptic forceps robot. Three types of experiments that used different target positions were conducted to confirm the effectiveness of the proposed method. In these experiments, the proposed motion-copying system succeeded in removing the phantom of a sarcoma, whereas the conventional method either failed to execute a grasping motion or applied excessive force. In order to extend the proposed method to a multi-DOF system, it is required to process a large amount of data, to select direction to implement the impedance control, and to reduce friction and inertia of the manipulator. Furthermore, if differences of environmental properties between the saving and loading phase are taken into account, viscosity may have to be changed. Chapter 6 also showed a method to clarify the features of human motions by elementally separating haptic information on the basis of the principle of motion control. The proposed method used a bilateral control system to extract haptic information and divided the haptic information into basic elements: transformation matrices, hybrid angles, pure position commands, and pure force commands. To validate the proposed method, a simulation and experiment using a robotic and a human operator were conducted. The proposed method successfully clarified the features of human motions despite the fact that it was difficult to recognize the differences from the original responses extracted through the bilateral control system. This study provides mathematical expression of human motion, that contributes toward revealing implicit knowledge. The mathematical expression shows motion features as a combination of the dual variables, control stiffness, and dominant control axes. Furthermore, since these obtained four elements are generally used in the conventional theory of motion control, it is possible to reproduce the human motion from these elements. This approach which is based on the bilateral control has an advantage over the other measurement approaches that use exterior sensors and force sensors, as the slave system itself can be used for the reproduction. The original motion can be certainly reconstructed and improved at the element level before the reproduction. For example, this approach allows us to modify the control stiffness or the grasping force according to the environmental impedance. Therefore, this method is considered an useful procedure to enhance the dexterity of robots. In addition, there is another benefit of using the bilateral control system. Since the system can decompose force information into human force and environmental reaction force, it is possible to estimate the stiffness of the human motion and the environment independently and simultaneously. As above, chapter 6 showed that the proposed approaches have usefulness to understand human motion.

Chapter 7 presented a method to facilitate the instruction of motions involving direct contact with ob-

jects by using a time-scaling technique to adapt the difference in location of target objects. The bilateral teleoperation system was introduced to directly extract human motions. The extracted information was used to automatically reproduce the motions. The main focus of this study was adaptation to the difference in location of target objects in the reproduction phase. The proposed method employed the position offset and the time-scaling technique. These were determined by the difference between the extracted and current force information in real-time. The validity of the proposed method was verified by comparative experiments. The proposed method succeeded to accurately reproduce the stored motion. This proposed method especially behaved extremely well and showed the usefulness in the duration of the contact state and the amplitude of the force. Furthermore, chapter 7 described realization method of physical human actions. The human actions were extracted by the bilateral control system using wearable tendon-driven robot, which has master-slave structure. The force control scheme and the modal transformation were employed in this study. The proposed approach was applied to the removal operation of a nut. The utility of the proposed method was experimentally verified by applying to the removal operation of a nut. It was confirmed that the realized motion can remove the nut regardless of the size and shape. Chapter 7 showed a quite practical approach and clarified that the proposed method realizes human motion artificially. The experimental results suggested extremely high possibility that robots can be physical agent of humans.

As stated above, this dissertation proposes a novel avenue for realization of adaptive human manipulation. The methodology to realize human motion will be a basic technology of human support, and it will greatly contribute to solve urgent problem of aging societies with falling birthrates and labor shortages. The force-based adaptiveness of the realized motion have a beneficial effect on various field such as future production process and rehabilitative therapy. To achieve high-mix low-volume production and to respond to individual differences, realization of adaptive motion is absolutely imperative. Needless to say, conventional positioning technique is also important to achieve precise operation. This dissertation provides a novel methodology to clarify successively expressed position-based precise motion and force-based adaptive motion by active utilization of haptic technology. The functionality-based design/redesign method, which is backbone of the proposed realization methodology, leads to exceptional prospects. The validity of the proposed methodology was confirmed theoretically and experimentally. Although the motion artificially realized in this dissertation is just simple operation, the basic concept and theory possess generality. The proposed methodology is anticipated to be applied to wider areas and expected to open the way to a bright future.

References

[1] Y. Yokokura, S. Katsura, and K. Ohishi, "Stability analysis and experimental validation of a motion-copying system", *IEEE Trans. Ind. Electron.*, Vol. 56, No. 10, pp. 3906–3913, Oct. 2009.

[2] S. Yajima and S. Katsura, "Motion-copying system based on velocity information for motion reproduction", In *Proc. Int. Conf. IEEE IECON*, pp. 221–226, Nov. 2011.

[3] E. A. Sisbot and R. Alami, "A human-aware manipulation planner", *IEEE Trans. Robot.*, Vol. 28, No. 5, pp. 1045–1057, Oct. 2012.

[4] P. Rouanet, P. Y. Oudeyer, F. Danieau, and D. Filliat, "The impact of human-robot interfaces on the learning of visual objects", *IEEE Trans. Robot.*, Vol. 29, No. 2, pp. 525–541, Apr. 2013.

[5] S. J. Kim and B. K. Kim, "Dynamic ultrasonic hybrid localization system for indoor mobile robots", *IEEE Trans. Ind. Electron.*, Vol. 60, No. 10, pp. 4562–4573, Oct. 2013.

[6] L. Renquan, Z. Li, C. Su, and A. Xue, "Development and learning control of a human limb with a rehabilitation exoskeleton", *IEEE Trans. Ind. Electron.*, to be published.

[7] W. Chung, C. Rhee, Y. Shim, H. Lee, and S. Park, "Door opening control of a service robot using the multi-fingered robot hand", *IEEE Trans. Ind. Electron.*, Vol. 56, No. 10, pp. 3975–3984, Oct. 2009.

[8] S. Komada, Y. Hashimoto, N. Okuyama, T. Hisada, and J. Hirai, "Development of a biofeedback therapeutic-exercise-supporting manipulator", *IEEE Trans. Ind. Electron.*, Vol. 56, No. 10, pp. 3914–3920, Oct. 2009.

[9] J. Jia, G. Wang, Y. T. Cham, Y. Wang, and M. Han, "Electrical characteristic study of a hybrid PEMFC and ultracapacitor system", *IEEE Trans. Ind. Electron.*, Vol. 57, No. 6, pp. 1945–1953, Jun. 2010.

[10] Y. Oonishi, S. Oh, and Y. Hori, "A new control method for power-assisted wheelchair based on the surface myoelectric signal", *IEEE Trans. Ind. Electron.*, Vol. 57, No. 9, pp. 3191–3196, Sep. 2010.

[11] T. Tsuji, K. Natori, H. Nishi, and K. Ohnishi, "Controller design method of bilateral control system", *Eur. Power Electron. Drives J.*, Vol. 16, No. 2, pp. 22–28, May 2006.

[12] T. Tsuji, K. Ohnishi, and A. Sabanovic, "A controller design method based on functionality", *IEEE Trans. Ind. Electron.*, Vol. 54, No. 6, pp. 3335–3343, Dec. 2007.

[13] X. Cao, B. Ning, P. Yan, and X. Li, "Selecting key poses on manifold for pairwise action recognition", *IEEE Trans. Ind. Informat.*, Vol. 8, No. 1, pp. 168–177, Feb. 2012.

[14] A. Suzumura and Y. Fujimoto, "Real-time motion generation and control systems for high wheel-legged robot mobility", *IEEE Trans. Ind. Electron.*, to be published.

[15] H. Cheng, H. Chen, and B. W. Mooring, "Accuracy analysis of dynamic-wafer-handling robotic system in semiconductor manufacturing", *IEEE Trans. Ind. Electron.*, Vol. 61, No. 3, pp. 1402–1410, Mar. 2014.

[16] C. Sun, W. L. Xu, J. E. Bronlund, and M. Morgenstern, "Dynamics and compliance control of a linkage robot for food chewing", *IEEE Trans. Ind. Electron.*, Vol. 61, No. 1, pp. 377–386, Jan. 2014.

[17] J. T. Klosowski, M. Held, J. S. B. Mitchell, H. Sowizral, and K. Zikan, "Efficient collision detection using bounding volume hierarchies of k-DOPs", *IEEE Trans. Visualization and Computer Graphics*, Vol. 4, No. 1, pp. 21–36, Jan. 1998.

[18] S. Ullrich and T. Kuhlen, "Haptic palpation for medical simulation in virtual environments", *IEEE Trans. Visualization and Computer Graphics*, Vol. 18, No. 4, pp. 617–625, Apr. 2012.

[19] R. J. Adams and B. Hannaford, "Stable haptic interaction with virtual environments", *IEEE Trans. Robot. Autom.*, Vol. 15, No. 3, pp. 465–474, Jun. 1999.

[20] K. Ohnishi, S. Katsura, and T. Shimono, "Motion control for real-world haptics", *IEEE Trans. Ind. Electron. Mag.*, Vol. 4, No. 2, pp. 16–19, Jun. 2010.

[21] S. Katsura, W. Yamanouchi, and Y. Yokokura, "Real-world haptics: reproduction of human motion", *IEEE Trans. Ind. Electron. Mag.*, Vol. 6, No. 1, pp. 25–31, Mar. 2012.

[22] J. K. Salisbury, "Active stiffness control of a manipulator in Cartesian coordinates", In *Proc. IEEE Conf. Decision Control Including Symp. Adapt. Process.*, pp. 95–100, Dec. 1980.

[23] M. T. Mason, "Compliance and force control for computer controlled manipulators", *IEEE Trans. Syst., Man, Cybern.*, Vol. SMC-11, No. 6, pp. 418–432, Jun. 1981.

[24] N. Hogan, "Impedance control: An approach to manipulation part1, 2 and 3", *Trans. ASME, J. Dyn. Syst.. Meas., Cont.*, Vol. 107, No. 1, pp. 1–24, Mar. 1985.

[25] J. Luh, M. Walker, and R. Paul, "Resolved-acceleration control of mechanical manipulators", *IEEE Trans. Automat. Contr.*, Vol. 25, No. 3, pp. 468–474, Jun. 1980.

[26] M. H. Raibert and J. J. Craig, "Hybrid position/force control of manipulators", *Trans. ASME, J. Dyn. Syst. Meas. Control*, Vol. 103, No. 2, pp. 126–133, Jun. 1981.

[27] O. Khatib, "A unified approach for motion and force control of robot manipulators: The operational space formulation", *IEEE Trans. Robot. Autom.*, Vol. RA-3, No. 1, pp. 43–53, Feb. 1987.

[28] K. Ohishi, Y. Ohba, and S. Katsura, "Kinematics and dynamics of motion control based on acceleration control", *IEEJ Trans. Ind. Appl.*, Vol. 127-D, No. 6, pp. 545–553, Jun. 2007.

[29] K. Ohnishi, M. Shibata, and T. Murakami, "Motion control for advanced mechatronics", *IEEE/ASME Trans. Mechatron.*, Vol. 1, No. 1, pp. 56–67, Mar. 1996.

[30] Y. Yildiz, A. Sabanovic, and K. Abidi, "Sliding-mode neuro-controller for uncertain systems", *IEEE Trans. Ind. Electron.*, Vol. 54, No. 3, pp. 1676–1685, Jun. 2007.

[31] A. Hace, K. Jezernik, and A. Sabanovic, "SMC with disturbance observer for a linear belt drive", *IEEE Trans. Ind. Electron.*, Vol. 54, No. 6, pp. 3402–3412, Dec. 2007.

[32] A. Tesfaye, H. S. Lee, and M. Tomizuka, "A sensitivity optimization approach to design of a disturbance observer in digital motion control systems", *IEEE/ASME Trans. Mechatron.*, Vol. 5, No. 1, pp. 32–38, Mar. 2000.

[33] T. Murakami, F. Yu, and K. Ohnishi, "Torque sensorless control in multidegree-of-freedom manipulator", *IEEE Trans. Ind. Electron.*, Vol. 40, No. 2, pp. 259–265, Apr. 1993.

[34] T. Murakami, N. Oda, Y. Miyasaka, and K. Ohnishi, "A motion control strategy based on equivalent mass matrix in multidegree-of-freedom manipulator", *IEEE Trans. Ind. Electron.*, Vol. 42, No. 2, pp. 123–130, Apr. 1995.

[35] M. Morisawa and K. Ohnishi, "Motion control taking environmental information into account", *EPE J.*, Vol. 12, No. 4, pp. 37–41, Nov. 2002.

[36] D. Ito, T. Kageyama, J. Suzuki, T. Tsuji, M. Morisawa, and K. Ohnishi, "A design of decentralized control system in unstructured environment", *IEEJ Trans. Ind. Appl.*, Vol. 123-D, No. 10, pp. 1219–1226, Oct. 2003.

[37] S. Katsura and K. Ohnishi, "Quarry of modal information from environment for advanced motion control", *IEEJ Trans. Ind. Appl.*, Vol. 126-D, No. 4, pp. 372–378, Apr. 2006.

[38] R. Kubo and K. Ohnishi, "An extraction method of environmental surface profile using planar end-effectors", In *Proc. 9th IEEE Int. Workshop AMC*, pp. 368–373, Mar. 2006.

[39] R. Kubo, T. Shimono, and K. Ohnishi, "Flexible controller design of bilateral grasping systems based on a multilateral control scheme", *IEEE Trans. Ind. Electron.*, Vol. 7, No. 3, pp. 62–68, Jan. 2009.

[40] R. A. Brooks, "A robust layered control system for a mobile robot", *IEEE J. Robot. Autom.*, Vol. RA-2, No. 1, pp. 14–23, Mar. 1986.

[41] D. Dimarogonas and K. Kyriakopoulos, "Connectedness preserving distributed swarm aggregation for multiple kinematic robots", *IEEE Trans. Robot.*, Vol. 24, No. 5, pp. 1213–1223, Oct. 2008.

[42] Z. Wang and D. Gu, "Cooperative target tracking control of multiple robots", *IEEE Trans. Ind. Electron.*, Vol. 59, No. 8, pp. 3232–3240, Aug. 2012.

[43] J. E. Hernandez, A. G. Loukianov, B. Castillo-Toledo, and V. I. Utkin, "Observer based decomposition control of linear delayed systems", In *Proc. IEEE Conf. Decision and Control*, pp. 1867–1872, Dec. 2001.

[44] S. Arimoto and P. T. A. Nguyen, "Principle of superposition for realizing dexterous pinching motions of a pair of robot fingers with soft-tips", *IEICE Trans. Fundam.*, Vol. E84-A, No. 1, pp. 39–47, Jan. 2001.

[45] M. Okada, K. Tatani, and Y. Nakamura, "Polynomial design of the nonlinear dynamics for the brain-like information processing of whole body motion", In *Proc. IEEE Int. Conf. Robot. Autom.*, pp. 1410–1415, May 2002.

[46] T. Tsuji, K. Natri, and K. Ohnishi, "A controller design method of bilateral control system", Vol. 4, pp. 123–128, Sep. 2004.

[47] T. Tsuji, H. Nishi, and K. Ohnishi, "A controller design method of decentralized control system", *IEEJ Trans. Ind. Appl.*, Vol. 126-D, No. 5, pp. 630–638, May 2006.

[48] A. Uemura, K. Yubai, and J. Hirai, "Realization of cooperative motions by a function-based decentralized control system for reconfigurable robots", *IEEJ Trans. Ind. Appl.*, Vol. 129-D, No. 10, pp. 995–1003, Oct. 2009.

[49] A. Sabanovic, M. Elitas, and K. Ohnishi, "Sliding modes in constrained systems control", *IEEE Trans. Ind. Electron.*, Vol. 55, No. 9, pp. 3332–3339, Sep. 2008.

[50] A. Sabanovic, "SMC framework in motion control systems", *Int. J. Adapt. Control Signal Process.*, Vol. 21, No. 8, pp. 731–744, Oct. 2007.

[51] S. Sakaino, T. Sato, and K. Ohnishi, "Modal transformation for bilateral control and cooperational robot motion - kinematics and dynamics -", Feb. 2009.

[52] S. Sakaino, T. Sato, and K.Ohnishi, "Realization of advanced hybrid control through oblique coordinate control", *IEEJ Trans. Ind. Appl.*, Vol. 130-D, No. 3, pp. 300–306, Feb. 2010.

[53] S. Sakaino, T. Sato, and K. Ohnishi, "Precise position/force hybrid control with modal mass decoupling and bilateral communication between different structures", *IEEE Trans. Ind. Informat.*, Vol. 7, No. 2, pp. 266–276, May 2011.

[54] S. Sakaino, T. Sato, and K. Ohnishi, "Multi-DOF micro-macro bilateral controller using oblique coordinate control", *IEEE Trans. Ind. Informat.*, Vol. 7, No. 3, pp. 446–454, Aug. 2011.

[55] Y. Nakajima, T. Nozaki, Y. Oyamada, and K. Ohnishi, "Object-coordinate-based bilateral control system using visual information", *IEEJ Trans. Ind. Appl.*, Vol. 132-D, No. 3, pp. 374–380, Mar. 2012.

[56] T. Nozaki, Y. Suzuki, and K. Ohnishi, "Transmission of force sensations by hand of multi-DOF master-slave robot using tendon-driven mechanism", *IEEJ Trans. Ind. Appl.*, Vol. 131-D, No. 3, pp. 297–303, Mar. 2011.

[57] Y. Saito, W. Motooka, T. Nozaki, D. Yashiro, and K. Ohnishi, "Development of two-link manipulator equipped with biarticular muscle mechanism using flexible actuator", *IEEJ Trans. Ind. Appl.*, Vol. 132-D, No. 3, pp. 397–403, Mar. 2012.

[58] Y. Kasahara, H. Kawana, S. Usuda, and K. Ohnishi, "Telerobotic-assisted bone-drilling system using bilateral control with feed operation scaling and cutting force scaling", *Int. J. Med. Robotics Comput. Assist. Surg.*, Vol. 8, No. 2, pp. 221–229, Jun. 2012.

[59] H. Tanaka, K. Ohnishi, H. Nishi, T. Kawai, Y. Morikawa, S. Ozawa, and T. Furukawa, "Implementation of bilateral control system based on acceleration control using FPGA for multi-DOF haptic endoscopic surgery robot", *IEEE Trans. Ind. Electron.*, Vol. 56, No. 3, pp. 618–627, Mar. 2009.

[60] W. Motooka, T. Nozaki, T. Mizoguchi, K. Sugawara, F. Mitome, K. Okuda, M. Miyagaki, D. Yashiro, T. Yakoh, K. Ohnishi, Y. Morikawa, and N. Shimojima, "Development of 16-DOF telesurgical forceps master/slave robot with haptics", In *Proc. Int. Conf. IEEE IECON*, pp. 2081–2086, Nov. 2010.

[61] B. Hannaford, "A design framework for teleoperators with kinesthetic feedback", *IEEE Trans. Robot. Autom.*, Vol. 5, No. 4, pp. 426–434, Aug. 1989.

[62] D. A. Lawrence, "Stability and transparency in bilateral teleoperation", *IEEE Trans. Robot. Autom.*, Vol. 9, No. 5, pp. 624–637, Oct. 1993.

[63] Y. Yokokohji and T. Yoshikawa, "Bilateral control of master-slave manipulators for ideal kinesthetic coupling-formulation and experiment", *IEEE Trans. Robot. Autom.*, Vol. 10, No. 5, pp. 605–620, Oct. 1994.

[64] P. Malysz and S. Sirouspour, "A kinematic control framework for single-slave asymmetric teleoperation systems", *IEEE Trans. Robot.*, Vol. 27, No. 5, pp. 901–917, Oct. 2011.

[65] Y. Matsumoto, S. Katsura, and K. Ohnishi, "An analysis and design of bilateral control based on disturbance observer", In *Proc. IEEE ICIT*, pp. 802–807, Dec. 2003.

[66] W. Iida and K. Ohnishi, "Reproducibility and operationality in bilateral teleoperation", In *Proc. 8th IEEE Int. Workshop AMC*, pp. 217–222, Mar. 2004.

[67] S. Katsura, Y. Matsumoto, and K. Ohnishi, "Realization of "law of action and reaction by multi-lateral control"", *IEEE Trans. Ind. Electron.*, Vol. 52, No. 5, pp. 1196–1205, Oct. 2005.

[68] I. Aliaga, A. Rubio, and E. Sanchez, "Experimental quantitative comparison of different control architectures for master-slave teleoperation", *IEEE Trans. Control Syst. Technol.*, Vol. 12, No. 1, pp. 2–11, Jan. 2004.

[69] O. Khatib and J. Burdick, "Motion and force control of robot manipulators", *Proc. of the 1986 IEEE Int'l Conf. on Robotics and Automation.*, Vol. 3, pp. 1381–1386, Apr. 1986.

[70] N. Tsunashima and S. Katsura, "Spatiotemporal coupler: storage and reproduction of human finger motions", *IEEE Trans. Ind. Electron.*, Vol. 59, No. 2, pp. 1074–1085, Feb. 2012.

[71] S. Shimmyo, T. Sato, and K. Ohnishi, "Biped walking pattern generation by using preview control based on three-mass model", *IEEE Trans. Ind. Electron.*, Vol. 60, No. 11, pp. 5137–5147, 2013.

[72] S. Sakaino, T. Sato, and K. Ohnishi, "A novel motion equation for general task description and analysis of mobile-hapto", *IEEE Trans. Ind. Electron.*, Vol. 60, No. 7, pp. 2673–2680, Jul. 2013.

[73] A. Suzuki and K. Ohnishi, "Frequency-domain damping design for time-delayed bilateral teleoperation system based on modal space analysis", *IEEE Trans. Ind. Electron.*, Vol. 60, No. 1, pp. 177–190, Jan. 2013.

[74] T. Nozaki, T. Mizoguchi, Y. Saito, D. Yashiro, and K. Ohnishi, "Recognition of grasping motion based on modal space haptic information using DP pattern-matching algorithm", *IEEE Trans. Ind. Informat.*, Vol. 9, No. 4, pp. 2043–2051, 2013.

[75] H. Tai and T. Murakami, "Equivalent mass matrix based bilateral control for multi-degrees-of-freedom systems", In *Proc. of 11th IEEE Int. Workshop AMC*, pp. 343–348, Mar. 2010.

[76] A. Lasnier and T. Murakami, "Workspace based force sensorless bilateral control with multi-degree-of-freedom motion systems", In *Proc. of 11th IEEE Int. Workshop AMC*, pp. 583–588, Mar. 2010.

[77] N. Motoi, R. Kubo, T. Shimono, and K. Ohnishi, "Bilateral control with different inertia based on modal decomposition", In *Proc. of 11th IEEE Int. Workshop AMC*, pp. 697–702, Mar. 2010.

[78] T. Nozaki, T. Mizoguchi, and K. Ohnishi, "Position/force decoupling for micro-macro bilateral control based on modal space disturbance observer", In *Proc. of 12th IEEE Int. Workshop AMC*, pp. 1–6, Mar. 2012.

[79] T. Ohta and T. Murakami, "A stabilization control of bilateral system with time delay by vibration index–application to inverted pendulum control", *IEEE Trans. Ind. Electron.*, Vol. 56, No. 5, pp. 1595–1603, May 2009.

[80] P. K. W. Abeygunawardhanai and T. Murakami, "Vibration suppression of two-wheel mobile manipulator using resonance-ratio-control-based null-space control", *IEEE Trans. Ind. Electron.*, Vol. 57, No. 12, pp. 4137–4146, Dec. 2010.

[81] S. Komada, N. Machii, and T. Hori, "Control of redundant manipulators considering order of disturbance observer", *IEEE Trans. Ind. Electron.*, Vol. 42, No. 2, pp. 413–420, Apr. 2000.

[82] N. Oda, H. Ohta, T. Murakami, and K. Ohnishi, "A robust impedance control strategy for redundant manipulator", In *Proc. Int. Conf. IEEE IECON*, pp. 1254–1259, Nov. 1995.

[83] N. Oda, T. Murakami, and K. Ohnishi, "A robust control strategy of redundant manipulator by workspace observer", *Journal of Robotics and Mechatronics*, Vol. 8, No. 3, pp. 235–242, Jun. 1996.

[84] Y. Izumikawa, K. Yubai, and J. Hirai, "Fault-tolerant control system of flexible arm for sensor fault by using reaction force observer", *IEEE/ASME Trans. Mechatron.*, Vol. 10, No. 4, pp. 391–396, Aug. 2005.

[85] S. C. Jacobsen, J. E. Wood, D. F. Knutti, and K. B. Biggers, "The Utah/MIT dextrous hand work in progress", *Int. J. Robot. Research*, Vol. 4, No. 3, pp. 21–50, Dec. 1984.

[86] M. E. Rosheim, "Evolution the development of anthrobotics", *John Wiley and Sons, Inc.*, 1994.

[87] H. Liu, J. Butterfass, S. Knoch, P. Meusel, and G. Hirzinger, "A new control strategy for DLR's multisensory articulated hand", *IEEE Control Systems*, Vol. 19, No. 2, pp. 47–54, Apr. 1999.

[88] H. Kawasaki and T. Komatsu, "Mechanism design of anthropomorphic robot hand: Gihu hand I", *J. of Robotics and Mechatronics*, Vol. 11, No. 4, pp. 269–273, 1999.

[89] H. Kawasaki, T. Komatsu, and K. Uchiyama, "Dexterous anthropomorphic robot hand with distributed tactile sensor: Gifu hand", *IEEE/ASME Trans. Mechatron.*, Vol. 7, No. 3, pp. 296–303, Sep. 2002.

[90] K. Haiya, S. Komada, and J. Hirai, "Tension control for tendon mechanisms by compensation of nonlinear spring characteristic equation error", *IEEJ Trans. Ind. Appl.*, Vol. 130-D, No. 6, pp. 816–823, Jun. 2010.

[91] G. H. Ballantyne, "Robotic surgery, telerobotic surgery, telepresence, and telementoring", *Surgical Endoscopy*, Vol. 16, No. 10, pp. 1389–1402, Oct. 2002.

[92] Mamoru Mitsuishi, "Medical robotics", *The J. of Japanese College of Angiology*, Vol. 46, pp. 759–767, Dec. 2006.

[93] Y. Suzuki, H. Kuwahara, M. Sato, K. Mikami, and K. Ohnishi, "Force sensation transmission with same-structured master-slave robot hands using flexible actuators", *J. of the Japan Society for Precision Engineering*, Vol. 76, No. 8, pp. 938–944, Feb. 2010.

[94] S. C. Jacobsen, H. Ko, E. K. Iversen, and C. C. Davis, "Antagonistic control of a tendon driven manipulator", In *Proc. 1989 IEEE Int. Conf. Robotics and Automation*, pp. 1334–1339, May 1989.

[95] S. C. Jacobsen, E. K. Iversen, D. F. Knutti, R. T. Johnson, and K. B. Biggers, "Design of the Utah/M.I.T. dextrous hand", In *Proc. 1986 IEEE Int. Conf. Robotics and Automation*, pp. 1520–1534, 1986.

[96] S. C. Jacobsen, H. Ko, E. K. Iversen, and C. C. Davis, "Control strategies for tendon-driven manipulators", *lEEE Control Systems Magazine*, Vol. 10, No. 2, pp. 23–28, Feb. 1990.

[97] S. Susa, T. Shimono, and K. Ohnishi, "Micro-macro bilateral control taking into account scaling of control gain", *IEEJ Trans. Ind. Appl.*, Vol. 129-D, No. 2, pp. 150–157, Feb. 2009.

[98] S. Susa, K. Natori, and K. Ohnishi, "Bilateral control of master-slave system with different scaling", *IEEJ Trans. Ind. Appl.*, Vol. 129-D, No. 7, pp. 682–690, Jul. 2009.

[99] T. Murakami and K. Ohnishi, "A study of stability and workspace decoupling control based on robust control in multi-degrees-of-freedom robot", *IEEJ Trans. Ind. Appl.*, Vol. 113-D, No. 5, pp. 639–646, May 1993.

[100] T. Yamashita and T. Shimono, "An approach to force-sensorless bilateral control in master-slave system with different configurations", *IEEJ Trans. Ind. Appl.*, Vol. 131-D, No. 6, pp. 777–784, Jun. 2011.

[101] N. Tsunashima, Y. Yokokura, and S. Katsura, "Saving and reproduction of human motion data by using haptic devices with different configurations", *IEEJ Trans. Ind. Appl.*, Vol. 131-D, No. 3, pp. 267–274, Mar. 2011.

[102] W. Yamanouchi, S. Katsura, and K. Ohishi, "Bileteral force feedback control with different configurations based on dimensional scaling for realization of mobile-hapto", *IEEJ Trans. Ind. Appl.*, Vol. 131-D, No. 2, pp. 180–186, Feb. 2011.

[103] T. Mizoguchi, H. Kuwahara, and K. Ohnishi, "A design method of force dependent velocity bilateral control based on gyrator property", *IEEJ Trans. Ind. Appl.*, Vol. 131-D, No. 3, pp. 304–310, Mar. 2011.

[104] H. Liu, "Exploring human hand capabilities into embedded multifingered object manipulation", *IEEE Trans. Ind. Informat.*, Vol. 7, No. 3, pp. 389–398, Aug. 2011.

[105] M. Kondo, J. Ueda, and T. Ogasawara, "Recognition of in-hand manipulation using contact state transition for multifingered robot hand control", *Robot. Autonomous Syst.*, Vol. 56, No. 1, pp. 66–81, Jan. 2008.

[106] K. Abe, H. Saito, and S. Ozawa, "Virtual 3-D interface system via hand motion recognition from two cameras", *IEEE Trans. Syst., Man, Cybern. A*, Vol. 32, No. 4, pp. 536–540, Jul. 2002.

[107] K. Natori, T. Tsuji, T. Yakoh, and K. Ohnishi:, "Bilateral teleoperation through networks", *IEEJ Trans. Ind. Appl.*, Vol. 126, No. 2, pp. 161–167, Feb. 2006.

[108] S. Hyodo, Y. Soeda, and K. Ohnishi, "Verification of flexible actuator from position and force transfer characteristic and its application to bilateral teleoperation system", *IEEE Trans. Ind. Electron.*, Vol. 56, No. 1, pp. 36–42, Jan. 2009.

[109] H. Kuwahara, T. Shimono, H. Tanaka, D. Yashiro, and K. Ohnishi, "Abstraction of action components unconstrained by alignment of haptic sensing points", *IEEE Trans. Ind. Electron.*, Vol. 58, No. 8, pp. 3196–3204, Aug. 2011.

[110] S. Katsura, Y. Matsumoto, and K. Ohnishi, "Analysis and experimental validation of force bandwidth for force control", *IEEE Trans. on Industrial Electronics*, Vol. 53, No. 3, pp. 922–928, 2006.

[111] K. Ogawara, J. Takamatsu, H. Kimura, and K. Ikeuchi, "Extraction of essential interactions through multiple observations of human demonstrations", *IEEE Trans. Ind. Electron.*, Vol. 50, No. 4, pp. 667–675, Aug. 2003.

[112] S. Katsura and K. Ohishi, "A realization of motion acquisition system based on interaction mode control", *IEEJ Trans. Ind. Appl.*, Vol. 127-D, No. 8, pp. 796–804, 2007.

[113] Y. Yokokura, S. Katsura, and K. Ohishi, "Motion copying system based on real-world haptics", In *Proc. of 10th IEEE Int. Workshop AMC*, pp. 613–618, 2008.

[114] T. Watanabe and S. Katsura, "Character recognition method by time-frequency analyses using writing pressure", *IEEJ Trans. Ind. Appl.*, Vol. 130-D, No. 4, pp. 498–504, 2010.

[115] T. Watanabe and S. Katsura, "Recognition and classification of road condition on the basis of friction force by using a mobile robot", *IEEJ Trans. Ind. Appl.*, Vol. 131-D, No. 3, pp. 357–363, 2011.

[116] Y. Kasahara, T. Shimono, H. Kuwahara, M. Sato, and K. Ohnishi, "Modal-power-based haptic motion recognition", *IEEJ Trans. Ind. Appl.*, Vol. 130-D, No. 4, pp. 477–484, 2010.

[117] H. Ghasemzadeh and R. Jafari, "Physical movement monitoring using body sensor networks: a phonological approach to construct spatial decision trees", *IEEE Trans. Ind. Informat.*, Vol. 7, No. 1, pp. 66–77, Feb. 2011.

[118] S. Jin, D. Kim, T. T. Nguyen, D. Kim, M. Kim, and J. W. Jeon, "Design and implementation of a pipelined datapath for high-speed face detection using FPGA", *IEEE Trans. Ind. Informat.*, Vol. 8, No. 1, pp. 158–167, Feb. 2012.

[119] C. Tran and M. M. Trivedi, "3-D posture and gesture recognition for interactivity in smart spaces", *IEEE Trans. Ind. Informat.*, Vol. 8, No. 1, pp. 178–187, Feb. 2012.

[120] A. Quagli, D. Fontanelli, D. Greco, L. Palopoli, and A. Bicchi, "Design of embedded controllers based on anytime computing", *IEEE Trans. Ind. Informat.*, Vol. 6, No. 4, pp. 492–502, Nov. 2010.

[121] A. Malinowski and H. Yu, "Comparison of embedded system design for industrial application", *IEEE Trans. Ind. Informat.*, Vol. 7, No. 2, pp. 244–257, May 2011.

[122] S. Katsura and K. Ohishi, "Acquisition and analysis of finger motions by skill preservation system", *IEEE Trans. Ind. Electron.*, Vol. 54, No. 6, pp. 3353–3361, Dec. 2007.

[123] H. Sakoe and S. Chiba, "Dynamic programming algorithm optimization for spoken word recognition", *IEEE Trans. Acoustics, Speech and Signal Processing*, Vol. 26, No. 1, pp. 43–49, Feb. 1978.

[124] T. Nozaki, Y. Suzuki, and K. Ohnishi, "Motion recognition using DP matching based on position and force information", In *Proc. 4th Conf. HSI*, pp. 104–109, May 2011.

[125] T. Nozaki, T. Mizoguchi, Y Nakajima, and K. Ohnishi, "Real-time skill providing system using human haptic information", In *Proc. 5th Conf. HSI*, Jun. 2012.

[126] S. Nakagawara, H. Kajimoto, N. Kawakami, S. Tachi, and I. Kawabuchi, "An encounter-type multi-fingered master hand using circuitous joints", *Proc. of the 2005 IEEE Int'l Conf. on Robotics and Automation*, pp. 2667–2672, April. 2005.

[127] H. Fang, Z. Xie, and H. Liu, "An exoskeleton master hand for controlling DLR/HIT hand", *Proc. of the 2009 IEEE/RSJ Int'l Conf. on Intelligent Robots and Systems*, pp. 3703–3708, October. 2009.

[128] J. Ota, S. Shiozaki, and T. Arai, "Motion recognition using DP matching", *JAPE Trans.*, Vol. 63, No. 6, pp. 812–818, 1997.

[129] J. Rosen, B. Hannaford, C. G. Richards, and M. N. Sinanan, "Markov modeling of minimally invasive surgery based on tool/tissue interaction and force/torque signatures for evaluating surgical skills", *IEEE Trans. Biomedical Engineering*, Vol. 48, No. 5, pp. 579–591, May 2001.

[130] M. Yang, N. Ahuja, and M. Tabb, "Extraction of 2D motion trajectories and its application to hand gesture recognition", *IEEE Trans. Biomedical Engineering*, Vol. 24, No. 8, pp. 1061–1074, Aug. 2002.

[131] B. K. Kim, W. K. Chung, and K. Ohba, "Design and performance tuning of sliding-mode controller for high-speed and high-accuracy positioning systems in disturbance observer framework", *IEEE Trans. Ind. Electron.*, Vol. 56, No. 10, pp. 3798–3809, Oct. 2009.

[132] Y. Kuniyoshi, M. Inaba, and H. Inoue, "Learning by watching: extracting reusable task knowledge from visual observation of human performance", *IEEE Trans. Robot. Autom.*, Vol. 10, No. 6, pp. 799–822, Dec. 1994.

[133] K. Ikeuchi and T. Suehiro, "Toward an assembly plan from observation. I. Task recognition with polyhedral objects", *IEEE Trans. Robot. Autom.*, Vol. 10, No. 3, pp. 368–385, Jun. 1994.

[134] M. Pardowitz, S. Knoop, R. Dillmann, and R. D. Zollner, "Incremental learning of tasks from user demonstrations, past experiences, and vocal comments", *IEEE Trans. Syst., Man, Cybern. B, Cybern.*, Vol. 37, No. 2, pp. 322–332, Apr. 2007.

[135] A. Alissandrakis, C. L. Nehaniv, and K. Dautenhahn, "Correspondence mapping induced state and action metrics for robotic imitation", *IEEE Trans. Syst., Man, Cybern. B, Cybern.*, Vol. 37, No. 2, pp. 299–307, Apr. 2007.

[136] A. Ude, A. Gams, T. Asfour, and J. Morimoto, "Task-specific generalization of discrete and periodic dynamic movement primitives", *IEEE Trans. Robot.*, Vol. 26, No. 5, pp. 800–815, Oct. 2010.

[137] S. M. Khansari-Zadeh and A. Billard, "Learning stable nonlinear dynamical systems with Gaussian mixture models", *IEEE Trans. Robot.*, Vol. 27, No. 5, pp. 943–957, Oct. 2011.

[138] A. Vakanski, I. Mantegh, A. Irish, and F. Janabi-Sharifi, "Trajectory learning for robot programming by demonstration using hidden Markov model and dynamic time warping", *IEEE Trans. Syst., Man, Cybern. B, Cybern.*, Vol. 42, No. 4, pp. 1039–1052, Aug. 2012.

[139] P. F. Hokayem and M. W. Spong, "Bilateral teleoperation: An historical survey", *Automatica*, Vol. 42, No. 12, pp. 2035–2057, Dec. 2006.

[140] C. D. Onal and M. Sitti, "A scaled bilateral control system for experimental one-dimensional teleoperated nanomanipulation", *Int'l Journal of Robotics Research*, Vol. 28, No. 4, pp. 484–497, Apr. 2009.

[141] C. D. Onal and M. Sitti, "Teleoperated 3-D force feedback from the nanoscale with an atomic force microscope", *IEEE Trans. Nanotechnol.*, Vol. 9, No. 1, pp. 46–54, Jan. 2010.

[142] G. Niemeyer and J. J. E. Slotine, "Stable adaptive teleoperation", *IEEE Journal of Oceanic Engineering*, Vol. 16, No. 1, pp. 152–162, 1991.

[143] K. H. Zaad and S. E. Salcudean, "Transparency in time delayed systems and the effect of local force feedback for transparent teleoperation", *IEEE Trans. Robot. Autom.*, Vol. 18, No. 1, pp. 108–114, February 2002.

[144] A. Haddadi and K. H. Zaad, "Bounded-impedance absolute stability of bilateral teleoperation control systems", *IEEE Trans. Haptics*, Vol. 3, No. 1, pp. 15–27, Jan. 2010.

[145] J. E. Colgate, "Power and impedance scaling in bilateral manipulation", In *the IEEE Int'l Conf. on Robotics and Automation*, Vol. 3, pp. 2292–2297, Apr. 1991.

[146] J. E. Colgate, "Robust impedance shaping telemanipulation", *IEEE Trans. Robot. Autom.*, Vol. 9, No. 4, pp. 374–384, Aug. 1993.

[147] T. F. Chan, S. E. Everett, and R. V. Dubey, "Variable damping impedance control of a bilateral telerobotic system", In *the Int'l Conf. Robotics Automat.*, Vol. 3, pp. 2033–2040, Apr. 1996.

[148] R. V. Dubey, S. E. Everett, and T. F. Chan, "Variable damping impedance control of a bilateral telerobotic system", *IEEE Control Systems*, Vol. 17, No. 1, pp. 37–45, Feb. 1997.

[149] K. Kaneko, H. Tokashiki, K. Tanie, and K. Komoriya, "Impedance shaping based on force feedback bilateral control in macro-micro teleoperation system", In *the IEEE Int'l Conf. Robotics and Automation*, pp. 710–717, Apr. 1997.

[150] A. Bolopion, H. Xie, D. S. Haliyo, and S. Regnier, "Haptic teleoperation for 3-D microassembly of spherical objects", *IEEE/ASME Trans. Mechatron.*, Vol. 17, No. 1, pp. 116–126, Feb. 2012.

[151] A. Sharon, N. Hogan, and E. D. Hardt, "High bandwidth force regulation and inertia reduction using a macro/micro manipulator system", In *1988 IEEE Int. Conf. on Robotics and Automation*, Apr. 1988.

[152] S. Khan, A. Sabanovic, and A. O. Nergiz, "Scaled bilateral teleoperation using discrete-time sliding-mode controller", *IEEE Trans. Ind. Electron.*, Vol. 56, No. 9, pp. 3609–3618, 2009.

[153] A. Hace and M. Franc, "FPGA implementation of sliding mode control algorithm for scaled bilateral teleoperation", *IEEE Trans. Ind. Informat.*, Vol. 9, No. 3, pp. 1291–1300, 2013.

[154] C. Ishii, K. Kobayashi, Y. Kamei, and Y. Nishitani, "Robotic forceps manipulator with a novel bending mechanism", *IEEE/ASME Trans. Mechatron.*, Vol. 15, No. 5, pp. 671–684, Oct. 2010.

[155] N. Tsunashima and S. Katsura, "Reproduction of human motion using motion-copying system based on coordinate modification", In *Proc. Int. Conf. IEEE IECON*, pp. 1609–1614, Nov. 2010.

[156] C. Sutherland, K. Hashtrudi-Zaad, R. Sellens, P. Abolmaesumi, and P. Mousavi, "An augmented reality haptic training simulator for spinal needle procedures", *IEEE Trans. Biomedical Eng.*, Vol. 60, No. 11, pp. 3009–3018, 2013.

[157] C. T. Asque, A. M. Day, and S. D. Laycock, "Haptic-assisted target acquisition in a visual point-and-click task for computer users with motion impairments", *IEEE Trans. Haptics*, Vol. 5, No. 2, pp. 120–130, Apr. 2012.

[158] D. Yashiro and K. Ohnishi, "Performance analysis of bilateral control system with communication bandwidth constraint", *IEEE Trans. Ind. Electron.*, Vol. 58, No. 2, pp. 436–443, Feb. 2011.

[159] Y. Bekiroglu, J. Laaksonen, J. A. Jorgensen, V. Kyrki, and D. Kragic, "Assessing grasp stability based on learning and haptic data", *IEEE Trans. Robot.*, Vol. 27, No. 3, pp. 616–629, Jun. 2011.

[160] J. M. Romano, K. Hsiao, G. Niemeyer, S. Chitta, and K. J. Kuchenbecker, "Human-inspired robotic grasp control with tactile sensing", *IEEE Trans. Robot.*, Vol. 27, No. 6, pp. 1067–1079, Dec. 2011.

[161] R. Balasubramanian, X. Ling, P. D. Brook, J. R. Smith, and Y. Matsuoka, "Physical human interactive guidance: identifying grasping principles from human-planned grasps", *IEEE Trans. Robot.*, Vol. 28, No. 4, pp. 899–910, Aug. 2012.

[162] S. Sakaino, T. Sato, and K. Ohnishi, "Task hierarchy for position limitation and bilateral control by oblique coordinate control", In *Proc. Int. Conf. IEEE IECON*, pp. 1794–1799, Nov. 2009.

[163] T. Nozaki, T. Mizoguchi, and K. Ohnishi, "Decoupling strategy for position and force control based on modal space disturbance observer", *IEEE Trans. Ind. Electron.*, Vol. 61, No. 2, pp. 1022–1032, 2014.

[164] J. Lee, P. Chang, and R. S. Jamisola, "Relative impedance control for dual-arm robots performing asymmetric bimanual tasks", *IEEE Trans. Ind. Electron.*, to be published.

[165] T. Nozaki, T. Mizoguchi, and K. Ohnishi, "A controller design method for multirobot systems based on task projection matrix", In *Proc. IEEE Int. Conf. Mechatronics*, pp. 213–218, Feb. 2013.

[166] E. Sariyildiz, D. Cattin, and K. Ohnishi, "Improving the performance of higher order disturbance observers: a position approach", In *the 2012 12th IEEE Int'l Workshop on Advanced Motion Control*, Mar. 2012.

[167] H. Kobayashi, S. Katsura, and K. Ohnishi, "An analysis of parameter variations of disturbance observer for motion control", *IEEE Trans. Ind. Electron.*, Vol. 54, No. 6, pp. 3413–3421, Dec. 2007.

[168] Y. Nakajima, T. Nozaki, and K. Ohnishi, "Heartbeat synchronization with haptic feedback for tele-surgical robot", *IEEE Trans. Ind. Electron.*, to be published.

[169] C. Paleologu, J. Benesty, and S. Ciochina, "A robust variable forgetting factor recursive least-squares algorithm for system identification", *IEEE Signal Process. Lett.*, Vol. 15, pp. 597–600, 2008.

[170] N. Sado, S. Sakai, and Y. Hori, "Road condition estimation for traction control in electric vehicle", In *Proc. ISIE*, pp. 973–978, Jul. 1999.

[171] M. Lopes and J. Santos-Victor, "A developmental roadmap for learning by imitation in robots", *IEEE Trans. Syst., Man, Cybern. B, Cybern.*, Vol. 37, No. 2, pp. 308–321, Apr. 2007.

[172] Y. Lin, S. Ren, M. Clevenger, and Y. Sun, "Learning grasping force from demonstration", In *Proc. IEEE Int. Conf. Robot. Autom.*, pp. 1526–1531, May. 2012.

[173] A. M. Schmidts, D. Lee, and A. Peer, "Imitation learning of human grasping skills from motion and force data", In *Proc. IEEE/RSJ Int. Conf. Intell. Robots Syst.*, pp. 1002–1007, Sep. 2011.

[174] T. Sato, S. Sakaino, and K. Ohnishi, "Motion reproduction system with haptic information for different environment location", In *Proc. Int. Conf. IEEE IECON*, pp. 1651–1656, Nov. 2009.

[175] M. T. Ravichandran and A. D. Mahindrakar, "Robust stabilization of a class of underactuated mechanical systems using time scaling and lyapunov redesign", *IEEE Trans. Ind. Electron.*, Vol. 58, No. 9, pp. 4299–4313, Sep. 2011.

[176] L. M. Capisani and A. Ferrara, "Trajectory planning and second-order sliding mode motion/interaction control for robot manipulators in unknown environments", *IEEE Trans. Ind. Electron.*, Vol. 59, No. 8, pp. 3189–3198, Aug. 2012.

[177] S. Yajima and S. Katsura, "Velocity based motion-copying system for grasping/manipulation motion reproduction", In *Proc. IEEE/SICE Int. Symp. Syst. Integr.*, pp. 515–520, Dec. 2011.

[178] S. Yajima and S. Katsura, "Velocity based motion-copying system for integrated reproduction of motion components", In *Proc. Int. Conf. IEEE IECON*, pp. 2628–2633, Oct. 2012.

[179] T. Shimono, S. Katsura, and K. Ohnishi, "A realization of haptic skill database by bilateral motion control", In *Proc. Int. Conf. IEEE IECON*, pp. 5252–5257, Nov. 2006.

[180] E. Sariyildiz and K. Ohnishi, "Bandwidth constraints of disturbance observer in the presence of real parametric uncertainties", *European J. of Control*, Vol. 19, No. 3, pp. 199–205, 2013.

[181] E. Sariyildiz and K. Ohnishi, "Analysis the robustness of control systems based on disturbance observer", *Int'l J. of Control*, to be published.

List of Achievements

Journals (First Author)

[1] <u>Takahiro Nozaki</u>, Takahiro Mizoguchi, and Kouhei Ohnishi, "Motion expression by elemental separation of haptic information," *IEEE Transactions on Industrial Electronics*. (Accepted for publication)

[2] <u>Takahiro Nozaki</u>, Takahiro Mizoguchi, and Kouhei Ohnishi, "Motion-copying system with variable impedance based on scaled bilateral control in one-degree-of-freedom robot," *IEEJ Journal of Industry Applications*, vol. 3, no. 1, pp. 1–9, 2014.

[3] <u>Takahiro Nozaki</u>, Takahiro Mizoguchi, and Kouhei Ohnishi, "Decoupling strategy for position and force control based on modal space disturbance observer," *IEEE Transactions on Industrial Electronics*, vol. 61, no. 2, pp. 1022–1032, 2014.

[4] <u>Takahiro Nozaki</u>, Takahiro Mizoguchi, Yuki Saito, Daisuke Yashiro, and Kouhei Ohnishi, "Recognition of grasping motion based on modal space haptic information using DP pattern-matching algorithm," *IEEE Transactions on Industrial Informatics*, vol. 9, no. 4, pp. 2043–2051, 2013.

[5] <u>Takahiro Nozaki</u>, Takahiro Mizoguchi, Yuki Saito, Tomohiro Nakano, and Kouhei Ohnishi, "Bilateral control method based on transformation matrix relating motion features and tool coordinates," *IEEJ Journal of Industry Applications*, vol. 2, no. 1, pp. 67–73, 2013.

[6] <u>Takahiro Nozaki</u>, Takahiro Mizoguchi, and Kouhei Ohnishi, "Real-world haptics for motion realization," *IEEJ Journal of Industry Applications*, vol. 2, no. 1, pp. 1–6, 2013.

[7] <u>Takahiro Nozaki</u>, Takahiro Mizoguchi, Kouhei Ohnishi, Yasuhide Morikawa, and Soji Ozawa, "Extraction of motion feature by using force scaling bilateral control," *Journal of Japan Society of Computer Aided Surgery*, vol. 14, no. 3, pp. 248–249, 2012. (in Japanese)

[8] <u>Takahiro Nozaki</u>, Takahiro Mizoguchi, Yusuke Suzuki, Daisuke Yashiro, and Kouhei Ohnishi, "Human combination motion recognition based on haptic information using similarly structured

master-slave robot hand," *IEEJ Transactions on Industry Applications*, vol. 132-D, no. 9, pp. 858–864, 2012. (in Japanese)

[8'] <u>Takahiro Nozaki</u>, Takahiro Mizoguchi, Yusuke Suzuki, Daisuke Yashiro, and Kouhei Ohnishi, "Recognition of human combined motion from haptic information using similarly structured master and slave robot hands," *Electronics and Communications in Japan*. (Accepted for publication)

[9] <u>Takahiro Nozaki</u>, Takahiro Mizoguchi, Kouhei Ohnishi, Yasuhide Morikawa, and Soji Ozawa, "Transmission of enhanced stiffness with teleoperation robot," *Journal of Japan Society of Computer Aided Surgery*, vol. 13, no. 3, pp. 312–313, 2011. (in Japanese)

[10] <u>Takahiro Nozaki</u>, Yusuke Suzuki, and Kouhei Ohnishi, "Transmission of force sensations by hand of multi-dof master-slave robot using tendon-driven mechanism," *IEEJ Transactions on Industry Applications*, vol. 131-D, no 3, pp. 297–303, 2011. (in Japanese)

[11] <u>Takahiro Nozaki</u>, Keisuke Sugawara, Kouhei Ohnishi, Yasuhide Morikawa, and Naoki Shimojima, "The basic principle of bilateral teleoperation," *Journal of Japan Society of Computer Aided Surgery*, vol. 12, no. 3, pp. 220–221, 2010. (in Japanese)

Journals (Co-author)

[1] Yu Nakajima, <u>Takahiro Nozaki</u>, and Kouhei Ohnishi, "Heartbeat synchronization with haptic feedback for tele-surgical robot," *IEEE Transactions on Industrial Electronics*. (Accepted for publication)

[2] Takahiro Mizoguchi, <u>Takahiro Nozaki</u>, and Kouhei Ohnishi, "Stiffness transmission of scaling bilateral control system by gyrator element integration," *IEEE IEEE Transactions on Industrial Electronics*, vol. 61, no. 2, pp. 1033–1043, 2014.

[3] Yu Nakajima, <u>Takahiro Nozaki</u>, Yuji Oyamada, and Kouhei Ohnishi, "An object-coordinate-based bilateral control system using visual information," *Electronics and communications in Japan*, vol. 96, no. 8, pp. 41–49, 2013.

[4] Keita Shimamoto, Kazuki Tanida, <u>Takahiro Nozaki</u>, and Kouhei Ohnishi, "Transmission of force sensation achieved by tendon-driven spherical joint mechanism," *IEEJ Transactions on Industry Applications*, vol. 133-D, no. 3, pp. 307–313, 2013. (in Japanese)

[5] Yuki Saito, Wataru Motooka, <u>Takahiro Nozaki</u>, Daisuke Yashiro, and Kouhei Ohnishi, "Development of two-link manipulator equipped with biarticular muscle mechanism using flexible actuator," *IEEJ Transactions on Industry Applications*, vol. 132-D, no. 3, pp. 397–403, 2012. (in Japanese)

[6] Yu Nakajima, <u>Takahiro Nozaki</u>, Yuji Oyamada, and Kouhei Ohnishi, "Object-coordinate-based bilateral control system using visual information," *IEEJ Transactions on Industry Applications*, vol. 132-D, no. 3, pp. 347–380, 2012. (in Japanese)

[7] Yu Nakajima, <u>Takahiro Nozaki</u>, Kouhei Ohnishi, Yasuhide Morikawa, and Soji Ozawa, "Bilateral control method with motion canceling for 2-DOF forceps robot," in *Journal of Japan Society of Computer Aided Surgery*, vol. 13, no. 3, pp. 336–337, 2011. (in Japanese)

[8] Yuki Saito, <u>Takahiro Nozaki</u>, Kouhei Ohnishi, Yasuhide Morikawa, and Soji Ozawa, "Scaling bilateral control of tendon-driven rotary actuator," in *Journal of Japan Society of Computer Aided Surgery*, vol. 13, no. 3, pp. 318–319, 2011. (in Japanese)

[9] Takahiro Mizoguchi, <u>Takahiro Nozaki</u>, Kouhei Ohnishi, Yasuhide Morikawa, and Soji Ozawa, "Workspace TGI bilateral control for systems with different structures," in *Journal of Japan Society of Computer Aided Surgery*, vol. 13, no. 3, pp. 316–317, 2011. (in Japanese)

[10] Fumiya Mitome, Wataru Motooka, <u>Takahiro Nozaki</u>, Takahiro Mizoguchi, Keisuke Sugawara, Keishi Okuda, Midori Miyagaki, Daisuke Yashiro, Takahiro Yakoh, Kouhei Ohnishi, Yasuhide Morikawa, and Naoki Shimojima, "Development of 8-DOF haptic robot assisted surgery," in *Journal of Japan Society of Computer Aided Surgery*, vol. 12, no. 3, pp. 208–209, 2010. (in Japanese)

International Conferences (First Author)

[1] <u>Takahiro Nozaki</u>, Kazuki Tanida, Takahiro Mizoguchi, Tomohiro Nakano, Yuki Saito, and Kouhei Ohnishi, "Extraction and realization of human actions," in *Proceedings of the 13th IEEE International Workshop on Advanced Motion Control, AMC 2014, Yokohama, Japan*, March 14–16, 2014.

[2] <u>Takahiro Nozaki</u>, Takahiro Mizoguchi, and Kouhei Ohnishi, "Motion reproduction using time-scaling for adaptation to difference in environmental location," in *Proceedings of the IEEE International Conference on Industrial Technology, ICIT 2014, Busan, Korea*, February 26–March 1, 2014.

[3] <u>Takahiro Nozaki</u>, Takahiro Mizoguchi, and Kouhei Ohnishi, "A controller design method for multirobot systems based on task projection matrix," in *Proceedings of the IEEE International Conference on Mechatronics, ICM 2013, Vicenza, Italy*, pp. 213–218, February 27–March 1, 2013.

[4] <u>Takahiro Nozaki</u>, Takahiro Mizoguchi, and Kouhei Ohnishi, "Bilateral control method for tendon-driven mechanism considering wire elongation," in *Proceedings of the 38th Annual Conference of*

the IEEE Industrial Electronics Society, IECON 2012, Montreal, Canada, pp. 2662–2667, October 25–28, 2012.

[5] Takahiro Nozaki, Takahiro Mizoguchi, Yu Nakajima, and Kouhei Ohnishi, "Real-time skill providing system using human haptic information," in *Proceedings of the 5th International Conference on Human System Interaction, HSI 2012, Perth, Australia*, pp. 144–151, June 6–8, 2012.

[6] Takahiro Nozaki, Takahiro Mizoguchi, and Kouhei Ohnishi, "Position/force decoupling for micro-macro bilateral control based on modal space disturbance observer," in *Proceedings of the 12th IEEE International Workshop on Advanced Motion Control, AMC 2012, Sarajevo, Bosnia and Herzegovina*, March 25–27, 2012.

[7] Takahiro Nozaki, Yusuke Suzuki, and Kouhei Ohnishi, "Motion recognition using DP matching based on position and force information," in *Proceedings of the 4th International Conference on Human System Interaction, HSI 2011, Yokohama, Japan*, pp. 104–109, May 19–21, 2012.

[8] Takahiro Nozaki and Kouhei Ohnishi, "Development of haptic data acquisition robot hand," in *Proceedings of the International Symposium on Application of Biomechanical Control System to Precision Engineering, ISAB 2010, Hukushima, Japan/*, July 22–24, 2010.

International Conferences (Co-author)

[1] Takahiro Mizoguchi, Takahiro Nozaki, and Kouhei Ohnishi, "Impedance correction in time delayed teleoperation system," in *Proceedings of the 13th IEEE International Workshop on Advanced Motion Control, AMC 2014, Yokohama, Japan*, March 14–16, 2014.

[2] Keita Shimamoto, Y. Ohno, Takahiro Nozaki, and Kouhei Ohnishi, "Time delay compensation for tendon-driven bilateral control using modal decomposition and communication disturbance observer," in *Proceedings of the IEEE International Conference on Industrial Technology, ICIT 2014, Busan, Korea*, February 26–March 1, 2014.

[3] Takahiro Mizoguchi, Takahiro Nozaki, and Kouhei Ohnishi, "A consideration to window problem in mechanical power factor calculation," in *Proceedings of the IEEE International Conference on Industrial Technology, ICIT 2014, Busan, Korea*, February 26–March 1, 2014.

[4] Takahiro Mizoguchi, Takahiro Nozaki, and Kouhei Ohnishi, "Free motion mechanical power factor; comparison between robots in different structure and coordinate," in *Proceedings of the International Power Electronics Conference, IPEC 2014, Hiroshima, Japan*, May 18–21, 2014.

[5] Takahiro Mizoguchi, Takahiro Nozaki, and Kouhei Ohnishi, "Power factor analyses in mechanical system focusing on trajectory and environment," in *Proceedings of the IEEE International Symposium on Industrial Electronics, ISIE 2013, Taipei, Taiwan*, May 27–31, 2013.

[6] Yuki Saito, Uichiro Nishio, Takahiro Nozaki, and Kouhei Ohnishi, "Acceleration-based position and force control for twist drive," in *Proceedings of the IEEE International Conference on Mechatronics, ICM 2013, Vicenza, Italy*, pp. 664–669, February 27–March 1, 2013.

[7] Tomohiro Nakano, Yuki Saito, Takahiro Nozaki, and Kouhei Ohnishi, "Variable tension control for master-slave tendon-driven robot hand," in *Proceedings of the IEEE International Conference on Mechatronics, ICM 2013, Vicenza, Italy*, pp. 588–593, February 27–March 1, 2013.

[8] Takahiro Mizoguchi, Takahiro Nozaki, and Kouhei Ohnishi, "The power factor in mechanical system," in *Proceedings of the IEEE International Conference on Mechatronics, ICM 2013, Vicenza, Italy*, pp. 576–581, February 27–March 1, 2013.

[9] Takahiro Mizoguchi, Takahiro Nozaki, and Kouhei Ohnishi, "A design method of bilateral control system based on interactive parameters," in *Proceedings of the 38th Annual Conference of the IEEE Industrial Electronics Society, IECON 2012, Montreal, Canada*, pp. 4382–4387, October 25–28, 2012.

[10] Kasun Prasanga, Yuki Saito, Takahiro Nozaki, and Kouhei Ohnishi, "Achievement of real haptic sensation with tendon driven segregated jaws for laparoscopic forceps," in *Proceedings of the 6th International Conference on Information and Automation for Sustainability, ICIAfS 2012, Beijing, China*, pp. 65–70, September 27–29, 2012.

[11] Yu Nakajima, Takahiro Nozaki, and Kouhei Ohnishi, "Synchronization performance improvement on motion canceling bilateral control using an extended dual sampling rate observer," in *Proceedings of the 5th International Conference on Human System Interaction, HSI 2012, Perth, Australia*, pp. 160–167, June 6–8, 2012.

[12] Takahiro Mizoguchi, Takahiro Nozaki, and Kouhei Ohnishi, "Examination of stability and characteristics of gyrator type bilateral control; toward controller and transfer impedance design," in *Proceedings of the 5th International Conference on Human System Interaction, HSI 2012, Perth, Australia*, pp. 116–123, June 6–8, 2012.

[13] Yu Nakajima, Takahiro Nozaki, Takahiro Mizoguchi, and Kouhei Ohnishi, "Transparency analysis of motion canceling bilateral control under sensing constraints," in *Proceedings of the 12th IEEE International Workshop on Advanced Motion Control, AMC 2012, Sarajevo, Bosnia and Herzegovina*, March 25–27, 2012.

[14] Uichiro Nishio, <u>Takahiro Nozaki</u>, and Kouhei Ohnishi, "A method of joint torque control for a tendon-driven system," in *Proceedings of the 12th IEEE International Workshop on Advanced Motion Control, AMC 2012, Sarajevo, Bosnia and Herzegovina*, March 25–27, 2012.

[15] Shinnosuke Yamaoka, <u>Takahiro Nozaki</u>, Daisuke Yashiro, and Kouhei Ohnishi, "Acceleration control of stacked piezoelectric actuator utilizing disturbance observer and reaction force observer," in *Proceedings of the 12th IEEE International Workshop on Advanced Motion Control, AMC 2012, Sarajevo, Bosnia and Herzegovina*, March 25–27, 2012.

[16] Yuki Saito, <u>Takahiro Nozaki</u>, and Kouhei Ohnishi, "Model-based compensation of wire elongation for tendon-driven rotary actuator," in *Proceedings of the 12th IEEE International Workshop on Advanced Motion Control, AMC 2012, Sarajevo, Bosnia and Herzegovina*, March 25–27, 2012.

[17] Takahiro Mizoguchi, <u>Takahiro Nozaki</u>, and Kouhei Ohnishi, "Scaling bilateral controls with impedance transmission using transfer admittance," in *Proceedings of the 12th IEEE International Workshop on Advanced Motion Control, AMC 2012, Sarajevo, Bosnia and Herzegovina*, March 25–27, 2012.

[18] Wataru Motooka, <u>Takahiro Nozaki</u>, Takahiro Mizoguchi, Keisuke Sugawara, Fumiya Mitome, Keishi Okuda, Midori Miyagaki, Daisuke Yashiro, Takahiro Yakoh, Kouhei Ohnishi, Yasuhide Morikawa, and Naoki Shimojima, "Development of 16-dof telesurgical forceps master/slave robot with haptics," in *Proceedings of the 36th Annual Conference of the IEEE Industrial Electronics Society, IECON 2010, Arizona, United States of America*, pp. 2075–2080, November 7–10 2010.

Domestic Conferences (First Author)

[1] <u>Takahiro Nozaki</u>, Takahiro Mizoguchi, and Kouhei Ohnishi, "Realization of physical action by tendon-driven robot," in *Papers of the IEEJ Technical Meeting on Mechatronics Control*, MEC-13-178, November 22–23, 2013. (in Japanese)

[2] <u>Takahiro Nozaki</u>, Takahiro Mizoguchi, and Kouhei Ohnishi, "Motion expression by manifold of haptic information," in *Papers of the IEEJ Technical Meeting on Industrial Instrumentation and Control*, IIC-13-148, pp. 73–78, March 7–8, 2011. (in Japanese)

[3] <u>Takahiro Nozaki</u>, Takahiro Mizoguchi, Kouhei Ohnishi, Yasuhide Morikawa, and Soji Ozawa, "Extraction of motion feature by using force scaling bilateral control," *The 21st Annual Congress of Japan Society of Computer Aided Surgery, JSCAS'12, Tokushima*, pp. 248–249, November 2–4, 2012. (in Japanese)

[4] Takahiro Nozaki, Takahiro Mizoguchi, Yuki Saito, Tomohiro Nakano, and Kouhei Ohnishi, "Bilateral control method based on physical coordinate system and function," in *Papers of the IEEJ Technical Meeting on Industrial Instrumentation and Control*, IIC-12, pp. 91–96, March 6–7, 2012. (in Japanese)

[5] Takahiro Nozaki, Takahiro Mizoguchi, Kouhei Ohnishi, Yasuhide Morikawa, and Soji Ozawa, "Transmission of enhanced stiffness with teleoperation robot," *The 20th Annual Congress of Japan Society of Computer Aided Surgery, JSCAS'11, Kanagawa*, pp. 312–313, November 22–24, 2011. (in Japanese)

[6] Takahiro Nozaki and Kouhei Ohnishi, "Rotation angle and tension control of the tendon-driven rotary actuator based on oblique coordinate control," in *Proceedings of the 2011 Annual Conference of the IEEJ Industry Application Society, JIASC '11*, no. 2-6, pp. II383–II388, September 6–8, 2011. (in Japanese)

[7] Takahiro Nozaki, Yusuke Suzuki, and Kouhei Ohnishi, "Human haptic motion recognition using master-slave robot hand," in *Papers of the IEEJ Technical Meeting on Industrial Instrumentation and Control*, IIC-11-43, pp. 101–106, March 8–9, 2011. (in Japanese)

[8] Takahiro Nozaki, Keisuke Sugawara, Kouhei Ohnishi, Yasuhide Morikawa, and Naoki Shimojima, "The basic principle of bilateral teleoperation," *The 19th Annual Congress of Japan Society of Computer Aided Surgery, JSCAS'10, Hukuoka*, vol. 12, no. 3, pp. 220–221, November 2–4, 2010. (in Japanese)

[9] Takahiro Nozaki and Kouhei Ohnishi, "Haptic comunication in shared mixed reality," in *Proceedings of the 2010 Annual Conference of the IEEJ Industry Application Society, JIASC '10*, no. 2-26, pp. II341–II346, August 24–26, 2010. (in Japanese)

[10] Takahiro Nozaki, Yusuke Suzuki, and Kouhei Ohnishi, "Realization of a bilateral robot hand using tendon drive mechanism," in *Papers of the IEEJ Technical Meeting on Industrial Instrumentation and Control*, IIC-10-130, pp. 13–18, March 8–9, 2010. (in Japanese)

Domestic Conferences (Co-author)

[1] Seiji Uozumi, Haruya Sato, Daiki Suzuki, Keita Shimamoto, Takahiro Nozaki, and Kouhei Ohnishi, "Design method of function mode considering shape of grasping object," in *Papers of the IEEJ Technical Meeting on Industrial Instrumentation and Control*, IIC-13, pp. 67–72, March 7–8, 2013. (in Japanese)

[2] Takahiro Mizoguchi, <u>Takahiro Nozaki</u>, and Kouhei Ohnishi, "Characteristics of gyrator type bilateral control under time-delay," in *Papers of the IEEJ Technical Meeting on Industrial Instrumentation and Control*, IIC-13, pp. 131–136, March 7–8, 2013. (in Japanese)

[3] Yuki Saito, Uichiro Nishio, <u>Takahiro Nozaki</u>, and Kouhei Ohnishi, "Realization of acceleration based control for strings transmission twist drive," in *Proceedings of the 2012 Annual Conference of the IEEJ Industry Application Society, JIASC '12*, no. 2-23, pp. II135–II140, August 21–23, 2012. (in Japanese)

[4] Yuki Saito, <u>Takahiro Nozaki</u>, Tomohiro Nakano, and Kouhei Ohnishi, "Analysis and compensation of wire elongation for tendon-driven rotary actuator based on four-element viscoelastic model," in *Papers of the IEEJ Technical Meeting on Industrial Instrumentation and Control*, IIC-12, pp. 123–128, March 6–7, 2012. (in Japanese)

[5] Keita Shimamoto, Kazuki Tanida, <u>Takahiro Nozaki</u>, and Kouhei Ohnishi, "Motion and tension control for tendon-driven spherical joint mechanism," in *Papers of the IEEJ Technical Meeting on Industrial Instrumentation and Control*, IIC-12, pp. 111–116, March 6–7, 2012. (in Japanese)

[6] Tomohiro Nakano, Haruya Sato, Yuki Saito, <u>Takahiro Nozaki</u>, and Kouhei Ohnishi, "Tendon arrangement and bilateral control of master-slave robot hand using tendon-driven mechanism considering grasping motion," in *Papers of the IEEJ Technical Meeting on Industrial Instrumentation and Control*, IIC-12, pp. 91–96, March 6–7, 2012. (in Japanese)

[7] Takahiro Mizoguchi, <u>Takahiro Nozaki</u>, and Kouhei Ohnishi, "A design method of bilateral control system with transfer impedance and admittance," in *Papers of the IEEJ Technical Meeting on Industrial Instrumentation and Control*, IIC-12, pp. 49–54, March 6–7, 2012. (in Japanese)

[8] Yu Nakajima, <u>Takahiro Nozaki</u>, Kouhei Ohnishi, Yasuhide Morikawa, and Soji Ozawa, "Bilateral control method with motion canceling for 2-DOF forceps robot," *The 20th Annual Congress of Japan Society of Computer Aided Surgery, JSCAS'11, Kanagawa*, pp. 336–337, November 22–24, 2011. (in Japanese)

[9] Yuki Saito, <u>Takahiro Nozaki</u>, Kouhei Ohnishi, Yasuhide Morikawa, and Soji Ozawa, "Scaling bilateral control of tendon-driven rotary actuator," *The 20th Annual Congress of Japan Society of Computer Aided Surgery, JSCAS'11, Kanagawa*, pp. 318–319, November 22–24, 2011. (in Japanese)

[10] Takahiro Mizoguchi, <u>Takahiro Nozaki</u>, Kouhei Ohnishi, Yasuhide Morikawa, and Soji Ozawa, "Workspace TGI bilateral control for systems with different structures," *The 20th Annual Congress*

of Japan Society of Computer Aided Surgery, JSCAS'11, Kanagawa, pp. 316–317, November 22–24, 2011. (in Japanese)

[11] Yu Nakajima, <u>Takahiro Nozaki</u>, and Kouhei Ohnishi, "Motion canceling method for bilateral control," *Proceedings of the 2011 Annual Conference of the IEEJ Industry Application Society, JIASC '11*, no. 2-106, pp. II813–II818, September 6–8, 2011. (in Japanese)

[12] Yuki Saito, Wataru Motooka, <u>Takahiro Nozaki</u>, and Kouhei Ohnishi, "Development of two link manipulator equipped with bi-articular muscle mechanism using flexible actuator," in *Papers of the IEEJ Technical Meeting on Industrial Instrumentation and Control*, IIC-11-23, pp. 107–112, March 8–9, 2011. (in Japanese)

[13] Yu Nakajima, <u>Takahiro Nozaki</u>, Yuji Oyamada, and Kouhei Ohnishi, "Object space coordinates based bilateral control system using a camera," in *Papers of the IEEJ Technical Meeting on Industrial Instrumentation and Control*, IIC-11-39, pp. 77–82, March 8–9, 2011. (in Japanese)

[14] Fumiya Mitome, Wataru Motooka, <u>Takahiro Nozaki</u>, Takahiro Mizoguchi, Keisuke Sugawara, Keishi Okuda, Midori Miyagaki, Daisuke Yashiro, Takahiro Yakoh, Kouhei Ohnishi, Yasuhide Morikawa, and Naoki Shimojima, "Development of 8-DOF haptic robot assisted surgery," *The 19th Annual Congress of Japan Society of Computer Aided Surgery, JSCAS'10, Hukuoka*, pp. 208–209, November 2–4, 2010. (in Japanese)

<u>Awards</u>

[1] Excellent Presentation Award

Technical Committee on Mechatronics Control (MEC), Industry Applications Society (IAS), the Institute of Electrical Engineers of Japan (IEEJ)

Date: January 10th, 2013

[2] Excellent Research Activity Award (Master Course)

School of Integrated Design Engineering, Graduate School of Science and Technology, Keio University

Date: March 29th, 2012

[3] The Best Paper Award, "Motion recognition using DP matching based on position and force information",

IEEE 4th International Conference on Human System Interaction HSI2011.

Date: May 19, 2011.

[4] Excellent Presentation Award

Industry Applications Society (IAS), the Institute of Electrical Engineers of Japan (IEEJ)

Date: March 31st, 2011

[5] Excellent Presentation Award

Technical Committee on Industrial Instrumentation and Control (IIC), Industry Applications Society (IAS), the Institute of Electrical Engineers of Japan (IEEJ)

Date: December 28th, 2010